Probabilistic fatigue limit assessment and improvement by experimental and numerical tests

Lujie Shi

Normandie Université

THESE

Pour obtenir le diplôme de doctorat

Spécialité Génie Mécanique

Préparée au sein de l'Institut National des Sciences Appliquées de Rouen Normandie

Probabilistic fatigue limit assessment and improvement by experimental and numerical tests

Présentée et soutenue par
Lujie SHI

Thèse soutenue publiquement le 25 janvier 2023 devant le jury composé de		
M. Stéphane Panier	Professeur, Université de Picardie Jules Verne	Président du jury
M. Thierry Palin-luc	Professeur, Arts et Métiers ParisTech Bordeaux campus	Rapporteur
M. Julien Baroth	Maître de conférences HDR, Université Grenoble Alpes	Rapporteur
Mme. Cécile Mattrand	Maître de conférences, Clermont Auvergne INP	Examinatrice
M. Eduardo Souza de Cursi	Professeur, INSA Rouen Normandie	Examinateur
Mme. Leila Khalij	Maître de conférences HDR, INSA Rouen Normandie	Directrice de thèse

Thèse dirigée par Mme. Leila KHALIJ,
Laboratoire de Mécanique de Normandie - LMN (EA 3828)

INSA INSTITUT NATIONAL DES SCIENCES APPLIQUÉES ROUEN NORMANDIE

ED PSIME

LMN

PROBABILISTIC FATIGUE LIMIT ASSESSMENT AND IMPROVEMENT BY EXPERIMENTAL AND NUMERICAL TESTS

Lujie Shi

Laboratory of Mechanics of Normandy
INSA Rouen Normandy, France

La vie consiste à se créer soi-même.

Acknowledgments

First and foremost I am grateful to my supervisor, Asst. Prof. Leila Khalij, whose expertise was invaluable in formulating the research questions and methodology. Her insightful feedback pushed me to sharpen my thinking and brought my work to a higher level. It is really my fortune to meet her as a mentor.

I would like to express my gratitude to Dr. Hao Bai for his wise ideas and wonderful collaboration. He assisted me with the research tools, choosing the right direction and reviewing the dissertation.

Dr. Christophe Gautrelet has been another guide in my Ph.D. research since the beginning. I would like to thank him for his technical support in the experimental study. Prof. Eduardo Souza De Cursi offered guidance on statistics. Asst. Prof. Emmanuel Pagnacco and Prof. Stéphane Panier were influential in shaping my research methods and critiquing the results. Asst. Prof. Younes Aouès and Asst. Prof. Didier Lemosse gave much valuable advice to my dissertation. Mrs. Elisabeth Lesage, the laboratory management assistant, also helped me on the way to finishing my PhD.

I appreciate the time and efforts of all committee members in reviewing this dissertation. I would also like to acknowledge the help from Prof. Changwu Huang, who offered the computation resources used in my research, and the help from Alain Guillet and Emmanuel Cadel for the SEM micrographs. Additionally, I would like to appreciate the financial support from China Scholarship Council.

Dr. Chen Shi and Dr. Julien Wang are kind and brilliant, with them I had a cherished time in the lab and social settings. There are many other colleagues in LMN, Dr. Hongbo Zhang, Dr. Shubiao Wang and Dr. Hadj kacem Mouna, whom I would like to thank for their amiability. It is a beautiful accident to meet friends Shuming Huang and Shengyue Ruan. It is their kind help and support that have made my study and life in France a wonderful time.

Most importantly, I would like to express gratitude to my parents and my little sister Mingzhi Shi. Family is always the beautiful land of life.

I wish to extend my special thanks to myself. Reaching out eagerly and bravely for a newer and richer experience. What is past is prologue.

L.S.

Abstract

This work is devoted to the improvement of the estimation of the mean and standard deviation of the fatigue limit from experimental tests and numerical simulations using a staircase method. Once a target life is chosen (e.g. 106 cycles), this approach consists in applying on each specimen a loading amplitude with ascending or descending steps until the specimen fails or not. The fatigue limit is then estimated from the median of a probability distribution. Nevertheless, the step size of the loading is known to be problematic because it can lead to a poor estimation of the standard. Thus, we proposed in this work, on the one hand, a non-parametric Kernel approach and, on the other hand, an approach based on Bayesian maximum entropy sampling combined with Latin hypercube sampling.

To obtain a first set of experimental data, the tests using the staircase protocol were performed in vibratory bending on an electro-dynamic exciter (shaker). Indeed, to reduce the dispersion on the estimation of the fatigue limit, a relatively high number of specimens is necessary, which can increase the costs and the time of tests, particularly on a conventional system limited in frequency. Thus, a first work was carried out to test steel specimens at a frequency close to the first resonance mode. Nevertheless, shakers are known to generate excitations in acceleration. We have therefore proposed a technique to achieve a strain control at constant amplitude with excitations close to the resonance. The system allows maintaining constant strain levels along the test despite the variation of the resonance frequency due to the presence of crack. Post-processing was performed on the experimental data to obtain fatigue limit distributions and evaluate the uncertainty on the staircase method by Bootstrap sampling. The results show a large uncertainty in the standard deviation. Thus, we considered a nonparametric distribution to improve the estimation of the fatigue limit and its dispersion.

Thus, we proposed a Kernel Density Estimation (KDE) approach combined with a non-linear correction of the standard deviation bias to optimize the bandwidth. To test this approach, numerical data were simulated in Python in order to perform a sensitivity study of a parameter set such as the number of specimens or the step size. The various comparisons have shown that the non-parametric method is more accurate than a classical method, especially regarding the estimated standard deviation.

Finally, in the last part of the work, in order to avoid the intrinsic limitations caused by the step size, a maximum entropy Bayes approach combined with Latin

Hypercube sampling (Bayes-LHS) has been proposed. This approach eliminates the requirement for the fixed stepsize and iteratively uses the information from the previous calculation step to reproduce the staircase method. Even if this work is not achieved, it tends to prove that the Bayes-LHS provides a fast computational protocol to arrive at a promising estimate.

Keywords Fatigue limit distribution, Staircase method, Vibratory strain control, Electro-dynamic shaker, High-cycle fatigue, Bootstrap sampling, Kernel Density Estimation, Bayesian maximum entropy sampling, Latin Hypercube Sampling (LHS)

Résumé

Cette thèse a pour objectif l'amélioration de l'estimation de la moyenne et de l'écart type de la limite de fatigue à partir d'essais expérimentaux et de simulations numériques au travers d'une méthode dite de l'escalier (ou staircase). Une fois la durée de vie cible fixée (e.g. 10^6 cycles), cette approche consiste à appliquer sur chaque éprouvette, une amplitude de chargement avec des paliers ascendants ou descendants jusqu'à rupture ou non de l'éprouvette. La limite de fatigue est alors estimée à partir de la médiane d'une distribution de probabilité. Cependant, le pas des paliers de chargement est connu comme étant problématique car, s'il est mal ajusté il peut mener à des erreurs dans l'estimation de l'écart type. Ainsi nous avons proposé d'une part, une approche non paramétrique de type Kernel et, d'autre part, une approche basée sur l'échantillonnage Bayésien à entropie maximale combinée à un échantillonnage Latin Hypercube.

Afin d'obtenir un premier jeu de données expérimentales, des essais utilisant le protocole staircase ont été réalisés en flexion vibratoire sur un excitateur électrodynamique (pot vibrant). En effet, pour réduire la dispersion sur l'estimation de la limite de fatigue, un nombre relativement élevé d'éprouvettes est nécessaire, ce qui peut augmenter les coûts mais aussi les durées des essais, notamment sur un système conventionnel limité en fréquence. Ainsi, un premier travail a été mené pour tester des éprouvettes en acier à une fréquence proche de leur premier mode de résonance. Cependant, les machines vibratoires de type pot vibrant sont connues pour générer une excitation en accélération. Nous avons donc proposé une technique pour réaliser un contrôle en déformation à amplitude constante avec une excitation au plus près de la résonance. Le système permet de maintenir des niveaux de déformation constants tout au long de l'essai malgré la variation de la fréquence de résonance due à la présence de fissure. Des post-traitements ont été réalisés sur les données expérimentales afin d'obtenir des distributions de la limite de fatigue et d'évaluer l'incertitude sur la méthode de l'escalier par un échantillonnage Bootstrap. Les résultats montrent que la méthode staircase présente une incertitude considérable sur l'écart-type. C'est pourquoi, nous avons envisagé une distribution non paramétrique pour améliorer l'estimation de la limite de fatigue et sa dispersion.

Ainsi, nous avons proposé une approche de type Kernel - KDE (Kernel Density Estimation) - combinée à une correction non linéaire du biais de l'écart type pour optimiser la largeur de bande. Pour tester cette approche, des données numériques

ont été simulées avec Python, afin de réaliser une étude de sensibilité d'un ensemble de paramètres, comme le nombre d'éprouvettes ou encore les pas entre les paliers de chargement. Les différentes comparaisons menées ont permis de démontrer que la méthode non-paramétrique est plus précise qu'une méthode classique, notamment en ce qui concerne l'écart type estimé.

Enfin, dans la dernière partie de ce travail, afin d'éviter les limitations intrinsèques causées par le palier de chargement, une approche de Bayes à entropie maximale combinée à un échantillonnage Latin Hypercube (Bayes-LHS) a été proposée. Cette approche abandonne complètement le pas fixe de chargement et utilise de manière itérative les informations de l'étape précédente pour reproduire la méthode de l'escalier. Cette approche, nécessitant encore des développements, est une première étape qui tend à prouver que le Bayes-LHS fournit un protocole de calcul rapide pour arriver à une estimation prometteuse.

Mots-clé Distribution de la limite de fatigue, méthode de l'escalier, contrôle de la déformation par vibration, excitateur électrodynamique, fatigue à grand nombre de cycles, échantillonnage Bootstrap, estimation de la Densité par Kernel (KDE), échantillonnage Bayésien à entropie maximale, échantillonnage Latin Hypercube

Contents

Acknowledgments v
Abstract vii
Résumé ix
List of Figures xv
List of Tables xix

Chapter 1 Introduction

1.1 Fatigue and fatigue limit . . . 2
1.1.1 Fatigue properties . . . 2
1.1.2 Strain-stress relationship in HCF . . . 6
1.2 Staircase test . . . 9
1.2.1 Staircase test protocol . . . 10
1.2.2 Staircase parameters . . . 11
1.3 Summary . . . 15

Chapter 2 Experimental strain-based vibration control to obtain the fatigue limit by the staircase method

2.1 Fatigue test machines and their control . . . 18
2.2 Experimental setup . . . 20
2.2.1 Specimen design and material . . . 20
2.2.2 Test bench . . . 23
2.2.3 Variability in the experimental test . . . 26
2.2.4 Linearity of the test system in acceleration control . . . 27
2.3 Strain control strategy . . . 28
2.3.1 Experimental development for fatigue tests . . . 29
2.3.2 Strain gauge and failure criterion . . . 32
2.3.3 Comparative study of fatigue test with strain control and acceleration control . . . 34
2.3.4 Fatigue curve . . . 39
2.4 Application of staircase method for the fatigue limit estimation . . . 42
2.4.1 Experimental procedure . . . 42
2.4.2 Test results and discussion . . . 44

2.5 Conclusion 53

Chapter 3 Uncertainty quantification using resampling methods

3.1 Background 56
3.2 Application of the leave-one-out resampling 57
3.3 Bootstrap resampling and results 59
3.3.1 Procedure 59
3.3.2 Experiment-based hyper-parameter sensitivity analysis 59
3.3.3 Results and discussion 62
3.4 Effect of specimen dimensions 63
3.4.1 Staircase tests 63
3.4.2 Application of the bootstrap sampling 66
3.5 Conclusion 69

Chapter 4 A non-parametric evaluation method in staircase test for improving fatigue limit assessment

4.1 Background 72
4.1.1 Existing evaluation techniques 72
4.1.2 Dixon-Mood method and corrections 74
4.1.3 Maximum Likelihood Estimation method 75
4.2 Non-parametric evaluation method and simulation procedure 75
4.2.1 Non-parametric fatigue limit estimation 76
4.2.2 Bandwidth selection 77
4.2.3 Bias correction on fatigue limit standard deviation 79
4.3 Numerical validation of the proposed evaluation method 80
4.3.1 Simulation procedure 80
4.3.2 Correction to Scott's rule 83
4.3.3 Sensitivity analysis of the KDE bandwidth 85
4.3.4 Comparison of the median value estimation 87
4.3.5 Comparison of the standard deviation estimation 88
4.3.6 Comparison of the probability distribution estimation 93
4.4 Application of KDE method on experimental data 94
4.5 Conclusion 96

Chapter 5 Bayesian improved staircase experimental design

5.1 Background 98
5.2 Bayesian theorem in fatigue test 99

5.2.1 Model parameter . . . 99
5.2.2 Likelihood with censored data . . . 100
5.2.3 Prior and posterior . . . 100
5.3 Bayesian maximum entropy sampling . . . 102
5.3.1 Shannon entropy . . . 102
5.3.2 Utility function . . . 103
5.3.3 Bayesian staircase method . . . 105
5.4 Improvement by using Latin Hypercube Sampling . . . 107
5.5 Application of the Bayes-LHS method for staircase representation . . . 108
5.5.1 Input parameters . . . 108
5.5.2 Bayes-LHS staircase protocol . . . 109
5.5.3 Example of Bayes-LHS procedure . . . 110
5.6 Numerical simulation of the Bayes-LHS test protocol . . . 113
5.7 Results and discussions . . . 114
5.7.1 Sensitivity analysis of input parameters . . . 114
5.7.2 Comparison of the Bayesian staircase and Bayes-LHS method . . . 116
5.7.3 Comparison to the conventional staircase using KDE . . . 117
5.8 Conclusion . . . 118

Chapter 6 Conclusion and perspective work

A Dynamics analysis of the specimen 125

A.1 Finite element modelling . . . 125
A.2 Dynamics characterization . . . 128

B Staircase test data 135

C Comparison study using the Dixon-Mood method 139

C.1 Dixon-Mood method . . . 139
C.2 Standard deviation correction for DM method . . . 140
C.3 Comparison results and discussions . . . 142
C.4 Conclusions . . . 144

D Comparison study with Maximum Likelihood Estimation 145

D.1 MLE method . . . 145
D.2 Comparison results and discussions . . . 148
D.3 Conclusion . . . 151

E Distributions: Normal, Lognormal and Weibull **153**

E.1 Normal distribution 154
E.2 Lognormal distribution 155
E.3 Weibull distribution 155

F Résumé en français **161**

F.1 Introduction générale 161
F.2 Chapitre 1 : Vue d'ensemble de la limite de fatigue 162
F.3 Chapitre 2 : Contrôle expérimental des vibrations basé sur la déformation 164
F.4 Chapitre 3 : Évaluation de l'incertitude par les méthodes de rééchantillonnage 166
F.5 Chapitre 4 : Méthode d'évaluation non paramétrique dans un test d'escalier pour la limite de fatigue 167
F.6 Chapitre 5 : Plan d'expérience optimal en escalier par échantillonnage bayésien à entropie maximale 169
F.7 Chapitre 6 : Conclusion et perspectives 170

Bibliography **173**

List of Figures

1.1 S-N curve illustration 3
1.2 S-N curve and the fatigue limit 4
1.3 Distribution representing the probabilistic nature of the fatigue tests . . 5
1.4 Stress-strain relationship 7
1.5 Typical plot of strain amplitude versus cycles to failure 8
1.6 S-N curve and the staircase test 9
1.7 Effect of the increment on the standard deviation estimation [38] 12
1.8 Framework of this study 15

2.1 Geometry and dimension of the symmetrical specimen (Unit: mm) 21
2.2 The finite element model of the specimen and measurement points 22
2.3 The first four mode shapes of the specimen. (The colors correspond to the normalized displacement. Red is the maximum) 22
2.4 FRF of strain response 23
2.5 Schematic of the testing setup 24
2.6 Pictures of test machine 24
2.7 Dimension of strain gauge (HBM 1-LM11-1.5/350GE) 25
2.8 FRF of the strain and the velocity to the base acceleration 27
2.9 Strain and velocity vs. the acceleration level 28
2.10 Schema of the change of the bench instrumentation 29
2.11 Sine Resonance Track-and-Dwell (SRTD) test with strain control 30
2.12 Test control and condition system for SRTD test 31
2.13 Fatigue test procedure with strain control 31
2.14 Crack length versus resonant frequency decrease of (a) 2% (b) 5% and (c) 8% 34
2.15 Comparison of sine sweep test with acceleration control and strain control 35
2.16 Comparison of SRTD test with acceleration control or strain control . . . 36
2.17 Landscape of the fracture surface 38
2.18 Direct observation of fracture surface by SEM 39
2.19 Experimental data and the related Basquin curve with strain control . . 41
2.20 Staircase test procedure 43
2.21 Up–and–down diagram for DC01 steel specimens 44

2.22 Frequency decrease and strain amplitude during SRTD test. The failure curves correspond to failed specimen ordinal i 45
2.23 The acceleration and velocity in same strain level(1380 µm/m) 46
2.24 Resonant frequency decrease progress of No. 22 specimen 47
2.25 Comparison about cracks and Change of Resonant Frequency (CRF) . . 49
2.26 PDF estimated from DM method 50
2.27 CDF estimated from DM method 51
2.28 The CDF of C20 steel [90] 53
2.29 A S–N curve of MCS 1018 steel [83] 53

3.1 PDFs of fatigue strain limits from Loo re-sampling 58
3.2 Uncertainty factor of the median for different values of M and N 61
3.3 Uncertainty factor of the standard deviation for different values of M and N 61
3.4 PDF of bootstrap resampling based on the experimental data 62
3.5 Median and standard deviation from the bootstrap resampling 62
3.6 Shape of the specimen with the same reduced section (Unit: mm) 63
3.7 Up–and–down diagram for specimen S1 64
3.8 Up–and–down diagram for specimen S2L 65
3.9 Fatigue limit PDFs obtained for the three kinds of specimens 65
3.10 Fatigue limit CDFs obtained for the three kinds of specimens 66
3.11 Bootstrap sampling applied to the three kinds of specimens 67
3.12 Distributions of median from the bootstrap results of S1, S2, and S2L . . 67
3.13 Distributions of standard deviation from the bootstrap results of S1, S2, and S2L 68

4.1 Estimated PDF from different bandwidths (SC: Scott; SI : Silverman; SJ: Sheather-Jones) 78
4.2 Estimated PDF from different bandwidths 79
4.3 Simulation procedure and evaluation for results 81
4.4 Normalised (a) median value and (b) standard deviation estimated with Kernel Density Estimation (KDE) for different bandwidth selectors and varying number of specimens 85
4.5 Normalised (a) median value and (b) standard deviation estimated with KDE for different bandwidth selectors and varying normalised step sizes 86
4.6 Distributions of median obtained from simulation for varying numbers of specimens for (a) $d = 1.0$ and (b) $d = 1.5$ normalised 87
4.7 Distributions of median obtained from simulation for different normalised step sizes for (a) $n = 30$ and (b) $n = 100$ 87
4.8 Distributions of standard deviation obtained from simulation for varying numbers of specimens for (a) $d = 1.0$ and (b) $d = 1.5$ normalised 88

4.9 Distributions of standard deviation obtained from simulation for different normalised step sizes for (a) $n = 30$ and (b) $n = 20$ 89
4.10 Estimated standard deviation and the number of used piecewise equation 90
4.11 Distributions of standard deviation obtained from simulation with the Normal distribution and CV=0.0125 90
4.12 Distributions of standard deviation obtained from simulation with the Normal distribution and CV=0.05 91
4.13 Distributions of standard deviation obtained from simulation with Lognormal distribution and CV=0.025 92
4.14 Distributions of standard deviation obtained from simulation with Weibull distribution and CV=0.025 92
4.15 PDF of the fatigue limit 94
4.16 CDF of the fatigue limit 95

5.1 Utility function diagram 104
5.2 Workflow of the Bayesian staircase procedure 105
5.3 Up-and-down diagram of a simulated Bayesian staircase 106
5.5 Posterior of the Bayesian staircase 106
5.4 Shannon entropy of the Bayesian staircase 107
5.6 An example of LHS 108
5.7 Workflow of the Bayes-LHS staircase procedure 109
5.8 Up-and-down diagram of a simulated Bayes-LHS staircase test 111
5.9 Posterior and estimation of a Bayes-LHS staircase test 112
5.10 Shannon entropy of a Bayes-LHS staircase test 112
5.11 Simulation procedure and evaluation of the results 113
5.12 Decrease of the Shannon entropy in case of $n = 30$ 114
5.13 Normalised (a) median value and (b) standard deviation with the different median ranges 115
5.14 Normalised (a) median value and (b) standard deviation with the different standard deviation ranges 115
5.15 Normalised (a) median value and (b) standard deviation with respect to the number of specimens 116
5.16 Normalised (a) median value and (b) standard deviation with respect to the number of specimens 117
5.17 Normalised (a) median value and (b) standard deviation with respect to step size in conventional staircase method 118

6.1 Decrease of strain mean value from Ti-6Al-4V specimens 123

A.1 Finite element model of the specimen 125

A.2 A sketch of the clamp in the shaker [76] 126
A.3 Deformed shape and contact pressure of the clamp [76] 126
A.4 Representation of the clamp in finite element model 127
A.5 The modals of the specimen with thickness 2mm 128
A.6 FRF of strain 129
A.7 Harmonic analysis and experiment result 129
A.8 Strain distribution for the first mode 131
A.9 Two positions for strain gauge 131
A.10 Stress gradient evolution from the center to the edge (orange line in Fig. A.9) 132
A.11 Comparison between the response in the specimen center and on edge obtained by experimental tests 133
A.12 Velocity response in specimen center and on the edge of the notch 133

C.1 Distributions of the median from DM - Number of specimens 142
C.2 Distributions of the median from DM - Normalised step size 142
C.3 Distributions of standard deviation from DM (corrections) - Number of specimens 143
C.4 Distributions of standard deviation from DM (corrections) - Normalised step size 143

D.1 Left and right censored data distribution and likelihood 146
D.2 Comparison of estimated PDF from MLE and MLE with censored data . 147
D.3 An example of likelihood function optimization 148
D.4 Distributions of median from MLE (Normal) - Number of specimens . . 149
D.5 Distributions of median from MLE (Normal)- Normalised step size . . . 149
D.6 Distributions of standard deviation from MLE (Normal) - Number of specimens 150
D.7 Distributions of standard deviation from MLE (Normal) - Normalised step size 150
D.8 Distributions of standard deviation from MLE (Lognarmal) 151
D.9 Distributions of standard deviation from MLE (Weibull) 151

E.1 Normal distribution test 154
E.2 Lognormal distribution test 156
E.3 Weibull distribution test 157

F.1 Courbe S-N et test de l'escalier 163
F.2 Diagramme up–and–down pour les échantillons d'acier DC01 165

List of Tables

1.1 Comparison of test protocols for fatigue limit distribution 6
1.2 Summary of staircase test and fatigue limit characteristics 14

2.1 Difference of fatigue test machines 18
2.2 Mechanical properties of the low carbon steel DC01 21
2.3 Chemical composition of the steel DC01 material 21
2.4 Configurations of the shaker 25
2.5 The selected specimens for fractography analysis 38
2.6 Empirical Coefficients $b_i(i = 1, 2, 3, 4)$ for K_{owen} 41
2.7 Empirical Coefficients $c_i(i = 1, 2, 3)$ for K_{owen} 41
2.8 The experimental parameters used in staircase test 42
2.9 The result data of specimens with thickness 2mm 48
2.10 Fatigue limit values with specified P–C levels 52
2.11 Comparison of fatigue limits of carbon steel 52

3.1 Effect of dimensions on the resonant frequency 63
3.2 Comparison of median and standard deviation (with DM) 66

4.1 Overview of existing evaluation techniques for staircase testing 72
4.2 The coefficients used in the correction equation (Eq. 4.13) 80
4.3 Parameters in simulation work 82
4.4 J-S divergence with different α parameter ($\times 10^{-2}$) 84
4.5 The J-S divergence of all the methods investigated in the study cases with d=1.0 and n=30 93
4.6 The median and standard deviation from different estimation 94

5.1 Different input parameters 115

6.1 Different treatments for Ti-6Al-4V specimens used in Fig. 6.1 123

A.1 The first resonant frequencies estimated for several boundary conditions . 127

B.1 Effect of dimensions on the resonant frequency 135
B.2 The specimen, test data and test results from staircase test of specimen S1 136
B.3 The specimen, test data and test results from staircase test of specimen S2L137

C.1 Constants used in standard deviation correction (Eq. C.6) 141

Glossaries

C : confidence level

E : Young's modulus

H : Shannon entropy

I : Shannon information

K_f : fatigue notch factor

K_t : stress concentration factor

M : number of resampling replications

N : the number of specimens in a single sampling

N_L : number of cycles fixed for defining fatigue limit

N_f : fatigue life (number of cycles to failure)

P : probability

P_f : probability of failure

S_a : load amplitude in staircase test

S_e : endurance limit (MPa)

S_f : fatigue limit (MPa)

$S_{a,0}$: lowest stress level in staircase test (MPa)

U : utility function

$\boldsymbol{\theta}$: distribution model parameters

δ_m : uncertainty factor of median

δ_s : uncertainty factor of standard deviation

σ_f : fatigue strength coefficient

σ_u : ultimate strength

σ_y : yield strength

σ_{max} : maximum stress value

σ_{min} : minimum stress value

ε : strain (μm/m)

ε_f : fatigue ductility coefficient

d : step size in staircase test

fr : resonant frequency (Hz)

h : KDE bandwidth

i : ordinal number of specimens

j : ordinal number of load levels

m : median value of samples

n : total number of specimens or sample size in staircase test

$n_{f,j}$: number of failures at load level j

$n_{s,j}$: number of survivals at load level j

s : standard deviation of samples

Abbreviations

BMES Bayesian Maximum Entropy Sampling

CDF Cumulative Density Function

CRF Change of Resonant Frequency

DM Dixon-Mood

DOF Degree Of Freedom

EDM Electrical Discharge Machine

FEA Finite Element Analysis

FEM Finite Element Method

FRF Frequency Response Function

HCF High Cycle Fatigue

KDE Kernel Density Estimation

LCF Low Cycle Fatigue

LHS Latin Hypercube Sampling

LMN Laboratory of Mechanics of Normandy

Loo Leave-one-out

Loocv Leave-one-out cross-validation

MCS Monte-Carlo Simulation

MLE Maximum Likelihood Estimation

MSE Mean Square Error

PDF Probability Density Function

SCF Stress Concentration Factor

SEM Scanning Electron Microscopy

SRTD Sine Resonance Track-and-Dwell

VHCF Very High Cycle Fatigue

Chapter 1
Introduction

While selecting a material for design, it is crucial to know its operating conditions. Under cyclic loading conditions, the fatigue limit or endurance limit is generally required to delimit the operating range under High Cycle Fatigue (HCF).

In this chapter, the preliminary background information on fatigue is given in order to understand the objective of the thesis work concerning the notion of fatigue limit. Section 1.1.1 introduces the fatigue properties of a material and the corresponding intrinsic variabilities leading to an estimate of the probabilistic distribution of the fatigue limit. The experimental tests being carried out in strain, Section 1.1.2 introduce the strain-stress linear relationship to provide a simple link between strain and stress in HCF. Section 1.2.1 describes the staircase methods used to estimate the fatigue limit, which is the object of this thesis. Section 1.2.2 examines the sensitivity of the staircase parameters based on the literature studies and analyses the advantages and disadvantages of the staircase method. The final section summarises the framework of the PhD study.

1.1. Fatigue and fatigue limit

As mechanical structures move toward lightweight and complexity, fatigue design becomes more and more critical. Fatigue is the leading cause of failure for mechanical components and structures. It has been estimated that fatigue causes 90% of all service failures of metal parts [1]. It is a progressive and localised structural damage that occurs when a material is subjected to cyclic loading. Damage in metallic materials involves the initiation - commonly considered from the material's surface - and propagation of cracks by the action of the cyclic loads. The cyclic action may eventually cause the mechanical part to fail even at low load levels (below the yield stress of the material). Fatigue failure can be divided into different forms, including thermal fatigue failure, corrosion fatigue failure and vibration fatigue failure. Vibration fatigue generally refers to fatigue failure and the process of structures under a vibration environment. In recent years, many engineering structures must be serviced in a severe vibration environment [2], resulting in increased structural fatigue. For example, the Airbus 330 aircraft encountered engine vibration spiked up in 2011 [3], in which the fuel pump supply line cracked due to high vibrations. In general, vibration fatigue resistance is an essential criterion for structural design for engineering structures working in a vibrating environment.

Fatigue properties are primarily associated with the S-N curve and endurance limit [4]. For some ferrous (iron-based) and titanium alloys, there is a threshold called endurance limit under which no fatigue failure occurs after an infinite number of repeated load cycles. For other materials (non-ferrous), this threshold does not exist, and it is therefore necessary to define a limit for a specific number of cycles. The evaluation of this fatigue limit is the purpose of the study. In practice, this parameter is hard to be determined accurately and normally it is considered as the fatigue strength which display at typically $1 \times 10^6 - 1 \times 10^7$ load cycles [5, 6, 7, 8, 9]. It must be identified by experimental fatigue tests using approaches such as staircase methods.

1.1.1. Fatigue properties

The fatigue properties can be defined from the S-N curve (Stress amplitude-Number of cycles to failure) as shown in Fig. 1.1. The S-N curve, also known as the Wöhler diagram, represents the fatigue property of a material, which is the most conventional design basis for fatigue analysis and is still used in engineering today.

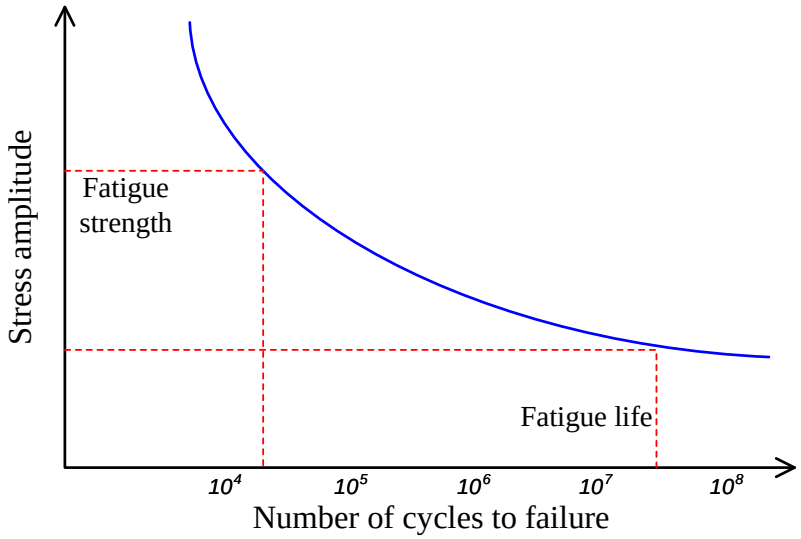

Figure 1.1: S-N curve illustration

The constant amplitude fatigue test was first initialled by Wöhler on railway axles in the 1850s. In general, the classical S-N curve illustrates only a uniaxial load. Fig. 1.2 illustrates the relationship between S-N curve and fatigue limit. High Cycle Fatigue (HCF) occurs at relatively large numbers of cycles (above 1×10^4 cycles) is mainly due to elastic strain under stress amplitudes without obvious macroscopic plastic deformation (below the yield strength σ_y). Typical examples of HCF are pistons, crankshafts, connecting rods or gas turbine engines and components subject to vibratory excitation (e.g. induced by airflow on airfoils or swell on offshore structures). It is usually expressed by the S-N curve, where the amplitude of cyclic stress is plotted versus the logarithmic scale of the number of cycles the specimen can sustain before failure. The fatigue test in Very High Cycle Fatigue (VHCF) - corresponding to fatigue life region beyond 10^7 cycles - leads to a long test time, and the failure mechanism in VHCF can be quite different from that in Low Cycle Fatigue (LCF) and HCF [10].

In the Fig. 1.2, S-N curve becomes horizontal at a higher number of cycles, which means that when the applied alternating stress is lower than the stress corresponding to the horizontal line, the structure can withstand an infinite number of stress cycles without fatigue fracture. The stress value corresponding to the horizontal line represents the endurance limit of the material [11]. The endurance is not easy to obtain with experimental tests because it is time-consuming even if relatively high frequency is used. So in this study, a fatigue limit is sought with a staircase approach below 1×10^7 cycles.

From the view of engineering, the endurance limit and the fatigue limit are often confused and considered similar. However, the endurance limit is the constant stress amplitude corresponding to the asymptotic value [9]. In some cases, the fatigue limit is chosen at a specific large number of cycles (e.g., 1×10^6 cycles) to reduce the testing

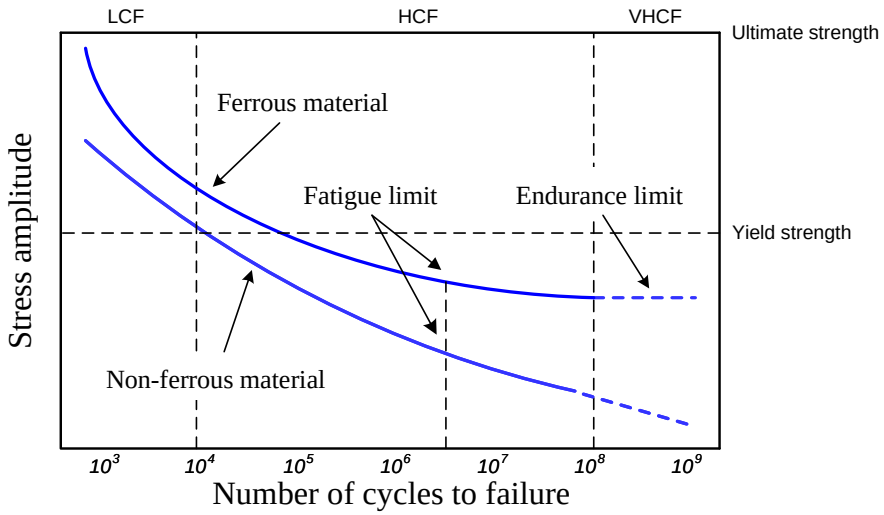

Figure 1.2: S-N curve and the fatigue limit

time or to depend on the structural design. Both parameters are important material properties for various engineering predictions on fatigue [12], in particular, to apply the mean stress correction through Goodman's method, for example [13]. In this dissertation the fatigue limit is defined: fatigue strength (stress amplitude) for a given number of cycles targeted 1 million from the S-N curve [4, 9, 14, 15].

In body-centred cubic materials (bcc, such as steel and titanium), a pronounced fatigue resistance can often be determined (endurance limit). In contrary, face-centred cubic materials (fcc, such as aluminium and copper) do not have a specific limit and will eventually fail even from small stress amplitudes, the S-N curve drops over the entire load cycle range for these materials [16]. Therefore, engineers try to design their parts to keep them under the fatigue limit during work.

However, the fatigue limit assessment has never been an easy task, as fatigue has considerable dispersion due to variability in the fracture process [17, 18] and uncontrolled test conditions in a rigorous manner, which is independent of the experimenter.

Pascual et al. [19] established a random fatigue limit model to describe the variability increment in fatigue life around the fatigue limit. As a result of inherent variation in fatigue data [20], the S-N curve and the fatigue limit must be drawn on the distribution. Most approaches evaluate the fatigue limit in the form of a distribution (Cumulative Density Function (CDF) or Probability Density Function (PDF)) to estimate a mean or median value of the fatigue limit but also a variance or standard deviation to give a measure of its variability. The distribution is also used to estimate the probability of failure or success of an experiment repeated several times. The median S-N curve and its dispersion (dotted curves) are schematically represented in Fig. 1.3. During real fatigue tests, the probabilistic fatigue limit performed at the given number of cycles (N_L) [21], which is restricted to the HCF region.

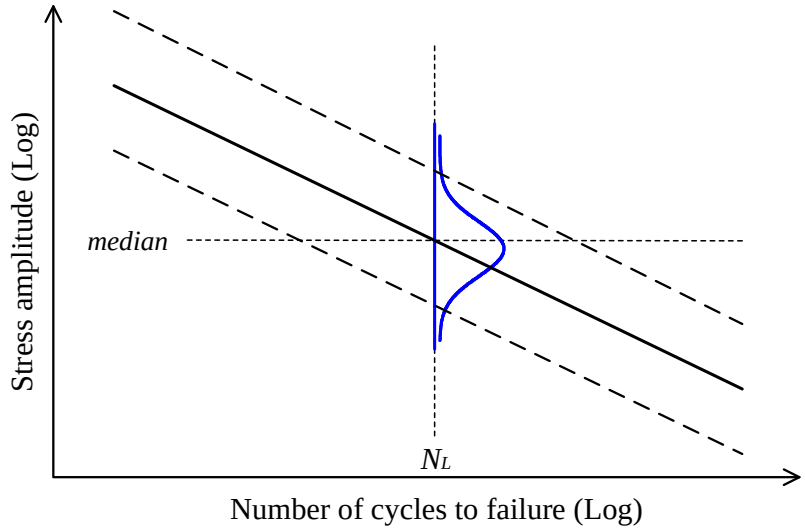

Figure 1.3: Distribution representing the probabilistic nature of the fatigue tests

In numerical design, the fatigue limits obtained from uniaxial tests (in torsion, bending or tension) are essential in evaluating fatigue strength when the structure is subjected to multiaxial loads. The stress-based criteria is expressed as inequality between the equivalent shear stress and a function of the fatigue limits. When the structure is submitted to random loads, the function of the fatigue limits, which is expressed as a probability distribution, can be used in a reliability study. Thus, Lambert et al. [22] proposed a probabilistic model from the Sines criterion using the extreme value theory to determine the equivalent shear stress distribution. The fatigue limit function can be obtained from experimental tests to complete the evaluation by the constraints-resistance approach. This work is in line with this objective because it is not easy to reach these distributions owing to the requirements of testing time and a large number of specimens.

The methods of obtaining the fatigue limit can be classified as follows:

(1) Probabilistic modelling of S-N curves. The statistical fatigue limits are derived from the probabilistic curves. However, this method is inaccurate because the data are distributed in the whole S-N curve rather than around the fatigue limit.

(2) Numerical methods. Firstly, Ray-projection and Parallel-projection methods [23]. These two methods extrapolate the HCF property from LCF test data to avoid long-time tests. Lin [23] proved the parallel-projection method provided reasonable results for fatigue limit distribution. However, this method gradually lost its advantage with the development of HCF test equipment. Secondly, Monte-Carlo simulation (MCS) method [24] aims to generate several fatigue limit values with different probabilities and confidence values from one reference fatigue limit according to a specific distribution. Thirdly, many researches [4, 9, 14, 25]

have proposed a fatigue limit prediction model considering the notch or defect in the structure. The numerical methods are based on previous fatigue information rather than a direct measurement.

(3) Experimental testing. In fact, the fatigue limits deduced from random fatigue performance should be verified by true test data. The experimental fatigue test is the main tool for assessing the fatigue limit of a material [26]. Several experimental evaluation test strategies have been proposed in the literature, mainly including staircase method [27], step stress method [28], locati method [29], prot method [30], probit method [31]. These methods are compared in Tab. 1.1. In addition, an experimental thermal method [32] can be used to measure the temperature change during the fatigue process to reach the limit. However, this method requires infrared thermography.

Table 1.1: Comparison of test protocols for fatigue limit distribution

Method	Number of specimens	Stress amplitude	Evaluation	Remarks
Staircase	multi	one stress per sample	distribution	- most widely used
Step stress	multi	multi stresses per sample	distribution	- much more test times than staircase
Probit	multi	one stress per sample	distribution	- much more test specimens than staircase
Locati	single	multi stresses per sample	mean value	- accelerated test time - need prior fatigue parameter (e.g. the slope of the S-N curve)
Prot	multi	multi stresses per sample	mean value	- statistical efficiency is less than that of probit and staircase methods [33]

Despite its drawbacks (mentioned in Section 1.2.2), many studies try to improve the estimation of the probabilistic fatigue limit by staircase methods. This method has advantages in both experiments (less number of specimens and less test time) and statistics (more efficient). This work, therefore, is focused on the staircase test method presented in Section 1.2.

1.1.2. Strain-stress relationship in HCF

High Cycle Fatigue (HCF) is a type of fatigue caused by small elastic strains under a high number of load cycles before failure occurs. The stress comes from a combination of mean and alternating stresses. Let us consider the case of a proportional load with constant amplitude calculated from the minimum and maximum stress values of

σ_{min} and σ_{max}:

$$\begin{array}{ll} \text{stress range} & \Delta\sigma = \sigma_{max} - \sigma_{min} \\ \text{mean stress} & \sigma_m = \frac{\sigma_{max}+\sigma_{min}}{2} \\ \text{stress amplitude} & \sigma_a = \frac{\Delta\sigma}{2} \\ \text{stress ratio} & R = \frac{\sigma_{min}}{\sigma_{max}} \end{array} \tag{1.1}$$

A power formula relating stress amplitude with the number of cycles, proposed by Basquin in the 1910s [34], is expressed as:

$$\sigma_a = C_1 \times N_f^{C_2} \tag{1.2}$$

where, C_1 and C_2 are constant related with material; σ_a is the stress amplitude and N_f is number of cycles to failure.

The S-N curve and the models for describing HCF are widely used to the present day. Nevertheless, strain-based formulations are required in this study to consider the measurement means used during the tests (strain gauges, for example). When a deformable solid (material) is subjected to a uniaxial loading state with a fully reversed cyclic stress (or strain) loading in the linearly elastic strain range, the stress and strain correlate linearly with Young's modulus E. For example, the Fig. 1.4 illustrates cyclic strain $\varepsilon(t)$ as a function of cyclic stress $\sigma(t)$. It is evident that the strain cycle (0-1-2-...-11-12) is the same as the stress cycle (0-1-2-...-11-12), and the stress-strain curve can be simplified as a straight line in the elastic domain.

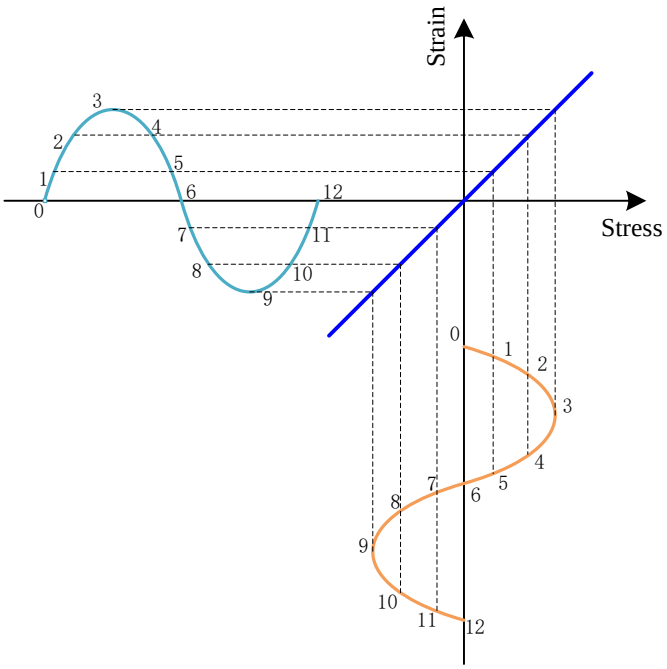

Figure 1.4: Stress-strain relationship

The fatigue limit lies in the high cycle fatigue domain, so the linear relationship between strain and stress is also valid. Thus, the specimens subjected to a load close to the fatigue limit have an elastic behaviour. Therefore it can be assumed that the specimens follow the general Hooke's law:

$$\sigma_{ij} = C_{ijkl}\varepsilon_{kl} \tag{1.3}$$

where σ_{ij} and ε_{kl} are the engineering stress and strain, respectively. C_{ijkl} is the elasticity tensor that depends only on the material. The fatigue Stress Concentration Factor (SCF) can be included in the analysis by multiplying the stress calculated in Eq. 1.3 by K_f given in Appendix A.2.3.

Fig. 1.5 shows a typical $log - log$ plot of strain amplitude versus the number of cycles to failure.

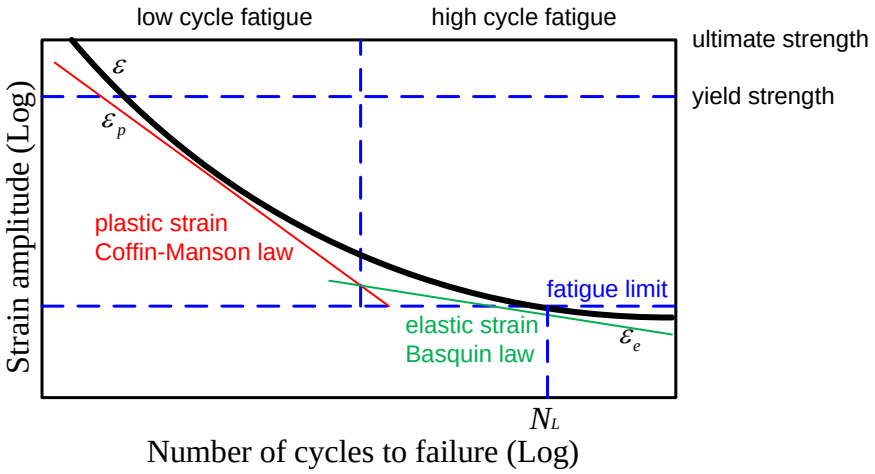

Figure 1.5: Typical plot of strain amplitude versus cycles to failure

The total strain (ε) can be considered as the sum of elastic strain (ε_e) and plastic strain (ε_p). The total strain occupies the main part in LCF while the plastic strain occupies the main part in HCF. Therefore, the strain-number of cycles to failure ($\varepsilon - N$) curve can be divided into two parts according to elastic strain and plastic strains. The plastic strain can be expressed by the Manson-Coffin law:

$$\varepsilon_p = \varepsilon_f \times N_f^c \tag{1.4}$$

where ε_f and c are fatigue ductility coefficient and the constant, respectively. The Basquin's law (given in stress in Eq. 1.2) also can be used to express the elastic strain as follows:

$$\varepsilon_e = \frac{\sigma_f}{E} \times N_f^b \tag{1.5}$$

where σ_f and b are the fatigue strength coefficient and a constant obtained from the slope of the log-log S-N curve, respectively.

Since the stress in HCF tests is usually within the elastic range, the present work focuses on the fatigue limit by considering only elastic strain under small deformation. If we focus on the range within fatigue limit, $\varepsilon_p = 0$ and $\varepsilon = \varepsilon_e$. Thus, the strain and stress have a linear relationship with Young's Modulus E. It can be concluded that stress control and strain control around the fatigue limit range can reach the same results when the same test conditions are considered. This strong assumption is important for this work because it provides us to use strain control in Chapter 2 to evaluate the fatigue limit.

1.2. Staircase test

The fatigue properties of materials can be appraised on statistical grounds. The fatigue limit used in the design must be fully characterized by its statistical nature. The probability fatigue limit can be deduced from probabilistic S-N curve. Tests are specially conducted to characterize fatigue limit distribution.

The specimens are tested at various stress levels, and the corresponding number of cycles (fatigue life) is evaluated. The experimental results are usually prepared as Fig. 1.6.

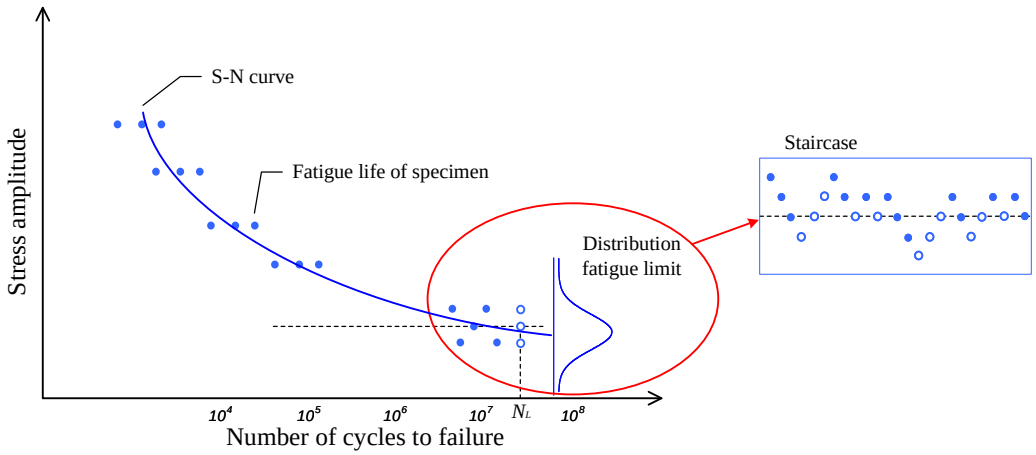

Figure 1.6: S-N curve and the staircase test

As the Fig. 1.6 shows, it is natural that the fatigue limit is deduced from S-N curve. The S-N curve can obtain a fatigue limit value but cannot provide a statistical distribution. Considering that the fatigue limit can be seen as a random value, the staircase method [27] is much more suitable for the fatigue limit estimation accuracy.

1.2.1. Staircase test protocol

Dixon and Mood [27] proposed the classical method for sensitivity tests in 1948, which is the staircase method. This method is widely used in machinery, medical, pyrotechnics, etc. Both standard ISO12107 [35] and the standard MIL-STD-331D [36] recommend this test procedure for experimental test.

As the staircase procedure, fatigue tests are carried out sequentially on specimens subjected to a constant amplitude stress cycle until a predetermined number of cycles N_L. The first specimen is tested at an initial load amplitude selected arbitrarily. Suppose the specimen "survival" (runout) until N_L cycles. The load amplitude applied to the next specimen is increased by a step size d. Conversely, the specimen is marked as "failure", and the load amplitude for the next specimen will be decreased by a step size d. The step size is usually constant during the entire experiment process. This procedure is repeated in sequence, with load levels being increased and decreased in increments until the number of specimens is reached. Therefore, the staircase approach provides a reasonable estimate of the median fatigue limit because about half of the specimens fail and the others do not [37].

Let n be the sample size of a staircase experiment, and the specimens that to be tested are denoted as random variables $X = [x_1, x_2, \ldots, x_i, \ldots, x_n]$. The X are chosen from a discrete and finite set of stress amplitude S_a, $S_a = [S_{a,1}, S_{a,2}, \ldots, S_{a,j}, \ldots, S_{a,j_{max}}]$. The S_a is discrete by step size d. After a specimen is tested in $x_i = S_{a,j}$, the next specimen must be treated one load level up or down as the current specimen. The responses of each specimen are denoted as the "0" survival and "1" failure. Repeating the same staircase rules turns a finite set of stress levels into random variables.

The staircase test methodology was extensively used to evaluate fatigue limit distribution due to its three outstanding features. Firstly, by its very nature, the staircase test tends to concentrate data near the median, leading to a high accuracy estimation of the median. Secondly, the staircase sequence design can result in "30 %to 40%" savings in the number of specimens compared with creating a whole S-N curve. Thirdly, it is the relative simplicity of the statistical analysis of staircase data.

However, the staircase method is not always working well because the standard deviation estimation is greatly affected by step size in the staircase method, which must be constant during the test, and leads to low standard deviation estimation accuracy. With this drawback, some simulation studies have shown that deviation bias is a function of both step size (d) and sample size (n) in staircase testing [38]. The staircase method cannot eliminate or avoid this problem. However, it can minimize the error of the standard deviation estimation value in optimizing the experimental design [39], improving the data processing [40] and creating the correct coefficient[38]. The detailed background are presented in Section 4.1 and Section 5.1.

1.2.2. Staircase parameters

Four parameters are input for the staircase method, including initial stress, stress step, number of specimens and the predetermined number of cycles.

(1) Initial stress ($S_{a,0}$)

Generally, the engineer could make a qualified guess about the expected fatigue limit based on the experience with the mechanical properties of the material that are derivatives from the literature and previous tests. Despite the fact that the engineer's experience with a particular component and the results from estimations may differ, it is indispensable to select the initial level. Some research [41] have studied the effect of initial stress on the staircase outcomes. Usually, the starting stress level should preferably be taken as close to the mean threshold stress as possible [42]. The initial level, which is a highly realistic boundary condition, is integrated into the simulation model. Roué et al. [39] choose a "median-$3/2d$" as an initial value in the simulation study to reduce the number of specimens to approach the median fatigue limit. Müller et al. [40] firstly proposed a function for choosing an initial level underlying the Lognormal distribution.

(2) Step size (d)

Step size is a significant parameter in the staircase method. The first reason is that if the value of the step is too small, there will be continuous survivals or failures, resulting in wasted specimen and time. Conversely, if the interval value is too large, the estimated standard deviation will be much more significant. In the conventional staircase method, the increment must be constant in one test. The other more crucial reason is that increments greatly influence standard deviation estimation.

In many researches, the increment was selected as a proper integer value without deliberate research such as 5 MPa, 10 MPa or 20 MPa.

A number of studies investigated the parameters in the staircase method. In the assumptions of Dixon-Mood, the increment should keep constant in every stress level, and the increment should be in the range of $0.5s-2s$ [27], where s donate the standard deviation of fatigue limit. Yoshimoto [43] recommended that the step size should be as close to the standard deviation of fatigue limit as possible in a small sample size test and applied linear regression analysis of the experimental $S-logN$ curve to find a "standard deviation". "5% criterion" [42] is a consensus and an engineering experience. When the fatigue strength determined by the conventional fatigue test method is known, the fatigue strength within 5% can be taken as the increment. However, this assumption relies on the constant increment being less than twice the actual standard deviation of the tested population. Grove [44] assumed that it is more robust to the choice of the increment in the range $s-2s$, where s is the standard deviation of the log-stresses. Pollak et al. [38] for a range of increment (Fig. 1.7) and

found that using larger step sizes in the $1.6s - 1.75s$ range can significantly reduce estimation bias. Çalişkan et al. [45] advised to use stress increment around $0.5s - 1.5s$.

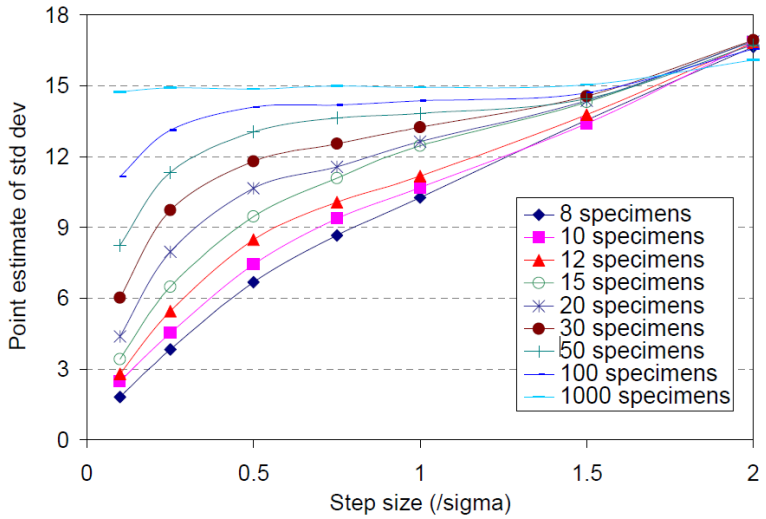

Figure 1.7: Effect of the increment on the standard deviation estimation [38]

So, the standard deviation is required prior to the test to determine the increment. Standard deviation is available from another testing of the material or similar material to provide a rough initial estimate of standard deviation.

(3) Number of specimens (n)

In the early research, the sample size of the staircase test should be large enough (40-50 specimens) for the staircase method. In recent years, staircase tests normally consist of 10-30 specimens. Pollak et al. [38] found that the method is robust for sample numbers as small as 5–10 specimens. We believe that too many samples will consume much test time and money, while too few samples do not yield accurate results and affect the subsequent probabilistic analysis. This observation is supported by the study of Roué et al. [39], which proved that a small sample size would greatly reduce the confidence of fatigue limit. Logically, the uncertainties decrease when the number of specimens increases for the same distribution (same fatigue test). ISO 12107 [35] and Strzelecki's research [46] demand that at least 15 specimens to estimate the mean and the standard deviation for exploratory research. Generally, the sample size is small, for example, less than 20.

The nominal sample size is used in both simulation and experimental studies to reduce the effect of starting load level. The nominal sample size [37, 47] is the number of specimens after and including the first pair of tests with opposite results. The number of specimens in this study (n) donates the nominal sample size.

(4) Number of cycles (N_L)

In practice experiment, it is hard to reach an infinite number of load cycles, and the

fatigue limit normally is considered as the fatigue strength which displays at typically 1×10^6 or 1×10^7 load cycles [5, 6, 7, 8]. In this study, we have chosen 1×10^6 cycles for defining the fatigue limit.

In the literature, fatigue limit tests based on the staircase method in recent years are summarized in Tab. 1.2.

In Tab. 1.2, m is the median (equal to mean in Normal distribution), s is the standard deviation, N_L is fatigue life for defining the staircase test method, and n is the number of specimens. The number of specimens is less than 30 in most studies. All tests were conducted considering stress levels, and results were calculated by the classical Dixon-Mood (DM) method (which is described in [27]) for Normal distribution unless otherwise specified.

In summary, the staircase methods have four outstanding features: (1) The simple protocol is the most obvious superiority. Each specimen was tested at given stress for a specified number of cycles or until failure, and only adjusted stress load for the different specimens. (2) This method tends to concentrate data near the median by its nature [37]. (3) In the following, the staircase method requires fewer tests. Compared with the Probit methods (See Tab. 1.1), it saves the tested number of specimens 30%-40% [27]. (4) Thanks to Dixon and Mood's research [27], there is the relative simplicity of the basic statistical analysis of staircase data.

However, the staircase method has three defects: (1) The staircase method test does not have mathematical optimization characteristics, and the accuracy of the estimation under the same sample size remains to be further increased, or the sample size needs to be further reduced under the same estimation accuracy. (2) The stress step size d should be estimated before the staircase test. If the step size is too large, the probability of generating invalid test data increases, increasing the test uncertainty. (3) The standard deviation estimation is systematically less accurate and lower than the true value. Therefore, this study carried out the experimental fatigue test by staircase method and improved it in terms of post-processing and test strategy.

Table 1.2: Summary of staircase test and fatigue limit characteristics

Materiel	N_L	Stress range (MPa)	d (MPa)	n	Statistical	Estimation	Ref
Lthium disilicate glass-ceramic	2.5×10^5	790-940N	50N	15	DM	m= 879.28	[48]
EN-GJS 700 ductile cast iron	2×10^6	190-230	18.88	7	DM	m= 210.90 s= 10.01	[49]
SAE 4340 steel	1×10^7	306.8-320.6	3.45	54	DM	m= 319.02 s= 20.03	[50]
Ti-6Al-4V	1×10^7	460-590	25	27	DM	m= 540 s= 60	[51]
Alloy A319 (120℃)	1×10^8	68.5-82.8	2.8	26	MLE (censoring)	m= 75 s= 4.2	[52]
Nodular cast iron	-	177.3-323.1	18.3	25	MLE (censoring)	m= 195.5 s= 17.6	[41]
Stainless steel	1×10^8	205-225	5	22	DM	m= 3.070 s= 3.2e-3	[47]
C45 steel	5×10^6	288-318	6	20	DM	m= 310.3 s= 11.4	[46]
Ti-6Al-4V	1×10^9	400-440	20	18	DM	m= 406.36 s= 11.65	[38]
EA4T axle steel	-	345-370	5	17	DM	m= 356 s= 13.4596	[24]
35NCDV12 steel Non-chromium	5×10^6	388-529	47	15	DM	m= 393.875 s= 39.088	[53]
35NCDV12 steel Chromium	5×10^6	151-341	115	15	DM	m= 239.214 s= 50.35	[53]
ASTM A743 CA6NM steel	2×10^6	337-392	14	15	DM	m= 361.625 s= 11.589	[54]
CL65 steel	-	410-420	5	15	DM	m= 414.64 s= 2.65	[24]
LZ50 axle steel	-	255-285	10	14	DM	m= 267.14 s= 5.3	[24]
High strength steel 300 M	1×10^9	690-790	20	14	Null	m=723±22	[55]
Aluminum A7N01S-T4	1×10^7	125-140	5	12	MLE fit	Lognormal m= 2.129 s= 2.469e-2	[56]
Bogie cast steel	-	134-146	4	12	DM	m= 139.23 s= 3.2479	[47]
Aluminium 7075 T7531	1×10^7	187-208	7	11	DM	m= 189 s= 3.7	[57]

Normal distribution: m: median(mean) s: standard deviation

1.3. Summary

Fatigue characterization has been a research topic in mechanical structure design for decades. A brief review of the fatigue limit and staircase method is presented in this chapter. Section 1.1 introduces fatigue limit - with its variability property - and describes the linear elasticity in the HCF test, which is the base of the strain control method proposed in this work. In Section 1.2, the staircase protocol and parameters sensitivity analysis are summarized. The studies below are carried out based on the advantages of the staircase method and aim to reduce the disadvantages.

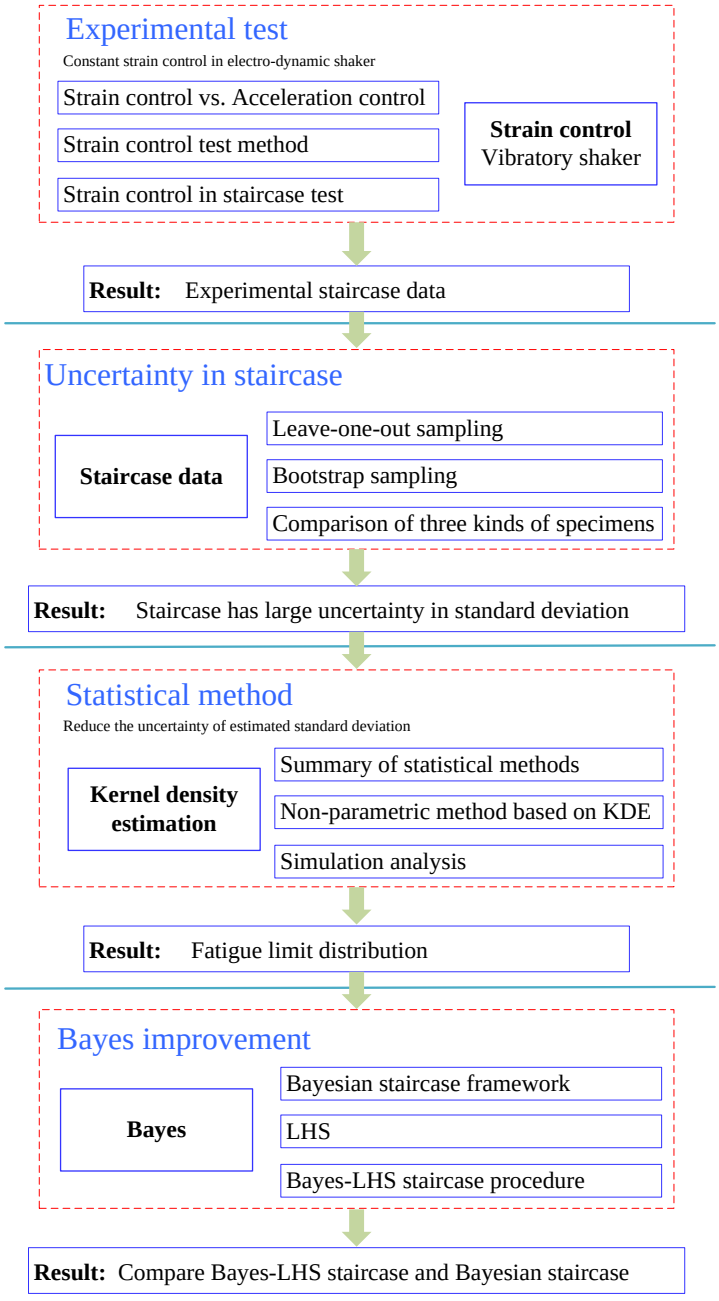

Figure 1.8: Framework of this study

The main contributions of this work are organized in 4 chapters as presented in Fig. 1.8:

Chapter 2 In this chapter, an experimental strain-based vibration control test method is introduced and conducted with an electro-dynamic shaker . This chapter details the use of a staircase test procedure on a vibration bending bench, including parameter selection and a fatigue limit estimation with the classical Dixon-Mood approach. The test results with the staircase method obtained in this chapter offer a dataset for uncertainty quantification and statistical study.

Chapter 3 The post-processing leads to one distribution after one staircase test. We want to evaluate the uncertainty from multi-staircase tests on the same experimental test system. Bootstrap is used to characterize the mean and standard deviation of the fatigue limit distribution from staircase data, as well as the uncertainty associated with the staircase test method. Using the bootstrap method, we also compared the fatigue limit distribution of the DC01 from different kinds of specimens.

Chapter 4 The use of different methods from the literature led us to investigate how to approach the statistical treatment to improve the standard deviation estimation of the fatigue limit distribution. We reached a new method based on Kernel Density Estimation, that we have detailed in this chapter. A simulation-based investigation is performed using several probability distributions with different coefficients of variation.

Chapter 5 In the logic of making improvements to the staircase methods, we chose to focus on the use of a test design process based on the Bayesian theorem. In an attempt to improve the results, we also proposed to include Latin Hypercube Sampling (LHS) regarding both the scientific consideration and the engineering requirement. The advantage of using the Bayesian theorem in the staircase method is that it eliminates the step size and makes the most of the previous test information to decide on the following test. LHS is also involved in preventing similar results from the same Bayesian Maximum Entropy Sampling (BMES). The results provide that the optimal staircase method has a faster convergence than the conventional staircase method.

This dissertation finally ends with general conclusion and perspective work.

Chapter 2
Experimental strain-based vibration control to obtain the fatigue limit by the staircase method

This chapter highlights the possibility of strain control with a vibration fatigue bench. The combination of a constant strain level and staircase methods provides a quick evaluation of the fatigue limit distribution.

Low carbon steel specimens with a reduced section were selected to carry out experimental tests. A staircase test procedure with a vibration bending bench is detailed in this work, including parameter selection. The results highlight the efficiency of the strain-controlled staircase method in reaching the fatigue limit.

Section 2.1 is a non-exhaustive overview of the fatigue test machines. Section 2.2 describes the specimen, the experimental vibratory bench and the instruments. Section 2.3 presents a methodology for strain control and a comparison with traditional acceleration control. Section 2.4 gives the validation for the experimental data and introduces the next chapter, which aims to provide improvements for the estimation of the statistical parameters of the fatigue limit distribution. This part has been published in an international journal [58].

2.1. Fatigue test machines and their control

As pointed out by Shawki [59], fatigue testing machines can be classified according to different criteria depending on the requirements. The method of load application is an essential criterion because it determines the amplitude of the applied force and the test duration. Usually, hydraulic machines are chosen for their ability to apply relatively high force amplitudes compared to machines using high frequencies to excite the components (such as electro-dynamic, electromagnetic, or ultrasonic systems). Other criteria are essential such as the type of loading (tension, bending, the combination of bending and torsion, ...) or the need to control by strain or stress.

There are three representative clusters of testing machines usually adopted to perform fatigue tests of structures: servo-hydraulic machine, electro-dynamic shaker, and ultrasonic testing system. The difference between these three machines is listed in Tab. 2.1.

Table 2.1: Difference of fatigue test machines

	Servo-hydraulic machine	Electro-dynamic shaker	Ultrasonic fatigue tester
Frequency	low ($\leqslant$30Hz)	high ($5-7000$Hz)	very high ($20-30$kHz)
Test time	long test time	large reduction of test time	large reduction of test time
Load	displacement or force	acceleration, velocity, displacement, force (with prestress)	displacement (strain)
Response	well-controlled	variations	well-controlled
Drawbacks	low frequency	indirect control	frequency effect thermal effect specific specimen

From Tab. 2.1, the main difference between these three kinds of testing systems is the working frequency range. In one way, the ultrasonic fatigue tester presents an excitation frequency of more than 20kHz and is mainly used for VHCF test. In another way, the load-controlled servo-hydraulic machine and electro-dynamic shaker are used in HCF tests. However, hydraulic machine may leads to a long time to achieve a large number of cycles around the fatigue limit due to the relatively low load frequency (20-50Hz). Whereas, electro-dynamic shaker has a significant advantage in saving the fatigue test time since they work on high load frequency. For example, it costs about 93 hours for 30 Hz in the servo-hydraulic machine to reach 1×10^7 cycles, while only 13 hours for 220 Hz in electro-dynamic shaker. Since testing such large numbers of cycles is time-consuming, it is desirable to accelerate the tests by electro-dynamic shaker to

reach a high number of cycles.

These systems offer different ways of applying the load. Hydraulic machine can directly perform fatigue testing in force (to control stress) or displacement (to control strain) on the structure. Electro-dynamic shaker is performed chiefly with base-excitation to obtain a large deflection of the structure with small input excitation. Furthermore, ultrasonic testing system control the displacement of the specimen through a piezoelectric actuator. The load application determines that the response of the servo-hydraulic machine and ultrasonic fatigue tester are well-controlled, but not for electro-dynamic shaker.

To sum up, the servo-hydraulic machine has reasonable constant load control but leads to a lengthy test duration. The electro-dynamic shaker has an advantage in reducing test time but has drawbacks in indirect control. The ultrasonic fatigue tester works in VHCF and must consider other problems like frequency effect and thermal effect in application [60].

The difficulty of using electro-dynamic shaker in the fatigue test lies in control. The shaker introduces the motion of the basement by controlling acceleration, velocity or displacement through a closed-loop system. However, the major drawback of base-excitation is that the stress or strain response is widely dispersed. Khalij et al. [61] used the base-excitation in acceleration to establish a fatigue diagram corresponding to the strain amplitude versus the number of cycles, which highlights the difficulty of controlling the strain amplitude levels for the same acceleration levels.

Several other works [62, 63] have proposed the development regarding the objection to keeping stress/strain steady for base-excitation of electro-dynamic shaker test systems. Among these, a simple approach is to use force as the input excitation. Hooreweder et al. [57] used an electro-shaker which directly controls the force through a stiff stinger at the free end of the specimen instead of base-excitation. However, force control requires a preload for the sensor and loses the advantage of resonant excitation with the shaker. Another typical approach is to use output sensors to calibrate the local stress (strain) in the fatigue zone. By measuring displacement, Xue et al. [55] focused on fatigue limit assessment and used an optical displacement sensor to measure displacement at the specimen free edge and then measure the applied stress. Morrissey et al. [51] performed the fatigue test by calibrating the displacement to give a feedback loop during testing to control the strain actively. Gautrelet et al. [64] used the linear relationship between the response in strain or velocity and the excitation in acceleration to calibrate the strain level of the fatigue zone. Kim [65] proposed a spectral damage prediction method based on acceleration response without any strain data, which is based on the spectral relationship between the energy of acceleration and fatigue damage. George et al. [66] used a laser sensor to measure the velocity of the specimen to calibrate to the maximum strain. Similarly, Ellyson et al. [67, 68]

used a closed-loop system to maintain a steady force and frequency of the base excitation, which is controlled against the displacement of a point on the sample. Česnik et al. [69] designed a closed-loop control system from two accelerometers as output-input based on a Y-shaped specimen to actually controll the stress in the fatigue zone, but no real-time was used. However, calibration to strain may be impossible if the sensor voltage exceeds the test software's limit in practice. Moreover, the relationship of output (displacement/velocity/acceleration) – strain/stress is susceptible not only to structure, such as dynamics characteristics, but also to other factors such as the material and the environmental temperature [65]. In brief, conventional experimental calibration measures strain rather than control of strain.

The literature dealing with the vibration-induced fatigue control method still focuses on indirectly controlling for stress/strain. Since the strain assessment depends on the frequency response magnitude, strain control is essential to reach the fatigue parameters.

In previous works, most fatigue tests were controlled by strain using the hydraulic machine. For example, the strain control fatigue test normally aims at stress-strain [70] and LCF behavior. A systematic study in this area is the work of strain–life curves. Procházka et al. [71] dealt with strain-controlled cyclic tests, the results of which enabled the construction of Manson-Coffin curves and assessment fatigue parameters. Williams [72] studied the development of accurate statistical strain–life curves, to predict LCF and HCF based on plastic strain and elastic strain. Carrion et al. [73] published the experimental data about the strain-controlled fatigue tests on TA6V at different strain ratios and various strain amplitudes.

In this study, we want to control strain in HCF vibration fatigue test. This section presents the difficulties encountered related to the use of a vibration system and the excitation at the resonant frequency of the specimen.

2.2. Experimental setup

2.2.1. Specimen design and material

For experiments, specimens were manufactured from plates using a wire electrical discharge machine (wire-cut EDM). A stress raiser zone was designed in the middle of the specimen to localize the crack far from the clamp. The quality level of the finished machining surface is better on the reduced section. More details about the specimen dimensions are shown in Fig. 2.1.

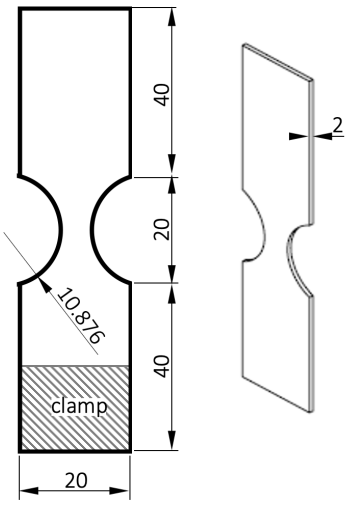

Figure 2.1: Geometry and dimension of the symmetrical specimen (Unit: mm)

The low carbon steel DC01 (EN 10130) [74] plate without heat-treatment is considered for the study. The fundamental mechanic properties and chemical composition of material are given in Tab. 2.2 and Tab. 2.3, respectively.

Table 2.2: Mechanical properties of the low carbon steel DC01

Density (kg/m^3)	Young's modulus (GPa)	Poisson's ratio	Yield Strength (MPa)
7850	205	0.3	350 [61]

Table 2.3: Chemical composition of the steel DC01 material

Element	C	Mn	Si	P	S	Ni	Cr	Al	Mo	N
Wt%	0.019	0.160	0.008	0.015	0.019	0.019	0.021	0.030	0.003	0.0024

A modal analysis by Finite Element Method (FEM) of the specimen used in experimental tests is performed using Ansys. The detailed analysis procedure is presented in Appendix A. Fig. 2.2 illustrates the finite element model and measure points. This analysis shows the first four mode shapes in Fig. 2.3 with the related normal displacements representing the deformations and the resonant frequencies.

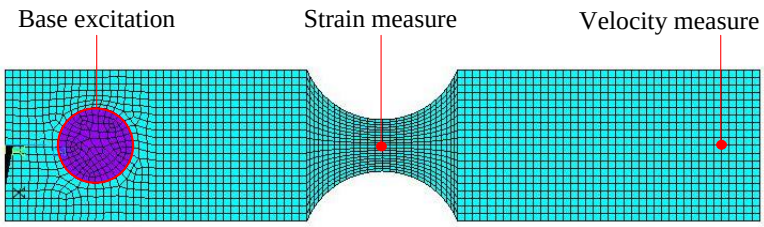

Figure 2.2: The finite element model of the specimen and measurement points

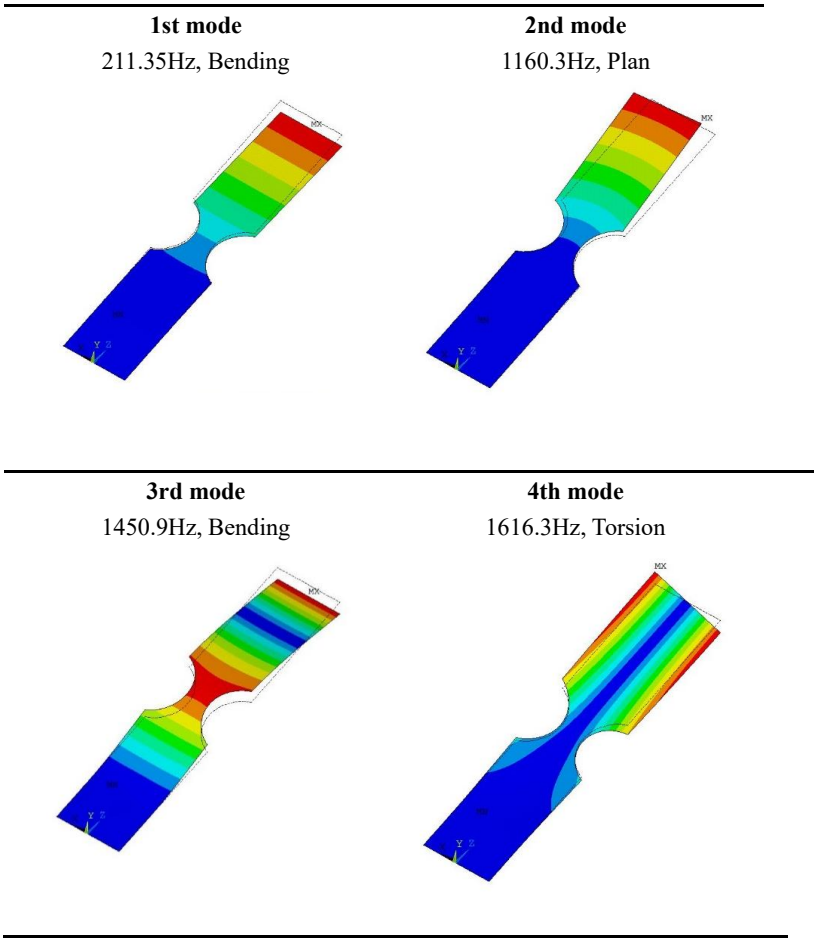

Figure 2.3: The first four mode shapes of the specimen. (The colors correspond to the normalized displacement. Red is the maximum)

From the FEM simulation, the resonant frequency of the first bending mode is 211.35 Hz. To avoid the effect of the second mode, the specimen has been designed in order to obtain the second mode away from the first. Besides, the Frequency Response Function (FRF) are obtained by harmonic analysis range of 100 Hz-2000 Hz under an acceleration of 3 g. The FRF of the strain in the central point (the location of strain gauge) is shown in Fig. 2.4. In this figure, only two peaks represent the first and third

modes. The plan mode and the torsion mode are not visible because of the normal measurement. Hence, the first bending leads to the largest deflection and, therefore, more damage in the reduction area. Therefore, the first mode is chosen for the fatigue tests.

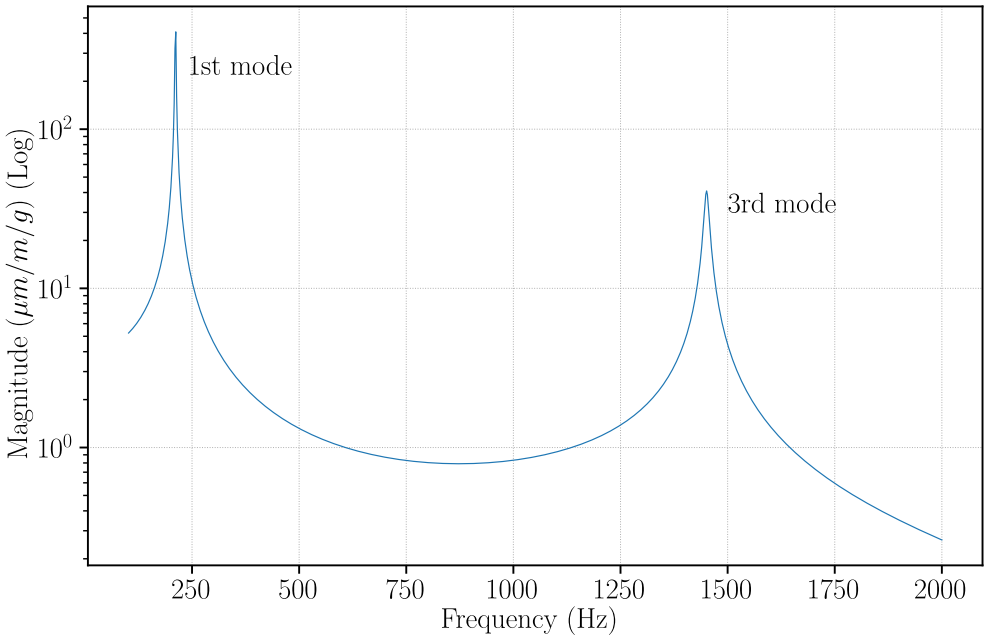

Figure 2.4: FRF of strain response

2.2.2. Test bench

The electro-dynamic shaker has the capability of the fatigue test with a high number of cycles, such as 1×10^6 cycles, in a short time. The Laboratory of Mechanics of Normandy (LMN) has acquired a vibration-based bending fatigue bench which consists of a motion table driven by a shaker presented in Fig. 2.5. The air-cooled electro-dynamic shaker is connected to the test specimen through a shaker table. A closed-loop vibration control ensures real-time adaptive control of tests. The experiments are performed on low carbon steel specimens subjected to cyclic sine excitation in bending deformation. Pictures of the machine are shown in Fig. 2.6.

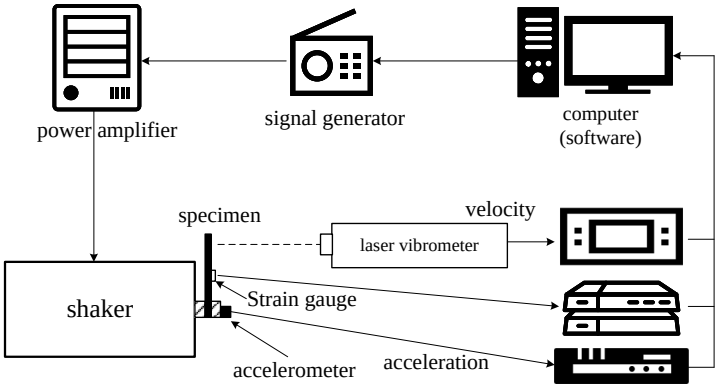

(a) Testing setup

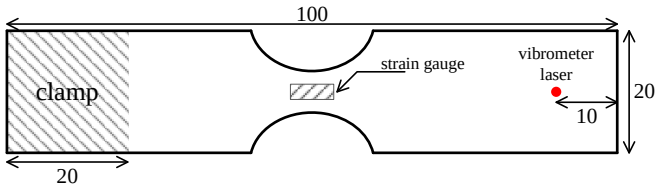

(b) Drawing of specimen showing position of instrumentation (Unit: mm)

Figure 2.5: Schematic of the testing setup

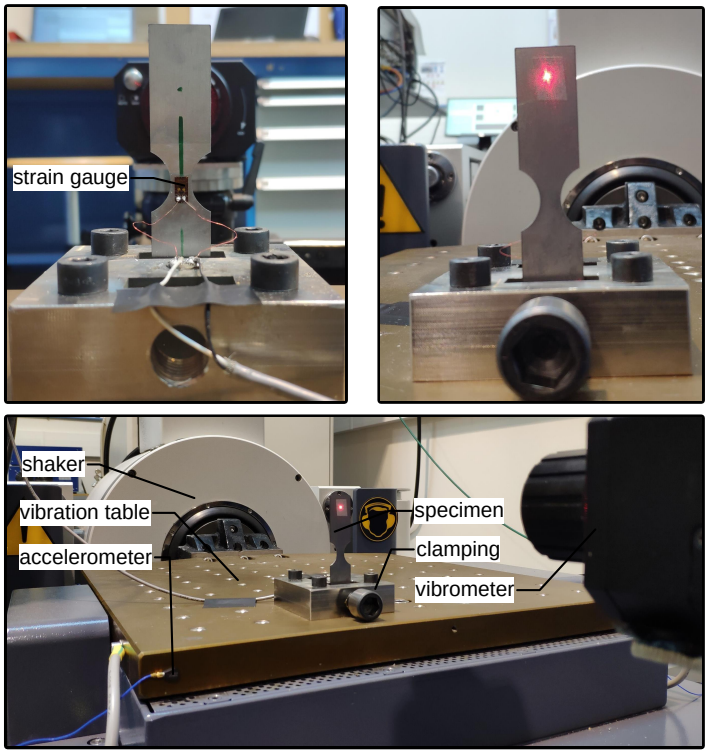

Figure 2.6: Pictures of test machine

For the Dongling GT500M shaker with a horizontal mobile table, the acceptable working conditions are listed in Tab. 2.4.

Table 2.4: Configurations of the shaker

Mass of mobile table	21.0 kg
Frequency range	5 Hz - 2000 Hz
Force in sine mode	3000 N (p)
Force in random mode (ISO-5344[75])	3000 N (eff)
Acceleration sine	14.6 g (p)
Acceleration random (ISO-5344[75])	14.6 g (eff)
Velocity	2 m/s (p)
Displacement	25 mm (pp)

(eff: effective value, p:peak value, pp:peak-peak value)

In this test, the instrumentation and software used to capture the signals are:

(1) A PCB 352A24 accelerometer with sensitivity 100 mV/g is fixed on the head of table.

(2) A HBM 350GE LM11 micro-measurement strain gauge with the ability of high resistance to alternating loads is glued on the stress concentration area of the specimen. The sensitivity is 0.5 mV/(µm/m). The performance of the strain gauge during the fatigue tests is discussed in Section 2.3.2 because the strain control has a great significance in this study. The shape and dimension of the strain gauge used in this study are presented in Fig. 2.7.

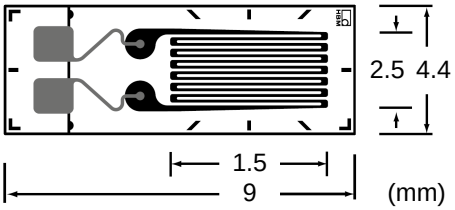

Figure 2.7: Dimension of strain gauge (HBM 1-LM11-1.5/350GE)

The roles of the strain gauge and the accelerometer have been permuted during the study to have :
- The accelerometer serves as the table control sensor to excite the specimen. In this case, the gauge measures the strain response of the specimen.
- The gauge is a control sensor of the specimen strain. In this case, the accelerometer becomes a device for measuring the acceleration that compensates for the displacement of the table according to the imposed strain.
In both cases, the two sensors can have a control role but can also be used to measure. Indeed, there is always a difference between the control set point and

the real imposed excitation.

(3) A Polytec OFV-3000 laser vibrometer with sensitivity 1000 mV/(m/s) is used in the test to measure the response in velocity on the free edge of the specimen. The modal characteristics of specimens can be determined by non-contacting vibrometer signals.

(4) "Data Physics 901 Series Vibration Control and Signal Analysis Systems" including software and hardware was used for test system control and data acquisition.

To carry out the fatigue test on the vibration table, the excitation frequency is selected near to the first resonance frequency of the specimen, and the specimen is forced to produce an enormous deflection response due to the resonance amplification.

2.2.3. Variability in the experimental test

Before fatigue testing, it is necessary to identify the factors that affect the test results. Since the main objective is to reduce uncertainty, this part helps to categorize these factors and make necessary assumptions. Most importantly, as described in Section 1.1.2, the strain and stress are linear in this high-cycle vibration fatigue testing.

To prevent uncertainty of the test system, the following arrangements have been adopted: (1) All tests were performed at constant room temperature; (2) The connection of the test specimen was ensured by clamp on accurate surfaces [76] with a constant tightened torque at $25\,\mathrm{N}\cdot\mathrm{m}$.

Alignment of testing machine and specimens The clamping in the vibration bench is not precise as the hydraulic machine. Even if the clamp is tightened with a torque wrench, the positioning of the specimens can have an impact on the resonance and damping. Moreover, the choice of the first resonance mode for testing is problematic, as shown in the work of Appert et al. [76]. That is why a reduced section has been added away from the clamp to reduce its effect.

Specimens mass The test results are highly dependent on the specimens. However, the specimens have variability in dimensions even if they come from the same manufacturing batch. Therefore, these dimension variations lead to mass (or density) variations, and the effect is not negligible when dynamic behaviour is considered.

Material and micro-structure The specimens being extracted from a plate, variability of the micro-structure and defects contained in the material, including size, type, distribution and morphology, have an effect on the fatigue behaviour [14, 77].

Crack initiation For the damage in HCF, there are micro-damages on the surface of

the deformed solid (Material) that lead to micro-cracks through slippage (crack initiation). Then the micro-cracks develop perpendicular to the direction of the load (crack propagation). It is assumed that cracks are always initiated from the side face of the reduced area and grow in the transverse direction.

2.2.4. Linearity of the test system in acceleration control

To prove that no other parameter affects the system (for example, plasticity), sine sweep tests at different acceleration levels were performed to validate the linearity of the test system. The sine sweep frequency is around the first resonant frequency, which is 190 Hz-220 Hz with a sweep speed of 0.3 Hz/s. From CES EduPack software[78], we know that the theoretical fatigue limit of the studied steel does not exceed 1800 µm/m. Therefore, the interest range can be focused on acceleration levels from 1 g to 4 g every 0.5 g. The FRF, representing the ratio in frequency between the response and the excitation, are plotted in Fig. 2.8.

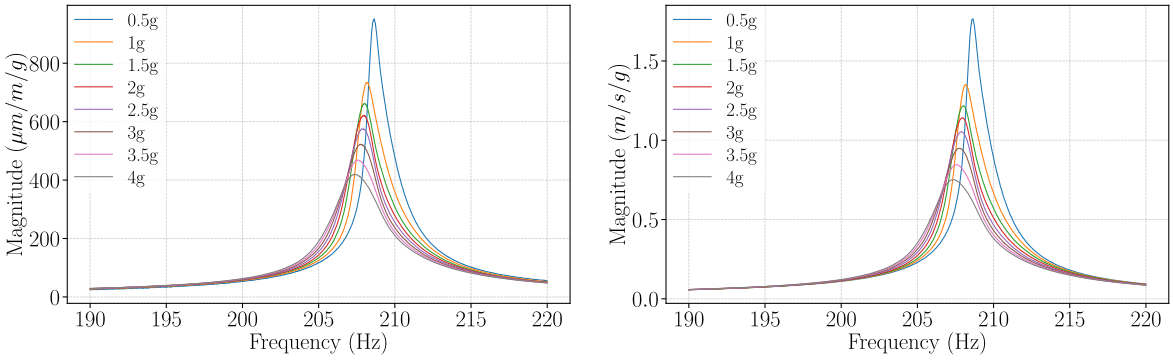

(a) FRF Strain

(b) FRF Velocity

Figure 2.8: FRF of the strain and the velocity to the base acceleration

These figures reveal a shift of the resonant frequency from 190 Hz to 220 Hz as well as a variation of the system damping factor in a range from 2.494×10^{-3} to 5.387×10^{-3} increasing with the acceleration levels. Besides, the maximum strain in Fig. 2.8 is 1684 µm/m, which corresponds to a stress close to 340 MPa. This stress is lower than the yield strength (Tab. 2.2) of steel DC01, which confirms that the material works in the elastic region in this acceleration range.

Gautrelet et al. [64] have determined the linearity range of the vibratory fatigue bench is 0-20g. According to this work, the linearity of the test system is studied from each response value at the frequency $fr - 5$Hz with different acceleration levels. The values were extracted to plot the relationship between the response (strain or velocity

response) and the excitation (acceleration levels). Here, fr is the resonant frequency, $fr - 5$ is arbitrarily chosen before the resonance peak to keep the phase between the input and the output less than 20° [69, 64]. Fig. 2.9 shows the relation between strain response and velocity response over the acceleration levels in resonant mode, and the linear curves are fitted by the least squares method.

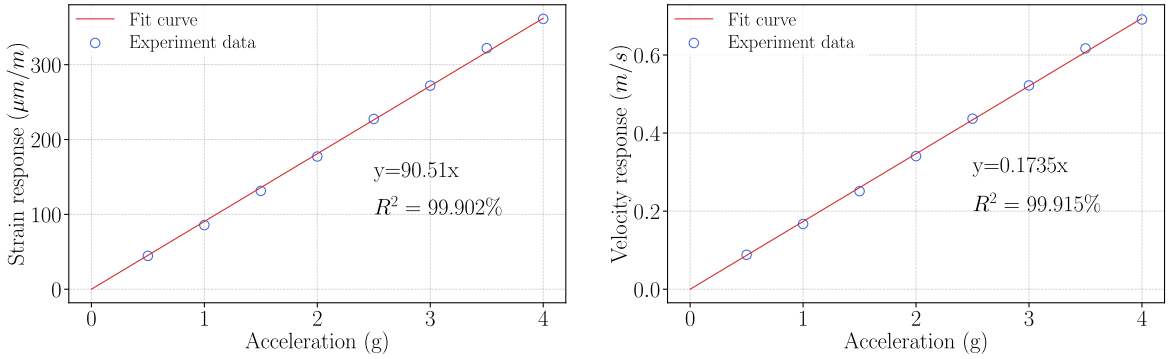

(a) strain (b) velocity

Figure 2.9: Strain and velocity vs. the acceleration level

The fatigue test in this study is conducted within the linearity range of the test system.

2.3. Strain control strategy

Because of the inherent feature of the vibratory system, the HCF test on vibratory shaker is usually controlled by acceleration [7, 61, 79, 80, 81]. By controlling the magnitude of the driving voltage, the acceleration of the vibration table is finally guaranteed to reach the specified value. This means the drive voltage of the vibration table can be adjusted slightly to keep the acceleration constant during the fatigue test. The strain measures obtained from acceleration control are dependent on the resonance amplification. Despite the use of identical specimens and the steady clamp, the dispersion in acceleration control leads to different strain amplitude values, so it is difficult to use in constant amplitude fatigue testing. That is why strain control is proposed in this study.

An experimental development on the shaker is conducted to define the strain level as an input control with a strain gauge placed on the specimen (see Fig. 2.10). In the left part of Fig. 2.10, the conventional vibration test on electro-dynamic shaker is usually controlled by the base acceleration (movements imposed on the clamping). Few recent controllers can be deflected to realize strain control.

On the contrary, the strain control in the right part makes sense in fatigue testing

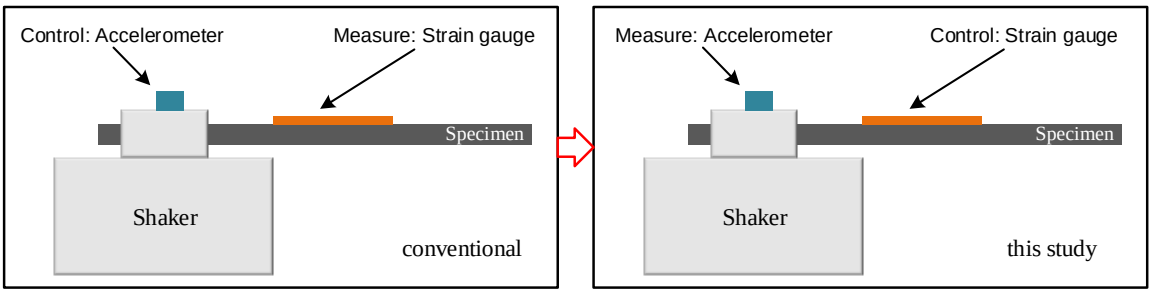

Figure 2.10: Schema of the change of the bench instrumentation

because the structure response is directly controlled. On the contrary, the acceleration and displacement depend on the FRF magnitude. The FRF of the test system shows variations with different specimens and clamping. These variations lead to large fluctuations of the stress or strain response amplitude, which may exceed 10% even for the same acceleration load. The fluctuation is too large to maintain stability, thereby reducing the reliability of vibration fatigue test results. Hence, strain control provides a constant stress or strain amplitude in the fatigue test. Besides, the vibration table works with the closed-loop control mode.

2.3.1. Experimental development for fatigue tests

In this study, the strain control fatigue test was implemented with the Sine Resonance Track-and-Dwell (SRTD) technique [77], which means the controller automatically maintains the resonance conditions during the test even though a change occurred (crack, for example). The SRTD test with strain control mode is illustrated in Fig. 2.11. This SRTD with strain control has two features. Firstly, the aim is to control the strain amplitude to keep a constant value. The shaker adjusts the base acceleration to reach the strain level needed for the fatigue test. Secondly, the SRTD maintains the phase difference between the excitation and response signals at 90 degrees. This ensures that the excitation frequency and resonant frequency of the specimen remain the same because a resonant frequency reduction is observed when a crack occurs. In general, the strain amplitude forms a closed-loop in SRTD test, which ensures a constant strain amplitude and working at the resonant frequency.

In the real test, the source signal for excitation is sent from the computer to the power amplifier and then driven the shaker to excite. The “Data Physics” software records the acceleration, velocity and strain signals in the frequency domain. The SRTD test makes it possible to record the evolution of the resonant frequency used in post-processing to define a criterion for assessing the presence of a crack on the

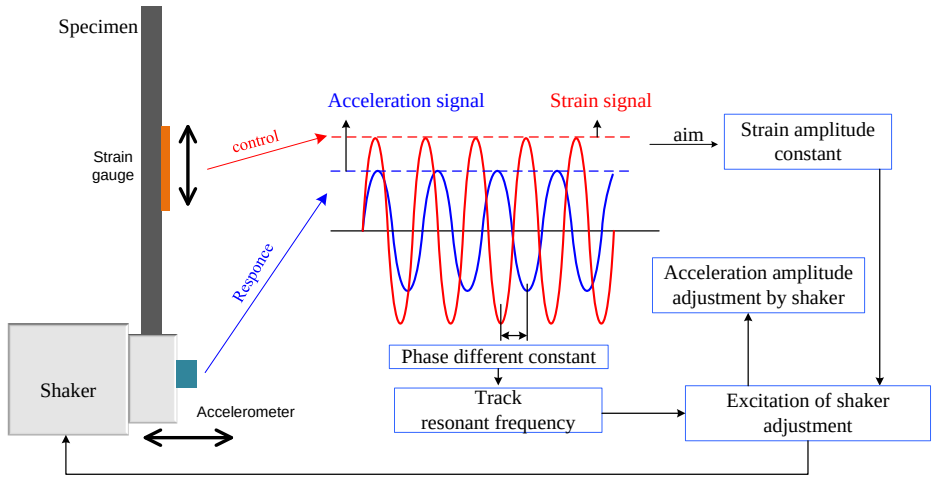

Figure 2.11: SRTD test with strain control

specimen.

The specimens were subjected to a sine excitation during the SRTD test, and the fatigue life under this strain amplification was subsequently identified. A schematic diagram of the data flow in the SRTD experiments is shown in Fig. 2.12. The source signals for excitation were sent from the computer to the power amplifier and then driven to the shaker to excite the specimens. The strain amplitude, initial resonant frequency, and the total number of cycles were defined at the beginning. The strain was controlled by a gauge and formed a closed-loop by the Data Acquisition (DAQ) system. The acceleration and velocity signals were also measured to obtain resonant frequency in real-time and calculate the number of cycles. The resonant frequency and the number of cycles were used to judge whether an SRTD test finishes. If both two criteria were not met, the resonant frequency was set as the excitation frequency for the amplifier to keep the test working at the resonant frequency. Otherwise, the SRTD test for one specimen was finished. All the signals of the acceleration, velocity, strain and excitation frequency were recorded in the time domain. The resonant frequency evolution recorded during the test was used in post-processing to define a criterion for evaluating the presence of cracks on the specimen.

According to Fig. 2.12, it is necessary to define the initial excitation frequency fr^0, strain amplitude ε, and the fatigue cycles N_L beforehand. The test system gives an excitation of the specimen to keep a constant strain response in resonant frequency. The system acquits phase shifts between input (strain) and output (acceleration) to obtain resonant frequency. The test maintains working frequency fr until 1×10^6 cycles, or stops due to instability caused by the critical crack.

With specimen DC01, the fatigue test procedures are depicted in Fig. 2.13. The test can be divided into two main steps for each specimen.

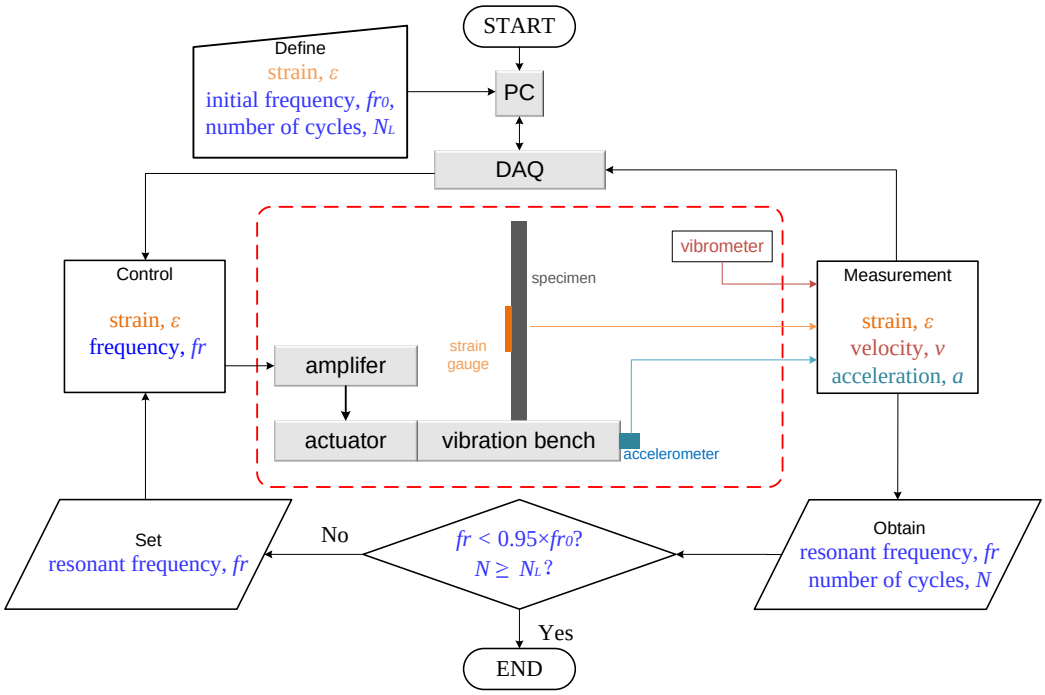

Figure 2.12: Test control and condition system for SRTD test

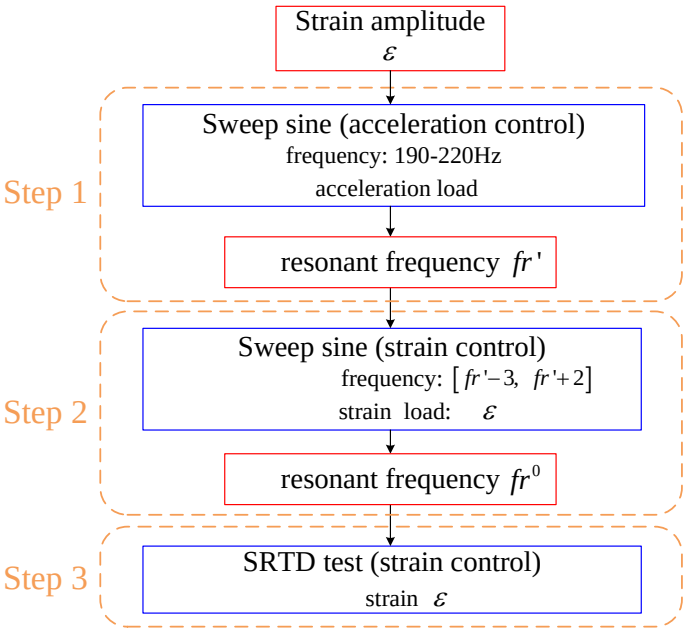

Figure 2.13: Fatigue test procedure with strain control

Note the desired strain amplitude by ε. For step 1, a sine sweep test with acceleration control (in base) is carried out from 190 Hz - 220 Hz. The excitation amplitude is arbitrarily chosen with the aim that it leads to a strain response close to ε. This step has two objectives. Firstly it is necessary to determine the resonant frequency for the next step with strain control. Secondly, the FRF of this sub-test can be used

as an examination of the test machine and specimen to reduce the uncertainty of the test.

The resonant frequency, donated as fr' and obtained by step 1, is used for step 2. It should be noted that a much higher excitation voltage is required for the amplifier to achieve the same response for control in strain relative to control in acceleration. Since the response depends on modal characteristics in excitation on base, it is hard to reach high deformation far away from the resonant frequency. Consequently, the excitation frequency should be close enough to the resonant frequency to avoid sudden changes in excitation voltage. Upon many tests, the frequency range is set in (fr'-3, fr'+2), in Hz, for carrying out the sine sweep in strain on the low carbon steel specimens. Based on this frequency range, a sine sweep test with strain control in desire level is conducted to record the FRF corresponding to the ratio between the strain (control on the response) and acceleration (measure on base) channels. Thanks to this FRF, the related resonant frequency, denoted by fr^0, is used as the initial excitation frequency in the SRTD test.

Step 3 is the main fatigue test carried with the SRTD test. The fr^0 from step 2 and ε are the input to SRTD test as shown in Fig. 2.12. The vibration excitation works at strain amplitude ε until the stop criterion.

2.3.2. Strain gauge and failure criterion

The fatigue damage of the strain sensor significantly affects the strain control strategy because both the specimen and the strain gauge are exposed to fatigue damage. Strain gauges are bonded to the center of the reduced zone to prevent premature gauge failure.

Empirically, the cracks were mainly observed on the face without the strain gauge. If the crack of the specimen leads to the fracture of a strain gauge, the specimen was not used for fatigue limit estimation to ensure all specimens reached the defined number of cycles.

Also, a threshold is required in the staircase method to define fatigue failure. The modal parameters of the mechanical system, such as resonant frequency and damping loss factor [69], shift when repetitive loading is applied to the system. However, Khalij et al. [61] have shown that the damping loss factor underestimates the number of cycles to failure. Therefore, the decrease in resonant frequency related to the crack presence and propagation was used in failure identification.

In order to avoid the different initial resonant frequency for each specimen, a normalized percentage rate changes between the resonant frequency of after (fr^{end}) and before (fr^0) SRTD test is used as s indicator defined as Change of Resonant Frequency (CRF), which is given by Eq. 2.1:

$$\%\text{CRF} = \frac{fr^0 - fr^{end}}{fr^0} \times 100 \tag{2.1}$$

To observe the strain gauge performance and related crack lengths to the thresholds, SRTD were carried out until CRF=2%, CRF=5% and CRF=8% of resonant frequency decrease. Fig. 2.14 reveals the relationship between frequency decrease and strain gauge measurement, as well as pictures obtained from a digital microscope (×300) of corresponding cracks on specimens. We can observe that:

(1) the strain keeps constant for a 2% decrease in frequency, and the cracks were not visible on the surface;
(2) the strain level drops for a decrease in the resonant frequency of 5% but only 40 µm/m (which is about 3% to defined strain amplitude). The crack length roughly reached half-width of the reduction area (about 3.3 mm);
(3) A dramatic drop of the strain value is observed after a 5% decrease in resonant frequency. The reason is that the crack on the surface of the specimen causes damage to the strain gauge. The crack extended over the whole width of the reduction area (6.8 mm) after an 8% frequency decrease.

In addition, the decrease in resonant frequency from 5% to 8% required a relatively small number of vibration cycles. Due to the severity of the crack, the strain gauge may lose its effectiveness after a decrease of 5%. Therefore, the stopping criterion for the staircase method is chosen at CRF = 5% which is also supported by the works of Gautrelet et al. [82].

To sum up, the following characteristics need to be considered to ensure the accuracy and stability of the strain control:

(1) Make sure that the strain gauges of each specimen are bonded at the same position, which means the center of the reduced section.
(2) Before the experiment, check whether the resistance value of the gauge is consistent with the nominal resistance value and balance the Wheatstone bridge before every test.
(3) The fatigue limit of strain gauge HBM 1-LM11-1.5/350GE is 2000 µm/m in 1×10^7 cycles, which is much higher than that of the specimen. The cracks are always occurred in the specimen, and there is no fatigue crack in strain gauge in this study.
(4) It must be noted that strain measurement is contact measurement, which means the effect of temperature evolution during the fatigue test should be examined first. Liakat et al. [83] deduced that the temperature of MCS 1018 carbon steel remains fairly unchanged in the HCF test, and the strain gauges are not sensitive to temperature during the room temperature range (20-30°C). Hence, the effect

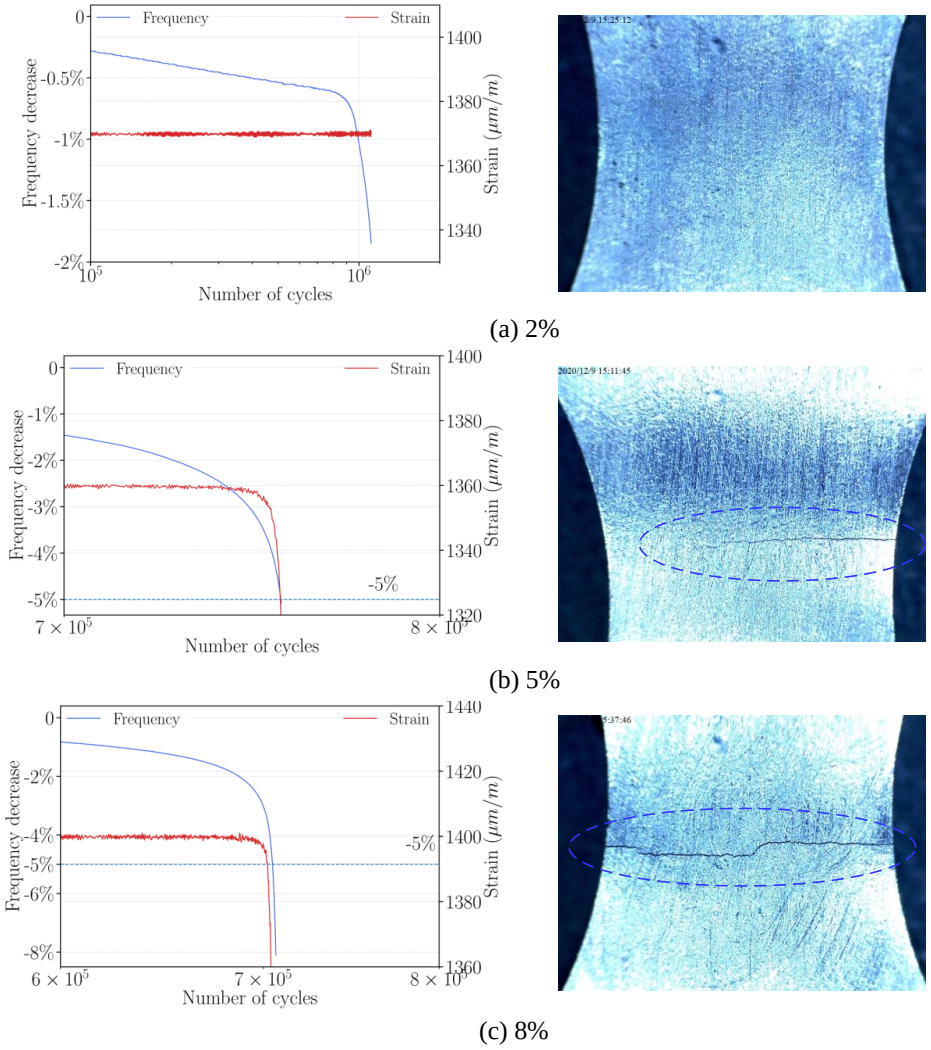

Figure 2.14: Crack length versus resonant frequency decrease of (a) 2% (b) 5% and (c) 8%

of temperature on the strain measurement of the fatigue test was considered negligible for DC01 steel.

2.3.3. Comparative study of fatigue test with strain control and acceleration control

The essential difference between acceleration control and strain control is that strain control realizes the control response during the fatigue process directly. In contrast, acceleration control is concerned with the input excitation of the specimen. The comparison between traditional acceleration control and proposed strain control is conducted on the sine sweep test and SRTD test to show the superiority of strain control.

2.3.3.1. Sine sweep test

Firstly, a sine sweep test was conducted on one specimen to obtain dynamic characteristics of the specimen by acceleration control in 5 g and strain control in 1400 µm/m. These two amplitudes are chosen because of similar deformation responses.

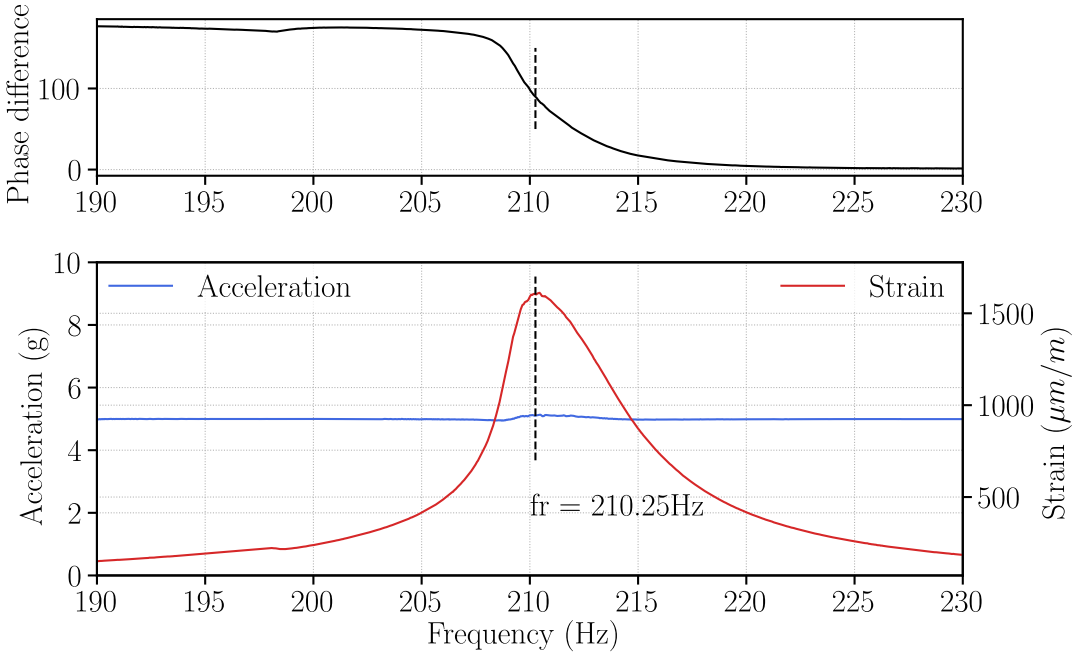

(a) Acceleration control in 5g

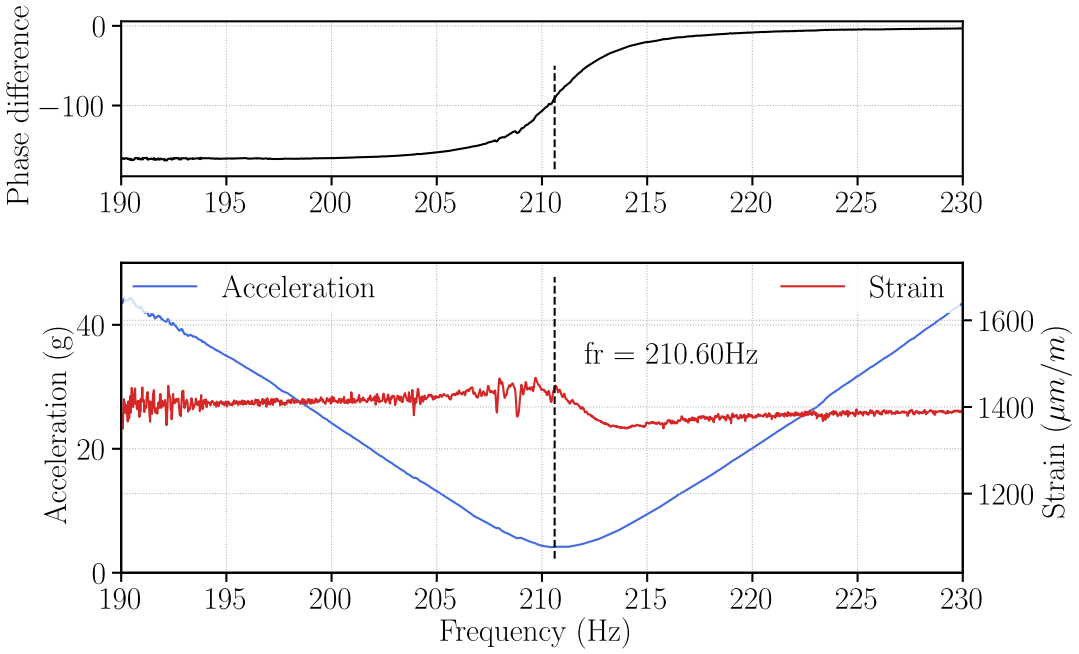

(b) Strain control in 1400 µm/m

Figure 2.15: Comparison of sine sweep test with acceleration control and strain control

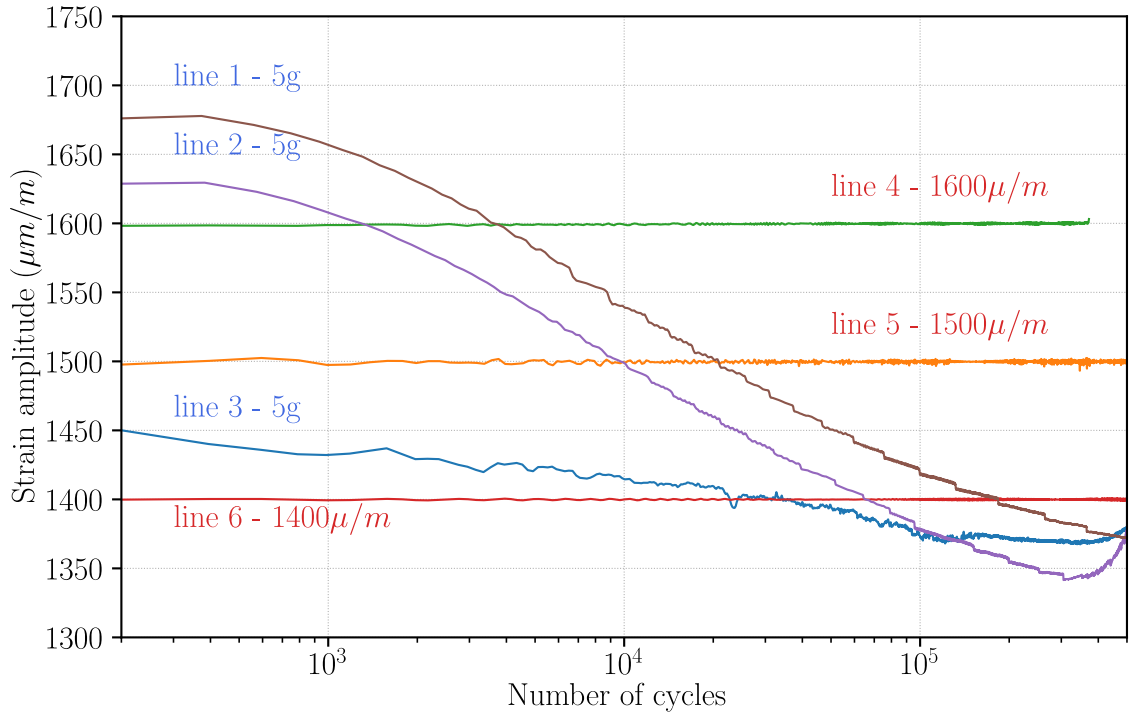

(a) Strain amplitude evolution

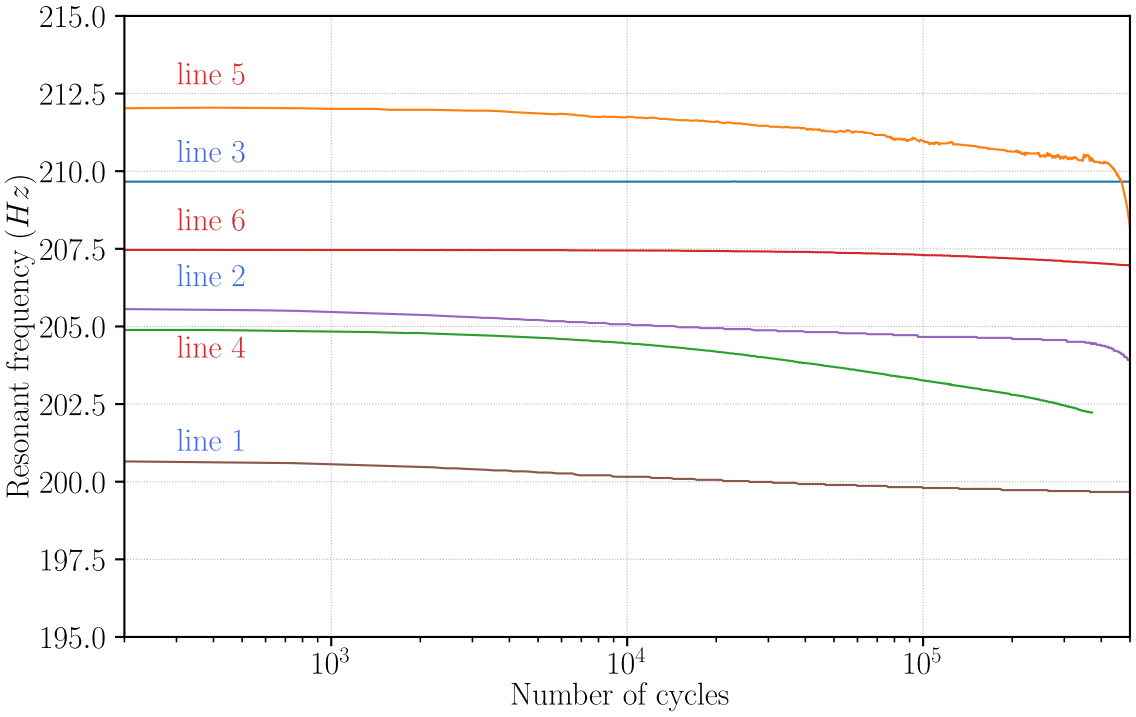

(b) Resonant frequency evolution

Figure 2.16: Comparison of SRTD test with acceleration control or strain control

As shown in Fig. 2.15, the resonant frequencies obtained for these two control modes, 210.25 Hz and 210.60 Hz, are almost the same. The damping loss factors calculated from the half-power bandwidth method are similar: 1.132×10^{-2} and 1.061×10^{-2}, respectively. In addition, the phase information is displayed by calculating the phase

difference between the acceleration signal and strain signal. Strain control is a new control mode that leaves the modal characteristics of the mechanical system unchanged.

2.3.3.2. Sine Resonant Track-and-Dwell test

Secondly, the Sine Resonance Track-and-Dwell (SRTD) test for three specimens with 5 g acceleration control and for another three with 1400 µm/m, 1500 µm/m, and 1600 µm/m strain control were carried out. The strain amplitude and resonant frequency evolution of the total 6 specimens during SRTD test is compared in Fig. 2.16(a) and Fig. 2.16(b), respectively.

In Fig. 2.16(a), lines 1-3 represent the acceleration control, which is variable in both the initial and the decreasing progress of strain amplitude. Khalij's vibration fatigue test [61] revealed a reduction in the peak of FRF with a resonant frequency shift. This leads to two effects: the change in response amplitude during the fatigue test and an inconsistent response for different specimens. It is the reason for the variation in acceleration control. Moreover, the existent control ways in base, regardless of acceleration, velocity, or displacement, have an inherent disadvantage of diversity in response [84]. While lines 4-6, representing strain control, show a stable and constant strain amplitude during the test under different defined strain levels. The resonant frequency of the 6 specimens given in Fig. 2.16(b) differs in both acceleration control and strain control. The dynamic response of the structure varies a lot with different specimens due to different modal parameters. It is known that the resonant frequency decreases when a crack occurs, and this decrease continues with the crack propagation [61]. Though there are many variations, the strain control keeps a constant strain amplitude independent of the resonant frequency.

Combining Fig. 2.15 and Fig. 2.16, though the strain control has large fluctuations in amplitude compared to acceleration control, especially close to the resonant frequency in the sine sweep test, the strain control has a very stable response in the SRTD test. Hence, strain control is desirable for the purpose of obtaining a stable response for base vibration.

2.3.3.3. Microstructure observations

Additionally, the fracture surface of two specimens with acceleration control and strain control was observed to complete the comparison. The fatigue test results of these two specimens are listed in Tab. 2.5. The specimens were scanned in a high vacuum chamber of the ThermoFisher microscope. The specimens were positioned vertically on a glued holder and fracture surfaces were placed perpendicular to the 15 kV electron beam. Fig. 2.17 and Fig. 2.18 display Scanning Electron Microscopy (SEM) images of fatigue crack surface from strain control and acceleration control.

Fig. 2.17 presents the landscapes of the fracture surfaces of strain control and

Table 2.5: The selected specimens for fractography analysis

	Specimen 1	Specimen 2
Control	Strain control 1360 µm/m	Acceleration control 5 g
Resonant frequency (Hz)	203.27 Hz	202.65 Hz
CRF(%)	15.76	25
Cycles ($\times 10^5$)	6.86078	7.24319

CRF: Change of resonant frequency Eq. 2.1

acceleration control. Following the fatigue test, the specimen with strain control is submitted to tensile to fracture - to observe the fracture surface - because the vibration fatigue test does not necessarily lead to complete separation. The crack growth direction is indicated by yellow arrows. It is observed that the cracks are initiated only from the surface without strain gauge (points B and C) in strain control, while there is crack initiation on both surfaces (points A, B, C and D) in acceleration control.

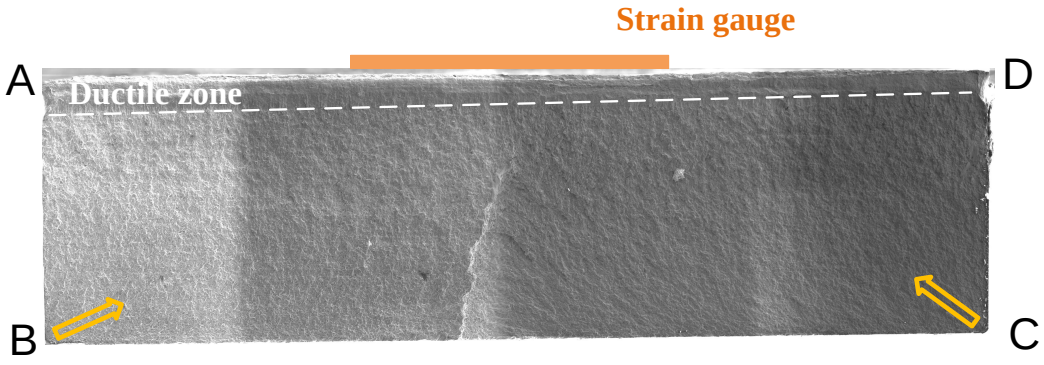

(a) Strain control

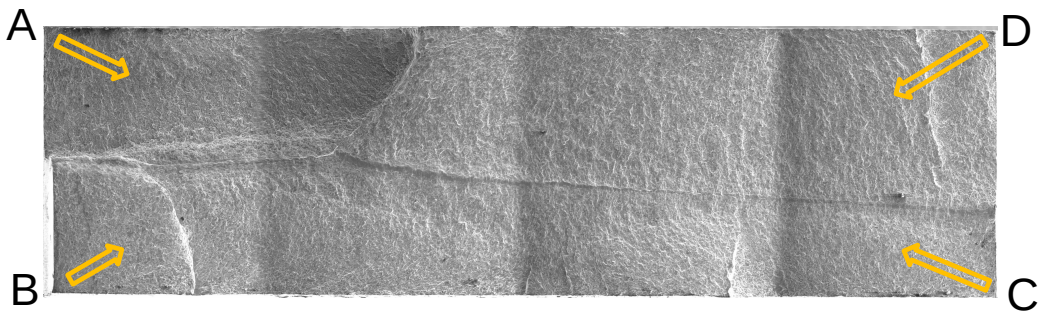

(b) Acceleration control

Figure 2.17: Landscape of the fracture surface

The details are shown in Fig. 2.18. A significant difference between the two control

modes is that we observed many intergranular fractures in strain control, as shown in Fig. 2.18(a). The intergranular spread over the fracture surface, including crack initiation and propagation. Nevertheless, the intergranular fracture occurred but not so much as shown in Fig. 2.18(b). In accordance with conventional fatigue fracture of low carbon steel [61], the transgranular fracture is the predominant part of acceleration control. Indeed, the river-line patterns representative of transgranular fracture are most noticeable in this figure. In our opinion, this observation could be ascribed to different kinds of excitation and therefore different stress states between strain and acceleration controls. The centerline presented in Fig. 2.17(b) leads to the conclusion that the deformation is of the bending type, whereas Fig. 2.17(a) corresponds more to a tensile fracture surface. This observation would require further investigation.

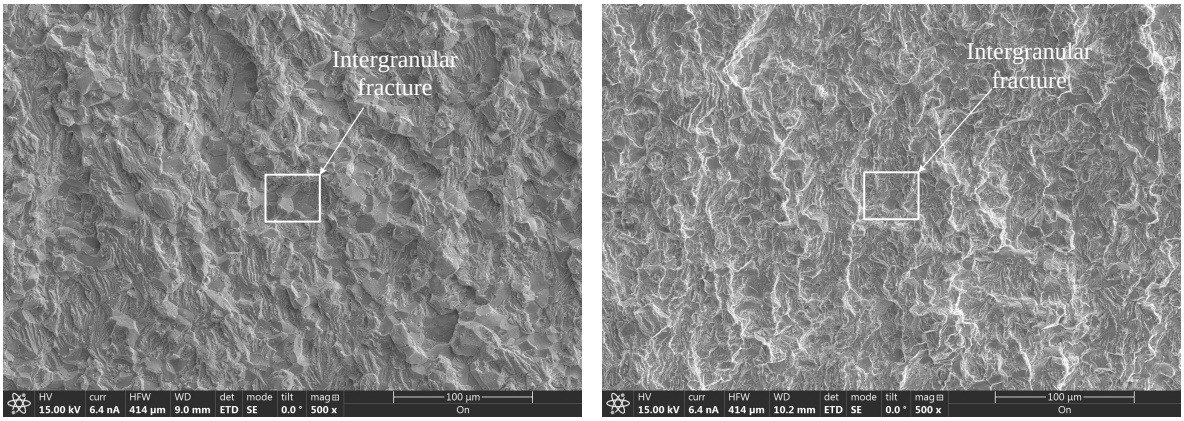

(a) Strain control (b) Acceleration control

Figure 2.18: Direct observation of fracture surface by SEM

2.3.4. Fatigue curve

To have a preliminary estimation of the fatigue limit, experimental tests with the strain control were carried out to obtain the $\varepsilon - N$ fatigue curve, the corresponding Basquin's equation and the confidence. Specimens are cyclically loaded using sinusoidal signals at specified strain levels (ε) until the specimen reaches recognizable failure. SRTD described in Section 2.3.3.2 is used to excite the specimens. Thus, a number of $\varepsilon - N$ points are plotted considering 5% decrease of the initial resonant frequency. Three strain amplitudes ε =1800 µm/m, 1500 µm/m, and 1200 µm/m are used as load levels, and three specimens are tested under each strain amplitude. The corresponding number of cycles to failure (N) - considered as the fatigue life - is then extracted to plot the fatigue curve depicted in Fig. 2.19 by double logarithmic axis.

The $\varepsilon - N$ equation is classically represented using the curve of the median fatigue data, but the variance information is then lost. It is necessary to construct a $\varepsilon - N$

curve that characterizes the confidence level and reliability, called the lower band curve, which ensures that the majority of the fatigue data falls above the lower bound value. The design curve can be derived by shifting the median $\varepsilon-N$ curve, as expressed in Eq. 2.2.

$$Y_{P,C} = \hat{Y} \pm K \times s \tag{2.2}$$

where the subscripts R and C denote the reliability and confidence levels. Y and $\hat{Y}$ donate the fatigue life (N) in the lower band curve and median fatigue curve, respectively, s is the standard deviation of Y on fatigue strength. $\pm$ reflects the lower limit or upper limit with specific reliability and confidence level. To calculate the multiplier K, the double-sided confidence intervals approach and the approximate Owen one-side tolerance limit approach are introduced as follows. The double-sided confidence intervals approach [85, 86] is used to obtain a confidence band with specific confidence given by:

$$K_{ASTM} = \pm\sqrt{2F_{C,(2,n-2)}} \times \sqrt{\frac{1}{2} + \frac{(X_i - \overline{X})^2}{\sum_{k=1}^{n}(X_i - \overline{X})^2}} \tag{2.3}$$

where $F_{C,(2,n-2)}$ is the F-distribution (also called Fisher–Snedecor distribution) value with the desired confidence interval C for $(2, n-2)$ degrees of freedom. n is the test sample size. K_{ASTM} takes the negative value for the upper confidence band whereas the positive value for the lower confidence band. The approximate Owen one-side tolerance limit approach [87] has been proposed to account for confidence and reliability.

$$\begin{aligned} K_{owen} &= K_D \times R_{owen} \\ K_D &= c_1 K_R + K_C\sqrt{c_3 K_R^2 + c_2 a} \\ R_{owen} &= b_1 + \frac{b_2}{f^{b_3}} + b_4\exp(-\mathrm{f}) \end{aligned} \tag{2.4}$$

in which,

$$\begin{aligned} K_R &= \Phi^{-1}(R) \\ K_C &= \Phi^{-1}(C) \\ f &= n - 2 \\ a &= \frac{1.85}{n} \end{aligned} \tag{2.5}$$

where Φ is the standard normal Cumulative Density Function (CDF). The coefficients for empirical forms of K_{owen} are shown in Tab. 2.6 and Tab. 2.7.

The double-sided confidence intervals provide a 95% confidence band, as presented in Fig. 2.19, accounting for the uncertainty of the median curve. The lower band curve is used for the design that ensures that there is a 95% possibility of survival with a

Table 2.6: Empirical Coefficients $b_i (i = 1, 2, 3, 4)$ for K_{owen}

Confidence level(C)	b_1	b_2	b_3	b_4
0.95	0.9968	0.1596	0.60	-2.636
0.90	1.0030	-6.0160	3.00	1.099
0.85	1.0010	-0.7212	1.50	-1.486
0.80	1.0010	-0.6370	1.25	-1.554

Ref: Page 116 in [86]

Table 2.7: Empirical Coefficients $c_i (i = 1, 2, 3)$ for K_{owen}

Confidence level(C)	c_1	c_2	c_3
$f \leqslant 2$	1	1	$\frac{1}{2f}$
$f > 2$	$1 + \frac{3}{4(f-1.042)}$	$\frac{f}{f-2}$	$c_2 - c_1^2$

Ref: Page 116 in [86]

90% of confidence level above this lower bound.

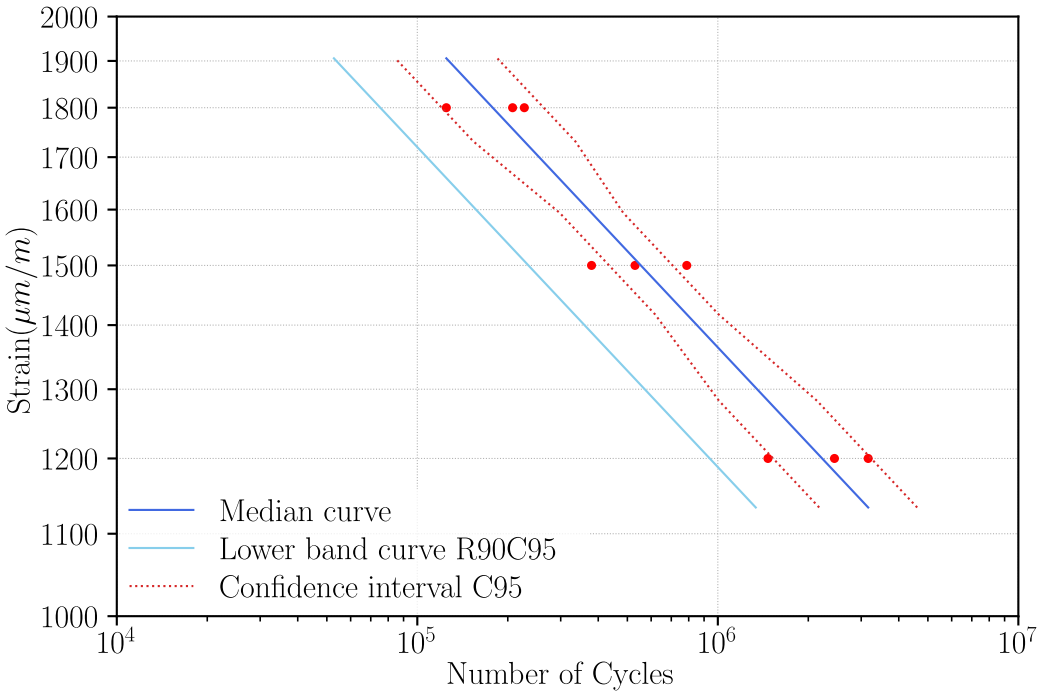

Figure 2.19: Experimental data and the related Basquin curve with strain control

The identification of the Basquin's parameters [34] leads to:

$$\varepsilon = 1.255 \times 10^4 \times N^{-0.1606} \tag{2.6}$$

Thus, the fatigue strength in 1×10^6 cycles - considered as fatigue limit in this study - is approached by the value of 1364.41 µm/m.

2.4. Application of staircase method for the fatigue limit estimation

This section describes the experimental staircase test with strain control. The test procedure and results are presented in this section.

2.4.1. Experimental procedure

The staircase test methodology [27] was extensively used to evaluate fatigue limit distribution by mean and standard deviation determination because of its simplicity and high accuracy. The specimens were tested sequentially, one at a time. The initial strain level ε_0 and strain step size d were determined before the test. The first specimen was tested at the initial strain level. If there is no crack (survival) for a pre-determined number of cycles N_L (for limit value), the strain amplitude of the following specimen is incremented by one step size. Conversely, if the specimen cracks (failure), the strain amplitude for the next specimen is decremented by one step size. This manner is repeated in sequence, with the strain levels increasing and decreasing with the step size. The outcome is that approximately half of the specimens fail, and the other half do not.

The increment d has a great influence on standard deviation estimation. Zhao & Yang [24] and Strzelecki & Sempruch [46], proposed the stress steps of 5 MPa and 6 MPa for a low carbon steel material. In accordance with these works, a strain step size of 20 µm/m is used in this study.

In this fatigue study, to carry out vibration tests, the 1×10^6 cycles are chosen for defining the fatigue limit. The first bending mode is excited because it gives the most severe damage compared to the other modes.

To summarize, the settings for the staircase tests are listed in the tab 2.8.

Table 2.8: The experimental parameters used in staircase test

Resonance mode	First bending
Step size (d)	20 µm/m
Stop criterion	CRF= 5%
Number of cycles (N_L)	1×10^6

With these set-up parameters, the test procedures for all specimens are schematically depicted in Fig. 2.20. In Fig. 2.13, each specimen was conducted with SRTD test (Section 2.3.3.2) until 1×10^6 cycles. After the fatigue test of one specimen, check the fatigue test results and determine the strain level for the next specimen. If the CRF was detected below 5% (survival) for 1×10^6 cycles, the strain level for the next specimen was incremented by one step size. Otherwise, it is decremented by a step size. After, the new strain level for another specimen is up to this test results. In the end, these steps were repeated on another until all specimens met the following three requirements for the staircase test.

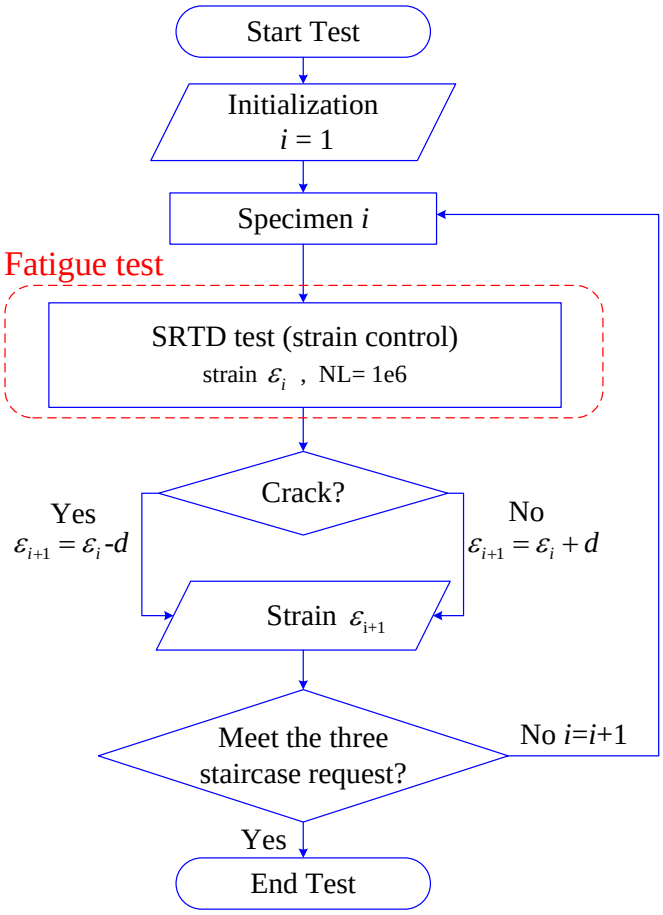

Figure 2.20: Staircase test procedure

(1) Taking the first reverse results as a starting point of valid data, the number of valid specimens should be no less than 30 [35].
(2) The test contains at least three strain levels.
(3) The strain level of the last specimen should be adjacent to the first strain level and have the opposite result [47].

2.4.2. Test results and discussion

In order to obtain the fatigue limit of steel plates, a total of 36 valid specimens were conducted at staircase strain levels with the resonant frequency, donated as i from 1 to 36. According to the results, the up-and-down diagram of the staircase test is shown in Fig. 2.21.

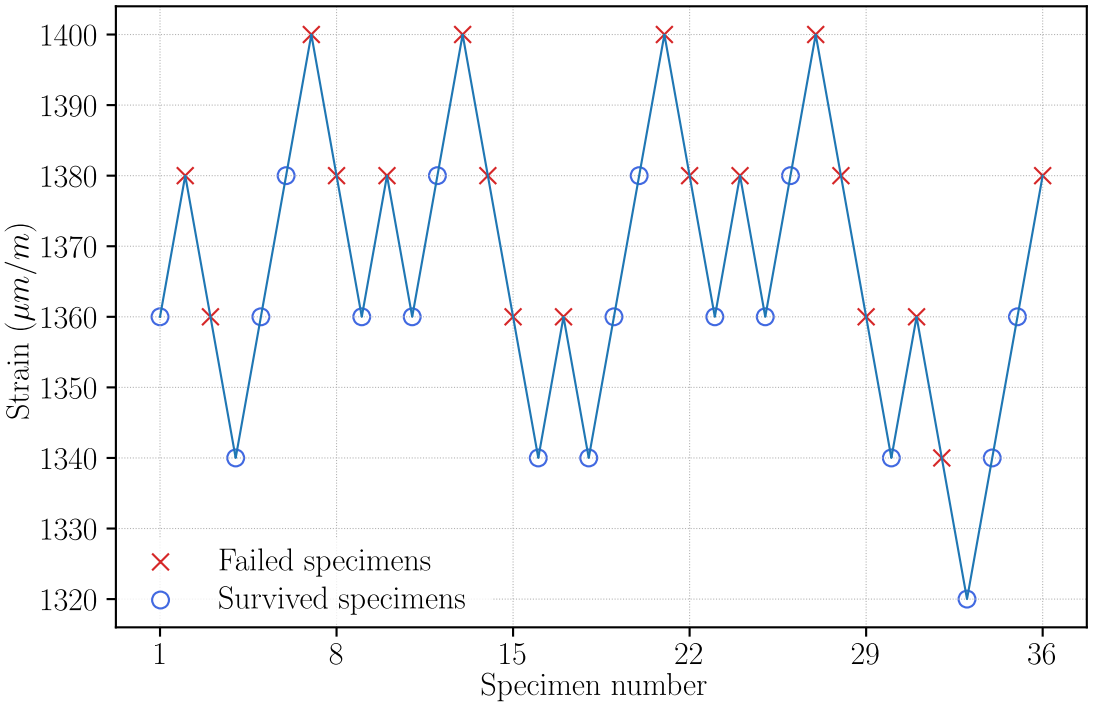

Figure 2.21: Up–and–down diagram for DC01 steel specimens

2.4.2.1. Resonant frequency evolution during the fatigue tests

When choosing the No.21-No.30 specimens for demonstration, the resonant frequency and strain amplitude recorded through the SRTD are presented in Fig. 2.22. The ordinal number of failed specimens is listed in the figures. Fig. 2.22(a) shows the decreased resonant frequency. Six specimens failed due to CRF exceeding 5%, while the other four survived. Correspondingly, Fig. 2.22(b) depicted the strain levels at the preset value and kept them constant during the test. The disabling process of gauge, in the end, is speedy and occurs after the stop criterion so that the strain value could be seen as constant through the SRTD test, regardless of the variation in frequency. These data demonstrate the reliability of strain control in vibration fatigue test on electro-dynamic shaker.

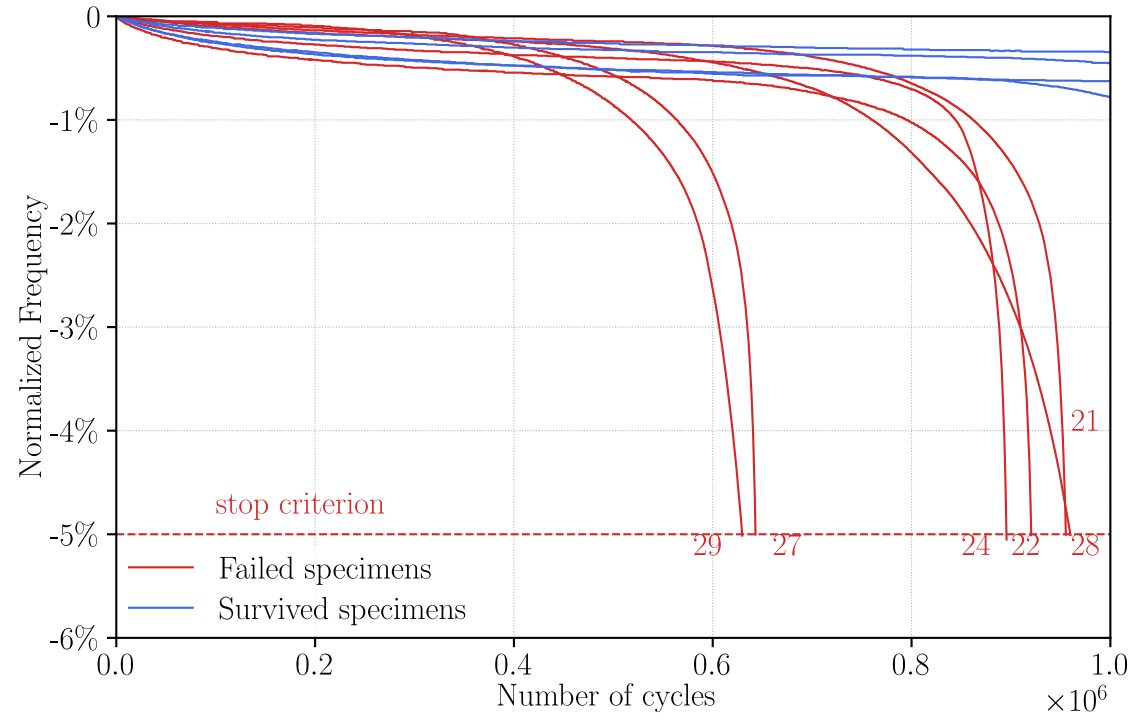

(a) Frequency decrease (normalized with the initial resonant frequency)

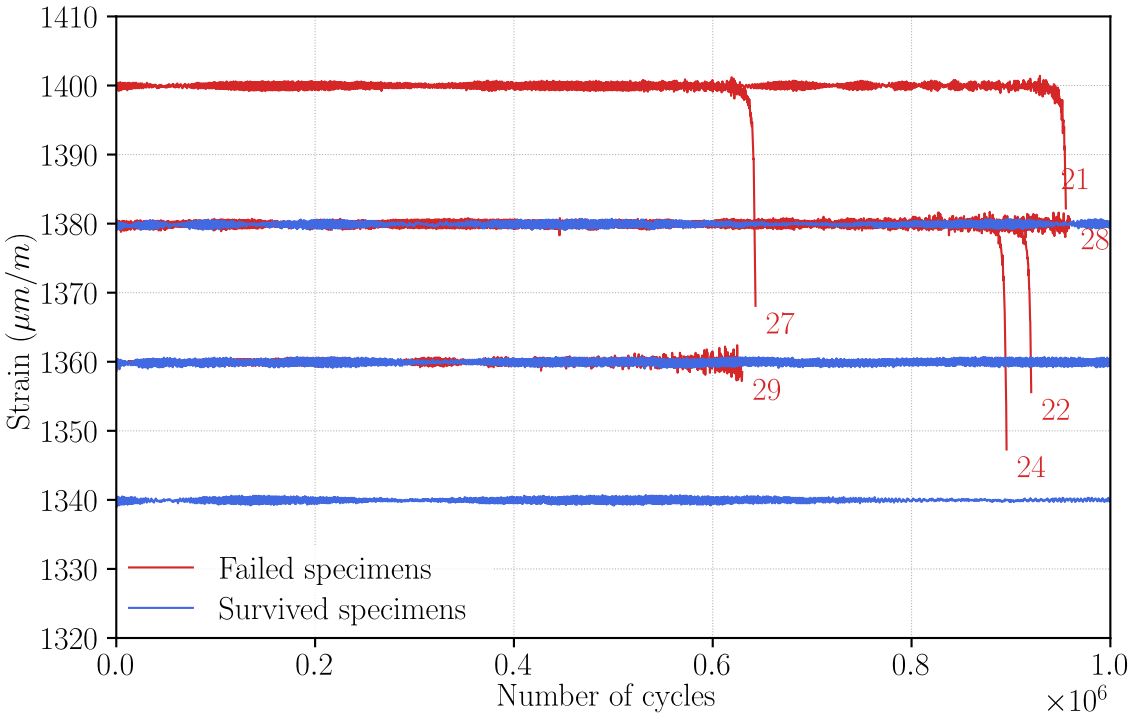

(b) Strain amplitude

Figure 2.22: Frequency decrease and strain amplitude during SRTD test. The failure curves correspond to failed specimen ordinal i

Choosing 11 specimens in the same strain level 1380 µm/m, Fig. 2.23 shows the acceleration and velocity amplitude with the number of cycles. We can see variability even with constant strain amplitude.

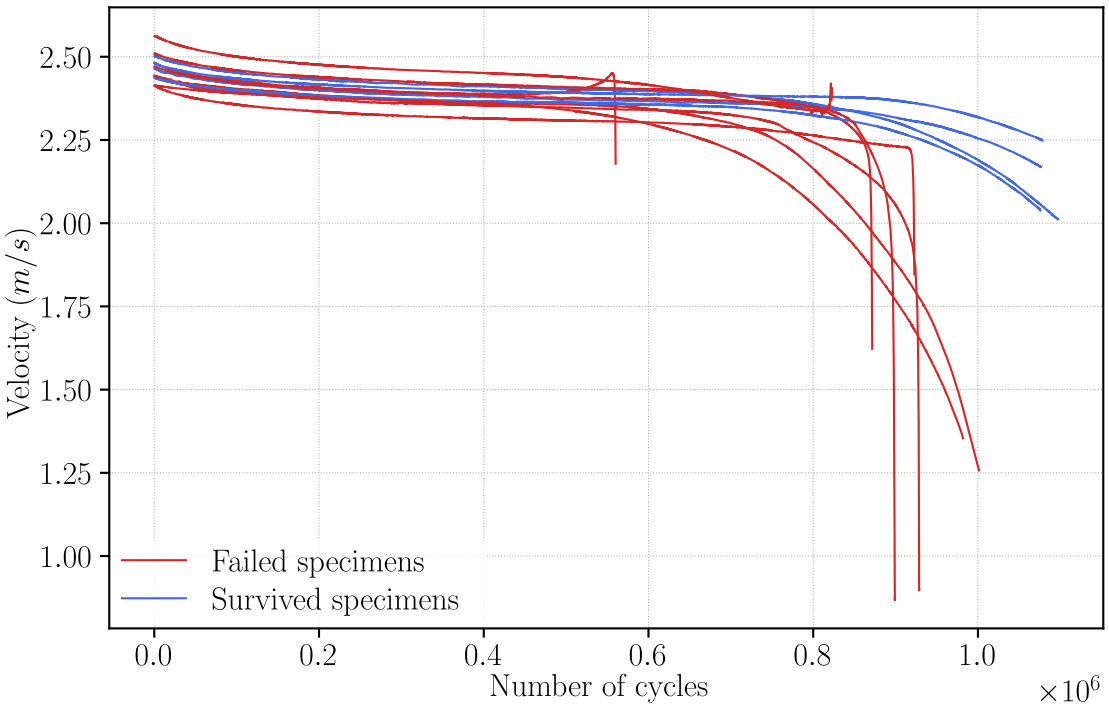

(a) Response velocity at same strain level

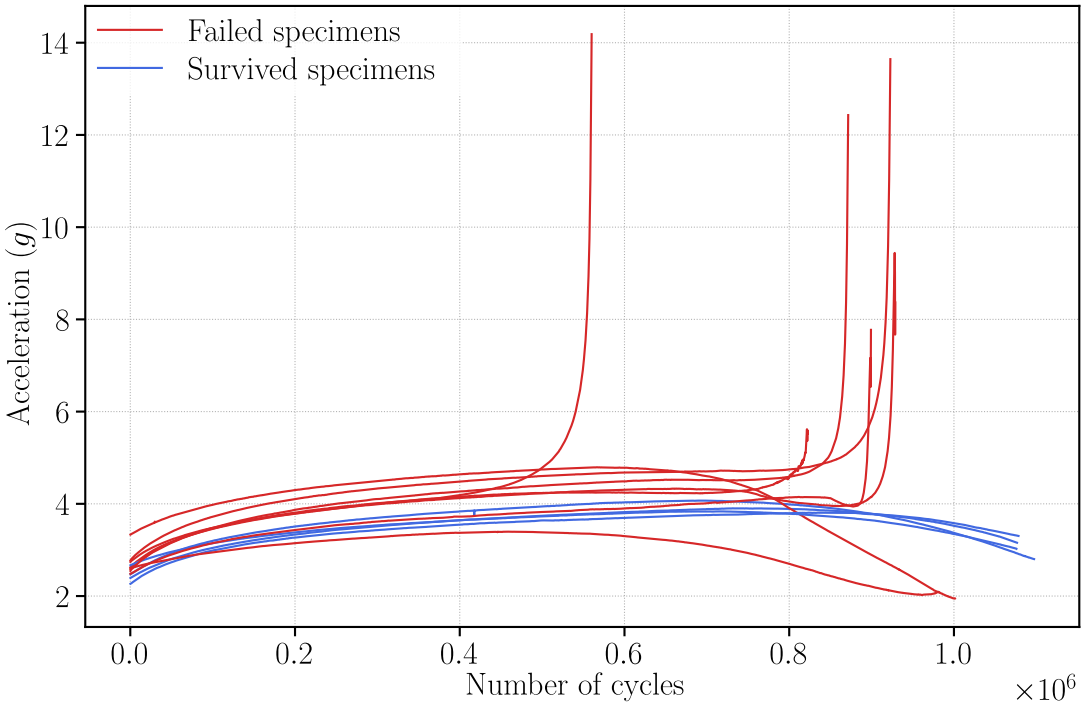

(b) Excitation acceleration in same strain level

Figure 2.23: The acceleration and velocity in same strain level(1380 µm/m)

In addition, taking the evolution of the frequency shift of the No. 22 specimen as an example in Fig. 2.24, three stages can be distinguished in the progress of frequency decrease: adaptation phase, quasi-stationary phase and rapid failure phase. The decrease in resonant frequency was observed when the crack occured, and the decrease

continues with the crack propagation [88]. Moreover, the 5% decrease chosen for the failure criterion is located in stage III.

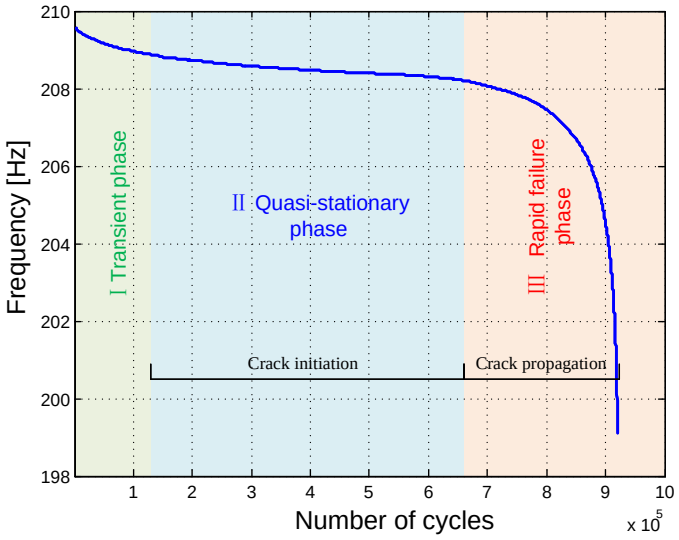

Figure 2.24: Resonant frequency decrease progress of No. 22 specimen

2.4.2.2. variability of the damage

The detailed test results data of the 36 specimens, including the number of cycles with respect to different CRF and the number of cracks, are listed in Tab. 2.9.

It can be seen from the second column that the mass is not identical for all specimens, and the first mode resonant frequency may differ by a few Hertz due to the variability of the test system. However, these two parameters have no direct relationship with the result (survival or failure) and the number of cracks.

Because each of the SRTD test dose not stopped at the same number of cycles, the number of cycles and CRF at the end of the test is not the same for every specimen. Hence, the cracks at the end of the specimens are also variable. For example, Fig. 2.25 illustrates the number of cracks with different CRF. Fig. 2.25 (a) and (b) show that the number of cracks may be different in the same CRF, while Fig. 2.25 (c) and (d) show that the crack lengths are different with respect to CRF. The location of crack initiation and the length of crack propagation are variable in real fatigue experimental tests. However, cracks always occur on the side without the strain gauge.

To sum up, the strain control in a vibratory shaker for the fatigue test is validated by the staircase method. The estimation of fatigue limit from staircase results is provided in the following section.

Table 2.9: The result data of specimens with thickness 2mm

Order i	Mass (g)	Strain $(\mu m/m)$	fr^0 (Hz)	Number of cycles $(N, \times 10^5)$ $\%CRF = 1$	$\%CRF = 2$	$\%CRF = 3$	$\%CRF = 4$	$\%CRF = 5$	Result (-)	End of the test $N_{end}(\times 10^5)$	$(\%CRF)$	Number of cracks
1	27.555	1360	207.41	9.32805	10.21816	10.49385	10.58351	10.61749	survival	10.64723	7.21	1
2	27.513	1380	206.51	7.98029	8.82029	9.0683	9.16992	9.22115	failure	9.28761	11.65	2
3	27.17	1360	205.25	7.64409	8.49476	8.68159	8.74068	-	failure	8.76143	4.87	1
4	27.486	1340	208.1	9.32047	10.49341	10.92247	11.13286	-	survival	11.14228	4.05	0
5	27.517	1360	206.51	-	-	-	-	-	survival	10.9229	0.58	0
6	27.482	1380	205.76	10.07389	-	-	-	-	survival	10.97323	1.4	0
7	27.469	1400	209.85	4.12443	5.37319	6.16511	6.69891	7.1896	failure	8.911	10	2
8	27.564	1380	207.3	4.7849	5.37969	5.52876	5.57474	5.59181	failure	5.60119	5.88	1
9	27.509	1360	206.76	8.8232	-	-	-	-	survival	9.99639	0.93	0
10	27.257	1380	204.04	7.56417	8.35942	8.55948	8.64134	8.67903	failure	8.716	8.32	2
11	27.584	1360	208.01	10.78161	-	-	-	-	survival	11.07563	1.11	0
12	27.255	1380	205.64	-	-	-	-	-	survival	10.76577	0.65	0
13	27.514	1400	207.19	6.25252	6.86953	6.99857	7.03288	7.04796	failure	7.06643	8.11	2
14	27.52	1380	205.05	8.20261	9.23962	9.64369	9.83689	9.96179	failure	10.01248	5.47	2
15	27.479	1360	208.21	6.48485	7.27884	7.47429	7.53749	7.56022	failure	7.57889	6.97	1
16	27.643	1340	207.79	-	-	-	-	-	survival	10.93247	0.62	0
17	27.456	1360	208.05	8.7732	9.66207	9.87187	9.93853	9.96492	failure	9.98718	7.27	1
18	27.233	1340	207.13	-	-	-	-	-	survival	11.14542	0.42	0
19	27.478	1360	207.66	8.92698	10.12819	10.47181	10.58444	10.66189	survival	10.73098	6.19	2
20	27.466	1380	206.4	10.19047	-	-	-	-	survival	10.75909	1.43	0
21	27.331	1400	207.47	8.61541	9.28369	9.45339	9.51826	9.55036	failure	9.61367	17.3	2
22	27.494	1380	209.61	7.94693	8.87729	9.09728	9.17367	9.20202	failure	9.22806	7.3	2
23	27.391	1360	201.31	-	-	-	-	-	survival	10.81194	0.64	0
24	27.605	1380	204.91	8.44418	8.76087	8.88198	8.93144	8.95403	failure	8.99245	11.2	2
25	27.617	1360	202.5	-	-	-	-	-	survival	10.8827	0.52	0
26	27.224	1380	200.83	10.74276	-	-	-	-	survival	10.78389	1.02	0
27	27.477	1400	203.52	5.63142	6.18471	6.34862	6.40395	6.4285	failure	6.45991	9.3	1
28	27.579	1380	201.28	7.59175	8.58759	9.09189	9.39481	9.59652	failure	9.81772	6.75	2
29	27.319	1360	203.27	5.17888	5.84764	6.06433	6.19833	6.29496	failure	6.86078	15.76	2
30	27.461	1340	202.59	-	-	-	-	-	survival	10.88091	0.36	0
31	27.619	1360	203.64	6.94097	7.446	7.61189	7.68253	7.71464	failure	7.72214	5.37	2
32	27.568	1340	203.85	7.54535	8.41179	8.74391	8.88915	8.95725	failure	9.09296	16.48	2
33	27.508	1320	203.75	-	-	-	-	-	survival	10.96331	0.34	0
34	27.611	1340	204.76	8.01821	9.39906	10.22085	10.86252	-	survival	10.94223	4.14	1
35	27.493	1360	204.57	11.06726	-	-	-	-	survival	11.95499	1.02	0
36	27.626	1380	203.83	7.09398	8.04198	-	-	-	failure	8.22478	2.74	1

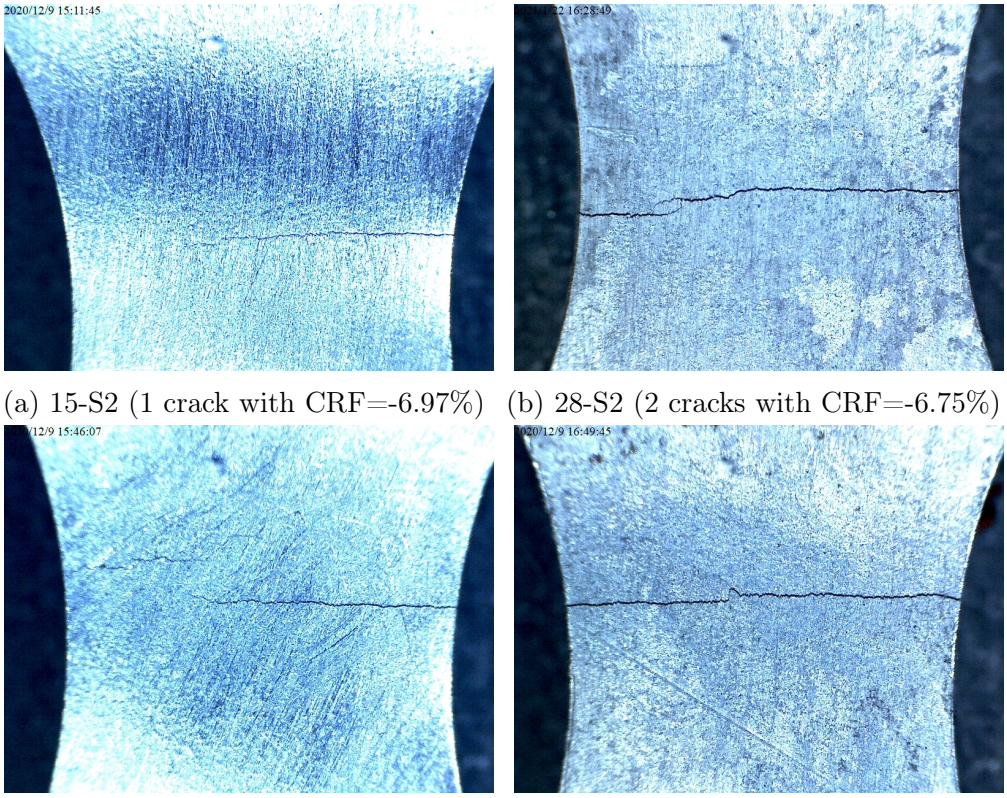

(a) 15-S2 (1 crack with CRF=-6.97%) (b) 28-S2 (2 cracks with CRF=-6.75%)

(c) 02-S2 (2 cracks with CRF=-11.65%) (d) 21-S2 (2 cracks with CRF=-17.3%)

Figure 2.25: Comparison about cracks and CRF

2.4.2.3. Distribution of the fatigue limit obtained from Dixon-Mood method

As described in Chapter 1, the Dixon-Mood (DM) method [27] is commonly involved in estimating the fatigue limit distribution. The DM method was proposed by Dixon and Mood [27] in 1948, which provides approximate formulas of maximum likelihood estimation to calculate the mean and standard deviation under the Normal distribution.

In DM method, only less frequent events, failure or survival, are used to evaluate the distribution. The stress amplitude span is split by a step size d into several load levels numbered by j, where $j = 0$ stands for the lowest load level and j_{max} stands for the maximum stress level. Denoting by $n_{c,j}$ the number of the fewer frequency events (survival or failure) at the load level j, two auxiliary values A and B can be calculated by Eq. 2.7:

$$
\begin{aligned}
A &= \sum_{j=0}^{j_{max}} j \times n_{c,j} \\
B &= \sum_{j=0}^{j_{max}} j^2 \times n_{c,j} \\
n_c &= \sum_{j=0}^{j_{max}} n_{c,j}
\end{aligned}
\tag{2.7}
$$

The auxiliary values are used to estimate the median value m_{DM} by Eq. 2.8 and the standard deviation s_{DM} by Eq. 2.9. The minus sign given in Eq. 2.8 is used if the failed specimens are evaluated; otherwise, the plus sign is applied.

$$
m_{DM} = S_{a,0} + d\left(\frac{A}{n_c} \pm \frac{1}{2}\right) \tag{2.8}
$$

$$
\begin{aligned}
s_{DM} &= 1.62 \times d\left(\frac{Bn_c - A^2}{n_c^2} + 0.029\right) \quad \text{if} \quad \frac{Bn_c - A^2}{n_c^2} \geqslant 0.3 \\
s_{DM} &= 0.53 \times d \qquad\qquad\qquad\qquad\quad \text{if} \quad \frac{Bn_c - A^2}{n_c^2} < 0.3
\end{aligned}
\tag{2.9}
$$

From up-and-down diagrams (Fig. 2.21), the Probability Density Function (PDF) and Cumulative Density Function (CDF) of fatigue limits calculated by the DM methods are shown in Fig. 2.26 and Fig. 2.27.

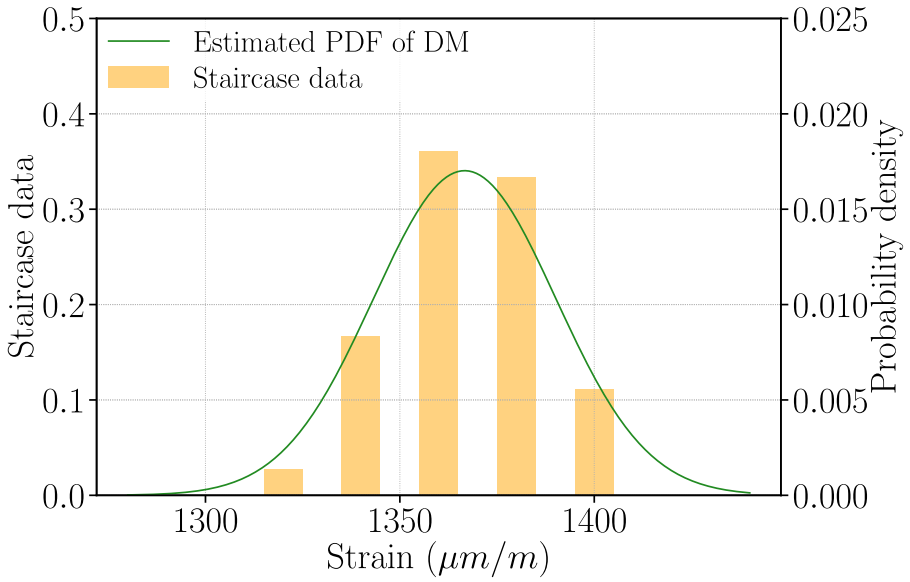

Figure 2.26: PDF estimated from DM method

The median and standard deviation are estimated as 1366.67 µm/m and 23.44 µm/m, respectively. In this case, the corresponding coefficient of variation is 0.01715. More-

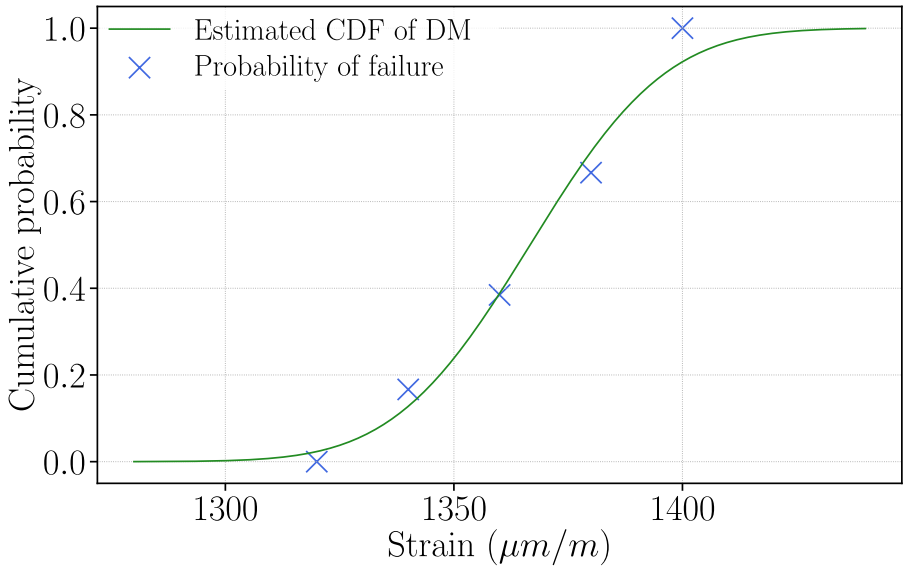

Figure 2.27: CDF estimated from DM method

over, we can observe that the median is close to the value obtained from the fatigue curve (1364.41 µm/m) in Section 2.3.4.

2.4.2.4. Lower limits of the fatigue limit

The rules of the staircase method make the test data concentrated near the median and distributed on both sides. Conducting fatigue tests at various strain levels in order to determine the median $\varepsilon - N$ curve gives a probability of failure of 50%. With the DM, it is assumed that the variation of the fatigue limit follows a normal distribution. The one-sided tolerance limit method is used in this study to calculate the probability of fatigue strength.

In the fatigue life analysis, there is no problem if the real life is larger than life expectancy, but it cannot be too small. Similarly, the fatigue limit can be underestimated for safety, and it will be dangerous if the fatigue limit is overestimated. In this study, the one-sided confidence interval of a normal distribution is provided below.

After the statistical parameters (the mean μ and the standard deviation s) and the number of specimens n are available, the lower limit of the fatigue limit value for different confidence levels (C) and survival probability (P) can be expressed as [35]:

$$\mu_{P-C} = \mu - k(P, 1-C, n)s \tag{2.10}$$

$$k = \frac{\mu_P + \mu_\gamma \sqrt{\frac{1}{n}[1 - \frac{{\mu_\gamma}^2}{2(n-1)}] + \frac{{\mu_P}^2}{2(n-1)}}}{1 - \frac{{\mu_\gamma}^2}{2(n-1)}} \tag{2.11}$$

where P means survival probability, $k(P, 1-C, n)$ is the coefficient for the one-sided

tolerance limit for a normal distribution with point P. μ_P and μ_γ are the standard Normal distribution values with the probability P and γ, respectively. Based on the μ =1366.67 µm/m and s =23.44 µm/m, the fatigue limit values with specified $P\breve{}C$ levels of DC01 steel by the previous approaches are exhibited in Tab. 2.10.

Table 2.10: Fatigue limit values with specified P–C levels

C \ P	0.5	0.9	0.95	0.99	0.999	0.9999
0.5	1366.67	1336.63	1328.11	1312.14	1294.23	1279.49
0.9	1361.60	1328.99	1319.30	1300.89	1280.05	1262.82
0.95	1360.11	1326.44	1316.31	1297.01	1275.12	1257.00
0.99	1357.21	1321.02	1309.90	1288.61	1264.37	1244.27

Unit: µm/m

2.4.2.5. Comparison to the steel fatigue limit in the literature

The Comparison of some fatigue limit values of carbon steel in fully reversed cycling from the literature is summarised in Tab. 2.11.

Table 2.11: Comparison of fatigue limits of carbon steel

Material	DC01	Carbon steel	C20 steel	MCS 1018 steel	C45 steel	SAE 1045 steel
Ultimate stress (MPa)	430.9	-	520	520	778	710
Fatigue limit (MPa)	280.26	268.7	265	263.2	274	300
Load mode	Bending	Bending	Tension	Tension	Tension	Tension
Load frequency	205	-	-	15	15	5
Number of cycles	10^6	-	2×10^6	10^6	-	10^6
Test method	Staircase test	-	Staircase test	S-N fitting	Staircase test	Intrinsic thermal dissipation
Reference	This study	Papuga [89]	Delahay et al. [90]	Liakat et al. [83]	Colombo et al. [91]	Teng et al. [92]

Low carbon steel is widely used in various building components, containers, furnaces, industrial machinery applications, etc. Thus, most research on the fatigue of steel has been carried out. In conventional stress-life domain, the database Papuga [89] gives the fatigue limit 268.7MPa of carbon steel for fully reverse bending. Delahay et al. [90] gave a probability distribution of the fatigue strength at 2×10^6 cycles against the stress amplitude for C20 steel, as Fig. 2.28 shows. Liakat et al. [83] presented a S-N curve of MCS 1018 steel form tension-compression fatigue tests, as Fig. 2.29 shows.

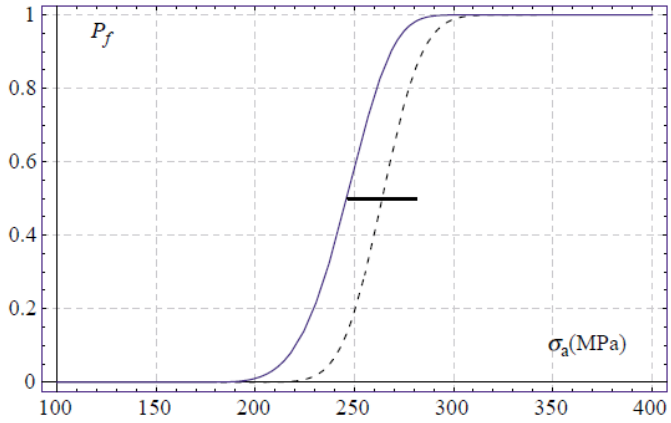

Figure 2.28: The CDF of C20 steel [90]

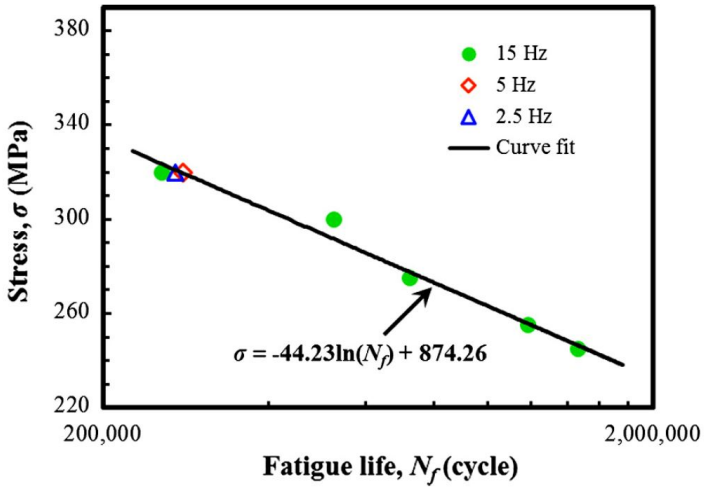

Figure 2.29: A S–N curve of MCS 1018 steel [83]

Though there are differences in load type and specimen geometry, an agreement between the results in this study and the literature data can be observed. While there is no standard test protocol for vibratory fatigue limit on the electro-dynamic shaker, this study provides a new experimental test and data processing method for estimating fatigue limit distribution.

2.5. Conclusion

This chapter proposes a strain control test method applied on an electro-dynamic shaker to conduct a constant amplitude fatigue test. The efficiency of the proposed approach has been demonstrated by testing DC01 steel plates in the first mode. The strain amplitudes measured on the specimens remain constant and independent of the resonant frequency with the strain control, avoiding the diversity response of

traditional acceleration control in the base. The results highlight the repeatability of the strain-controlled test with the staircase method. The DM method provides an estimation of the fatigue threshold and the scatter.

The staircase approach provides a reasonable estimate of the median fatigue limit because about half of the specimens fail and the others do not [37]. Nonetheless, it has a poor performance on the estimation of the standard deviation, especially for small sample tests [93, 94]. The results are: (1) It is more difficult to get an accurate measuring of dispersion due to the concentration of the data points near the median. (2) Usually, for the real fatigue tests, the fatigue limit distribution is hard to evaluate with a small number of specimens ($n \leqslant 30$). (3) Since the step size is chosen constant, the estimation of the fatigue limit is less accurate. Otherwise, a large number of specimens would be required to estimate the fatigue limit accurately. To avoid this, we propose, in the following chapter, to use bootstrap sampling to estimate the uncertainties. The next chapter presents a new statistical approach to improve the fatigue limit distribution estimation.

Chapter 3
Uncertainty quantification using resampling methods

In the last part of the previous chapter, the post-processing estimates the fatigue limit distribution from one experimental staircase test. However, the question arises as to whether the fatigue limit remains the same if the staircase test is conducted more than once under the same conditions.

In this chapter, the uncertainty analysis was carried out using the resampling method. A brief background of uncertainty for the staircase method is given in the first section. The second section details the resampling methods - leave-one-out and bootstrap - on the staircase data to evaluate the fatigue limit. Based on the experimental staircase test results of steel DC01, the uncertainty of the staircase test was evaluated by the bootstrap method. Then, the bootstrap was applied to the experimental data obtained for three kinds of specimens. The chapter ends with a brief conclusion. This part has been presented in an international congress [93].

3.1. Background

Since the fatigue limit is mainly estimated through experiments, uncertainties are consequently introduced into the assessment due to the inherent properties of the specimen as well as the environment of the experiment. These uncertainties may lead to an inaccurate estimation of the fatigue limit distribution. The uncertainty may originate owing to the fatigue limits of each specimen are random, and the fatigue process is affected in practice by many factors, such as the grain size, the type, the morphology and the loading [14]. The measurement uncertainty of the test results also affects the fatigue test confidence. Hence, the assessment of measurement uncertainty is still required to evaluate the test results.

Therefore, it is commonly accepted that the fatigue design, including fatigue limit estimates, without considering uncertainties, may not be efficient. Pascual et al. [19] proposed a random fatigue-limit model to describe the variation in the fatigue limit and all fatigue curves. Rabb [41] analyzed the confidence level of outcomes of staircase and reliability of the standard deviation estimation based on the Monte-Carlo simulation (MCS). Wallin [42] provided a study of the uncertainty of the Maximun Likelihood Estimation (MLE) method on staircase data. Jamalkhani Khameneh et al. [49] deduced the mean, standard deviation and lower and upper scatter-band of the fatigue limit at different confidence levels from the staircase experiment. Karolczuk et al. [95] used to predict fatigue life uncertainty by Monte Carlo and Latin Hypercube Sampling techniques.

However, fatigue limits can be expected to vary not only from specimen to specimen in one staircase test but also between different staircase tests. It is interesting to consider whether one staircase data can represent the real fatigue limit distribution. Hence, a question is what is the confidence level of one staircase test result.

Intending to evaluate the confidence of a fatigue limit distribution, this chapter describes the design and implementation of the resampling method on staircase test data. The resampling method, also used in statistical machine learning, is investigated in this paper as a possible means of assessing this uncertainty. By convention, no more than 30 specimens are loaded into an experimental staircase test for cost and time considerations. Resampling methods allow samples to be extracted repeatedly from the dataset and obtain additional information without more expensive tests.

This chapter discusses two resampling methods, including Leave-one-out cross-validation (Loocv) and bootstrap. Loocv is a resampling method that splits all datasets one by one and computes a statistic with left-out one sample. The bootstrap method, developed by Efron [96], provides an efficient way to reproduce more samples from the small-size dataset. It is a reasonable way to estimate the epistemic uncertainty and provide non-parametric statistical inferences without any assumption about the

distribution describing the quantity under consideration. In a case that combined resampling and staircase test, Pollak et al. [38] used the bootstrapping algorithm to reduce the potential of sizeable standard deviation errors in the staircase tests. Leonetti et al. [97] employed the Bootstrap method to linear regression of the S-N curve. A literature review indicated that almost no such resampling method had been mentioned for the staircase test uncertainty evaluation. We focused on the bootstrap method analysis, which allows the uncertainty assessment of the fatigue limit based on only existing test data. In this study, the bootstrap to extract more information from the limited experimental data is applied initially to assess the uncertainty of the staircase test data.

3.2. Application of the leave-one-out resampling

Leave-one-out cross-validation (Loocv) is a typical cross-validation method in machine learning, especially for small samples conditions. Cross-validation means that the dataset is randomly divided into k parts, of which there are $k-1$ parts in the training set and 1 part in the test set. The first data group can be used to test the model fit based on the remaining $k-1$ pieces of data, and then the second data group can be used as a test set to examine the adequacy of the corresponding training set.

It is commonly known that the larger the number of specimens, the more accurate the staircase data can represent the true fatigue limit distribution. In the literature of the last decades, there is almost no real experimental staircase test that exceeds 30 specimens. Inspired by the Loocv method, a similar Leave-one-out (Loo) resampling method can be used to measure the number of specimens. For the staircase test, every single piece of data represents an observation of one specimen in the real test. Therefore, each strain (or stress) value can be regarded as a part, and all test data is divided into n parts, where n is the total number of specimens in a staircase test. Assuming that $N = n - 1$ samples are taken out in each sampling to realize, leave one sample is left out. Using all staircase load (e.g. stress or strain amplitude) data as the dataset, the general procedure is according to Algorithm 3.1. As a resampling method, Loo has two main advantages:

(1) It is much less biased. We use a repeated sampling set containing $n-1$ observations, which is almost identical to all observations in the entire data set. Therefore, the Loo method will not lead to other data errors like other cross-validation methods.

(2) It is not computationally expensive to perform the Loo procedure.

Algorithm 3.1: Leave-one-out resampling

1 The staircase dataset that including n specimens is represented as $X = [x_1, x_2, ..., x_n]$
2 Let $N = n - 1$, N is the number of samplings
3 Resampling N data from X, to produce n times combination data $\widetilde{X}$, which is donated as $\widetilde{X} = [x_1, x_2, ..., x_N]$
4 **foreach** *combination data* $\widetilde{X}_i$ **do**
5 Regard $\widetilde{X}_i$ as a new staircase test results
6 Shuffle $\widetilde{X}_i$ randomly
7 Estimate fatigue limit distribution by the same DM method
8 **end foreach**
9 Calculate the uncertainty factors.

The analysis of the Loo method is performed to determine the efficiency of a single specimen. In this analysis, the number of samples N is chosen as $N = n-1 = 35$ in the numerical test, and a total of 36 times resampling (M) is used. With Loo resampling method, the distributions from all resampling data are shown in Fig. 3.1.

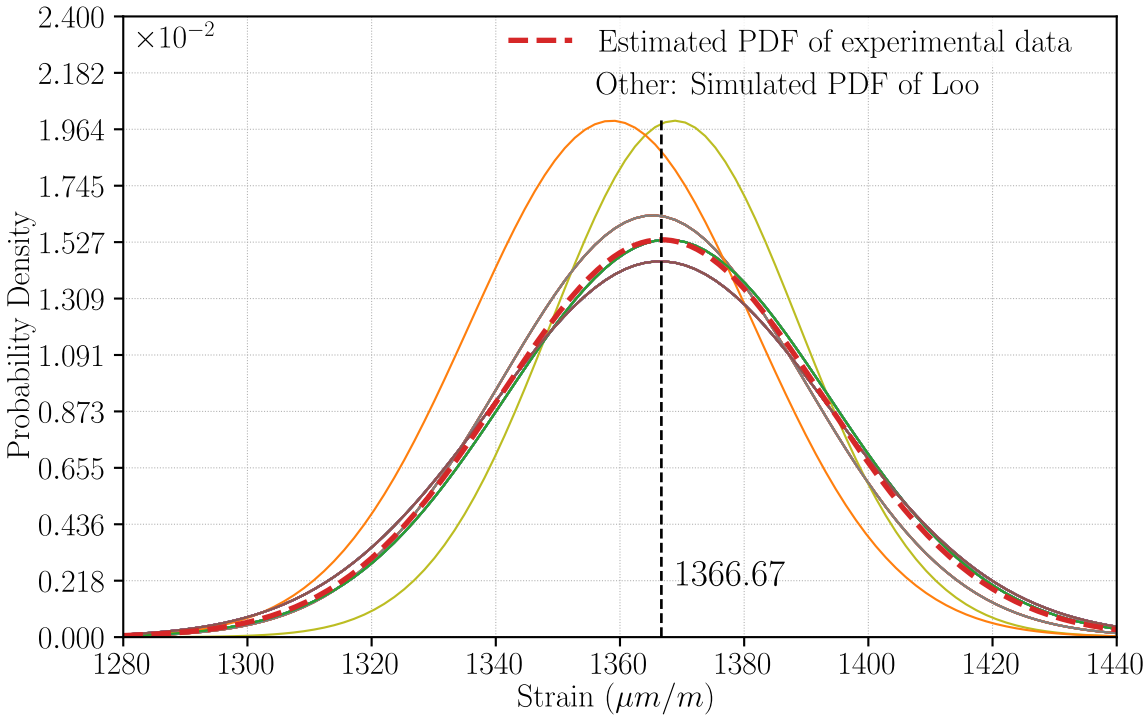

Figure 3.1: PDFs of fatigue strain limits from Loo re-sampling

Each line in Fig. 3.1 provides one Loo resampled result. The Loo excludes one data (tested strain level) at each sampling, so 36 samplings were repeated in this case. However, the Loo sampling for eliminating the same tested strain value leads to the same result. The maximum difference between the estimated median and standard

deviation between the experimental data and resampled data is 0.096% and −5.26%, respectively. It means that the number of specimens, $n = 36$, is sufficient in this experimental test. The test with one more specimen will change the result slightly.

3.3. Bootstrap resampling and results

3.3.1. Procedure

The fatigue limit is regarded as a random variable, while the staircase is an experimental method to estimate the distribution of this variable. Bootstrap provides a non-parametric method that relies on resampling the observed samples. That is, it uses several empirical distributions to approximate the population distribution. This method fully uses the given observation information without other assumptions of the numerical model and adds any new observations. The critical point of the bootstrap is unordered sampling with replacement. Combined with the staircase method, a bootstrap procedure is proposed in Algorithm 3.2. (N is the number of specimens in a single bootstrap sampling, and M is the number of bootstrap replications).

In order to evaluate the resampling results, the uncertainty factors of the median and standard deviation, δ_m and δ_s, are defined as:

$$\begin{aligned} \delta_m &= \frac{m - m_{ex}}{m_{ex}} \times 100\% \\ \delta_s &= \frac{s - s_{ex}}{s_{ex}} \times 100\% \end{aligned} \tag{3.1}$$

where m and s are the median and standard deviation, subscript "ex" is the value from experimental data.

This bootstrap procedure utilizes multiple samples randomly drawn from experimental test results to make a statistical evaluation of the primary dataset. Several advantages of using bootstrap on the staircase data can be noted. Firstly, compared with the Loo method, the bootstrap can avoid the problem of reducing the data by resampling. Secondly, the bootstrap can also create randomness in the data, which prevents the time-consuming repeated real staircase tests.

3.3.2. Experiment-based hyper-parameter sensitivity analysis

As described in Algorithm 3.2, there are two parameters M and N in the bootstrap method, where N is the number of specimens in a single sampling and M is the number of bootstrap replications. A question is how to find a suitable value for M and N with

Algorithm 3.2: Bootstrap

The staircase dataset including n simples is represented as $X = [x_1, x_2, ..., x_n]$, and the step size is d
Define N as the number of samples in a single sampling and M as the number of bootstrap replications
Find all strain (or stress) levels $L = [l_1, l_2, \dots l]$
Divide X to different part according to different strain (or stress) level l, let $X^l = [x_1^l, x_2^l, ..., x^l]$, that is $X^1 \cup X^2 \cup ...X^l = X$
Pre-define: select randomly a test strain level l
get all test data in strain level l
foreach *i in M* **do**
    Reset staircase dataset $X = [x_1, x_2, ..., x_n]$
    foreach *j in N* **do**
        Sample a data x from X^l randomly
        if *the sampled specimen x is failure* **then**
            $l = l - d$ // the next sample is selected from specimens in lower level
        else
            $l = l + d$ // the next sample is selected from specimens in upper level
        end if
        get all test point in new level X^l
    end foreach
    get sampling results: $\widetilde{X} = [x_1, x_2, ..., x_N]$
    estimate fatigue limit distribution by the same post-processing method
end foreach
get all sampling results: $[\widetilde{X}_1, \widetilde{X}_2, ..., \widetilde{X}_M]$ and corresponding uncertainty factors.

the bootstrap algorithm. Therefore, a sensitivity analysis is carried out to simulate the change in the uncertainty factor with M and N in the range of 10 to 200. The proposed analysis is implemented in Python. To avoid the potential influence of the number of seeds used in the random process, the proposed procedure is run by 5 times with different numbers of seeds. All 5 runs converge to the same result, indicating that the proposed procedure is independent of the random or numerical configurations. A typical result on the change of M and N are shown in the form of heatmaps in Fig. 3.2 and Fig. 3.3.

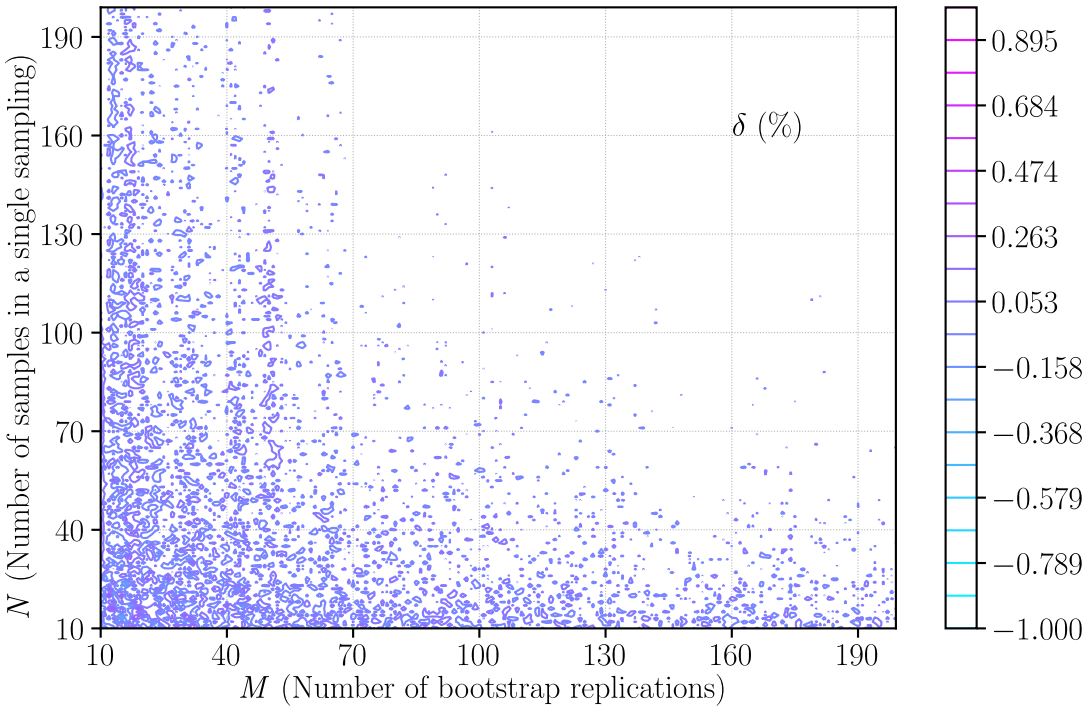

Figure 3.2: Uncertainty factor of the median for different values of M and N

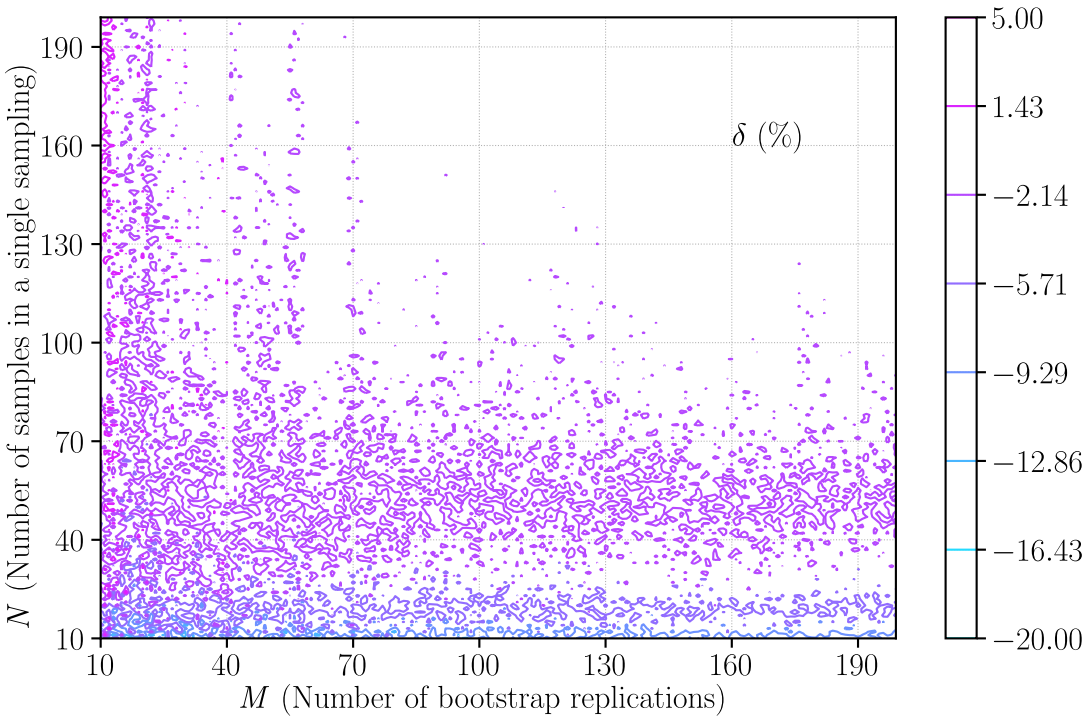

Figure 3.3: Uncertainty factor of the standard deviation for different values of M and N

In Fig. 3.2 and Fig. 3.3, the abscissa is the number of bootstrap replications (M), and the ordinate is the number of samples in a single sampling (N). The content is

uncertainty factors δ_m and δ_s that are scaled as the color bar on the right. It can be seen from the figures that there are blank areas in the upper-right part of the figures, which means the uncertainty factors values become stable with larger M and N. That is, uncertainty factors are not sensitive to M and N after 100 samples. Therefore, the $M = 100$ and $N = 100$ are used in the following analysis.

3.3.3. Results and discussion

The bootstrap was performed 100 times with 100 samples in each sampling. The results are shown in Fig. 3.4. The light blue lines are all bootstrap resampling results, the blue dash represents an average Probability Density Function (PDF) of all sampled data, and the red dash represents PDF of the experimental data.

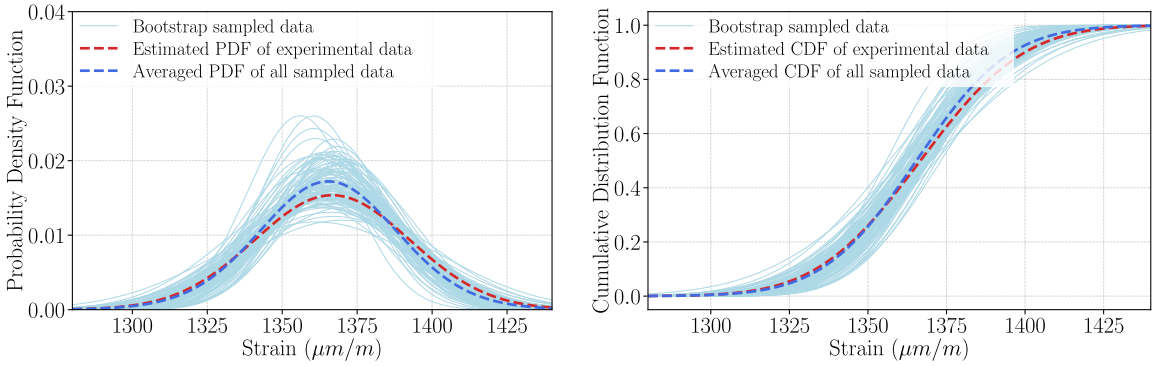

(a) PDF (b) CDF

Figure 3.4: PDF of bootstrap resampling based on the experimental data

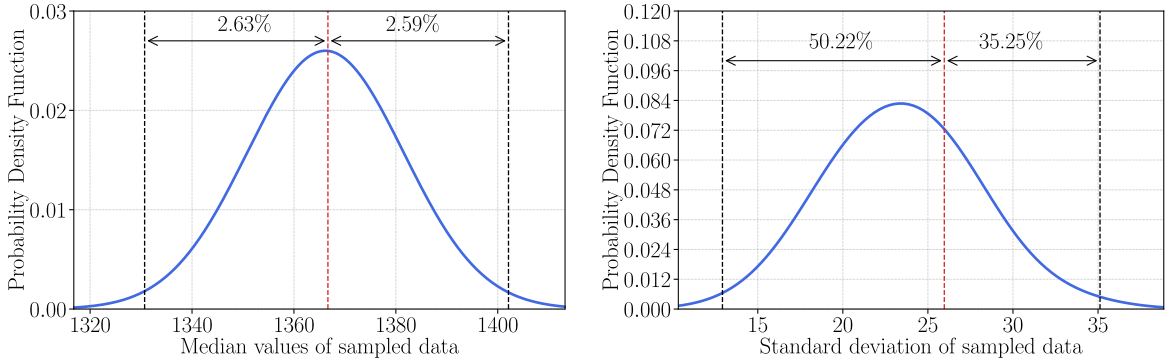

(a) Median values (b) Standard deviation values

Figure 3.5: Median and standard deviation from the bootstrap resampling

Each bootstrap result leads to a median value and a standard deviation value. The distributions of all these 100 median and standard deviation values are shown in Fig. 3.5. The vertical red dashes in Fig. 3.5(a) and (b) represent the estimated

median and standard deviation of the experimental data. The black dashes represent 5^{th} percentile and 95^{th} percentile. We can see that the range of 5^{th} percentile and 95^{th} percentile is no more than 3% for the median value, but it is almost more than 30% for the standard deviation value. The uncertainty for the standard deviation estimation is substantial, and much higher than the median estimation.

3.4. Effect of specimen dimensions

Two other kinds of specimens are used in this section to investigate the frequency and thickness impacts on the fatigue limit uncertainties. The results are also analyzed by bootstrap sampling.

3.4.1. Staircase tests

Three kinds of specimens, including the one described in Chapter 2, have the same specimen shape and reduced section, as shown in Fig. 3.6. The structural difference in thickness and length affects the resonant frequency. The resonant frequencies are obtained from the experimental sine-sweep test of each kind of specimen. The differences in thickness, length and resonant frequency are listed in Tab. 3.1.

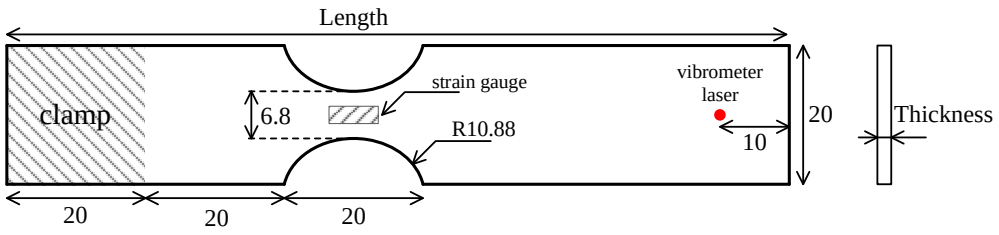

Figure 3.6: Shape of the specimen with the same reduced section (Unit: mm)

Table 3.1: Effect of dimensions on the resonant frequency

Specimen ID	Thickness (mm)	Length (mm)	Resonant frequency (Hz)
S1	1	100	105
S2	2	100	207
S2L	2	170	107

The material (steel DC01), manufacture, surface treatment and experimental environment are identical for these specimens. Using the experimental setup and test

procedures described in Section 2.4, tests on the other two specimens are conducted with strain control. The same step size d=20 µm/m for the staircase method. The test results are detailed in Appendix B, including frequency, cracks, and so on. The up-and-down diagrams for specimens S1 and S2L are shown in Fig. 3.7 and Fig. 3.8, respectively. Similarly to Section 2.4.2.3, the DM method is used to estimate the distribution of staircase results, as shown in Fig. 3.9 and Fig. 3.10. These figures show a difference in fatigue limit between the three kinds of specimens. The estimated distributions of S1, S2 and S2L are represented by orange, blue and pink lines, respectively. The cross marks used in Fig. 3.10 represent the probability of failure for each test strain amplitude.

The means and standard deviations are reported in Tab. 3.2. The fatigue limit medians are different. Indeed, the fatigue limit of S1 is 50.84 µm/m higher than the S2 value, and fatigue limit of S2 is 54.46 µm/m higher than S2L value. Less difference in the estimated standard deviation is observed.

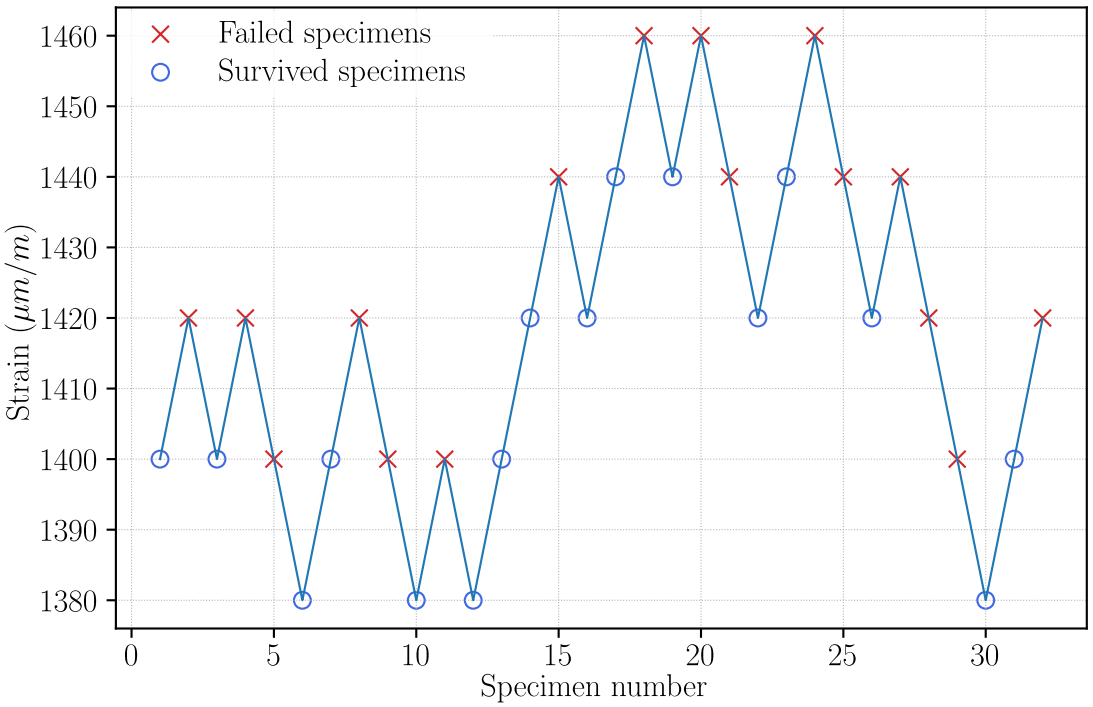

Figure 3.7: Up–and–down diagram for specimen S1

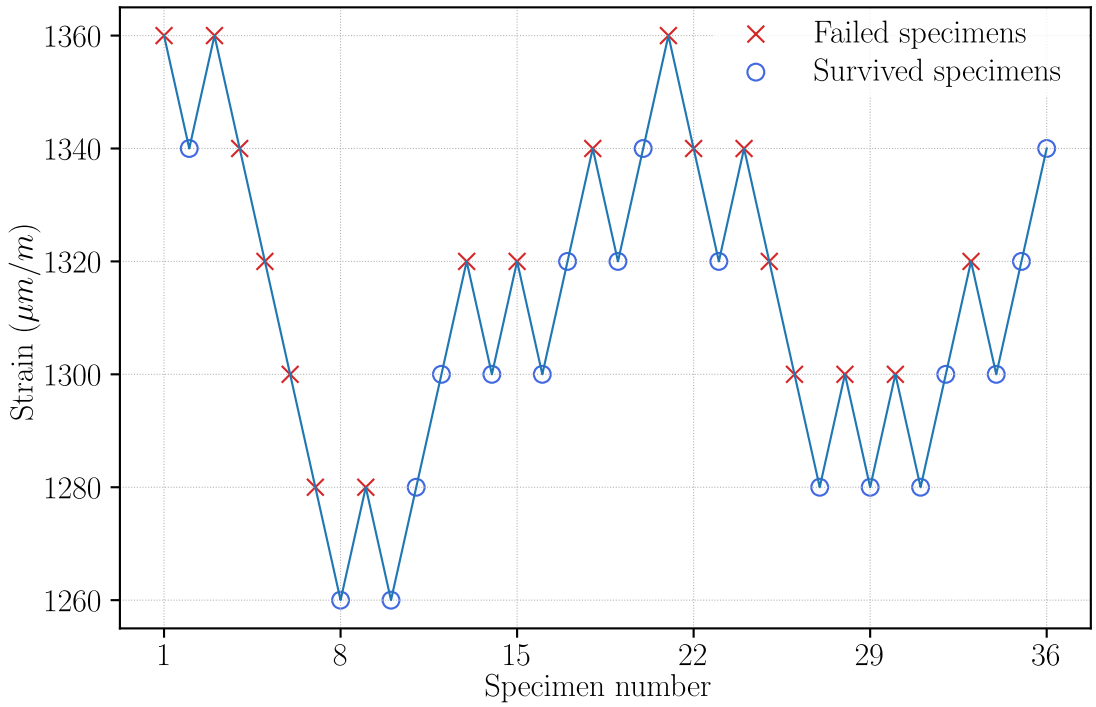

Figure 3.8: Up–and–down diagram for specimen S2L

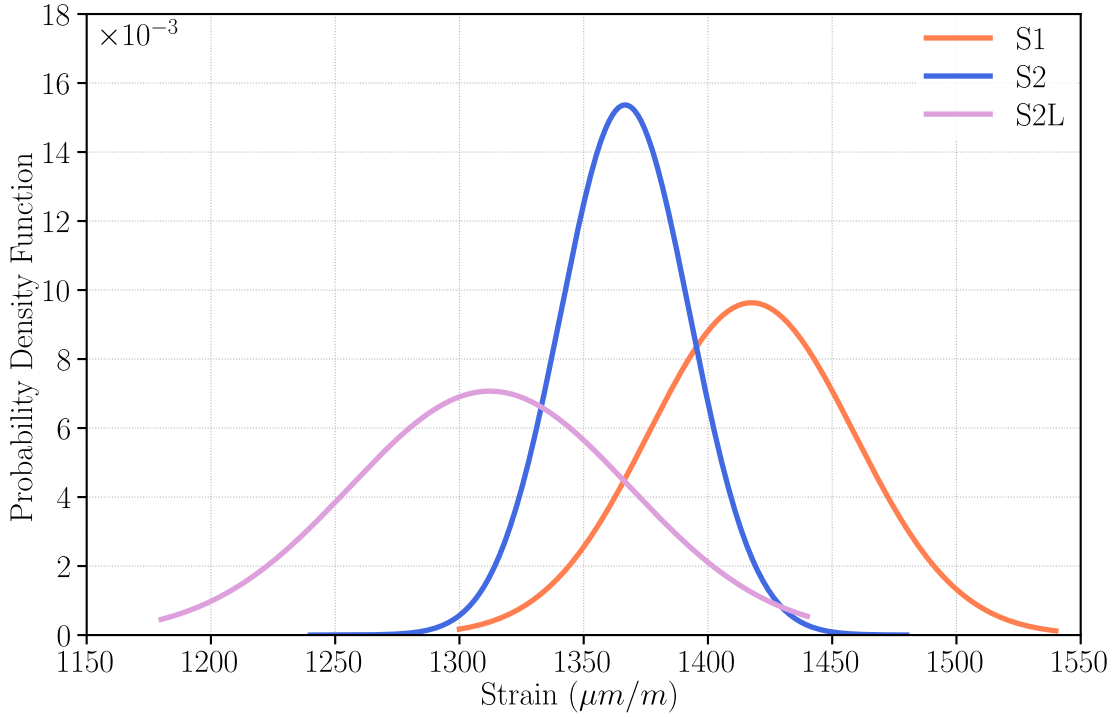

Figure 3.9: Fatigue limit PDFs obtained for the three kinds of specimens

Based on these different results, the bootstrap is used in the next section to analyze the uncertainties.

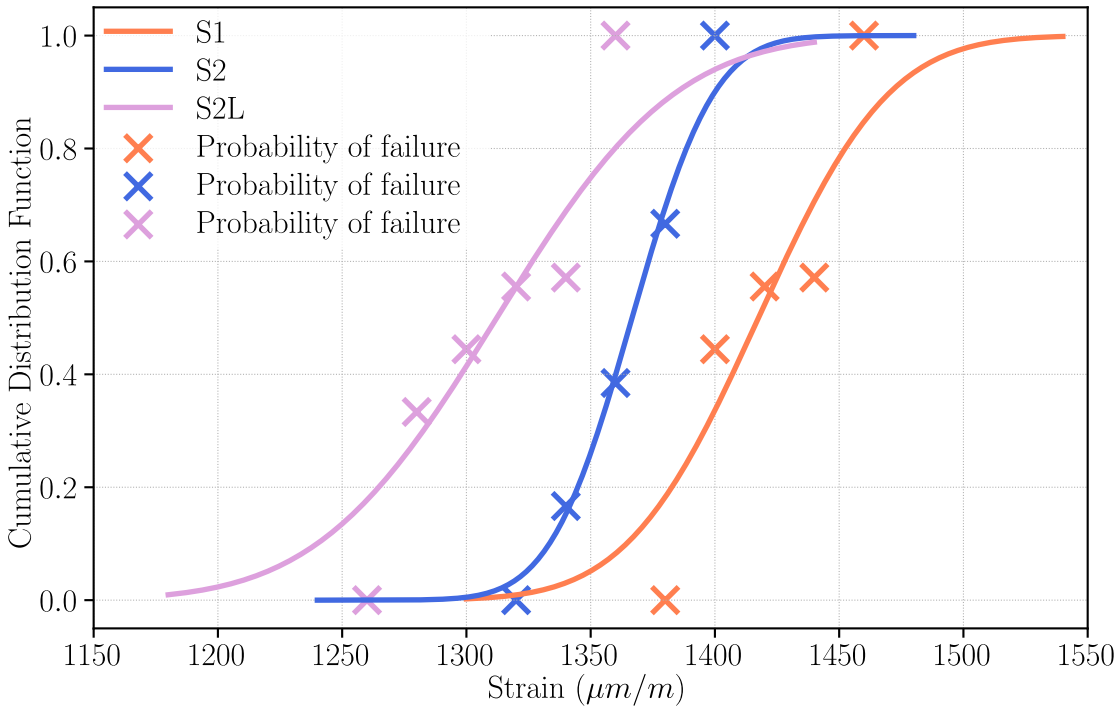

Figure 3.10: Fatigue limit CDFs obtained for the three kinds of specimens

Table 3.2: Comparison of median and standard deviation (with DM)

Specimen ID	Thickness (mm)	Length (mm)	Resonant frequency (Hz)	Median (m)	Standard deviation (s)
S1	1	100	105	1417.51	41.41
S2	2	100	207	1366.67	25.96
S2L	2	170	107	1312.21	56.43

3.4.2. Application of the bootstrap sampling

Choosing $N = 100$ and $M = 100$, the bootstrap results obtained for the three kinds of specimens are shown in Fig. 3.11. The thick lines represent the distribution estimated from the experimental data by DM method. The thin lines represent distributions estimated from the bootstrap data. In order to compare the overlapping of the three clusters of PDF, the median values of all sampled results are marked as pentagon, star and circle, respectively. From this figure, we can see that there is no overlap between the three PDFs. We relied on the literature. In this study, the specimens have two main differences: loading frequency (due to the change in the length of the specimens) and geometry dimensions, such as the thickness of the cross-section and the length.

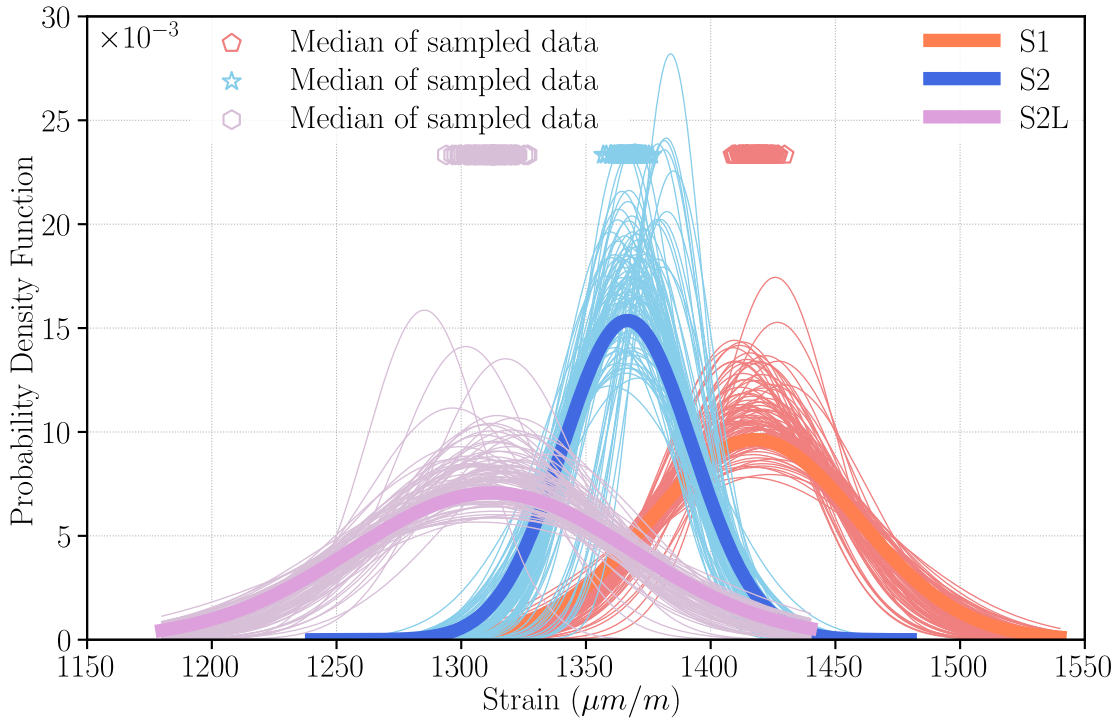

Figure 3.11: Bootstrap sampling applied to the three kinds of specimens

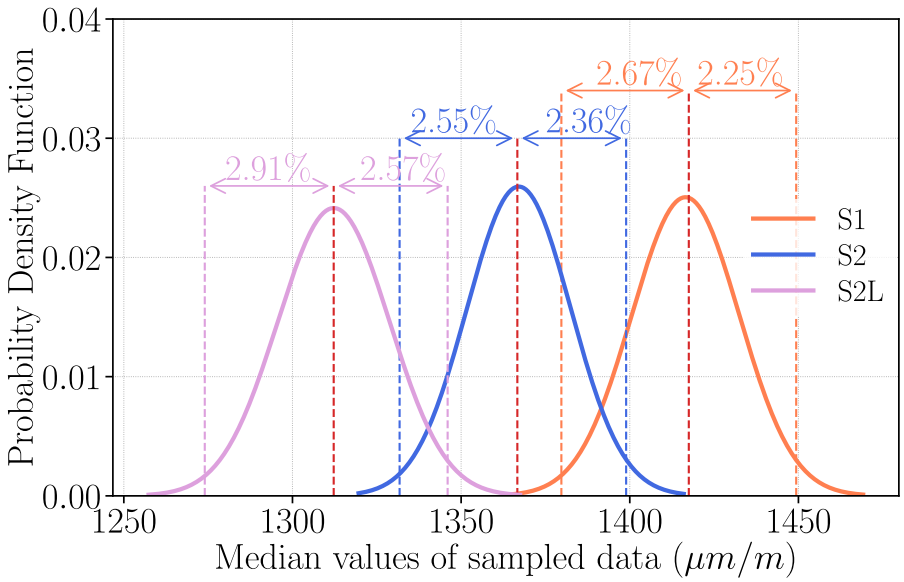

Figure 3.12: Distributions of median from the bootstrap results of S1, S2, and S2L

Based on all the resampled results in Fig. 3.11, the distributions of all these median and standard deviation values from different specimens are shown in Fig. 3.12 and Fig. 3.13.

In Fig. 3.12 and Fig. 3.13, the vertical red dashes represent the estimated median and standard deviation of the experimental data, other vertical dashes represent 5^{th} percentile and 95^{th} percentile of each kind of specimen. Similar to the observations

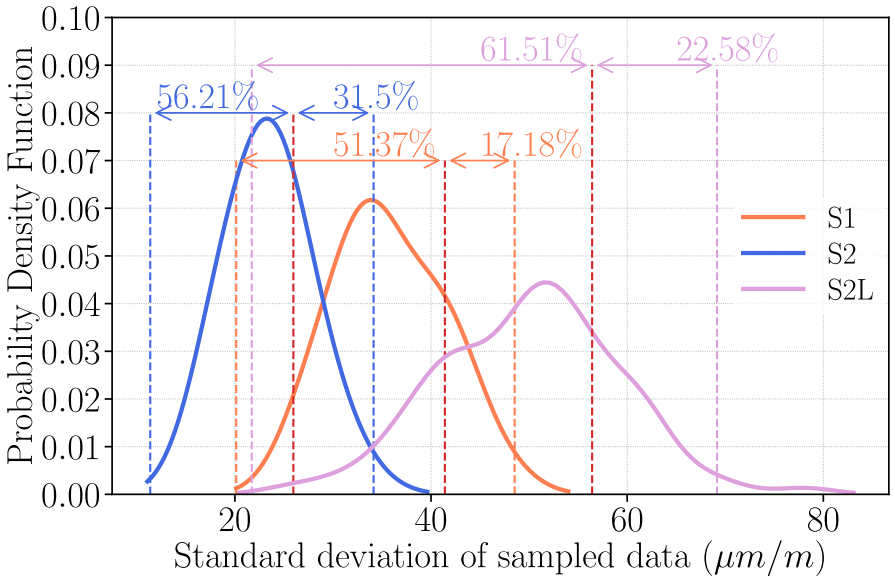

Figure 3.13: Distributions of standard deviation from the bootstrap results of S1, S2, and S2L

from Fig. 3.5, the uncertainty for the standard deviation estimation is much higher than the median estimation. From Fig. 3.13, it can be found that the bootstrap results always have a more significant deflection on the left of the experiment result (red dash). It is proof that the estimation of the standard deviation is systematically less accurate and lower than the true value [98].

Regarding frequency effect, Tsutsumi et al. [99] highlighted the frequency effect by comparing the fatigue tests at 20 kHz and 10 Hz. The stress-strain curves also highlighted this effect at a relatively high strain rate by Khalij et al. [61]. However, the excitation frequency (when less than 200Hz) has little effect on the fatigue limit, according to the research of Dallali et al. [100] and Tsutsumi et al. [99].

In our opinion, it is the combination of several parameters that affect the fatigue limit, especially since the tests were carried out in vibration. The biggest difference here is seen when a change in length and thickness is combined (comparison between S1 and S2L). It could therefore highlight the effect of bending stress gradient. Indeed, Narumoto et al. [101] considered that the difference in bending stress gradient is one of the causes of the size effect. They also showed that the stress intensity factor increases with thickness, resulting in faster crack growth. Narumoto et al. [101] and Bhuyan et al. [102] showed that the fatigue strength decreases with increasing thickness. However, the authors studied plates with greater thicknesses. In another work, Bhuyan et al. [102] found that the proportion of total fatigue life spent in crack initiation increases with the thickness decrease. They pointed out that the strain rate, induced by the thermally activated movement of dislocations in the ferritic microstructure of low carbon steel, has an effect on the fatigue limit.

3.5. Conclusion

This part presents an evaluation of statistical uncertainty in the staircase test for fatigue limit based on resampling methods. To avoid repetition of the real staircase tests, a Loo and the bootstrap procedure is used to produce more artificial staircase data based on one staircase test. Experimental staircase data from the vibration bending fatigue test on DC01 steel specimens were analyzed.

From the resampling results, the obtained conclusions could be listed as follows:

(1) Loo method can be used to judge if the number of specimens is sufficient in a staircase test.

(2) To get a steady result, it is necessary to use $N \geqslant 100$ specimens and conduct $M \geqslant 100$ times of staircase test.

(3) The results from bootstrap resampling show that the standard deviation of fatigue limit is more dispersive with more than 20%, leading to a conclusion that it should be conservative to use staircase results in fatigue design.

However, variability in the fatigue experiment test is unavoidable. Several main factors are involved in the scattering of fatigue test results. Some of these have been addressed by Murakami et al. [10]. Due to this considerable uncertainty in standard deviation estimation, the improvement to the staircase method from post-processing is conducted in the next chapter.

Chapter 4
A non-parametric evaluation method in staircase test for improving fatigue limit assessment

The previous works provided experimental staircase test results and the uncertainties of the result. The estimation of uncertainties cannot be obtained directly by experimental tests because it requires many specimens and time. Under this, a numerical post-processing method is needed. In this chapter, a new evaluation method based on Kernel Density Estimation (KDE) is proposed to estimate the fatigue limit distribution from staircase tests without prior knowledge. This chapter aims to summarize the methods, improve the estimation performance, and validate KDE effectiveness by comparing it to other evaluation techniques.

The first section presents a brief survey of existing statistical methods for staircase data. Then a novel non-parametric method was proposed based on KDE. A simulation-based investigation was performed to compare the effectiveness of the proposed method to other evaluation methods in the following section. The obtained results in the third section reveal that the proposed technique offers a better estimate of the median, the standard deviation and the probability distribution of the fatigue limit. The non-parametric method applied to experimental data is presented in the fourth section. The work of this part has been published in Probabilistic Engineering Mechanics [103].

4.1. Background

4.1.1. Existing evaluation techniques

As described in Chapter 1, the staircase test method [27] is commonly involved in characterizing the fatigue limit distribution. However, several researchers have investigated ways to improve the accuracy of the fatigue limit estimation by improving evaluation techniques in post-processing. Müller et al. [40] compared several evaluation techniques through Monte-Carlo simulation for evaluating experimental results. However, the fatigue scatter is still strongly dependent on step size. This background is introduced in detail in following.

The inadequacy of standard deviation estimation on staircase tests has received considerable attention in the literature. Several evaluations techniques [23, 38, 40, 42, 54] have been proposed since the first development of the staircase method. Tab. 4.1 highlights some notable methods in recent years.

Table 4.1: Overview of existing evaluation techniques for staircase testing

Methods	Algorithms	Prior Distribution	Remarks
Dixon-Mood method [27] (DM)	MLE	Normal	- Simplification - Recommended by ISO standard [35] - Strong dependence on step size
Svensson-Lorén [38] correction on DM			- Function of sample size
Braam-Zwaag [104] correction on DM			- Function of sample size and step size - Worse estimation with small sample size
Pollak's [38] correction on DM			- Function of sample size and step size
Bootstrap [38, 98]			- Reduce the estimation uncertainty - Increase in the amount of computation
MLE with censored data [40]	MLE	Yes	- Classical method
Correction on MLE [39]			- Function of sample size - Valid only for logarithmic standard deviation
Zhang-Kececioglu [105] method (ZK)	Suspended item and MLE	Yes	- Applicable to variable step size - Worse than DM in the negative skew distribution [23] - Underestimate the standard deviation[23] - Overestimate evaluation on mean [24]
Generalized MLE [24]	S-N curve and MLE	Yes	- Incorporate fatigue life in likelihood function - Paired failure-survival specimens
Wallin's [42] method	Binomial Probability(BP) and MLE	Use BP to select distribution	- Binomial Probability to fit staircase data - Strong dependence on step size
IABG [40] method	MLE	Normal or Lognormal	- Based on logarithmic values of data - All specimens are evaluated - discarded invalid data, add fictitious data
Deubelbeiss' [40] method	Probability of failure	No	- Fitting from probabilities of failure - Large bias in estimation

As the author of the staircase test method, Dixon et al. [27] proposed the Dixon-Mood (DM) method based on Maximun Likelihood Estimation (MLE). However, several studies reveal that this evaluation technique gives a reasonable estimation of the mean value but underestimates the standard deviation of the fatigue limit. To address this bias, some researchers enlarged the DM estimation on the standard deviation by correcting factors. Svensson [20] proposed a correction function with number of specimens as variable, Braam et al. [104] used a correction function with number of specimens and step size but has been proved worse estimated with small sample size. Pollak et al. [38] improved the estimation by a non-linear function. For tests with a small number of specimens, Pollak [98] suggested combining the bootstrap sampling technique with correcting factors to get a better estimate.

An alternative usage of MLE in post-processing staircase data is to use the censored data [39, 40, 56] with or without a correcting function on the standard deviation bias. Meanwhile, other research has introduced statistical techniques into the staircase data processing. Wallin [42] proposed an evaluation method based on binomial probability to analyze staircase data, whereas the method yields an acceptable estimation only when the staircase test step size is close to the real value of the standard deviation. Zhao et al. [24] developed a general maximum likelihood approach (GMLA) to assess the fatigue limit by constructing physically paired local S-N relations for all failure or survival specimens from staircase tests. The IABG (Industrieanlagen-Betriebsgesellschaft) method [40] provides an estimator by omitting invalid test results and adding fictitious data. From the simulation study [40], the differences between the IABG and MLE methods are negligible. Other methods such as Zhang-Kececioglu method (ZKA) [105] have no inherent improvement in standard deviation estimation and have been proven to perform less than MLE [40, 47]. Deubelbeiss' method is deduced from the regression of the failure probability, but leads to a significant bias on the standard deviation [40].

To sum up, firstly, most of the proposed statistical analysis methods are based on the MLE. Therefore, these methods have to make assumptions about the underlying distribution ineluctably. Secondly, these evaluation techniques lead to different accuracy, more or less correct. However, the drawback of the strong dependence on the step size still exists. Among all these kinds of evaluation techniques, the MLE and the DM method are generally accepted by researchers. Thus, these two methods are used as references in this work. The simulation on DM and MLE are illustrated in Appendix C and Appendix D respectively.

4.1.2. Dixon-Mood method and corrections

The DM method was proposed by Dixon and Mood [27] in 1948, which provides approximate formulas of maximum likelihood to estimate the mean and the standard deviation. It assumes that the fatigue limit should follow the Normal distribution. Only the less frequent events, failure or survival, are used to evaluate the distribution. The stress amplitude span is split by a step size d into several load levels numbered by j, where $j = 0$ stands for the lowest load level and j_{max} stands for the maximum stress level. Denoting by $n_{c,j}$ the number of the fewer frequency events (survival or failure) at the load level j, two auxiliary values A and B can be calculated by Eq. 4.1:

$$\begin{aligned} A &= \sum_{j=0}^{j_{max}} j \times n_{c,j} \\ B &= \sum_{j=0}^{j_{max}} j^2 \times n_{c,j} \\ n_c &= \sum_{j=0}^{j_{max}} n_{c,j} \end{aligned} \tag{4.1}$$

The auxiliary values are used to estimate the median value m_{DM} with Eq. 4.2 and the standard deviation s_{DM} with Eq. 4.3. The minus sign given in Eq. 4.2 is used if the failed specimens are evaluated and otherwise, the plus sign is applied.

$$m_{DM} = S_{a,0} + d\left(\frac{A}{n_c} \pm \frac{1}{2}\right) \tag{4.2}$$

$$\begin{aligned} s_{DM} &= 1.62 \times d\left(\frac{Bn_c - A^2}{n_c^2} + 0.029\right) \quad \text{if} \quad \frac{Bn_c - A^2}{n_c^2} \geqslant 0.3 \\ s_{DM} &= 0.53 \times d \qquad\qquad\qquad\qquad\quad \text{if} \quad \frac{Bn_c - A^2}{n_c^2} < 0.3 \end{aligned} \tag{4.3}$$

As listed in Tab. 4.1, some corrections to the DM method have been proposed to reduce the effect of the step size. The simulation on DM in Appendix C proved that the correction factor (Eq. 4.4) proposed by Svensson-Lorén (SL) [38] gives a better improvement to the standard deviation estimation:

$$s_{SL} = \frac{n}{n-3} \times s_{DM} \tag{4.4}$$

Therefore, the SL correction is used as a reference method in this simulation-based investigation.

4.1.3. Maximum Likelihood Estimation method

The Maximun Likelihood Estimation (MLE) provides an appropriate tool for solving the general problem of estimating the "best fit" line through censored test data. Thus, the resulting estimates are those that agree most closely with the observed data. MLE gives a more precise estimate than any other methods, and is adaptive. It can be used for any kind of method with any type of distribution. Its main drawback is that the likelihood function has a different form for each specific distribution.

The purpose of the MLE method is to use the known sample results to infer the most likely, in other words, the maximum probability parameter values that lead to such results. When the stress amplitude S_a of the staircase test is known, the failed and survived specimens give information about the probability:

$$\begin{aligned} \mathrm{P}(x > S_a) &= 1 - F(S_a) \\ \mathrm{P}(x \leqslant S_a) &= F(S_a) \end{aligned} \tag{4.5}$$

where $F(\cdot)$ denotes the Cumulative Density Function (CDF).

Let $n_{f,j}$ be the number of failures and $n_{s,j}$ be the number of survivals at the stress level $S_{a,j}$, the maximum likelihood function L is given by:

$$\mathrm{L} = \prod_{j=0}^{j_{max}} F(S_{a,j})^{n_{f,j}} \left(1 - F(S_{a,j})\right)^{n_{s,j}} \tag{4.6}$$

The maximization of L results in the estimation of probability distribution parameters. Although an assumption about the underlying distribution is required when performing the MLE method, this method can deal with the non-Normal distribution of the fatigue limit and is also widely used in the literature [40]. The simulation study of MLE method is presented in Appendix D.

4.2. Non-parametric evaluation method and simulation procedure

In order to improve the standard deviation estimation on fatigue limit for small sample tests, an evaluation technique based on Kernel Density Estimation (KDE) and non-linear correction is proposed in this work to post-process staircase tests. The KDE was applied to estimate the fatigue limit from experimental staircase tests by the authors [58]. The current work focuses majorly on:

— Implementation of a parameter-free estimator resulting in an accurate estimation of both the median and the standard deviation of the fatigue limit.

— Effectiveness of the proposed method is less dependent on the test parameters from the staircase method, especially the step size.
— Probabilistic fatigue limit estimation without prior knowledge of the fatigue limit distribution.

4.2.1. Non-parametric fatigue limit estimation

As a non-parametric method to estimate the PDF of random variables, KDE has been proven to be suitable for post-process experiment data like staircase tests [106]. Compared to other post-processing methods reviewed in the previous section, the KDE method has the advantage of being non-parametric and non-required on the prior knowledge of the underlying distribution. In the case of staircase tests, Dixon [37] pointed out that the load levels fluctuate around the median value of the fatigue limit. The fatigue limit can be considered as a random variable. Based on the staircase experiment rules, the ratio between the number of specimens at each load level and the total number of specimens represents the probability of the fatigue limit at this load level. The greater the number of specimens is, the higher the probability of the fatigue limit occurring, i.e., (Eq. 4.7):

$$P\{x = S_f\} \propto \frac{n_j}{n} \tag{4.7}$$

where, S_f is the fatigue limit, n_j is the number of specimens at the load level j and n is the total number of specimens (or samples). Let a random data set $\mathbf{X} = \{x_1, x_2, ..., x_n\}$ in the probability space χ, denote all the load amplitudes in the staircase test, the PDF of the fatigue limit distribution estimated by KDE is:

$$\hat{f}_h(x) = \frac{1}{nh} \sum_{i=1}^{n} \mathrm{K}\left(\frac{x - x_i}{h}\right) \tag{4.8}$$

where, $h > 0$ is a smoothing parameter called bandwidth, K is the non-negative kernel function using the standard Gaussian Kernel [107] defined as:

$$\mathrm{K}(u) = \frac{1}{\sqrt{2\pi}} \exp\left(-\frac{u^2}{2}\right) \tag{4.9}$$

Eq. 4.9 is applied to each sample from staircase tests. The PDF of all samples is then estimated by the sum of these kernel densities on every data point. The KDE estimator does not distinguish between specimens with and without failure. To optimize the performance of KDE in fatigue limit estimation, we compared different bandwidth (h) methods of KDE as described in the next section.

4.2.2. Bandwidth selection

In KDE method, a smoothing parameter (a.k.a. bandwidth h) is required to control the smoothing scale and the density estimation of the underlying distribution [108]. Several methods have been proposed to optimally select this hyperparameter [109, 110].

If the Gaussian kernel function is used to approximate data for an underlying Gaussian distribution, Scott's rule (Eq. 4.10) and Silverman's rule (Eq. 4.11) are two efficient ways:

$$h_{SC} = \left(\frac{4s^5}{3n}\right)^{1/5} \approx 1.06 \times sn^{-1/5} \tag{4.10}$$

$$h_{SI} = 0.9 \times \min(s, IQR/1.35)n^{-1/5} \tag{4.11}$$

where, n is the number of samples, s is the standard deviation of the data and IQR is the interquartile range. In addition, some research applied the Sheather-Jones method which reintroduces a non-stochastic term to reduce bias in estimation without inflating variance [111]. The Sheather-Jones method is more suitable for processing multimodality distribution.

These data-based methods give a variable bandwidth and it is challenging to delimit whether it fits the staircase data. Consider the DC01 staircase experimental data (in Section 2) as an example, the estimated PDF from SC (Scott), SI (Silverman), SJ (Sheather-Jones) bandwidths are shown in Fig. 4.1.

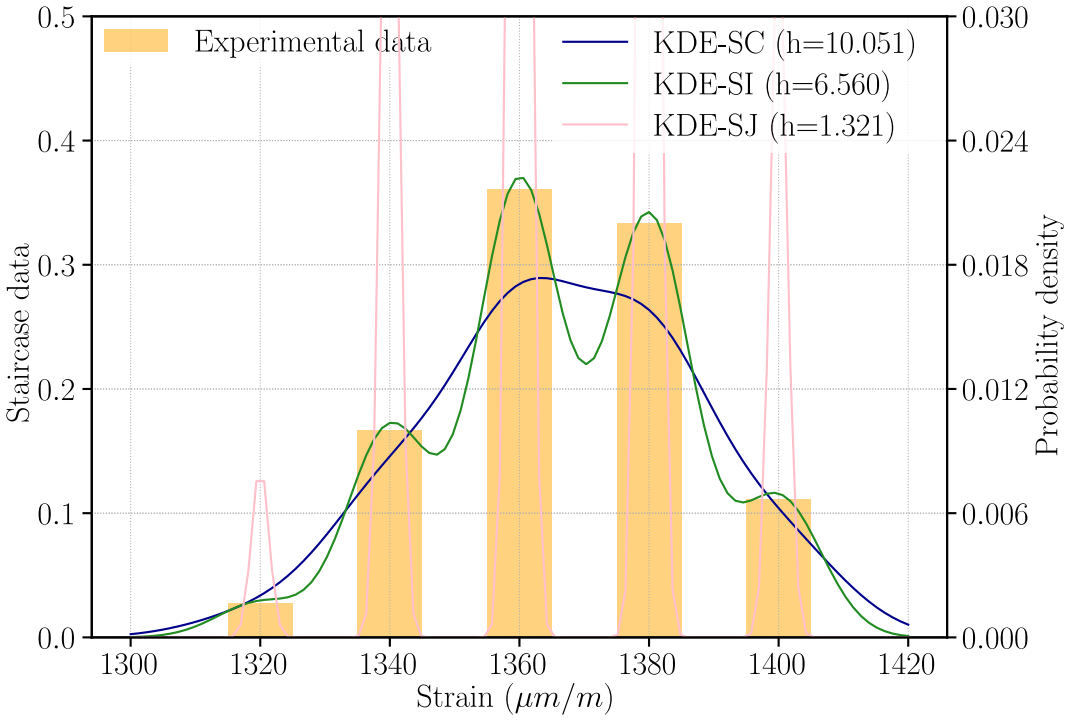

Figure 4.1: Estimated PDF from different bandwidths (SC: Scott; SI : Silverman; SJ: Sheather-Jones)

With the left y-axis in Fig. 4.1, the orange bars represent staircase experimental data at five strain levels. The right y-axis corresponds to the estimated PDF from SC, SI, SJ bandwidths, with the value of the bandwidth listed in the right legend. It should be noted that the fatigue limit distribution should be subject to flat unimodal distribution because we only consider one mode of failure. Nevertheless, these four kinds of bandwidth all give non-smooth distributions. Comparatively, SC uses the largest bandwidth and only one peak in PDF. Conversely, SJ method uses the smallest bandwidth and produces extreme multi-peaks PDF curve. SI and Normal-reference method also leads to obvious multipeaked distribution. SC is only one bandwidth selector that leads to one peaked distribution but still has signs of multimodality. In order to make the estimated distribution consistent with the physical meaning of fatigue, this study try to enlarge the coefficient in SC equation (Eq. 4.10) based on MCS. For optimizing the bandwidth, the corrected equation based on SC is shown as:

$$h_{opt} = \alpha \times \left(\frac{4s^5}{3n}\right)^{\frac{1}{5}} \tag{4.12}$$

where α is the coefficient that adapted to Scott's rule. The simulation study on how to adjust the parameter is presented in Section 4.3.2, and $\alpha = 1.15$ is determined in the end.

Based on experimental data, the KDE estimation with Scott's rule, given in

Eq. 4.10 and the improved bandwidth given in Eq. 4.12 are shown in Fig. 4.2. It is obvious that the improved bandwidth leads to a smooth estimated PDF.

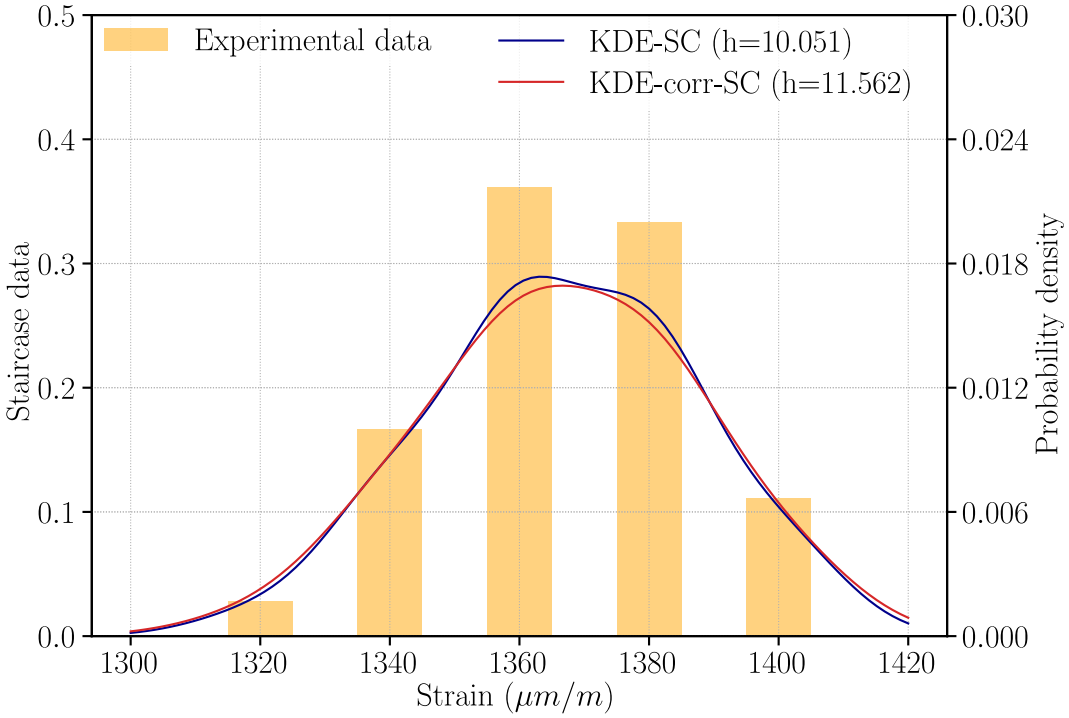

Figure 4.2: Estimated PDF from different bandwidths

4.2.3. Bias correction on fatigue limit standard deviation

Since it is known that linear correction enlarges the estimation uncertainty [38], this study developed a nonlinear approach to reduce the standard deviation bias as follows:

$$\begin{cases} s_{KDE} = \left(\frac{s}{d} + As\right)^c & \text{if} \quad s > d \\ s_{KDE} = \left(\frac{s}{d} + Bs\right)^c & \text{if} \quad s \leqslant d \end{cases} \tag{4.13}$$

where, s is the standard deviation from KDE with optimized bandwidth, s_{KDE} is the corrected standard deviation. This study proposes this formula based on correction equations in the literature. Some of them are introduced and simulated in Appendix C. The coefficients A, B and c, shown in Tab. 4.2, are correction coefficients depending on the coefficient of variation (CV).

Tab. 4.2 was determined by simulation tests as described in the following Section 4.3.1. In order to correct the estimated standard deviation s close to the initial true standard deviation, we carried out lots of tests to determine the coefficients A, B,

Table 4.2: The coefficients used in the correction equation (Eq. 4.13)

CV	A	B	c
0.0125	13	7	0.44
0.025	13	7	0.53
0.05	13	7	0.59

and c with respect to different values of CV, like Fig. 4.10. In this study, the coefficient of variation (CV) is expressed as the ratio of the standard deviation to the mean:

$$\mathrm{CV} = \frac{s}{\mu} \tag{4.14}$$

The proposed KDE-based fatigue limit estimation with bias correction is expressed by the pseudo-code in Algorithm 4.1.

Algorithm 4.1: Non-parametric fatigue limit estimation method

Data: The staircase dataset: $\mathbf{X} = \{x_1, x_2, ..., x_n\}$, the step size: d

1 Calculate the bandwidth h by Scott's rule;

2 (m, s) from KDE with bandwidth h ;

3 Correction to s ;

Result: The estimated median m and the estimated standard deviation s of the fatigue limit distribution

4.3. Numerical validation of the proposed evaluation method

4.3.1. Simulation procedure

In order to evaluate the effectiveness of the proposed method, a numerical simulation modeling the staircase test was practiced. The staircase simulation is configured as shown in Fig. 4.3. Similar simulation procedure and result evaluation to Reference [39] were conducted in this work, but more distributions and coefficients of variation were investigated.

Firstly, a simulated fatigue limit distribution was initialized by a distribution model and a coefficient of variation (CV) selected by the authors. Since the mean value μ_0 was considered constant in this study, CV controls the standard deviation of the fatigue limit s_0 directly. The simulated fatigue limit distribution is then generated by the mean value μ_0 and the standard deviation s_0 with different distribution models, including Normal, Lognormal and Weibull distributions. In this step, the

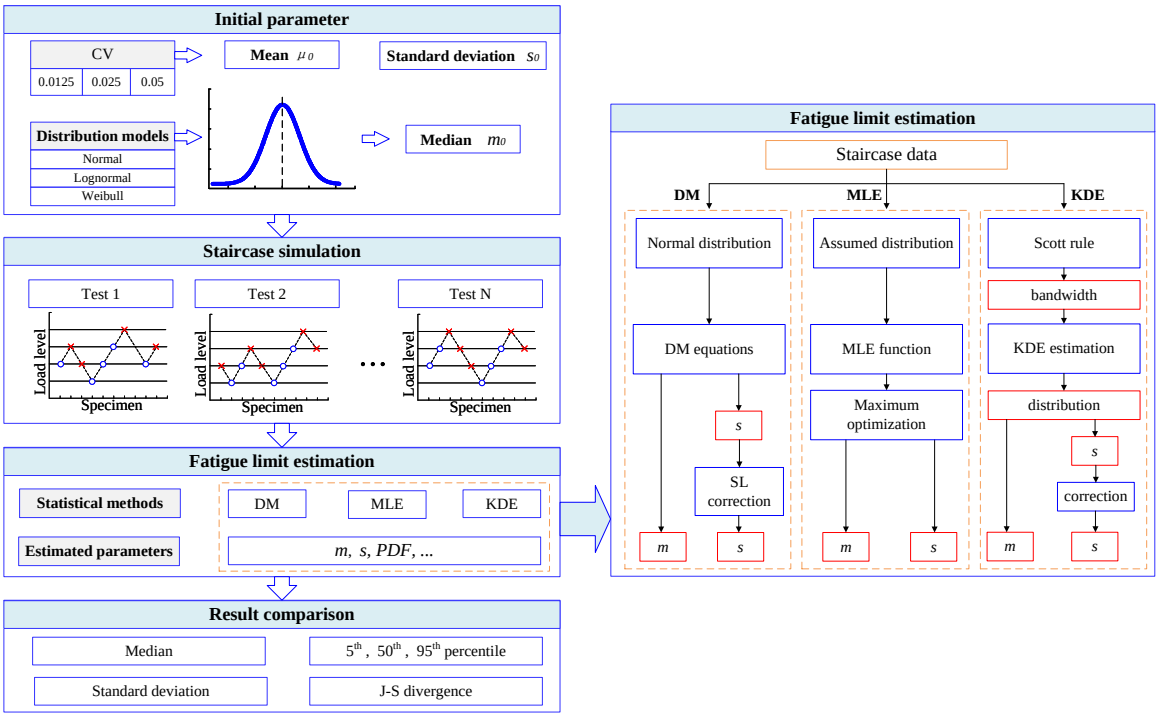

Figure 4.3: Simulation procedure and evaluation for results

mean is arbitrarily fixed at $\mu_0 = 400$, and the standard deviation is controlled by CV (CV=0.0125, 0.025, 0.05). These three values selected in this study come from Roué et al. [39] and previous experimental data. Then, the distribution was constructed by mean ($\mu_0 = 400$) and standard deviation ($s_0 = \text{CV} \times \mu_0$). The shape, location and scale parameters were calculated from the mean and standard deviation. However, as pointed out by Müller et al. [40] and Roué et al. [39], the fatigue limit estimated from the staircase test represents the median threshold with a failure probability of 50%. Consequently, the median value and the standard deviation were used in this work to describe the fatigue limit distribution. The mean value (μ) and the standard deviation (s) can be calculated by the discrete PDF as Eq. 4.15. The median (m) can be obtained from the discrete CDF with cumulative probability 50%.

$$\begin{aligned} \mu &= \sum_{i=0}^{max} x_i P(x_i) \\ s^2 &= \sum_{i=0}^{max} \frac{(x_i - \mu)^2 P(x_i)}{\sum_{i=0}^{max} P(x_i)} \end{aligned} \tag{4.15}$$

where i is ordinal number, x_i is random variable, $P(x_i)$ is the probability density of variable x_i.

Secondly, in the numerical simulation, the specimens were generated successively with respect to the staircase method. For the i^{th} specimen, a value (a.k.a. fatigue limit of i^{th} specimen) was randomly extracted from the fatigue limit distribution set

in the initialization step. All random processes involved in the work are practiced by "scipy.stats.rv_continuous" class from SciPy package [112]. This value was then compared to the load level (a.k.a. applied stress amplitude) of the i^{th} specimen. Just as in experimental tests, the specimen is donated as "survival" if the applied stress amplitude is below the fatigue limit, otherwise, the specimen is donated as "failure". The survival/failure state of the i^{th} specimen determines the stress amplitude that will be applied to the $(i+1)^{th}$ specimen. Then, the step size between load levels is fixed to a constant d. In other words, if the i^{th} specimen is survival at the load level S_a^i, the stress amplitude S_a^{i+1} for the $(i+1)^{th}$ specimen equals to $S_a^i + d$. Contrarily, if the i^{th} specimen is failure, the stress amplitude S_a^{i+1} for the $(i+1)^{th}$ specimen equals to $S_a^i - d$. As for the initial specimen (i.e., $i = 1$), the load level $S_a^{i=1}$ is set at the mean fatigue limit μ_0 of the given distribution. The above steps are repeated until enough specimens of n are generated. With the consideration of reducing the effect of starting load level, n is the nominal sample size [37, 47] in this study, which means that the tests are only valid after the first pair of tests with opposite results..

Thirdly, all results obtained from the staircase simulation are post-processed by three different evaluation techniques, including KDE, MLE and DM, as compared on the right side of Fig. 4.3. Each post-processing method estimates the median value m_k, standard deviation s_k and probability distribution for the k^{th} staircase test with $k = 1, \cdots, N$.

In order to evaluate the effectiveness of post-processing methods in fatigue limit estimation, five cases were constructed by combining a probability distribution with a CV. For each study case, a total number of $N = 1000$ trials [39] were performed to investigate the quality of the estimates with respect to the number of specimens $n \in 10, 15, 20, 25, 30, 35, 40, 50, 70, 100$ and the normalised step size $d \in 0.1, 0.2, \cdots, 2$ listed in Tab. 4.3. The evaluation methods and simulation variables are to be assigned to each case.

Table 4.3: Parameters in simulation work

	Probability Distribution	CV	Evaluation method	Variable	Result
Case 1	Normal	0.025	KDE MLE DM	n = 10 to 100 d/s_0 = 0.1 to 2	(m_k, s_k) for $k = 1, \cdots, 1000$
Case 2	Normal	0.0125			
Case 3	Normal	0.05			
Case 4	Lognormal	0.025			
Case 5	Weibull	0.025			

In most researches, the fatigue limit distribution is assumed to be the Normal distribution by default [27, 42]. However, the probability distribution shape may have little effect on the fatigue limit mean estimate but its tail is important for estimating

the dispersion [39]. Some recent studies have revealed that the distribution shape of the fatigue limit is not symmetric [113] and have suggested the usage of Lognormal distribution [40, 41, 56]. Moreover, the Weibull distribution was also proved to be a suitable estimation for the fatigue limit standard deviation [39, 45, 114]. Hence, these three probability distributions (i.e., Normal, Lognormal, and Weibull) are applied in this work to study the usability of the proposed KDE-based evaluation method. The CV value close to 0.0125 obtained in the experimental staircase tests carried out by Shi et al. [58] is used in this work. Meanwhile, Roué et al. [39] proposed to investigate the CV of 0.025 and 0.05 in the simulation-based staircase test. These three values are accordingly investigated with the Normal distribution in cases 1 to 3, since it is the only probability distribution that can be estimated by all evaluation methods, namely DM, MLE and KDE methods. To analyse the effect of the underlying probability distribution, the CV was fixed to 0.025 by the authors in cases 4 and 5. Only the MLE and KDE methods were applied to perform the estimation of the fatigue limit distribution in these cases, since the DM method assumes that the fatigue limit should be a Normal distribution [27].

The evaluation of the estimate quality is carried out by normalising the estimated median value m_k and the estimated standard deviation s_k to the true median value m_0 and the true standard deviation s_0 of the given probability distribution, respectively. The 5^{th}, 50^{th} (a.k.a. median), and 95^{th} percentiles were also estimated by the post-processing method and were used to evaluate the robustness of the compared method performance. In addition, the Jensen–Shannon divergence [115], denoted as D_{JS}, was used as a measure of difference between the estimated probability distribution and the true probability distribution:

$$D_{JS}(\hat{P}||Q) = \frac{1}{2}D_{KL}(\hat{P}||M) + \frac{1}{2}D_{KL}(Q||M) \text{ with } M = \frac{\hat{P}+Q}{2} \tag{4.16}$$

In Eq. 4.16, $\hat{P}$ denotes the estimated probability distribution from DM, MLE or KDE(Eq. 4.8) method. Q denotes the true distribution initialized in the first step of the simulation (Fig. 4.3). D_{KL} is Kullback–Leibler divergence that defines the relative entropy from Q to $\hat{P}$ in probability space χ:

$$D_{KL}(\hat{P}||Q) = \sum_{x\in\chi} \hat{P}(x)\log(\frac{\hat{P}(x)}{Q(x)}) \tag{4.17}$$

4.3.2. Correction to Scott's rule

Based on this simulation model, we want to find the optimal bandwidth by tuning α in Eq. 4.12. This bandwidth can lead the estimated distribution most approach to the true distribution. The J-S divergence is selected as the factor to evaluate the esti-

mated PDF. The average J-S divergence of 1000 staircase simulated trials with change of $\alpha = [1, 1.05, ..., 1.4]$ are list in Tab. 4.4. The J-S divergence of true distribution and empirical probability density function is selected as the true J-S divergence.

Table 4.4: J-S divergence with different α parameter ($\times 10^{-2}$)

Case	Setup	TRUE	1	1.05	1.1	1.15	1.2	1.25	1.3	1.35	1.4
Normal CV=0.025	n=30 dn=1.0	1.75	2.08	1.97	1.88	1.81	**1.76**	1.72	1.71	1.69	1.51
Normal CV=0.025	n=30 dn=0.1	51.04	**49.51**	49.09	48.67	48.25	47.82	47.39	46.96	46.53	46.10
Normal CV=0.025	n=30 dn=2.0	9.83	9.33	9.44	9.59	**9.76**	9.94	10.14	10.34	10.55	10.76
Normal CV=0.05	n=30 dn=1.0	0.88	1.59	1.33	1.14	0.98	**0.86**	0.76	0.68	0.61	0.56
Normal CV=0.0125	n=30 dn=1.0	32.13	30.53	31.01	31.48	31.92	**32.35**	32.75	33.13	33.49	33.83
Logormal CV=0.025	n=30 dn=1.0	1.91	2.18	2.08	2.00	1.94	**1.90**	1.88	1.87	1.88	1.90
Logormal CV=0.025	n=30 dn=0.1	50.57	**48.99**	48.57	48.14	47.71	47.28	46.85	46.42	45.98	45.54
Logormal CV=0.025	n=30 dn=2.0	9.84	9.35	9.46	9.61	**9.78**	9.96	10.16	10.36	10.57	10.79
Logormal CV=0.05	n=30 dn=1.0	13.09	13.36	**12.91**	12.47	12.04	11.62	11.20	10.78	10.37	9.97
Logormal CV=0.0125	n=30 dn=1.0	15.07	**15.05**	15.31	15.59	15.89	16.20	16.52	16.86	17.20	17.55
Weibull CV=0.025	n=30 dn=1.0	18.07	18.64	18.34	**18.05**	17.78	17.52	17.26	17.02	16.79	16.56
Weibull CV=0.025	n=30 dn=0.1	37.20	**34.21**	33.80	33.38	32.96	32.54	32.12	31.71	31.29	30.87
Weibull CV=0.025	n=30 dn=2.0	15.77	16.72	16.45	16.24	16.08	15.95	15.84	**15.77**	15.71	15.67
Weibull CV=0.05	n=30 dn=1.0	19.82	20.59	20.13	**19.69**	19.26	18.83	18.41	17.99	17.58	17.17
Weibull CV=0.0125	n=30 dn=1.0	32.29	32.73	32.56	32.42	**32.30**	32.19	32.10	32.02	31.96	31.92

dn: Normalised step size

In the Tab. 4.4, the first column lists distribution and CV, the second column lists number of specimens and normalised step size. The J-S divergence of KDE with bandwidth approaching to true distribution are listed in third column. The value of α are listed in other columns, and it equals to original Scott's rule when $\alpha = 1$. The most approaching to the true value are maker with bold text. $\alpha = 1.15$ is suitable for

most case. Therefore, the bandwidth selector in this study is determined as Eq. 4.18 .

$$h_{opt} = 1.15 \times \left(\frac{4s^5}{3n}\right)^{\frac{1}{5}} \tag{4.18}$$

4.3.3. Sensitivity analysis of the KDE bandwidth

A sensitivity analysis was carried out in this section to validate the proper bandwidth by comparing different bandwidth selectors. The KDE results with different bandwidth selectors are compared in the following.

Fig. 4.4 shows the median and standard deviation estimations for the different numbers of specimens. Here, the step size is arbitrarily chosen equal to the true standard deviation $d = s_0$. Similarly, Fig. 4.4 and Fig. 4.5 show the median and standard deviation estimates for different step sizes with a number of specimens equal to 30.

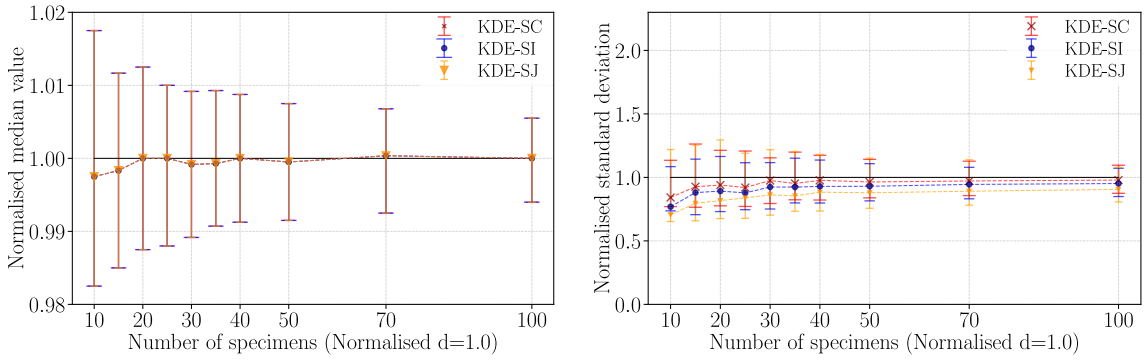

(a) (b)

Figure 4.4: Normalised (a) median value and (b) standard deviation estimated with KDE for different bandwidth selectors and varying number of specimens

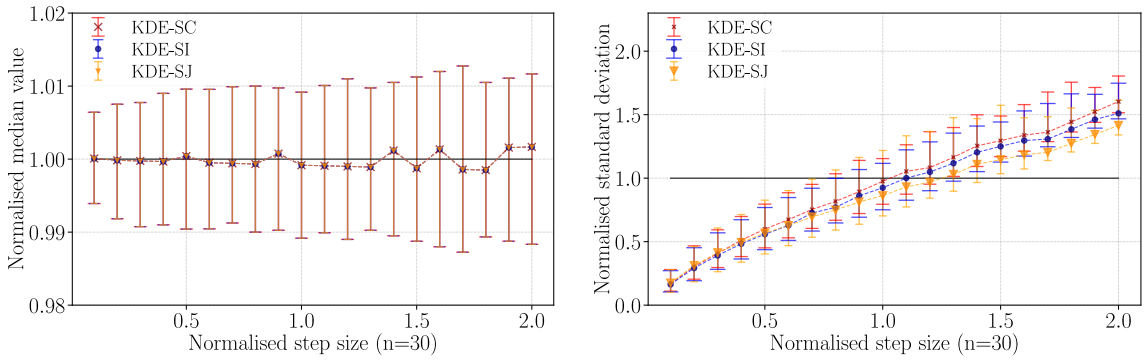

(a) (b)

Figure 4.5: Normalised (a) median value and (b) standard deviation estimated with KDE for different bandwidth selectors and varying normalised step sizes

In Fig. 4.4 and Fig. 4.5, corrected Scott's rule (SC), Silverman's rule (SI) and Sheather-Jones (SJ) method are illustrated by the red line, blue line and orange line, respectively. Each vertical bar's top and bottom represent the 5^{th} and 95^{th} percentile. The central marker is the estimated median from the 1000 staircase trials. From the comparison of the results obtained with the three bandwidths, it can be concluded that:

(1) From Fig. 4.4(a) and Fig. 4.5(a), three kinds of lines overlap, which means that the estimation of the median values is not sensitive to the bandwidth selector.
(2) Fig. 4.4(b) shows that the bandwidth of all methods has no effect on the standard deviation when the number of specimens increases (higher than 25-30).
(3) According to Fig. 4.5(b), the standard deviation estimation from these three bandwidths are all affected by the step size significantly.
(4) Focus on Fig. 4.5(b), the difference in the three bandwidth kinds is reflected in the normalised $d > 1$. However, the relative difference of the three methods is smaller compared to the absolute estimation error.

The estimations from corrected Scott's rule (SC) are closed to the true values when the normalised step size is equal to 1. The mean J-S divergences of the three bandwidth selectors in the case of $n = 30$ are 0.02115 (for SC), 0.03231 (for SI) and 0.04982 (for SJ). It is clear that the SC gives the smallest J-S divergence and is therefore applied to the proposed KDE approach. However, Fig. 4.5(b) shows that the estimated standard deviation obtained from SC is still far from the true value. Therefore, a correction is introduced to improve the results of the standard deviation estimation.

4.3.4. Comparison of the median value estimation

It is generally known that the staircase protocol concentrates data near the center [42], resulting in a high accuracy estimation of the median value of fatigue limit distribution. The comparative study firstly focuses on the median estimation. Fig. 4.6 shows the influence of the number of specimens for $d = 1.0$ and $d = 1.5$ normalised, and Fig. 4.7 shows the effect of the step size for a small number of specimens ($n = 30$) and a larger one ($n = 100$).

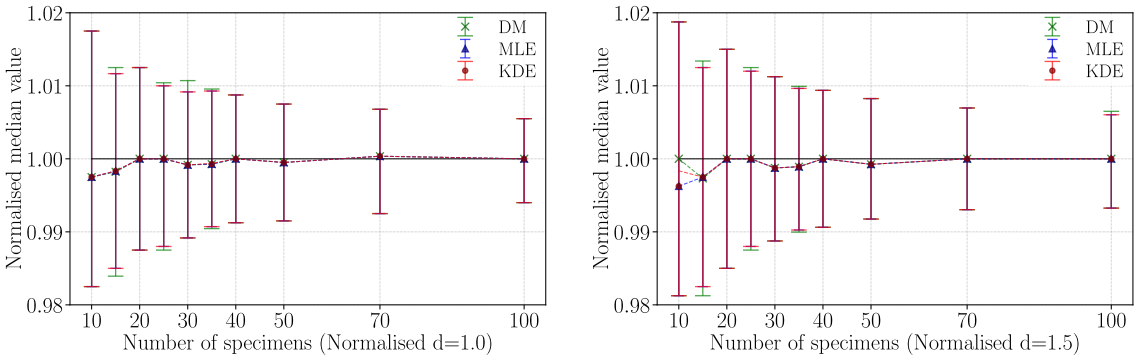

(a) (b)

Figure 4.6: Distributions of median obtained from simulation for varying numbers of specimens for (a) $d = 1.0$ and (b) $d = 1.5$ normalised

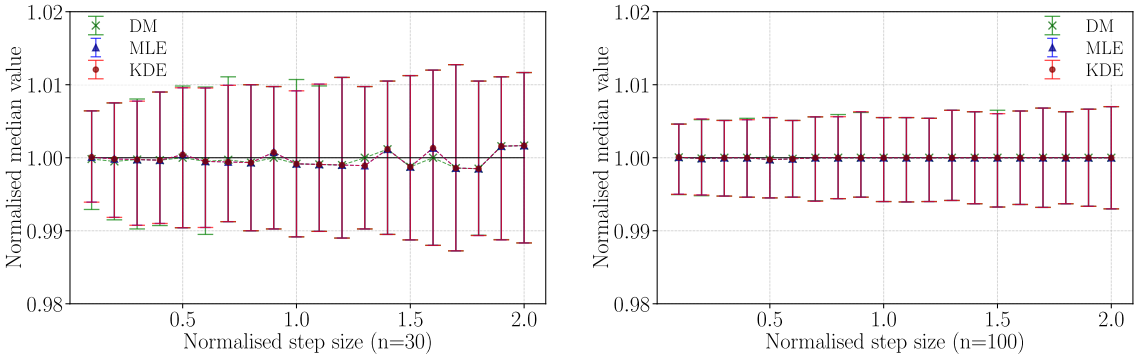

(a) (b)

Figure 4.7: Distributions of median obtained from simulation for different normalised step sizes for (a) $n = 30$ and (b) $n = 100$

In Fig. 4.6, the DM, MLE and KDE methods are illustrated by the green, blue and red lines, respectively. The estimation uncertainty decreases with the increase of the specimens number for all three methods. Furthermore, it can be seen from Fig. 4.7 that the step size has little effect on the median value estimation, but a larger step

size (normalised $d > 1$) leads to a small bias of median estimation when $n = 30$. Since all three methods give a reasonable median estimation, the following study presents only the results for the standard deviation estimation.

4.3.5. Comparison of the standard deviation estimation

4.3.5.1. Comparison of standard deviations with the Normal distribution (case 1)

The divergence of the different statistical methods is mainly reflected in the standard deviation estimation. To prove the robustness of the KDE method, the standard deviation estimates of the number of specimens and step sizes are presented with setup case 1, i.e., Normal distribution and CV=0.025. The results obtained with different numbers of specimens and step sizes are presented in Fig. 4.8 and Fig. 4.9, respectively.

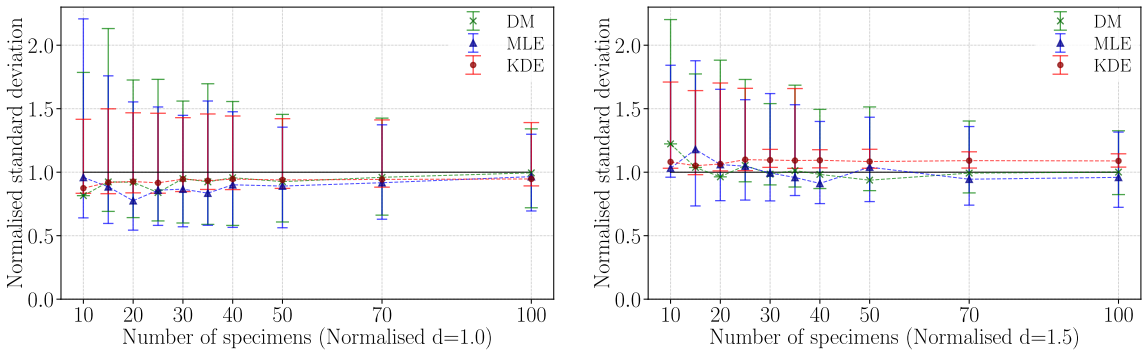

(a) (b)

Figure 4.8: Distributions of standard deviation obtained from simulation for varying numbers of specimens for (a) $d = 1.0$ and (b) $d = 1.5$ normalised

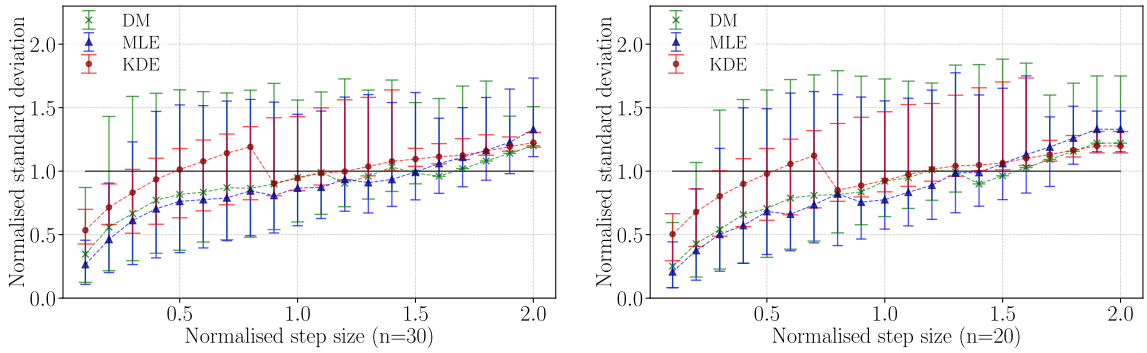

(a) (b)

Figure 4.9: Distributions of standard deviation obtained from simulation for different normalised step sizes for (a) $n = 30$ and (b) $n = 20$

The comparison of the three methods suggests the following conclusions:

(1) According to Fig. 4.8, all three methods have relatively stable performance for different numbers of specimens. For each method, the number of specimens has no effect on the 50^{th} percentile of all estimations but reduces the uncertainty.

(2) From the red line in Fig. 4.9, the KDE works better for standard deviation estimations when normalised $d = 1 - 1.5$.

(3) According to Fig. 4.9, there are slight differences between DM and MLE methods for a Normal distribution. This observation was also pointed out by [40].

(4) According to Fig. 4.9(a) and (b), the KDE method shows the closest results to the true value in most cases of step sizes with smaller uncertainty. This makes sense because the correction equation focuses on the small sample size.

(5) There is a transition between the normalised step sizes $0.7 - 0.8$ in Fig. 4.9. This discontinuity comes from the piecewise correction equation Eq. 4.13. Taking simulation case 1 ($n = 30$) as an example, the estimated standard deviation (s) and the number of used piecewise equation is shown in Fig. 4.10.
In the upper part of Fig. 4.10, the blue lines represent the results of KDE without correction, and the red lines represent the results of KDE with correction. In the lower part of Fig. 4.10, the red line is the number of first piecewise equation ($s > d$) used, and the blue line is the number of second piecewise equation ($s \leqslant d$) used. A total of 1000 trials have been performed in the simulation. The horizon axis is the normalised step size in the range of [0.1-2.0]. It is necessary to note that the green arrow in Fig. 4.10 indicates the crossing point between the blue line and the red line, as well as the discontinuity of 50% estimation. The reason that this point locates between 0.7 and 0.8 instead of 1.0 is that the staircase method has an inherent low biased estimation of the standard deviation [38, 40], due to concentrating the majority of the data points near the median.

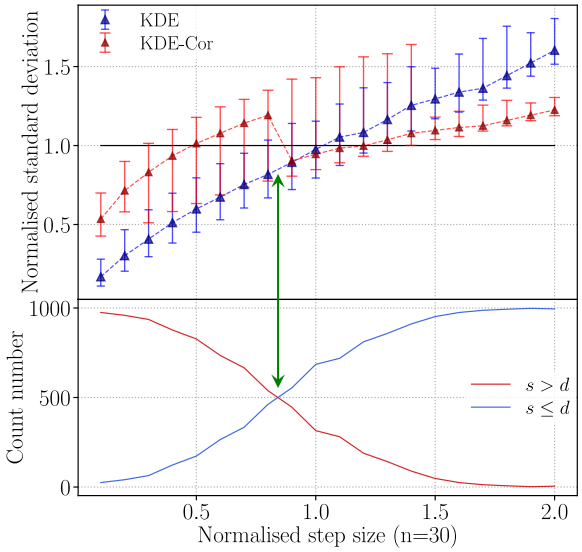

Figure 4.10: Estimated standard deviation and the number of used piecewise equation

(6) The scatter of the estimation is significantly reduced by applying the KDE method, especially for step sizes in the range of $1.5s_0 - 2.0s_0$.

In this case, the KDE method has the slightest uncertainty regarding the number of specimens and the step size. It achieves the goal of reducing the effect of step size and reducing uncertainty.

4.3.5.2. Comparison of standard deviations with different coefficients of variation (cases 2 and 3)

Since the mean is considered constant, the standard deviation varied with the coefficient of variation CV=0.0125 and CV=0.05. The results of the related standard deviation estimation are plotted against the number of specimens in Fig. 4.11 and Fig. 4.12.

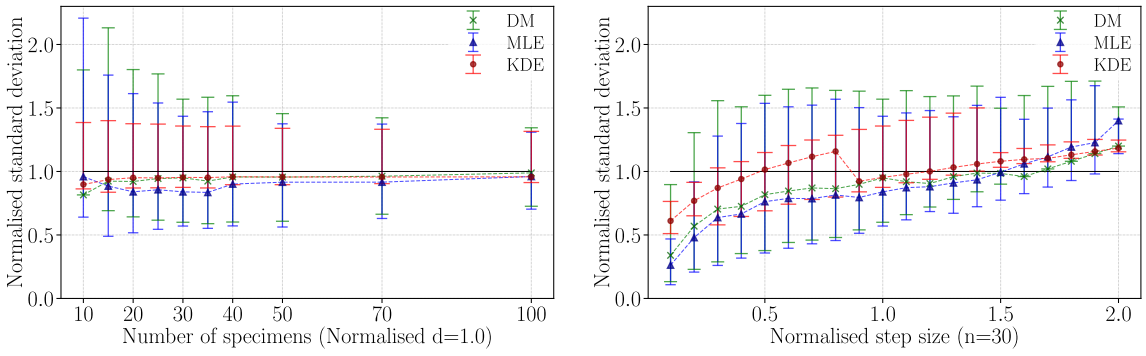

Figure 4.11: Distributions of standard deviation obtained from simulation with the Normal distribution and CV=0.0125

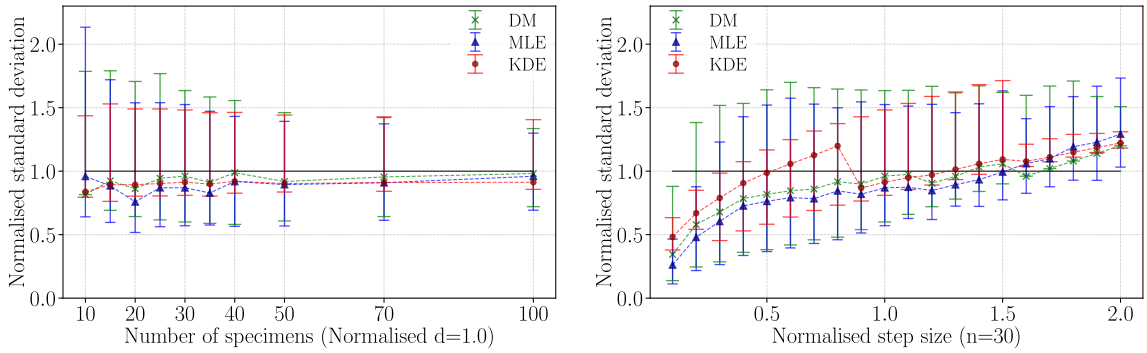

(a) (b)

Figure 4.12: Distributions of standard deviation obtained from simulation with the Normal distribution and CV=0.05

It is clear that the KDE method shows the best estimation properties in the case of CV=0.0125 and CV=0.05, which leads to the same conclusions for CV=0.025. With the help of the correction equation (Eq. 4.13), the estimated standard deviation is less affected by CV. The results analyzed with the knowledge of the coefficient of variation highlight the interest of KDE.

4.3.5.3. Comparison of the standard deviation with Lognormal and Weibull distributions (cases 4 and 5)

In the previous sections, the KDE method was evaluated with the Normal distribution compared to other evaluation methods. It should be noted that the KDE method requires no prior information about the underlying distribution. Therefore, it is necessary to evaluate the effectiveness of the proposed method with other probability distributions, such as Lognormal and Weibull distribution. Since the DM method is incapable of estimating the non-Normal distribution of the fatigue limit, the KDE method will be compared to the MLE method in this section. The estimation of the standard deviation with respect to the step sizes is shown in Fig. 4.13 for the Lognormal distribution and Fig. 4.14 for the Weibull distribution.

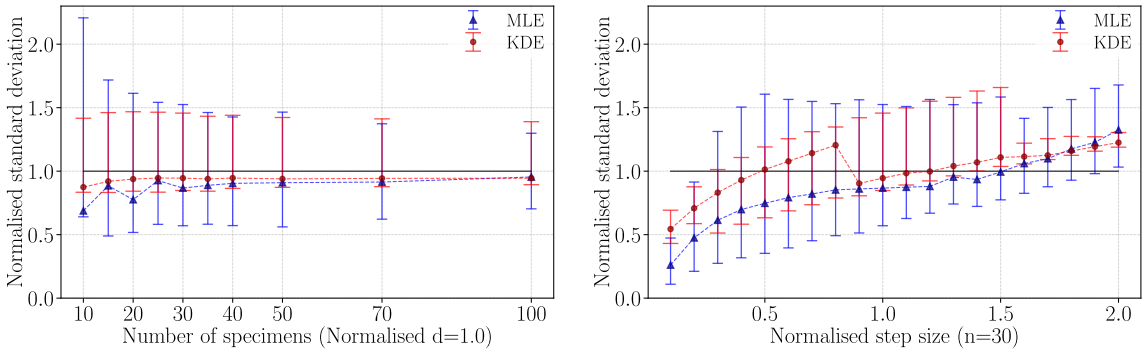

(a) (b)

Figure 4.13: Distributions of standard deviation obtained from simulation with Lognormal distribution and CV=0.025

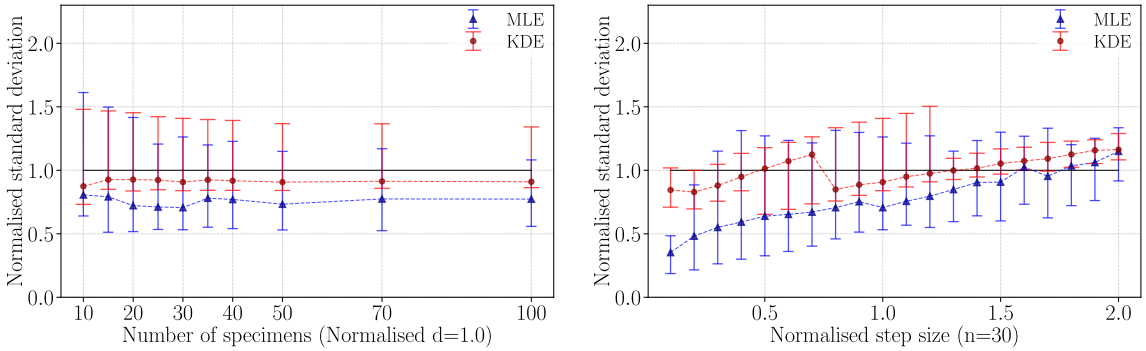

(a) (b)

Figure 4.14: Distributions of standard deviation obtained from simulation with Weibull distribution and CV=0.025

From Fig. 4.13, the outcome considering the Lognormal distribution presents the same main conclusions as that of the Normal distribution. From Fig. 4.14, the MLE estimation is not capable of providing reliable information regarding the Weibull staircase data. Focusing the KDE results (red line) in Fig. 4.13(b) and Fig. 4.14(b), the KDE method has better performance for Weibull distribution. From the results of this work, the KDE method combined with the Weibull distribution will achieve better performance for the experimental test. Therefore, the KDE is a distribution-free statistical assessment method that works better than the MLE even if the MLE fits the data distribution perfectly.

4.3.6. Comparison of the probability distribution estimation

To complete the performance evaluation of the proposed method in terms of median and standard deviation estimation, the J-S divergence is introduced in this section as a means of evaluating the estimate quality with respect to the probability distribution. The average J-S divergence $\bar{D}_{JS}$ reported in Tab. 4.5 is computed from 1000 trials in each case.

Table 4.5: The J-S divergence of all the methods investigated in the study cases with d=1.0 and n=30

	Probability Distribution	CV	$\bar{D}_{JS}^{DM}$	$\bar{D}_{JS}^{MLE}$	$\bar{D}_{JS}^{KDE}$
Case 1	Normal	0.025	0.04235	0.04534	0.02088
Case 2	Normal	0.0125	0.04331	0.04858	0.02131
Case 3	Normal	0.05	0.03248	0.03773	0.01708
Case 4	Lognormal	0.025	-	0.04841	0.02196
Case 5	Weibull	0.025	-	0.19293	0.05780

From case 1 to case 3, all the investigated methods provide a stable estimate of the probability distribution, as the average J-S divergence is nearly constant for each method throughout these cases, which reveals that the estimate quality is less affected by CV. The $\bar{D}_{JS}^{KDE}$ is always smaller than that of the DM and MLE methods. This means that the KDE-estimated probability distribution is relatively less different from the true probability distribution.

As for the cases 1, 4 and 5, the $\bar{D}_{JS}^{KDE}$ is also better than that of the MLE method. However, both $\bar{D}_{JS}^{KDE}$ and $\bar{D}_{JS}^{MLE}$ are increased in case 5. Considering that the KDE method has offered a good estimation of the median and standard deviation in the same study case, the reason for the increase in $\bar{D}_{JS}^{KDE}$ is probably caused by the negative skewness of the Weibull distribution. Since the kernel function used by KDE in this work is symmetric, the estimated probability distribution is relatively less accurate when the underlying distribution is highly skewed. This leads to future research on the kernel functions used in the proposed KDE-based evaluation method.

In this study, the proposed KDE method is simulated and compared with different distribution models and different CV. Based on the simulation study, it is possible for the proposed method to generalize for many material.

4.4. Application of KDE method on experimental data

The non-parametric method is applied in this section in order to characterise the fatigue limit of the DC01 low carbon steel specimens by using the data in the up-and-down diagram given in Chapter 2. The estimated PDF and CDF of fatigue limits calculated by the KDE with optimized bandwidth and DM method are shown in Fig. 4.15 and Fig. 4.16. Correspondingly, the median and standard deviation of fatigue limit resulting from the density estimation are shown in Tab. 4.6.

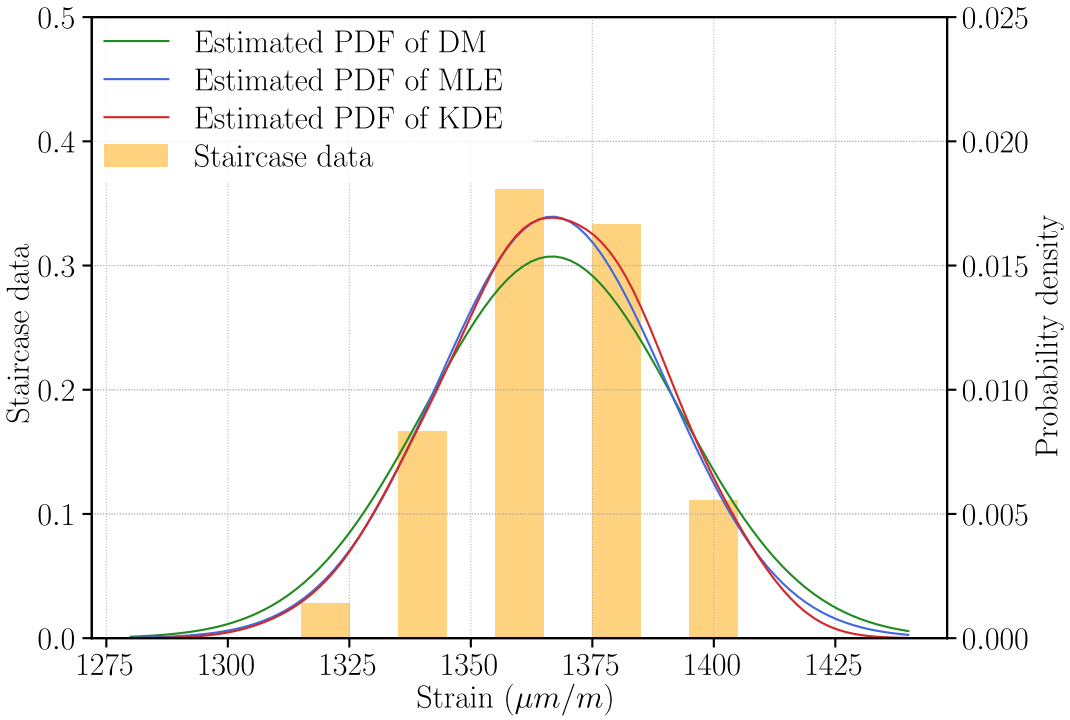

Figure 4.15: PDF of the fatigue limit

Table 4.6: The median and standard deviation from different estimation

Methods	Median	Standard deviation
DM	1366.67	25.96
MLE (Normal distribution)	1366.71	22.51
KDE ($h = 11.56$)	1366.66	22.61 12.21(corrected by Eq. 4.13)

Combining the estimated distributions and Tab. 4.6, the following results can be

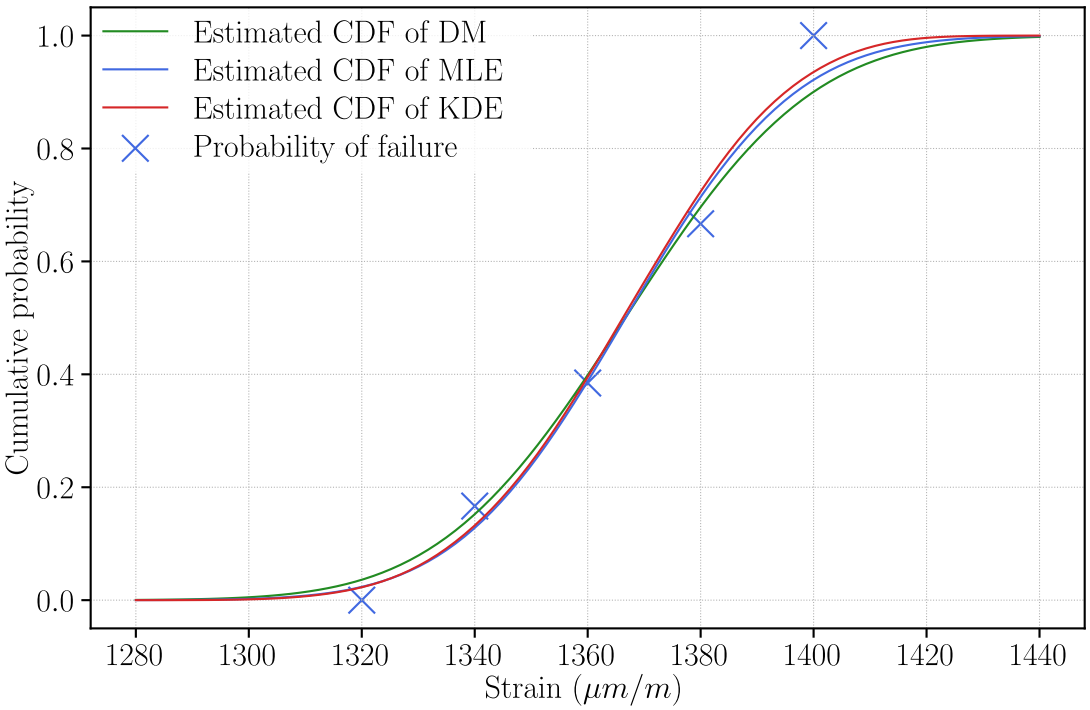

Figure 4.16: CDF of the fatigue limit

drawn:

(1) The bending fatigue limit of DC01 was obtained in strain domain as 1366.66 µm/m with the standard deviation 12.21 µm/m ;

(2) For the present results, three methods use different experimental informations. The sample size by DM is 18 (failure) while by MLE and KDE are 36 (total). Moreover, the MLE distinguishes the specimens by failure or survival result, while KDE does not require this information.

(3) Three methods lead to almost same median estimation.

(4) It is apparent that KDE has an estimated results accordance with MLE method. The median and standard deviation values by KDE and MLE estimations converge to each other.

(5) All estimated median value are consistent with the observed fatigue strength from $\varepsilon - N$ curve in Chapter 2 and comprise in the 95% confidence interval.

(6) A larger standard deviation of fatigue limit is obtained from DM. After the correction of the standard deviation in KDE method, the predicted value becomes much smaller.

4.5. Conclusion

In this chapter, a non-parametric evaluation method is proposed in this work to estimate the fatigue limit from the staircase test. The method originally combines the Kernel Density Estimation (KDE) with nonlinear bias correction. The performance of the proposed method is optimized by setting dynamically the bandwidth of the KDE. A simulation-based study is carried out to evaluate the estimate quality compared to other widely used evaluation methods like the Dixon-Mood (DM) and Maximun Likelihood Estimation (MLE) methods. In the numerical study, the underlying distribution of the fatigue limit is presumed to be characterized by a couple of probability distributions and coefficients of variation (CV). The numerical experiment involves three probability distributions (i.e., Normal, Lognormal and Weibull) that have been widely studied in related work. The dependence of the estimate quality on the sample size and the step size of the staircase test was investigated. From the numerical results, the proposed KDE-based method outperforms the MLE and DM in terms of estimations of the median, standard deviation and probability distribution of the fatigue limit. For the normally distributed fatigue limit, all the methods investigated (i.e., DM, MLE and KDE) result in a good estimation on the median value. But DM and MLE provide poor estimates of the standard deviation of the fatigue limit, especially for small sample tests, i.e., when the number of specimens is less than 30. In contrast, the proposed method offers an estimate that is relatively closer to the true standard deviation regardless of the number of specimens. This outstanding performance is also observed for the J-S divergence which measures the similarity between two probability distributions. The fatigue limit distribution estimated by the KDE method always returns a smaller J-S divergence, in other words, the estimated distribution is closer to the presumed Normal distribution. Not to mention that the estimate quality of the KDE method is stable with respect to the different CV coupled with the Normal distribution.

The proposed method is also applied to experimental data, which obtain the fatigue distribution from staircase data. With respect to the non-Normal distribution of the fatigue limit (i.e., Lognormal and Weibull), the estimations made by the proposed method are always better than those of the MLE method. The estimated standard deviation of the fatigue limit is really noticeable with the KDE method and the Weibull distribution, nevertheless the estimate quality measured by the J-S divergence is relatively poor. This leads to further research on the kernel functions of the proposed KDE-based method.

In the following chapter, a staircase procedure improvement is presented.

Chapter 5
Bayesian improved staircase experimental design

To address the essential deficiency of the conventional staircase test method, this chapter proposes an optimized test method based on Bayesian Maximum Entropy Sampling (BMES) and Latin Hypercube Sampling (LHS) to determine the fatigue limit distribution of the structure. The proposed method integrates the prior information from samples to obtain the posterior probability as well as the fatigue limit distribution. It reduces the statistical analysis error caused by the small number of samples in the fatigue limit test.

The current chapter is structured as follows: a summary of the staircase problems and several optimizations for test protocol are given in Section 5.1. The background of fatigue limit test, the Bayesian theory, the BMES and the LHS methods are interpreted in Section 5.2, Section 5.3 and Section 5.4, respectively. Then, Section 5.5 introduces the proposed improved Bayes-LHS staircase method based on BMES and LHS. Section 5.6 defines the numerical simulation setup for the conventional staircase method, the Bayesian staircase method and the proposed improved Bayes-LHS method. Lastly, Section 5.7 presents the simulation results, and evaluates the effectiveness of the proposed Bayes-LHS method by comparing the estimated distributions under the same condition.

5.1. Background

It is well known that the estimated sample median (or mean) from the staircase method is usually much closer to the true value. However, due to the nature of the staircase test, it is challenging to obtain a proper estimation of the sample standard deviation [41].

The improvement of the accuracy of the fatigue limit estimation can be classified into the evaluation techniques and the experimental protocol. In the last decades, several researchers have investigated ways of post-processing. For example, Pollak et al. [38] formulated a non-linear correction on the standard deviation of fatigue limit and involved bootstrapping sampling for a small number of specimens. Müller et al. [40] compared several evaluation techniques through Monte-Carlo simulation (MCS) and introduced the usage of statistical hypothesis tests in evaluating experimental results. Nevertheless, both methods didn't solve the disadvantage of the dependency to step size of fatigue limit test.

Due to the intrinsic limitations of the staircase method, recent studies focus on improving the test protocol. To date, several studies have focused on experimental design optimization. Wallin [42] simulated a modified staircase procedure with a small step size to cover all anticipated standard deviation ranges. However, a small step size may lead to larger sample size. Bai et al. [56] proposed a Monte-Carlo method that offers higher test data efficiency and can be variable in step size. However, the step size still needs to be guessed before the test, and the result strongly depends on the step size. Roué et al. [39] developed a new experiment staircase procedure and reduced the uncertainty in the standard deviation estimation by reloading unbroken specimens. Magazzeni et al., Magazzeni et al. [116, 117] proposed protocols using Bayesian Maximum Entropy Sampling (BMES), in which a faster convergence is obtained.

To the moment of writing, the application of parametric models based on robust initial assumptions, enriched by the Bayesian theorem, provides a more reliable fatigue characterization of materials without resorting to black boxes. The Bayesian staircase strategy was firstly proposed by Engler-Pinto et al. [118]. Then, Engler-Pinto et al. [118] incorporated the Bayesian staircase strategy into Life-Regression Models (S-N curve) [52]. Alcalá-Quintana et al. [119] carried out a numerical study to compare the fixed-step-size and the Bayesian staircase method. The authors found that the standard deviation of Bayesian estimates is systematically lower than that of the conventional staircase in the same condition.

Based on the idea of Bayesian theory in the experimental test [120, 121], an application is carried out by using maximum entropy sampling as a criterion for choosing experiments to maximize the gain in information regarding prediction at unsampled

sites. Sebastiani et al. [122] introduced an extension of the Bayesian principle to the estimation problems. Magazzeni et al. [117] described the improved staircase method using Bayesian Maximum Entropy Sampling (BMES) with details.

According to these studies, the Bayesian staircase method requires very little information about the sample set prior to the testing. The Bayes and the LHS are proposed to improve the conventional staircase tests in this work. The LHS [95] are incorporated into BMES to make sampling more uniform in the cumulative density probability domain. The current chapter focuses majorly on the implementation of BMES and LHS for improving conventional staircase protocol, in which the stress step size is not constant and is calculated after every test.

5.2. Bayesian theorem in fatigue test

Let be a random data set $\boldsymbol{x} = \{x_1, x_2, ..., x_n\}$ that denotes the specimens from fatigue limit test, $\boldsymbol{x}$ is subject to a PDF $P(\boldsymbol{x}|\boldsymbol{\theta})$ where, $\boldsymbol{\theta}$ is model parameter, and $\boldsymbol{x}$ is the fatigue limit (test results in fatigue test). Bayes rule is built as:

$$P(\boldsymbol{\theta}|\boldsymbol{x}) = \frac{P(\boldsymbol{x}|\boldsymbol{\theta})P(\boldsymbol{\theta})}{P(\boldsymbol{x})} \tag{5.1}$$

where, $P(\boldsymbol{x}|\boldsymbol{\theta})$ is the likelihood function, $P(\boldsymbol{\theta})$ is the prior probability, $P(\boldsymbol{x})$ is the observations from experimental test (a.k.a, marginal probability), $P(\boldsymbol{\theta}|\boldsymbol{x})$ is the posterior probability on the left side of the equation.

5.2.1. Model parameter

In the practical computation, the matrix $\boldsymbol{\theta}$ includes all possible model parameters that are described by shape, location, and scale (see Appendix E). For example, the $\boldsymbol{\theta}$ in Normal distribution is created as:

$$\boldsymbol{\theta} = \begin{bmatrix} (m_1, s_1), & (m_2, s_1), & \dots, & (m_a, s_1) \\ (m_1, s_2), & (m_2, s_2), & \dots, & (m_a, s_2) \\ \dots, & \dots, & \dots, & \dots \\ (m_1, s_b), & (m_2, s_b), & \dots, & (m_a, s_b) \end{bmatrix} \tag{5.2}$$

where, m and s are the location and scale for Normal distribution . The mean range and standard deviation range are discredited with the number of a and b. For example, $a = 100$ and $b = 100$ are used in the following analysis.

The model parameters also define all possible stresses for tested specimens. That is, $\boldsymbol{S}_a = [m_1, m_2, \dots, m_{max}]$. Each stress amplitude S_a corresponds to a result x (failure or survival).

5.2.2. Likelihood with censored data

Considering the one result x from a staircase test, the likelihood that contains information in test results (e.g., failure or survival) is:

$$\boldsymbol{L} = P(x|\boldsymbol{\theta}) = \int_{S_{a,low}}^{S_{a,up}} f(S_a, \boldsymbol{\theta}) dS_a = F(S_a, \boldsymbol{\theta}) \tag{5.3}$$

where, $f(\boldsymbol{\theta})$ and $F(\boldsymbol{\theta})$ are the PDF and CDF for the model parameter $\boldsymbol{\theta}$, S_a is the stress amplitude, $S_{a,low}$ and $S_{a,up}$ are the boundary limits of the stress S_a.

For example, based on the Normal distribution, the model parameter $\boldsymbol{\theta}$ consists of all possible median and standard deviation values. The aim is to calculate the CDF related to a chosen stress amplitude S_a based on the model parameters $[m, s]$ in $\boldsymbol{\theta}$. In case of Normal distribution, $\boldsymbol{F}$ is a CDF that has same dimensions with $\boldsymbol{\theta}$.

$$\boldsymbol{F} = \Phi(S_a, \boldsymbol{\theta}) \tag{5.4}$$

In practice, it should be distinguished between the survival stress amplitude and the failed stress amplitude and calculate separately the CDF with these stress amplitudes. There are two kinds of likelihood on one specimen with left- or right-censoring:

$$L_i = \begin{cases} L_i^f = F(S_a, i) \\ L_i^s = 1 - F(S_a, i) \end{cases} \tag{5.5}$$

where, i is the ordinal number of the specimen, S_a, i is the stress amplitude of i^{th} specimen.

Total likelihood with all previous specimens $\boldsymbol{x} = x_{i_{max}}, x_2, \ldots, x_{i_{max}}$:

$$\boldsymbol{L} = P(\boldsymbol{x}|\boldsymbol{\theta}) = \prod_{i=1}^{i_{max}} L_i \tag{5.6}$$

In computational practice, the likelihood ($\boldsymbol{L}$) is in the logarithm form. With the prior in logarithm, the Eq. 5.6 is carried out as follows:

$$\ln \boldsymbol{L} = \ln P(\boldsymbol{x}|\boldsymbol{\theta}) = \sum_{i=1}^{i_{max}} \ln L_i \tag{5.7}$$

5.2.3. Prior and posterior

The prior and posterior are usually done in the logarithm form to avoid numerical issues with small values. The prior (or posterior) is built as a discrete matrix with the same dimensions as $\boldsymbol{\theta}$.

Here we present how to update the posterior by prior after a single test. During the staircase test, after i^{th} specimen has been tested, the prior before i^{th} specimen becomes:

$$P(\boldsymbol{\theta}) = P(\boldsymbol{\theta}|\boldsymbol{x}_{1:i-1}) \tag{5.8}$$

In the logarithmic form:

$$\ln P(\boldsymbol{\theta}|\boldsymbol{x}_{1:i-1}) = \sum_{t=1}^{t=i-1} \ln P(\boldsymbol{\theta}|x_t) \tag{5.9}$$

where t is the iteration number.

In the experimental staircase test, the $\boldsymbol{x}$ and $\boldsymbol{\theta}$ are discrete values, and the total probability equation is:

$$\begin{aligned} P(\boldsymbol{x}) &= \sum_{\boldsymbol{\theta}} P(\boldsymbol{\theta}) \cdot P(\boldsymbol{x}|\boldsymbol{\theta}) \\ &= \sum_{\boldsymbol{\theta}} P(\boldsymbol{\theta}|\boldsymbol{x}_{1:i-1}) P(x_i|\boldsymbol{\theta}) \end{aligned} \tag{5.10}$$

Taking Eq. 5.8 and Eq. 5.10 into Eq. 5.1, the update of the prior for the i^{th} specimen $P(\boldsymbol{\theta}|\boldsymbol{x}_{1:i})$ according to $P(\boldsymbol{\theta}|\boldsymbol{x}_{1:i-1})$ is described as:

$$\begin{aligned} P(\boldsymbol{\theta}|\boldsymbol{x}) &= \frac{P(\boldsymbol{x}|\boldsymbol{\theta})P(\boldsymbol{\theta})}{P(\boldsymbol{x})} \\ P(\boldsymbol{\theta}|\boldsymbol{x}_{1:i}) &= \frac{P(x_i|\boldsymbol{\theta})P(\boldsymbol{\theta}|\boldsymbol{x}_{1:i-1})}{\sum_{\boldsymbol{\theta}} P(\boldsymbol{\theta}|\boldsymbol{x}_{1:i-1})P(x_i|\boldsymbol{\theta})} \end{aligned} \tag{5.11}$$

where i is the specimen ordinal number. The posterior $P(\boldsymbol{\theta}|\boldsymbol{x}_{1:i})$ calculated from the prior of the previous specimens $P(\boldsymbol{\theta}|\boldsymbol{x}_{1:i-1})$. $P(x_i|\boldsymbol{\theta})$ is the likelihood L_i.

In practice, incorporating Eq. 5.7 and Eq. 5.9, the update of posterior (Eq. 5.11) in logarithm is described as:

$$\ln P(\boldsymbol{\theta}|x_{1:i}) = \ln[P(\boldsymbol{\theta}|\boldsymbol{x}_{1:i-1})P(x_i|\boldsymbol{\theta})] - \sum_{\boldsymbol{\theta}} \ln[P(\boldsymbol{\theta}|\boldsymbol{x}_{1:i-1})P(x_i|\boldsymbol{\theta})] \tag{5.12}$$

In order to simplify the description, a normalized matrix $\boldsymbol{M}$ is defined by:

$$\begin{aligned} \boldsymbol{M} &= \ln[P(\boldsymbol{\theta}|\boldsymbol{x}_{1:i-1})P(x_i|\boldsymbol{\theta})] \\ &= \ln[P(\boldsymbol{\theta}|\boldsymbol{x}_{1:i-1})] + \ln[P(x_i|\boldsymbol{\theta})] \end{aligned} \tag{5.13}$$

It must be ensured that the element of $\boldsymbol{M}$ is greater than 0. For the element less than 0, it is set to a tiny number (such as 1×10^{-7}).

With Eq. 5.13, Eq. 5.12 can be written as:

$$\ln P(\boldsymbol{\theta}|x_{1:i}) = \boldsymbol{M} - \sum_{\boldsymbol{\theta}} \boldsymbol{M} \tag{5.14}$$

The posterior after i^{th} specimen is the prior for $(i+1)^{th}$ specimen.

It is necessary to define a initial prior matrix before the test. The fully flat initialised to the prior has been proved to work better in convergence [116]. A flat prior is equivalent to assuming no prior at all, which means it is created by an array of equal values. Consistent with the calculation of posterior in Eq. 5.11 and Eq. 5.14, the matrix $\boldsymbol{M}$, as described in Eq. 5.13, is initialised as:

$$\boldsymbol{M} = \boldsymbol{J}_{a,b} \tag{5.15}$$

where a, b are the dimensions of $\boldsymbol{\theta}$, the $\boldsymbol{J}_{a,b}$ is all-ones matrix of the same dimension as $\boldsymbol{\theta}$. The initial prior is obtained by taking Eq. 5.15 into Eq. 5.14.

5.3. Bayesian maximum entropy sampling

Bayesian Maximum Entropy Sampling (BMES) contributes to predicting the expected result by maximizing the entropy gain. After testing i specimens, the stress amplitude for $(i+1)^{th}$ specimen can be selected by maximizing the expected gain in Shannon information in the posterior.

5.3.1. Shannon entropy

The Shannon entropy measures the uncertainty of the system. Shannon information I included in the posterior is:

$$I(P(\boldsymbol{\theta}|\boldsymbol{x})) = -\ln(P(\boldsymbol{\theta}|\boldsymbol{x})) \tag{5.16}$$

This information indicates the uncertainty of the posterior $P(\boldsymbol{\theta}|\boldsymbol{x})$. According to this information, the Shannon entropy is defined as:

$$H(P(\boldsymbol{\theta}|\boldsymbol{x})) = E(I(P(\boldsymbol{\theta}|\boldsymbol{x}))) = -\int_{\boldsymbol{\theta}_{min}}^{\boldsymbol{\theta}_{max}} d\theta P(\boldsymbol{\theta}|\boldsymbol{x}) \ln P(\boldsymbol{\theta}|\boldsymbol{x}) \tag{5.17}$$

where we see that the Shannon entropy is the product of the probability and the uncertainty. When taken from a discrete $\boldsymbol{\theta}$ and finite samples $\boldsymbol{x}$, the Shannon entropy

formula can be explicitly written as follows:

$$H(P(\boldsymbol{\theta}|\boldsymbol{x})) = -\sum_{\theta} P(\boldsymbol{\theta}|\boldsymbol{x}) \ln P(\boldsymbol{\theta}|\boldsymbol{x}) \tag{5.18}$$

After the i^{th} specimen, we need to find the proper stress amplitude for the next $(i+1)^{th}$ specimen based on Bayesian progression.

In order to obtain an optimized stress amplitude, the objective is to maximize the information of the test stress amplitude. The entropy for $(i+1)^{th}$ specimen is defined as:

$$\boldsymbol{H}(P(\boldsymbol{\theta}|\boldsymbol{x}_{1:i+1})) = -\sum_{\theta} P(\boldsymbol{\theta}|\boldsymbol{x}_{1:i+1}) \ln P(\boldsymbol{\theta}|\boldsymbol{x}_{1:i+1}) \tag{5.19}$$

where $P(\boldsymbol{\theta}|\boldsymbol{x}_{1:i+1})$ is posterior for the $(i+1)^{th}$ specimen with design of stress amplitude S_a and result x_i. The model parameters $\boldsymbol{\theta}$ are kept unchanged during the staircase test.

Note: The gain in entropy ($\Delta\boldsymbol{H}$, entropy difference between the $(i+1)^{th}$ and i^{th} specimen) can also be used to replace the Eq. 5.19. However, the same results are obtained but with more computation.

Shannon entropy provides the information of staircase data but not the quality of the estimation results. The minimum Shannon entropy may not consist of the best posterior for estimation. The minimum Shannon entropy could not be used as a stopping criterion for the test.

5.3.2. Utility function

After testing i specimens, the next stress is chosen to maximize the expected information gained by sampling at a subsequent specimen x_{i+1}.

In the staircase test, a utility function is built by considering the expected information with both results of a specimen, survival or failure, at the expected stress amplitude (a stress amplitude possible to be tested). The utility function with the stress amplitude $S_{a,i+1}$ is defined as:

$$U(S_{i+1}) = H^s(S_{a,i+1}, \boldsymbol{x}) p^s(\boldsymbol{x}|S_a) + H^f(S_{a,i+1}, \boldsymbol{x}) p^f(\boldsymbol{x}|S_a) \tag{5.20}$$

where, U is the utility function that describes the entropy gain with the result x_{i+1}. $\boldsymbol{x}$ is a vector of all previous tests. U, H, p are all (float) values. The superscript "s" represents the "survival" and superscript "f" represents the "failure".

Similar to Eq. 5.18, the Shannon entropy is expressed as Eq. 5.21:

$$\begin{aligned} H^s(S_{a,i+1}, \boldsymbol{x}) &= -\sum_{\theta} P(\boldsymbol{\theta}|\boldsymbol{x}) \ln P(\boldsymbol{\theta}|\boldsymbol{x}) \text{ with survival} \\ H^f(S_{a,i+1}, \boldsymbol{x}) &= -\sum_{\theta} P(\boldsymbol{\theta}|\boldsymbol{x}) \ln P(\boldsymbol{\theta}|\boldsymbol{x}) \text{ with failure} \end{aligned} \tag{5.21}$$

The difference between these two equations is posterior $P(\boldsymbol{\theta}|\boldsymbol{x})$, which is calculated with Eq. 5.11. Two cases, including survival and failure, are considered for posterior with different likelihood as Eq. 5.5.

It should be noted that the probabilities p^s and p^f are the multiplication of the likelihood and the prior, after integrating to reach the marginal probability.

$$\begin{aligned} p^s(S_{a,i+1}, \boldsymbol{x}_{1:i}) &= \sum_{\boldsymbol{\theta}} [P(\boldsymbol{\theta}|\boldsymbol{x}_{1:i+1}) \cdot (1 - \Phi(S_{a,i+1}))] \\ p^f(S_{a,i+1}, \boldsymbol{x}_{1:i}) &= \sum_{\boldsymbol{\theta}} [P(\boldsymbol{\theta}|\boldsymbol{x}_{1:i+1}) \cdot \Phi(S_{a,i+1})] \end{aligned} \tag{5.22}$$

To summarise, the calculation of the utility function is illustrated in the flowchart of Fig. 5.1.

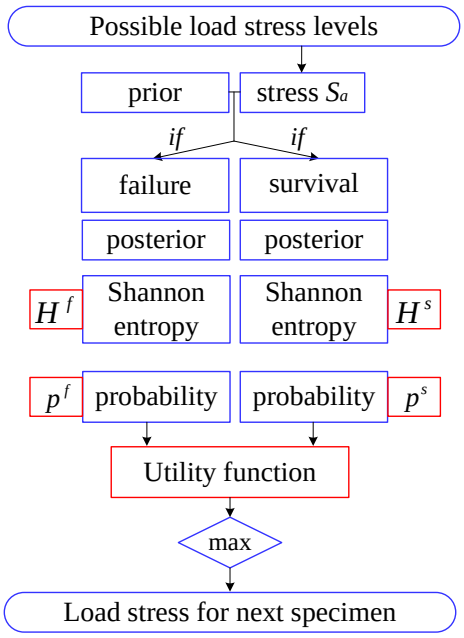

Figure 5.1: Utility function diagram

In this study, the utility function is calculated by the differential evolution optimization method, and the stress corresponding to maximum utility is the expected load level for the next specimen.

5.3.3. Bayesian staircase method

By applying the utility function to select the stress amplitude, the Bayesian staircase procedure [116] can be shown as Fig. 5.2.

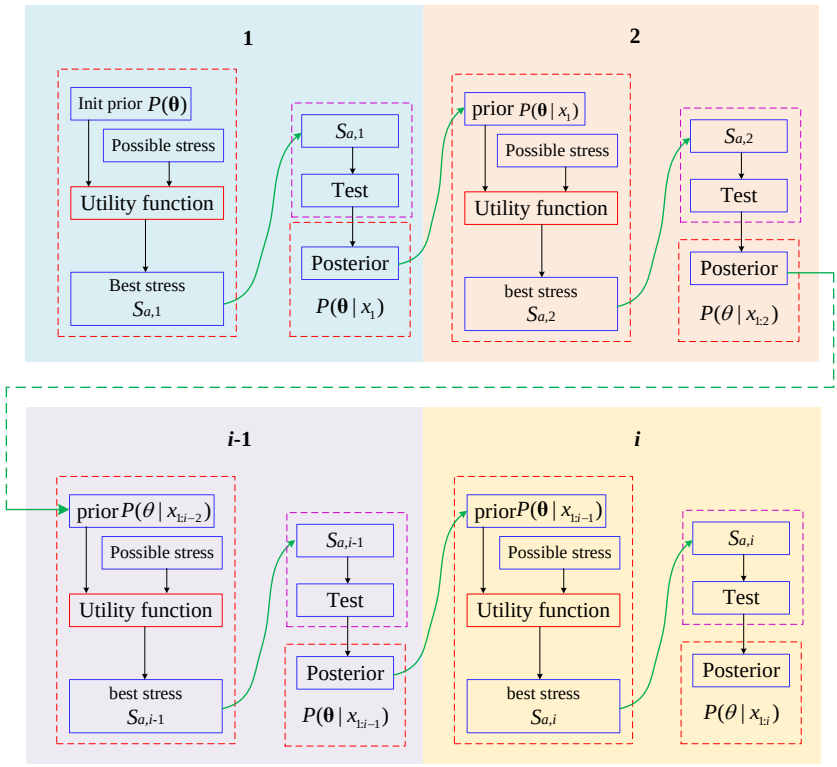

Figure 5.2: Workflow of the Bayesian staircase procedure

Assuming that the number of specimens is $n = 30$, an example of an up-and-down result is shown in Fig. 5.3. It can be seen that the first test is searched as the center of the mean range because there is no prior information. The second test is located closer to the boundary in a large load amplitude. Then, the load amplitude gradually decreases, until the opposite result appears. After that, the tests converged to near the mean value. All load amplitudes are optimized by the utility function as described before. So we can find variable load amplitudes during the simulated staircase test. In this study, the number of specimens $n = 30, 35, 40, 50, 70, 100$ are simulated, and similar results are found. The variable step size is used to maximize the utility function that based on Shannon entropy and probability.

From the Fig. 5.3, the Bayesian staircase method has two shortcomings. Firstly, this method relies on BMES to select the stress amplitude but ignores the test results (failure or survival). Secondly, the stress amplitudes gradually converge to the same values. Similarly, as shown in Fig. 5.4, Shannon entropy has a slower decrease rate after several tests. The fatigue tests in the later stages provide less information for searching for the best fit distribution. In order to improve the Bayesian staircase

in Magazzeni et al. [116] study, this part introduces the Latin Hypercube Sampling (LHS) into the Bayesian framework.

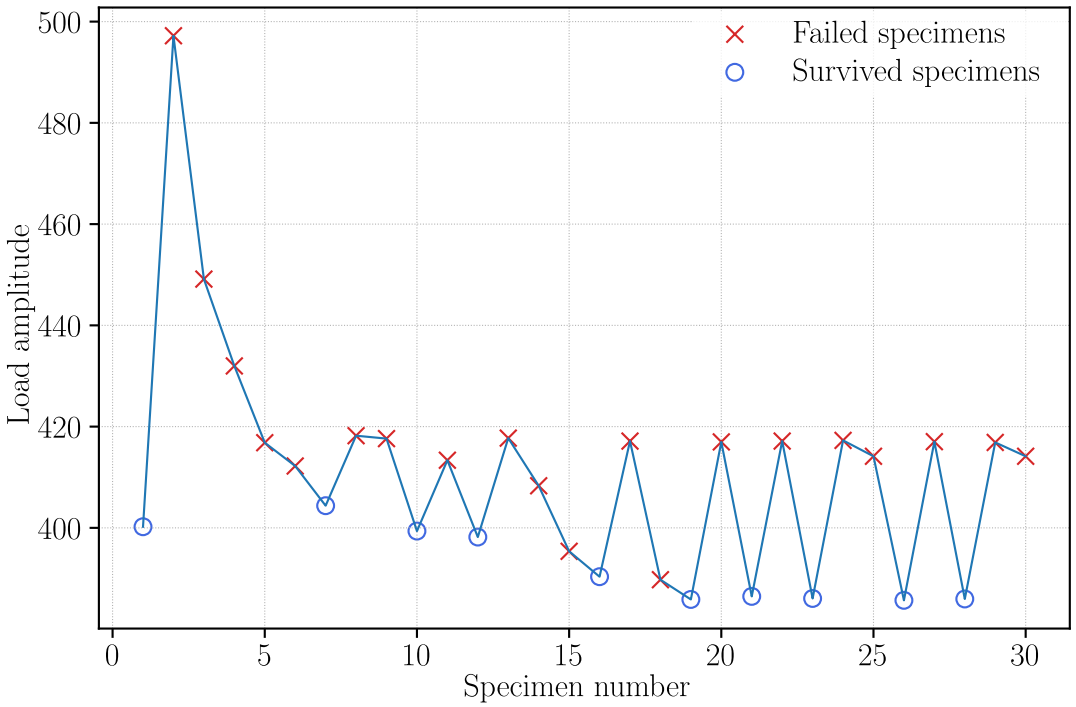

Figure 5.3: Up-and-down diagram of a simulated Bayesian staircase

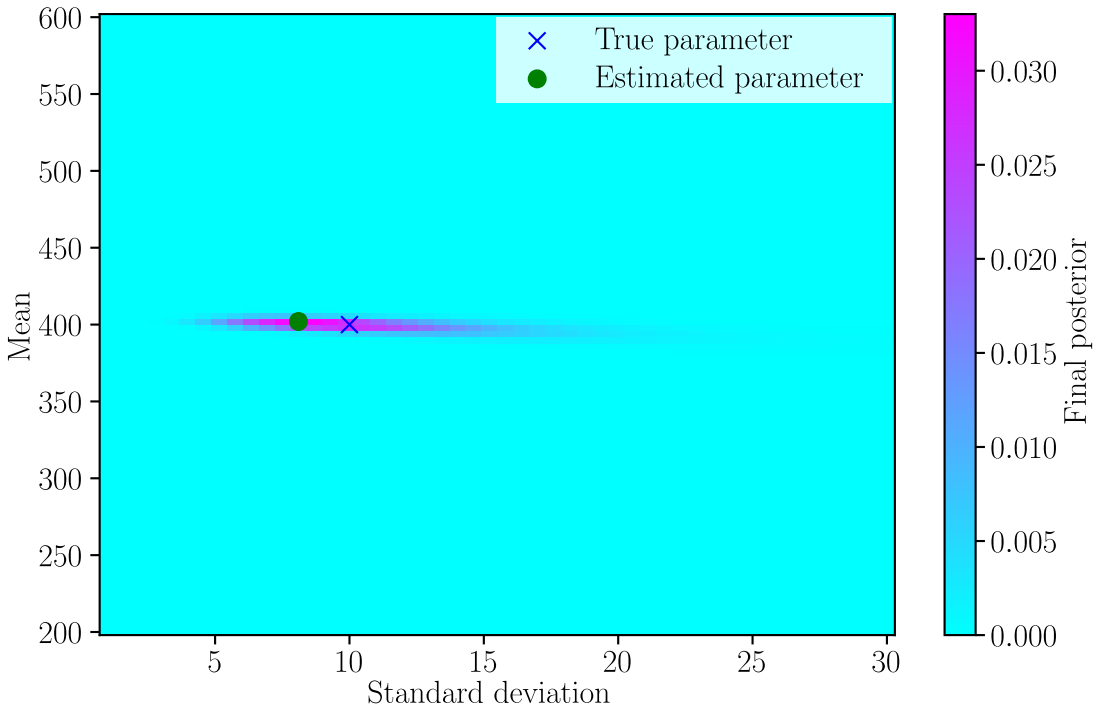

Figure 5.5: Posterior of the Bayesian staircase

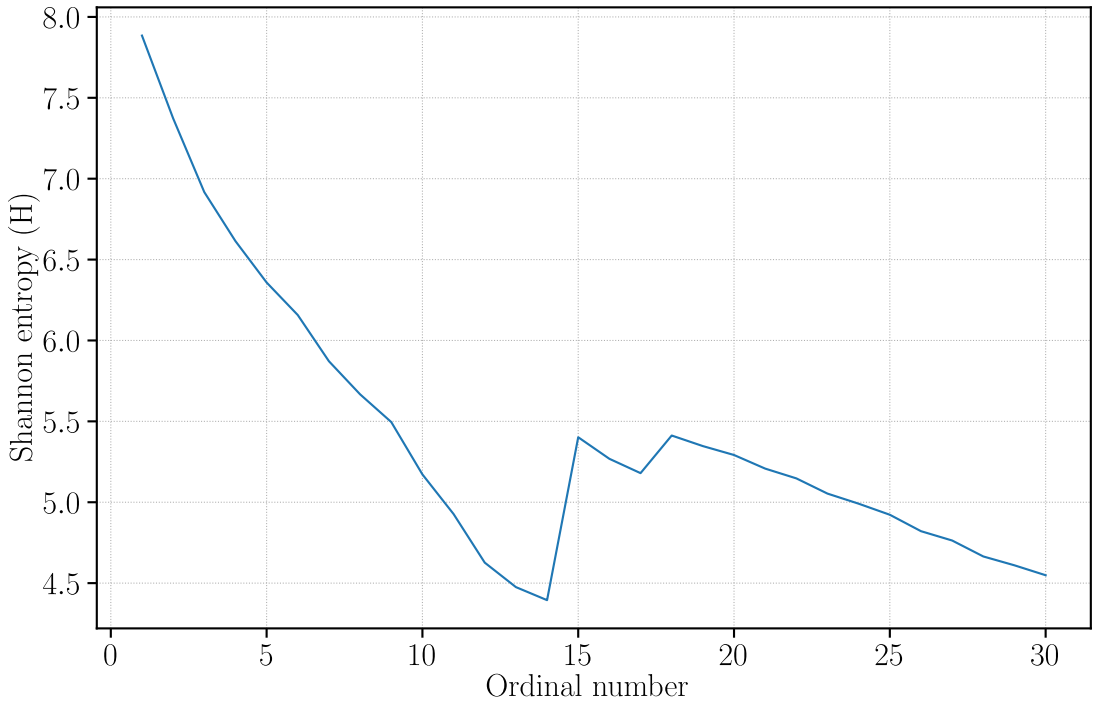

Figure 5.4: Shannon entropy of the Bayesian staircase

5.4. Improvement by using Latin Hypercube Sampling

Latin Hypercube Sampling (LHS) is a statistical method for generating a near-random sample of parameter values from a distribution [123]. As one-dimension LHS sampling strategy, the cumulative distribution function $[0, 1]$ is firstly divided into N equal parts to get $[0, 1/N]$, $[1/N, 2/N]$, ..., $[(N-1)/N, N]$. For these N partitions, a sampling point can be randomly selected in each partition, and then obtains N sampling values. This strategy maintains the independence between the samples at the same time.

The LHS has good uniformity with regard to the individual sub-layer. The CDF and PDF of an example of LHS are presented in Fig. 5.6. The 10 points sampled from a Normal distribution subject to $N(400, 10^2)$ in CDF and PDF can be shown in Fig. 5.6.

In the Fig. 5.6(a), the CDF curve is divided into 10 non-overlapping layers along y-axis (the blue lines). So that each interval (red lines) has the same cumulative probability. Selecting centring points (green points) in each interval, and total 10 sampling results (purple points) are obtained. Correspondingly, these sampling data with PDF is shown in the Fig. 5.6(b).

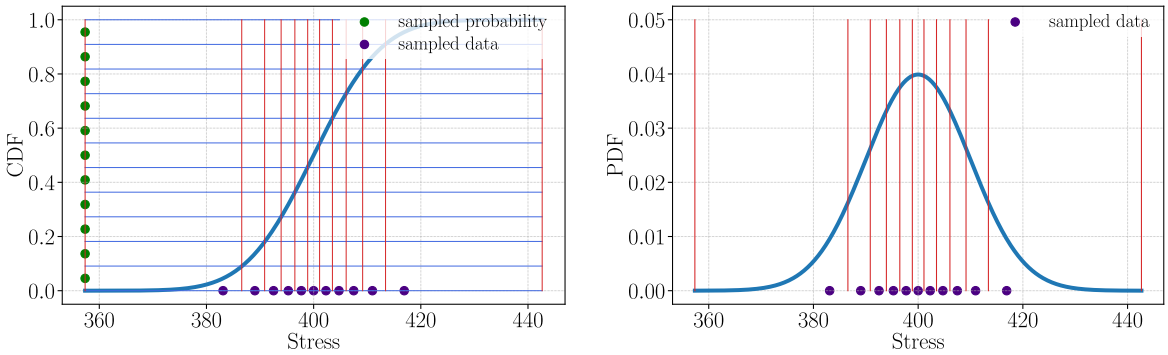

(a) CDF from LHS

(b) PDF from LHS

Figure 5.6: An example of LHS

In protocol design, the sampling procedure takes into account the previous stress amplitude. The LHS divides the CDF into N intervals and samples N points. To maintain uniformity during all the tests, the interval with the least number of specimens is selected as the stress amplitude.

An assumed distribution is needed to use the LHS in the experimental design. Hence, the LHS is used after BMES. Besides, the LHS requires less calculation and works faster than BMES

5.5. Application of the Bayes-LHS method for staircase representation

5.5.1. Input parameters

For the Bayes-LHS staircase test protocol, the parameters that need to be set before the test are:

(1) **The distribution type**. In this work, the Normal distribution is chosen to conduct the simulation study, though other models such as Weibull distribution and Lognormal distribution are also examined.

(2) **The possible range of the median of the fatigue limit distribution.** This proposed method is not sensitive to predefined ranges. In the practical application of this protocol, the median range in model parameter can be selected from a small value to yield strength.

(3) **The possible range of the standard deviation of the fatigue limit distribution.** The selection of the standard deviation range should come from the references and rely on the engineering experience.

The input parameters under the Normal distribution can be expressed as:

$$\begin{bmatrix} \boldsymbol{m} \\ \boldsymbol{s} \end{bmatrix} = \begin{bmatrix} m_1, & m_2, & \ldots, & m_a \\ s_1, & s_2, & \ldots, & s_b \end{bmatrix} \tag{5.23}$$

where m is the median and s is the standard deviation. Based on the input range, all possible model parameters ($\boldsymbol{\theta}$) for the fatigue limit distribution are created as a combination of the shape, location and scale according to the specific distribution initially assigned.

5.5.2. Bayes-LHS staircase protocol

The flowchart of the Bayesian staircase procedure is presented in In Fig. 5.7. The specimens tested by BMES are indicated as light blue, while the LHS are indicated as light red. i is the ordinal number of the specimens. The improved experimental procedure includes the stress amplitude determined from BMES and LHS.

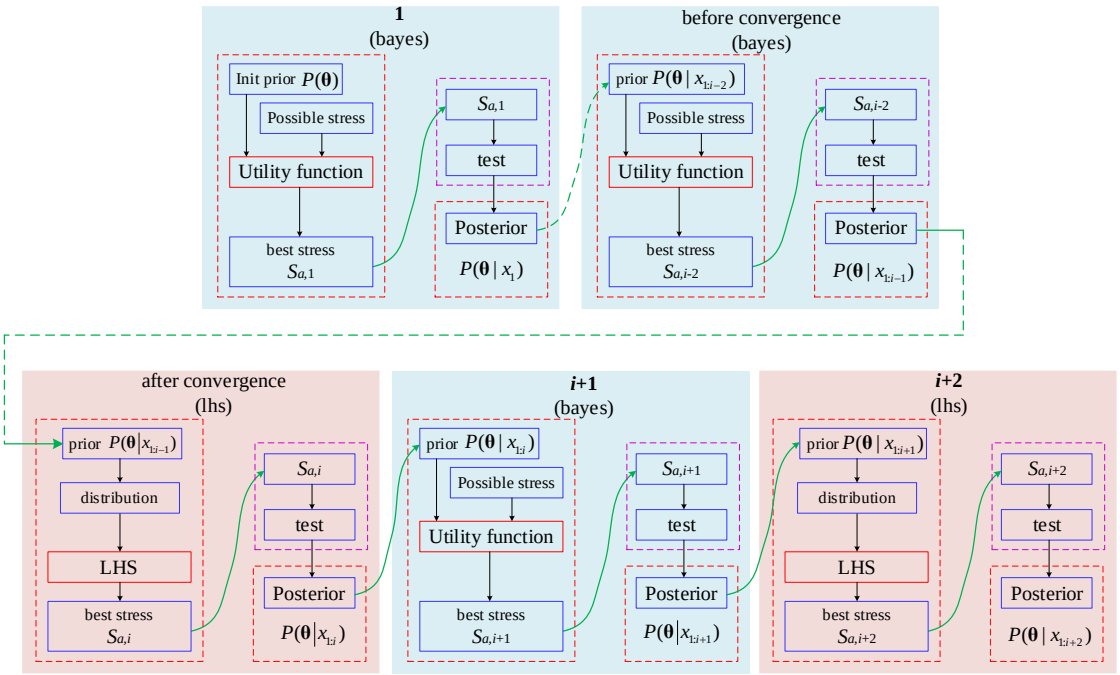

Figure 5.7: Workflow of the Bayes-LHS staircase procedure

For the first step (first specimen), the initial prior is created as described in Section 5.2.3. The possible stress values are chosen from the median range of the input parameter. The utility function, as described in Section 5.3.2, is used for searching this stress amplitude. After experimental test, the stress amplitude and test result (survival or failure) are obtained, and the posterior $P(\boldsymbol{\theta}|\boldsymbol{x}_{1:i+1})$ is updated based on this test result. This posterior is the prior for the next specimen.

The same procedure is repeated identically for other samples with BMES until the posterior has a convergence. The convergence means only one distribution corresponds to the maximum posterior. In the next step, the LHS is applied to determine the stress amplitude and update the posterior.

Then, the LHS and BMES are alternately used to determine the stress amplitude. The posterior is updated after each test. Finally, the posterior $P(\boldsymbol{\theta}|\boldsymbol{x}_{1:n})$ is obtained after the total n specimens.

The resulted posterior, $P(\boldsymbol{\theta}|\boldsymbol{x}_{1:n})$, presents the probability of the observations under the given possible model parameters. The estimated model parameters are obtained by searching the maximum in the posterior after the last step (last specimen). In summary, the improved staircase protocol is detailed in Algorithm 5.1.

Algorithm 5.1: Framework of Bayes-LHS staircase protocol

Data: Distribution; ranges of median and standard deviation;
Generate model parameter $\boldsymbol{\theta}$ Initial the prior $P(\boldsymbol{\theta})$
if $P(\boldsymbol{\theta}|\boldsymbol{x}_{1:i})$ *convergence* **then**
  Determine the load stress amplitude by BMES
else
  Determine the load stress amplitude by LHS and BMES alternatively
end if
Test the specimen
Calculate the posterior $P(\boldsymbol{\theta}|\boldsymbol{x}_{1:n})$ and Shannon entropy after each test
Final posterior
Result: The estimated median m and the estimated standard deviation s of the fatigue limit distribution

Compared to the Bayesian staircase method in Section 5.3.3, this Bayes-LHS method enriched it in two areas: Firstly, the principle is kept since the stress amplitude must decrease after a failure result. In contrast, the load level must increase after a survival result. Secondly, the LHS is applied as a tool to select the stress amplitude, which offers more choice for stress amplitudes.

5.5.3. Example of Bayes-LHS procedure

Based on the Normal distribution assumption, an example in the case of $n = 30$ is presented in this section. The up-and-down figure from Bayes-LHS is shown in Fig. 5.8.

Similar to the conventional staircase procedure, the specimens are tested separately. The first few specimens perform a preliminary search of the median fatigue limit, and the test data gradually converge towards the solution. After posterior convergence to a single estimated distribution, the BMES and LHS alternate in picking

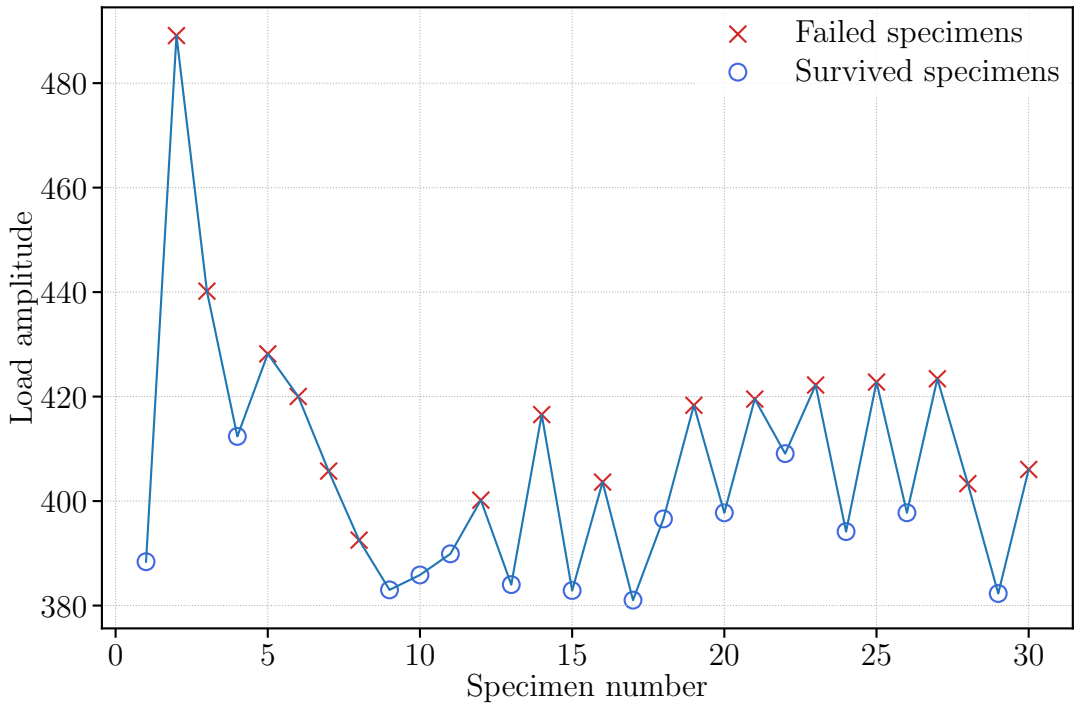

Figure 5.8: Up-and-down diagram of a simulated Bayes-LHS staircase test

the stress amplitude, with each sample using the previous posterior information. In the end, the maximum value in the final posterior is the estimated distribution, as shown in Fig. 5.9. The evolution curve of Shannon entropy during the test is reflected in Fig. 5.10.

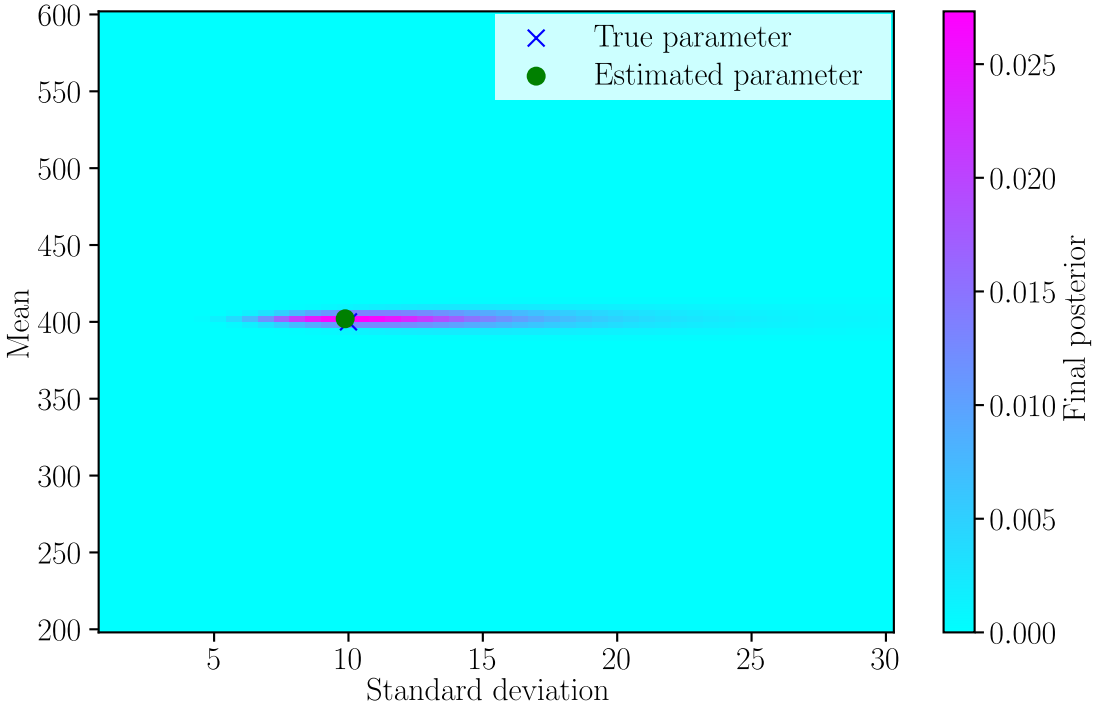

Figure 5.9: Posterior and estimation of a Bayes-LHS staircase test

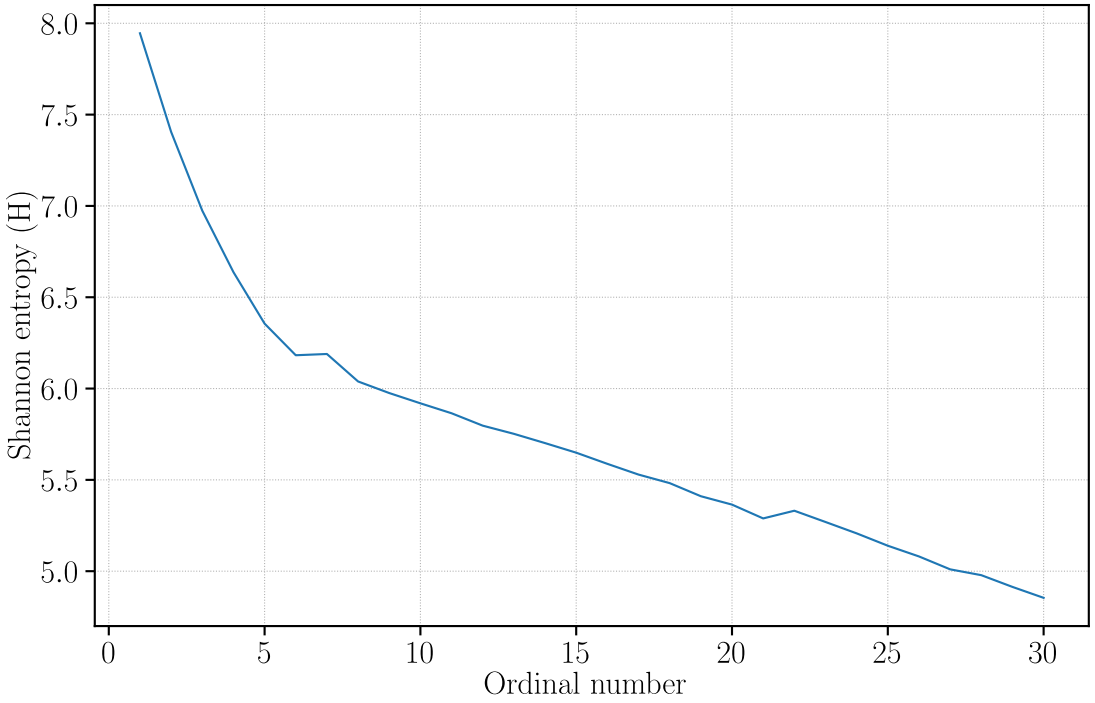

Figure 5.10: Shannon entropy of a Bayes-LHS staircase test

5.6. Numerical simulation of the Bayes-LHS test protocol

In this study, the possibly unknown distribution is asymptotically approached by the Normal distribution. However, other distribution models, such as Lognormal distribution and Weibull distribution, can also be used as the underlying distribution.

In order to evaluate the effectiveness of the proposed method, a numerical simulation modelling the staircase test is carried out. The staircase simulation is configured as shown in Fig. 5.11.

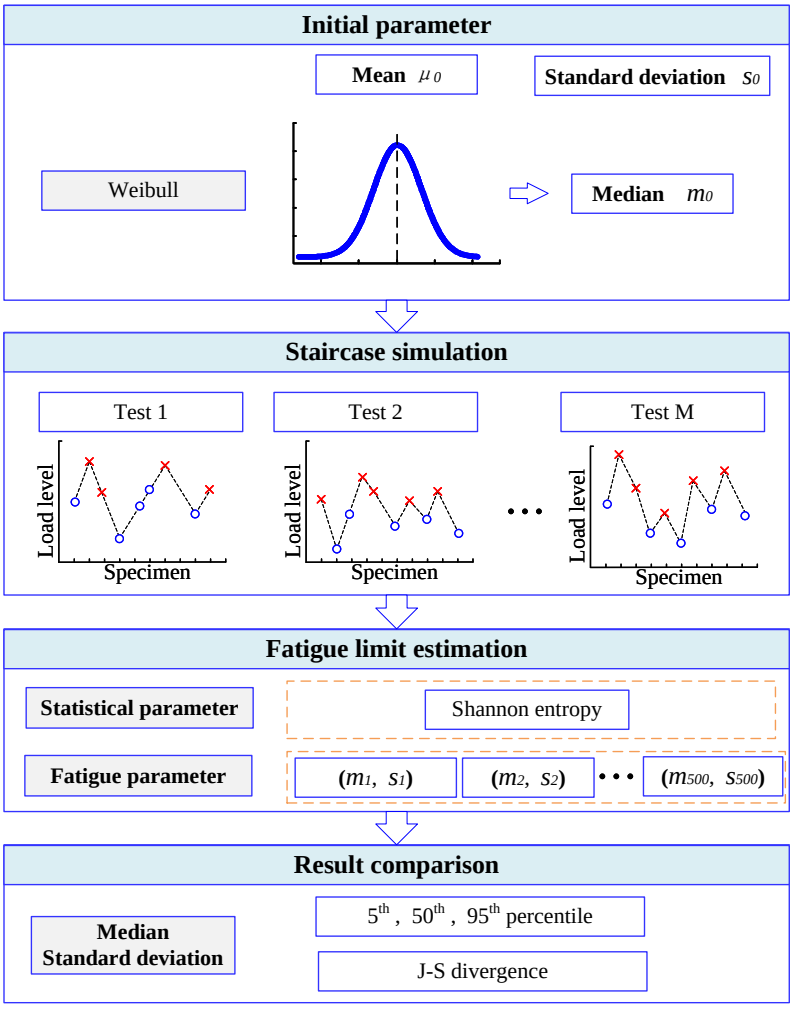

Figure 5.11: Simulation procedure and evaluation of the results

5.7. Results and discussions

A total of 400 trials are conducted for the Bayesian staircase and the Bayes-LHS staircase, respectively. Firstly, the evolution in the Shannon entropy indicates the efficiency of the test. Taking the $n = 30$ as an example, the decrease of Shannon entropy within a test from 400 simulations is shown in Fig. 5.12.

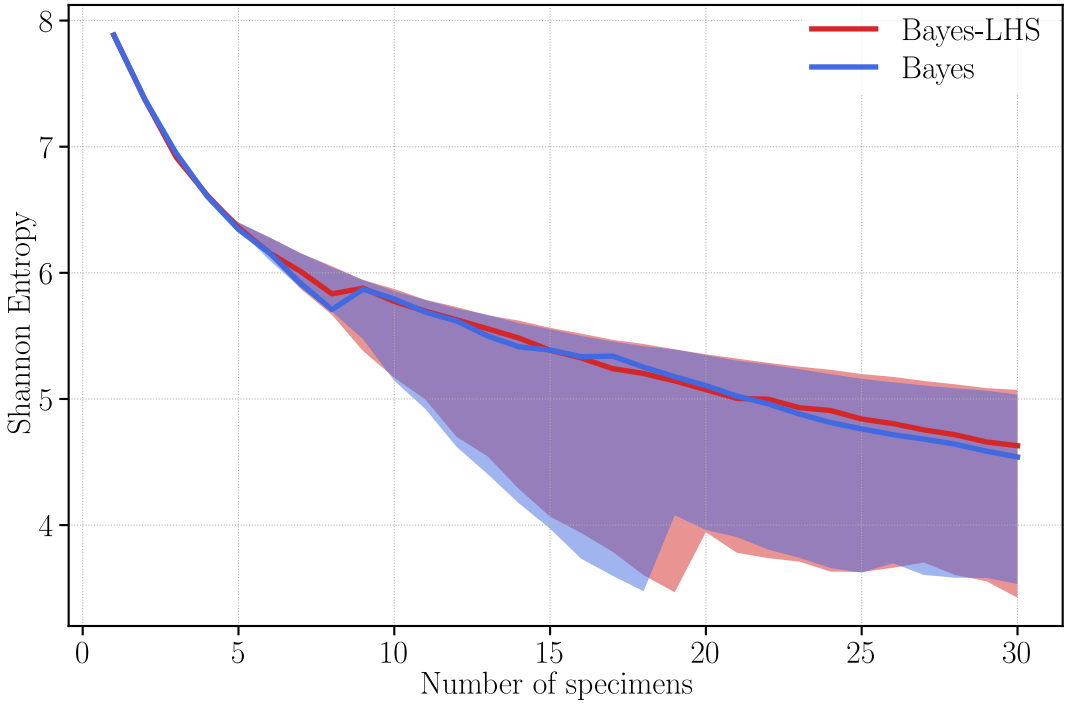

Figure 5.12: Decrease of the Shannon entropy in case of $n = 30$

In the Fig. 5.12, the blue area represents $5^{th} - 95^{th}$ percentile of the Shannon entropy from the Bayesian staircase method, while the red area represents that from the Bayes-LHS method. The blue and red lines are 50^{th} percentile of all entropy values. It can be found that both methods give the same tendency for entropy to decrease. The entropy value decreases fastest for the first several specimens, which also have the same results because the both methods start from the same model parameters ($\boldsymbol{\theta}$).

5.7.1. Sensitivity analysis of input parameters

To reach the better solution, it is necessary to analyse their sensitivity to input parameters, including guessed median range and standard deviation range. This study chooses three different median ranges and three standard deviation ranges for the simulation work, as listed in Tab. 5.1. Note that the true distribution is assumed as a Normal distribution $[400, 10^2]$. 200 trials are simulated for the comparison.

Table 5.1: Different input parameters

	Probability Distribution	Median range	Standard deviation range
Case 1	Normal	300-500	1-20
Case 3	Normal	200-600	1-20
Case 2	Normal	100-700	1-20
Case 4	Normal	200-600	1-30
Case 5	Normal	200-600	1-40

The estimated results for the median and the standard deviation are compared in Fig. 5.13 and Fig. 5.14 which show the effect of median range and the effect of standard deviation range, respectively.

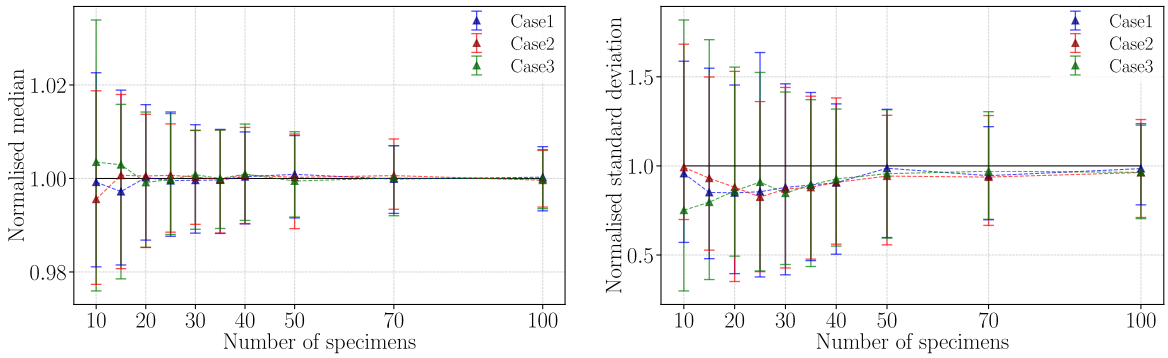

(a) (b)

Figure 5.13: Normalised (a) median value and (b) standard deviation with the different median ranges

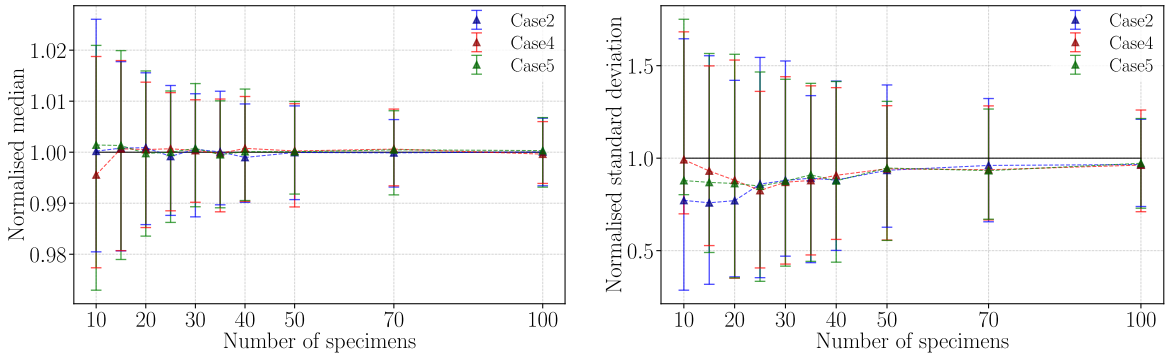

(a) (b)

Figure 5.14: Normalised (a) median value and (b) standard deviation with the different standard deviation ranges

In Fig. 5.13 and Fig. 5.14, case 2, case 4, case 5 (as listed in Tab. 5.1) are illustrated by the blue, red and green line, respectively. Each vertical bar represent the 5^{th} and 95^{th} percentiles, and the central marker represent the 50^{th} percentile (median).

From Fig. 5.13, the difference occurs for a number of specimens less than 20. For the Bayes-LHS test with a number of specimens greater than 20, the input median range has almost no influence on the estimation results. It is possible to choose between a small value and the yield stress as the median range in a real experiment. The same findings can be observed in Fig. 5.14. The estimated standard deviation does not rely on the guessed standard deviation range.

In a word, the Bayes-LHS method is not sensitive to input parameters with a sufficient number of specimens in the test ($n \geqslant 20$).

5.7.2. Comparison of the Bayesian staircase and Bayes-LHS method

Choosing Case 4 of Tab. 5.1 as input, the estimated results for median and standard deviation is shown in Fig. 5.15.

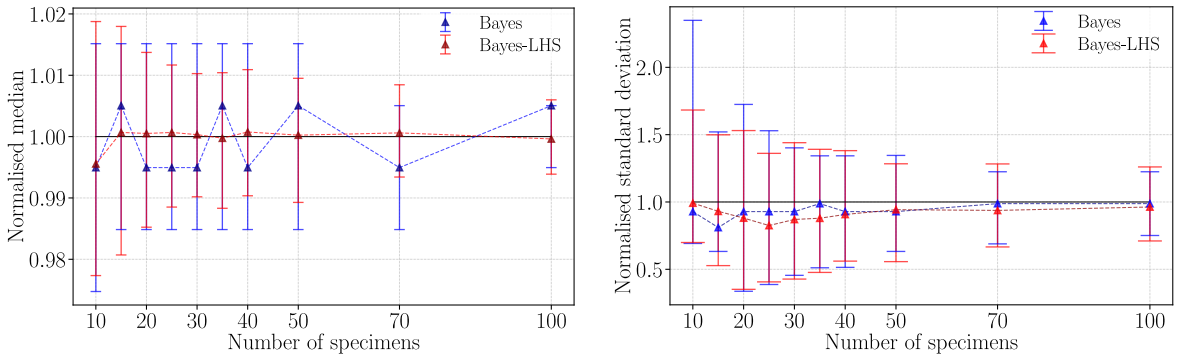

(a) (b)

Figure 5.15: Normalised (a) median value and (b) standard deviation with respect to the number of specimens

In Fig. 5.15, the Bayesian staircase and Bayes-LHS method are illustrated by the blue line and the red line, respectively. It can be observed that:

(1) Similar to the conventional staircase method, the estimated results of the Bayes staircase and Bayes-LHS method become more accurate with more specimens.

(2) From Fig. 5.15(a), the Bayes-LHS method is more stable on the median estimation. The estimated median is centred on the true value.

(3) From Fig. 5.15(b), the estimated standard deviation obtained from the Bayesian staircase method and Bayes-LHS method have almost the same uncertainty. More-

over, both methods have an underestimated bias for the standard deviation, especially with fewer number of specimens.

5.7.3. Comparison to the conventional staircase using KDE

In order to show the advantage of the Bayesian staircase method, the comparison between Bayes-LHS method and the conventional staircase method using KDE is presented in this section. In this comparison, the number of specimens is fix at 30. For the step size only existed in the conventional staircase method, the normalized step size 0.5, 1.0, 1.5 are selected for comparison. 200 trials are conducted for each method.

For Bayes-LHS method, the input parameter of Case 4 (see Tab. 5.1) is adopted. The conventional staircase is simulated as the procedure given in Section 4.2. For comparison with respect to the number of specimens $n = 30$ (Fig. 5.16), we choose the normalised step size d=0.5, 1.0 and 1.5 as examples. Since there is no step size in the Bayes-LHS method, the results are presented for comparison with respect to the step size (Fig. 5.16(b)). Based on 200 trials, the estimated median and standard deviation is shown in Fig. 5.16 and Fig. 5.17.

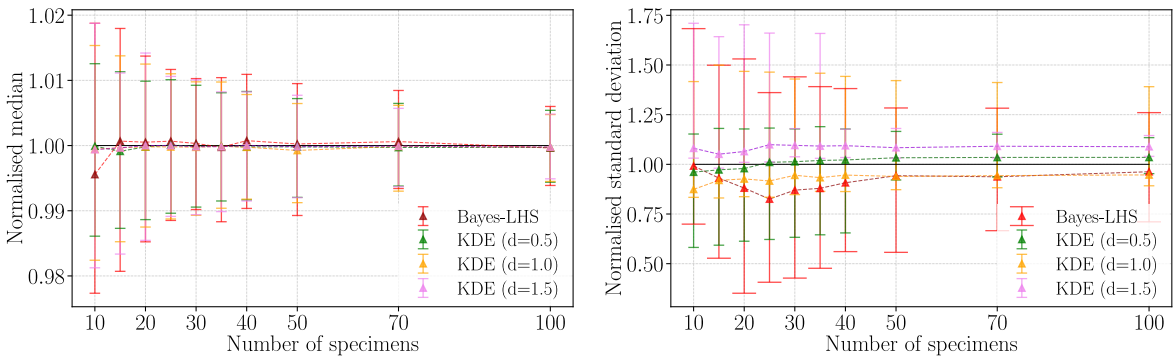

(a) (b)

Figure 5.16: Normalised (a) median value and (b) standard deviation with respect to the number of specimens

It can be observed that:

(1) From Fig. 5.16(a), four line kinds almost overlap. The estimated median results obtained from the Bayes-LHS method and KDE are almost identical. The Bayes-LHS method is worse when the number of specimens is less than 20. The same observation can also be made for Fig. 5.17(a).

(2) From Fig. 5.16(b), the estimated standard deviation of Bayes-LHS method always

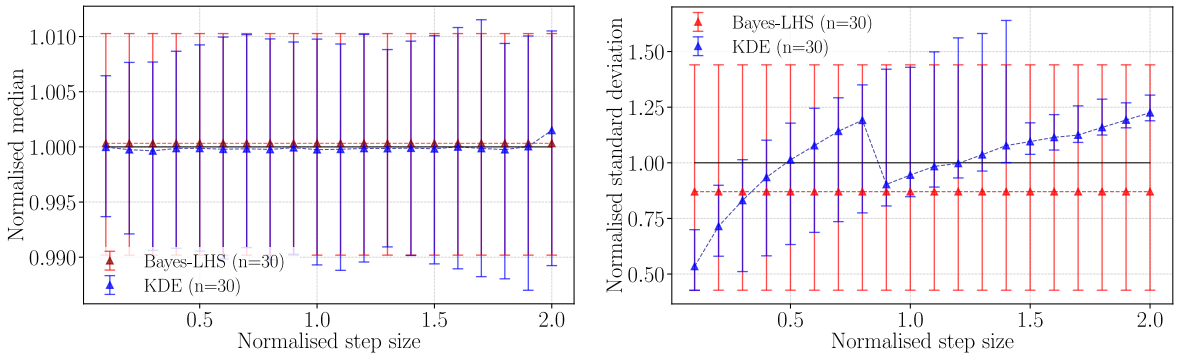

(a) (b)

Figure 5.17: Normalised (a) median value and (b) standard deviation with respect to step size in conventional staircase method

includes the true value, while that of the conventional staircase is affected by the step size. However, the vertical red line is longer than others, which means that the estimation uncertainty of Bayes-LHS method is lower than KDE with correction.

(3) From Fig. 5.17(b), the results of the conventional staircase method are dependent on the step size even though the correction is applied to KDE.

(4) From Fig. 5.16(b) and Fig. 5.17(b), the horizontal red dash are below the horizontal black line. This means, the Bayes-LHS method has a disadvantage of underestimating the standard deviation, especially when the number of specimens is in the range of [20-40].

5.8. Conclusion

This chapter presents an improved experimental staircase procedure, Bayes-LHS method, based on Bayesian Maximum Entropy Sampling (BMES) and Latin Hypercube Sampling (LHS). This method uses the BMES and LHS to select the stress amplitude (load level) in staircase testing, which removes the step size parameter. A simulation is conducted to compare the Shannon entropy and estimated median and standard deviation for the numerical validation of this new protocol.

Compared to the conventional staircase method, the advantage of Bayes-LHS method can be listed as follows:

(1) The Bayes-LHS method avoids the use of guessed start stress and fixed step size. It should artificially select a range of possible model parameters before the Bayesian staircase test.

(2) Due to the non-sensitivity of input parameters, very little information is required on the sample set before the test.

(3) The conventional staircase method with corrected KDE has an advantage in re-

ducing the estimation uncertainty. Therefore, it is suitable if the standard deviation is well-guessed. Otherwise, the Bayes-LHS method is recommended for the fatigue limit distribution assessment.

(4) There is no need to use a post-processing method. The distribution model parameter is obtained directly from the posterior.

Chapter 6
Conclusion and perspective work

The present work depicts the subject of fatigue limit assessment. The thesis covers aspects from mechanical fatigue experiments to statistical methods. This final chapter summarises what we have learned from previous works and points out the most promising directions for future research.

According to the literature review, fatigue limit assessment is a challenging practical problem as the structure is exposed to vibration conditions, thus is crucial a reliable structural design. To achieve probability distribution of the fatigue limit, the critical challenges come from the experimental test method and an advanced evaluation technique of the test data.

The fatigue limit assessment begins with the experiment test. A vibration bench is a reasonable solution to reduce fatigue test time. In contrast, the fatigue limit test requires the specimen to be subjected to a constant stress amplitude for a certain number of cycles. A strain control technique applied to an electro-dynamic shaker is proposed to conduct a constant strain amplitude test. The efficiency of the proposed approach has been demonstrated by testing in bending DC01 steel plates at their first resonant frequency. The strain control on resonance (amplification of the signal) and relatively high-frequency excitation leads to a reduction of the testing time to reach a large numbers of cycles. This approach is therefore effective for testing the staircase method. The fatigue threshold and the scatter of steel DC01 is estimated by the staircase results.

The statistical method offers approaches to provide the fatigue limit distributions for each staircase test. The key question is: what results from a re-conducting execution of the staircase test? Uncertainty analysis is carried out to evaluate the fatigue limit distributions of a material obtained from the staircase test. For this purpose we applied the resampling method, leave-one-out and bootstrap on the staircase data in order to deduce the scatter of the mean and standard deviation of the distribution. The results of this study highlighted the high inherent uncertainty in the standard deviation estimation.

To reduce this uncertainty, we propose to use the Kernel density estimation (KDE) in this study due to its non-parametric and independence from the distribution model. To compare it with other assumption-based methods, the KDE is tested on different

distributions to validate its efficiency. The dependency of the KDE hyperparameter is also studied and optimized to improve its performance in in assessing fatigue limit. Moreover, as the staircase method requires to define an initial step size, a non-linear corrected factor is formulated to reduce its influence in estimating the standard deviation. The numerical approach uses the Monte-Carlo simulation and allows to examine the effect of the number of specimens and the step size. The estimation performance is evaluated on the mean and standard deviation of the fatigue limit involving different distributions and coefficient of variation.

Intending to solve the limitation of step size in the staircase method, a Bayes-LHS staircase protocol is presented to remove the step size in the conventional staircase. The Bayesian theory in fatigue test and Bayesian Maximum Entropy Sampling (BMES) are detailed, and then the Bayesian staircase protocol is provided with an example. This study called Bayes-LHS method enriched the Bayes approach with the Latin Hypercube Sampling (LHS). This proposal is described for staircase procedure. The results are sufficiently optimistic to consider that the Bayes-LHS protocol could replace the conventional staircase method for fatigue limit estimation.

The original contributions of our work mainly involve:

1. For the present approach, staircase tests for deducing the fatigue limit are accessible by using the strain control method. The strain control is effective for low-carbon steel and provides a stable vibration control method to reach the High cycle fatigue domain in a relatively short time.
2. The bootstrap resampling is applied to evaluate the uncertainty of the staircase test. It provides a numerical sampling method to avoid the real experimental tests.
3. A non-parametric evaluation method based on Kernel Density Estimation (KDE) estimates the fatigue limit distribution in a data-driven way rather than using handcrafted heuristic strategies. The proposed method estimates the fatigue limit distribution without prior knowledge. It is not sensitive to its hyperparameter, and is less affected by the test parameters of the staircase method, such as the number of specimens and the step size.
4. Bayesian including the LHS for optimizing the staircase method to eliminate the effect of the step size. The improved test procedure uses the previous information during the test, and requires less information before numerical testing. Also, there is no need to use a post-processing method such as Maximun Likelihood Estimation (MLE) or KDE. Because the distribution model parameter is obtained directly from the posterior.

In the experiment part of this study, low carbon steel specimens were selected to carry out fatigue tests with strain control. We found that this material is the simplest

to study with this type of excitation (control of the deformation in vibration). We had previously tested Ti-6Al-4V and steel 304L. However, for some unknown reasons (different hypotheses were put forward but none of them gave satisfaction), it was possible to test materials in acceleration but not in strain control. In fact, the balance point (zero) of the strain measurement is shifted during the test.

Lots of Ti-6Al-4V and steel 304L specimens were tested with strain control. Some Ti-6Al-4V specimens with different treatments are presented as examples in Fig. 6.1. In this figure, different treatment for specimens and load strain amplitude are list in Tab. 6.1

Table 6.1: Different treatments for Ti-6Al-4V specimens used in Fig. 6.1

Curve	Vibration stress relief	Heat-treatment (℃)	Resonant frequency (Hz)	Strain ($\mu m/m$)
C1-1200	-	-	331	1200
C1-1500	-	-	330	1500
C2-700	√	-	359	700
C2-900	√	-	353	900
C2-1200	√	-	353	1200
C2-1500	√	-	357	1500
C3-3000	-	650	340	3000
C4-900	-	1050	335	900
C4-1200	-	1050	327	1200

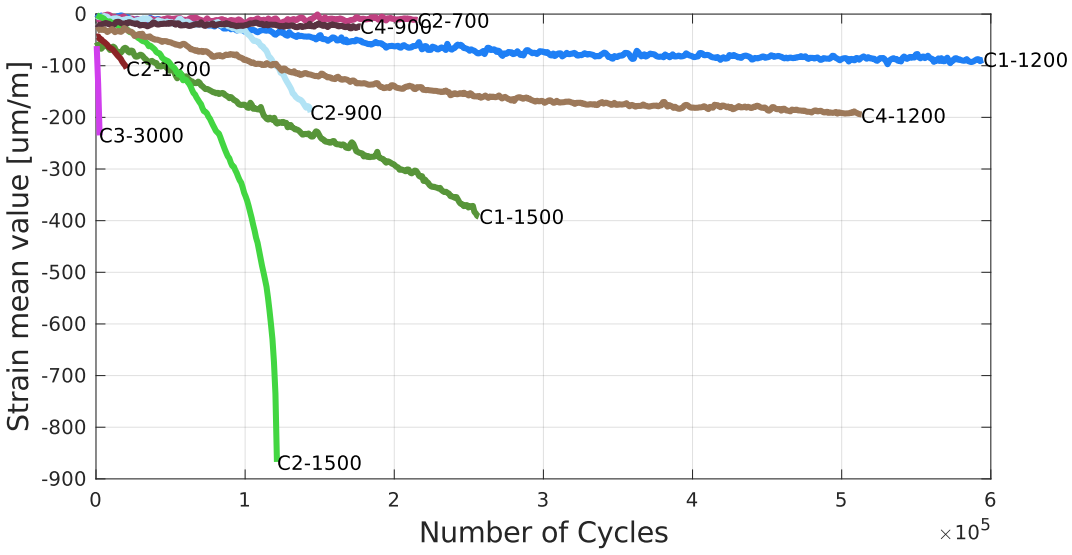

Figure 6.1: Decrease of strain mean value from Ti-6Al-4V specimens

From the Fig. 6.1, the obtained strain signals show a decrease with the number of cycles. The higher strain amplitude for the specimens with the same treatment leads to a faster decrease. Comparing C1 and other cases, the vibration stress relief and the heat-treatment before the track dwell test did not improve the test performance.

Indeed, we have found that strain control is not possible on Ti-6Al-4V titanium alloy and 304L stainless steel. One of the reasons is stated by Barbier [124] who indicates that 304L has a cyclic behavior that evolves over several cycles and does not stabilize even beyond several million cycles. Therefore, we preferred to direct this study toward standard steel. Hence, a research is required to evaluate the applicability of strain control for different materials.

To improve the study, several other ways will be investigated for further work:

1. Another investigation concerns the effect of frequency and geometric dimensions of the specimens on the fatigue limit. Because this research could lead to a "perfect" specimen to reach the fatigue limit distribution
2. An improvement of the Bayes-LHS approach is necessary to achieve a well-performing approach. For example, a way is to use the chaos polynomial to fit the distribution. The interest can be to adjust the coefficients on the basis of the uncertainties related to the experimental tests (e.g. the clamp).
3. In this work, we have carried out the tests on the bending mode. Another way would be to perform the tests in torsion mode. The torsional fatigue limit could then be used to build a reliability model as presented in the work of Lambert et al. [22].

Appendix A
Dynamics analysis of the specimen

Before the experiment fatigue test, it is desirable to obtain the dynamics characterization of the specimen by numerical model. In this study, the numerical model is established by finite element analysis (FEA) based on Ansys software [1].

A.1. Finite element modelling

A.1.1. Mesh and element

In this study, the shell 181 element is used to create the Finite Element model. Shell 181 is a four-node element with six Degree Of Freedom (DOF), that is suitable for analyzing thin shell structures in out-of-plane excitation. The FE model is shown in Fig. A.1 and it is built from 2293 nodes and 2267 elements, the size of elements is 1 mm.

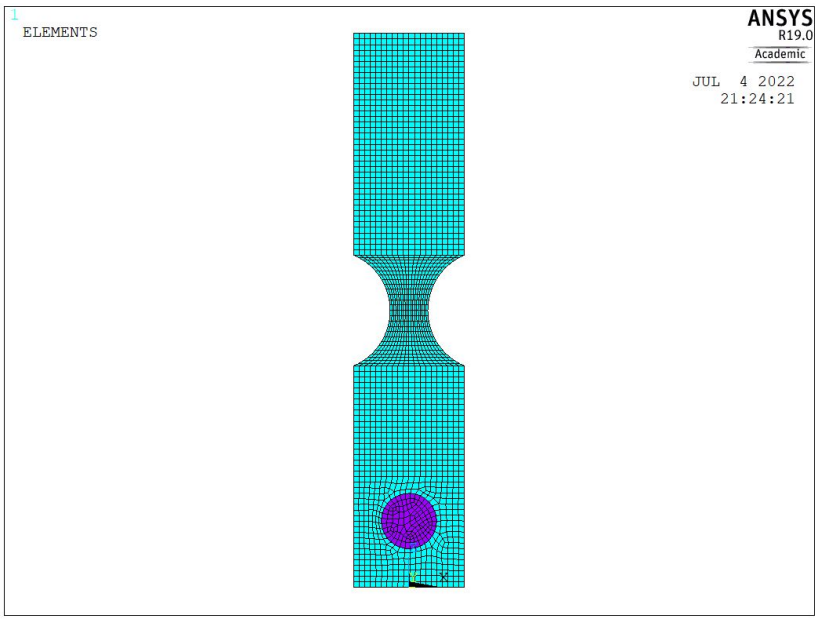

Figure A.1: Finite element model of the specimen

1. Ansys® Academic Research Mechanical, Release 17.0

A.1.2. Boundary condition

The second issue in modelling is how to simulate the constraints in experiment, that is boundary condition of the FE model . The specimen is fixed in the shaker by two mass blocks and pre-tightened by machine screw. The clamping of the shaker is illustrated in Fig. A.2.

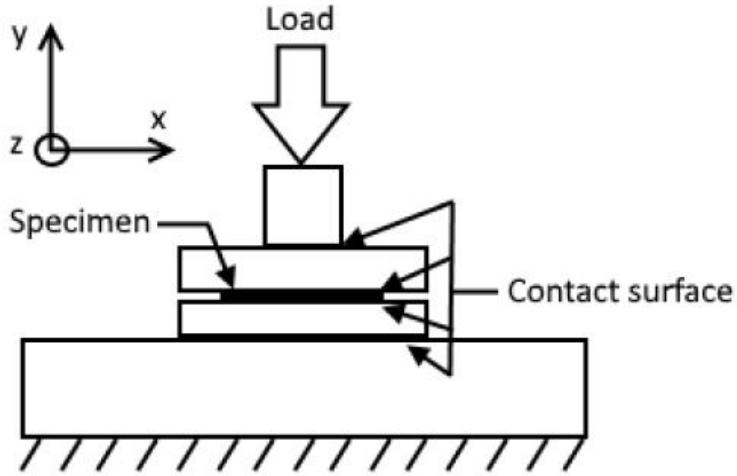

Figure A.2: A sketch of the clamp in the shaker [76]

A previous study was carried out by Appert et al. [76] on the same kind of clamping. The authors carried out a non-linear quasi-static finite element analysis in Code Aster to study the contact pressure in the fixture. The resulting design is reported in Fig. A.3, where the red color corresponds to no pressure and blue color corresponds to maximal pressure. Both two faces of the specimen have same pressure state.

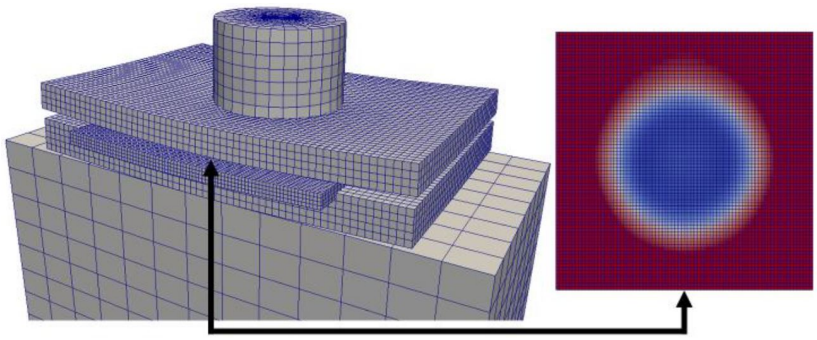

Figure A.3: Deformed shape and contact pressure of the clamp [76]

From Appert's conclusion, it is clear that the specimen is clamped only close to the screw. The screw is modeled as a regular cylinder in Appert's research. Therefore, the outer circumference line of the screw is used to define the clamp as the boundary condition.

To check the effects of the constraints on the first mode, we tested different combinations of the 6 DOFs. The results on the resonant frequency are listed in Table A.1. DX, DY, DZ represent the displacement and DRX, DRY, DRZ the rotation along x, y and z.

Table A.1: The first resonant frequencies estimated for several boundary conditions

DX	DY	DZ	DRX	DRY	DRZ	frequency (Hz)
√	√	√	√	√	√	211.35
√	√	√	√	×	×	211.14
√	√	√	×	√	×	205.96
√	√	√	×	×	√	206.66
√	√	√	×	√	√	206.36
√	√	√	√	×	√	211.35
√	√	√	√	√	×	211.14
√	√	√	×	×	×	205.96

Note: √: Constraint; ×: Free

As shown in Fig. A.2, the experimental clamping is intended to ensure a high rigidity in the translate direction of DX, DY and DZ. Also, the rotation DRZ is fixed by two plates. DRY is fixed by the lower plate, DRX is also fixed because the mass of specimens is much lower than the vibratory bench (not directly connected with the shaker armature) [76]. The boundary condition of all 6 DOFs in FE model is marked in Fig. A.4.

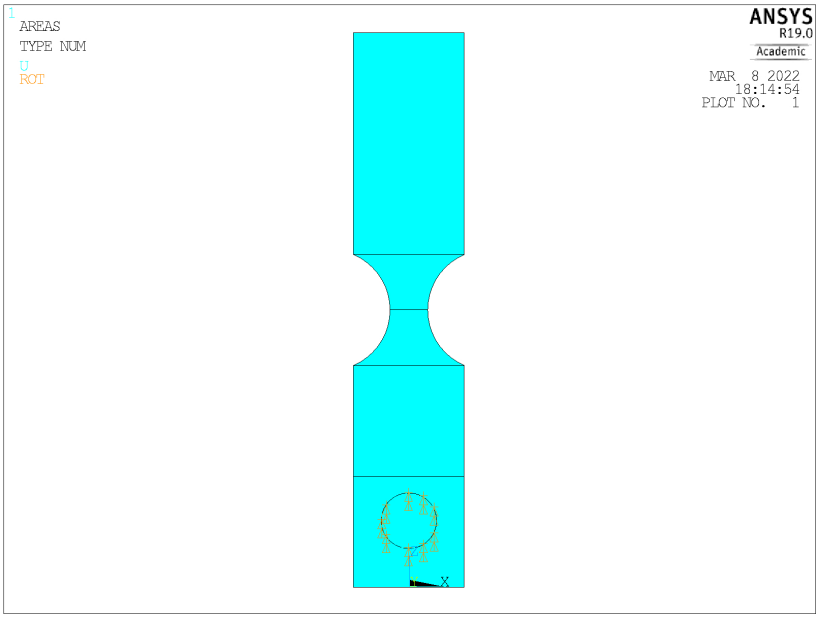

Figure A.4: Representation of the clamp in finite element model

From Tab. A.1 and Fig. A.4, the constraints in DX, DY, DZ, DRY, DRZ are adopted in this study.

A.2. Dynamics characterization

A.2.1. Modal analysis

A FEM of the experimental specimen is studied based on Ansys . Considering the clamp in the base, the modal behaviour of the specimen is shown in Fig. A.5.

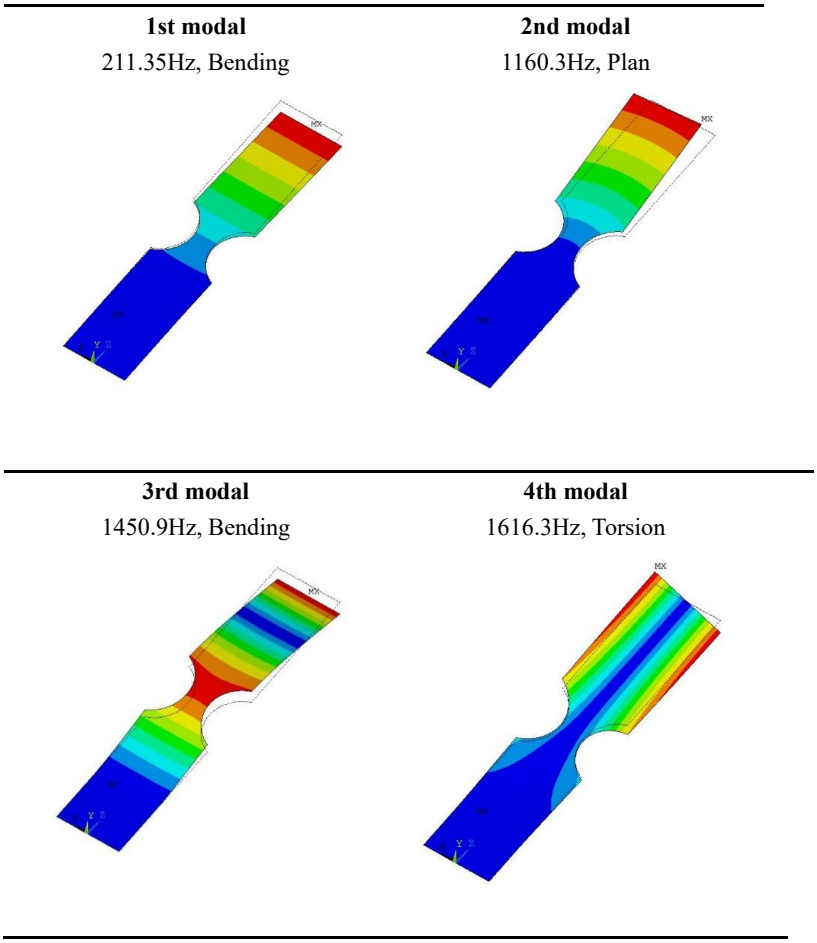

Figure A.5: The modals of the specimen with thickness 2mm

A.2.2. Harmonic analysis and test validation

Firstly, the FRF are obtained by harmonic analysis range of 100 Hz-2000 Hz under acceleration 3 g. The FRF of stress in central point (the location of strain gauge) is shown in Fig. A.6.

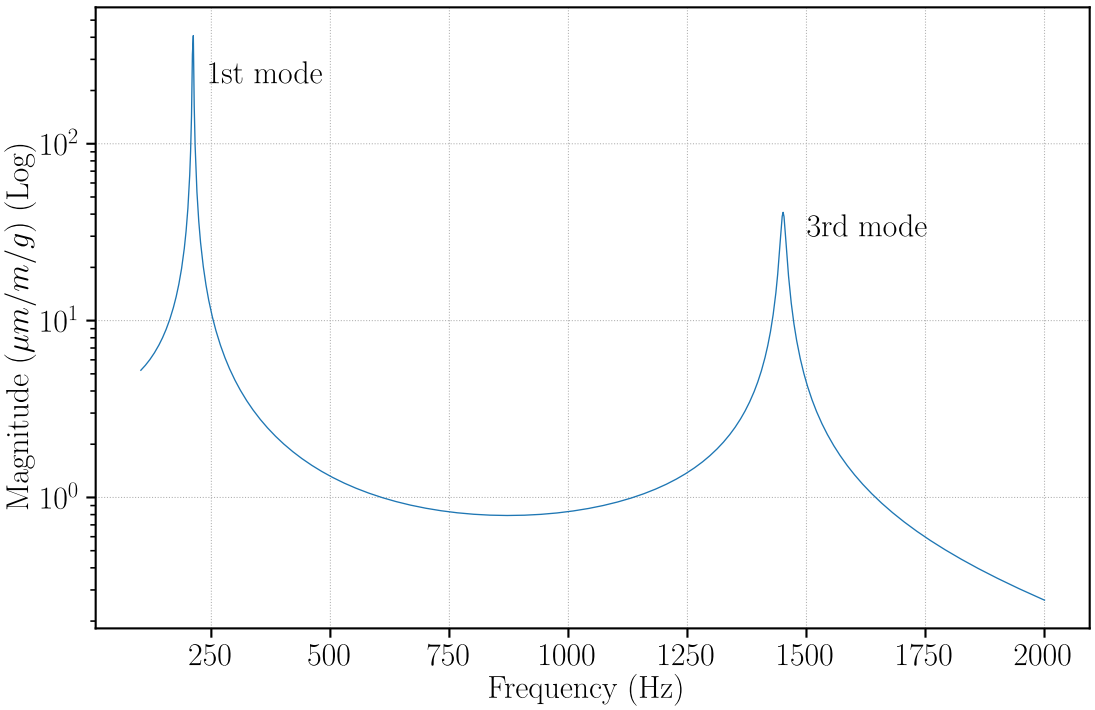

Figure A.6: FRF of strain

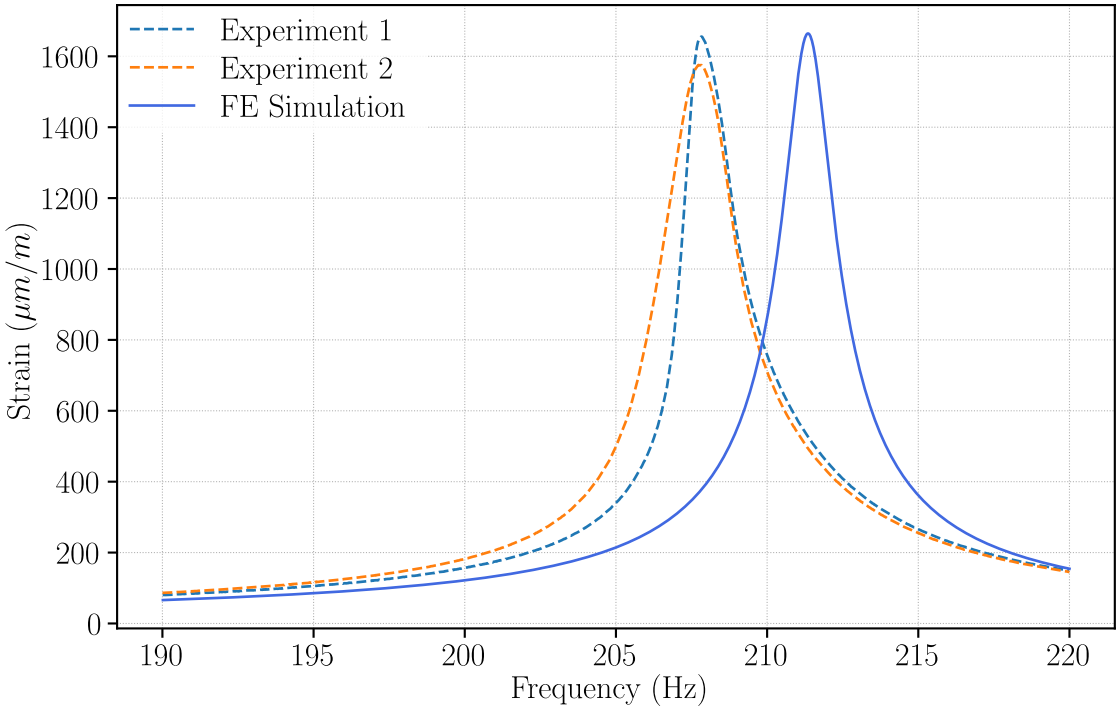

Figure A.7: Harmonic analysis and experiment result

According to the FEM simulation, the resonant frequencies of the first bending mode of the specimens with thickness 2 mm is 211.35 Hz. The second mode is far away from the first mode. Comparing these four modes, the first bending leads to the most

large damage in reduction area. Therefore, the first bending is chosen in fatigue test.

Secondly, the harmonic analysis and the two sine sweep experiments are carried out in range of 190 Hz-220 Hz under acceleration 3 g. The strain response are compared in Fig. A.7.

It can be seen that the resonant frequency and the strain response from simulation and experiment are close. These results provide verification for the FE model .

A.2.3. Stress concentration factor

At the notch area of the specimen, the local stress is much greater than the nominal stress, which is known as stress concentration. Fatigue failure typically occurs at the notched edge because the local stress is much greater than the nominal stress. To simplify the description, two sample models are established: specimen without notch (SWON) for nominal stress, and specimen with notch (SWN) for maximum stress.

The Stress Concentration Factor (SCF) can be expressed as:

$$K_t = \frac{\sigma_{max}}{\sigma_{nom}} \tag{A.1}$$

σ_{max} is the local maximum stress and σ_{nom} is nominal stress. Assuming the axial force ($F = 1N$) and the dimension of specimen without notch, σ_{nom} is given by:

$$\sigma_{nom} = \frac{My}{I_x} = \frac{F(L - L_r)\frac{h}{2}}{\frac{bh^3}{12}} = 3.38\,\text{MPa} \tag{A.2}$$

This result is in accordance with the results of Ansys. Then, the static SCF is calculated as:

$$K_t = \frac{10.6}{3.2958} = 3.21621 \tag{A.3}$$

In terms of the fatigue limit, tests indicate [86] that the presence of a notch on specimen under cycling nominal stresses reduces the fatigue strength of the smooth specimen by a fatigue notch factor K_t given by:

$$K_f = \frac{\text{unnotched fatigue limit}}{\text{notched fatigue limit}} \tag{A.4}$$

In general, K_f is equal to or less than K_t. The K_f is related to both the notch root radius and ultimate tensile strength. More information about K_f can be found in Liu et al. [4].

A.2.4. Location of strain gauge

There is an important experimental particularity about strain gauge which must be addressed. For the first mode, the strain is homogeneous as shown in Fig. A.8.

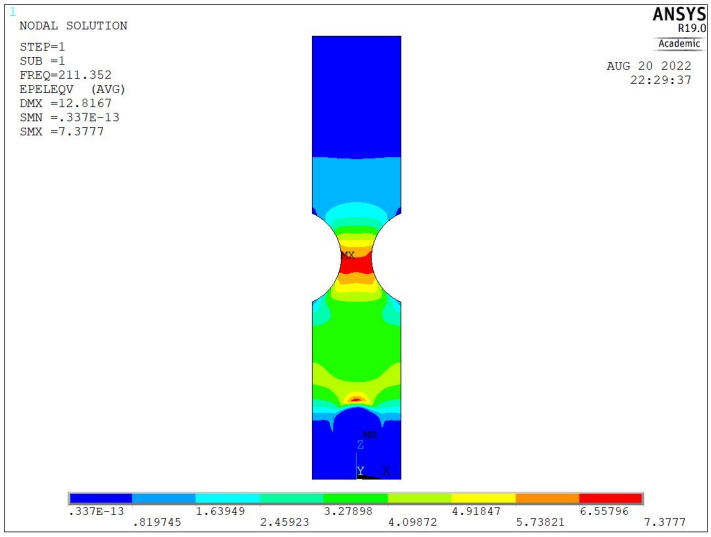

Figure A.8: Strain distribution for the first mode

The real maximum stress occurred in the edge of the arc, while it is easier to manipulate if the gauge is placed at the center of the notch area (as shown in Fig. A.9) So, it needs a calibration test to investigate both positions in stress estimation. This problem is discussed here with respect to numerical study, sine sweep test and track dwell test.

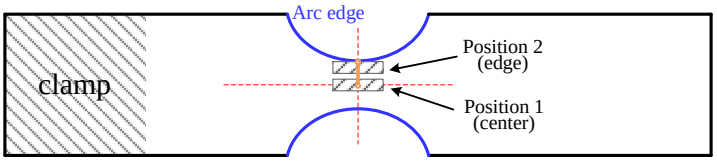

Figure A.9: Two positions for strain gauge

Firstly, the stress at two different locations can be calculated from a harmonic analysis. The maximum stress at the notch edge is about 1.325 (tension) and 1.06 (bending) higher than the stress in the middle of the specimen, as can be seen in Fig. A.10.

Secondly, Ansys results were also verified by testing. Two strain gauges are mounted in the center and on the edge of the reduced section of one specimen. The sine sweep test and SRTD are performed respectively to compare responses from these two locations of interest. The strain responses in the sine sweep test with acceleration control

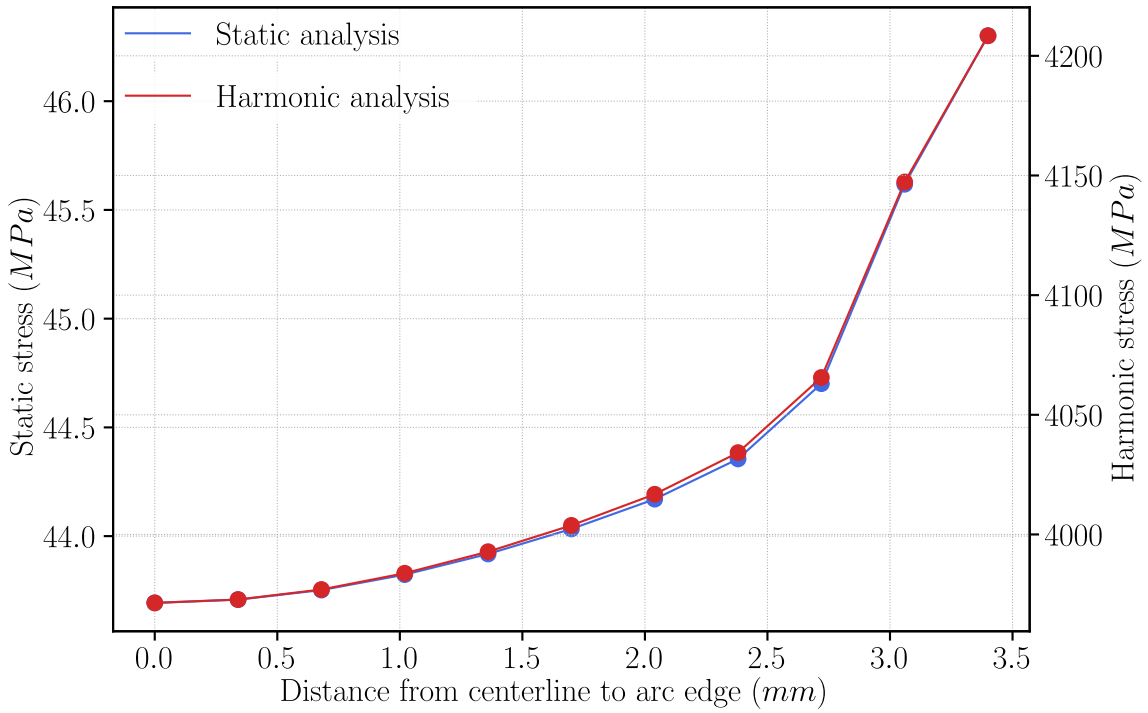

Figure A.10: Stress gradient evolution from the center to the edge (orange line in Fig. A.9)

in 2 g, 4 g, 6 g and 8 g are shown in Fig. A.11. The red line and blue dash are the values obtained from the strain gauge in the arc and the center of the stress concentration zone respectively. The strain value close to the notched edge is 1.015 times as high as the strain value in the center of the specimen.

Thirdly, the track dwell test controlled by the strain in 760 µm/m for 280 s, the responses of the velocity are shown in Fig. A.12. The highest strain at the notched edge is only 0.55% higher than the strain at the middle of the specimen, as presented in Fig. A.12.

In conclusion, the strain value at the edge and the middle of the specimen reduced section are almost the same as predicted by the numerical model in Fig. A.8. Considering the feasibility of sticking the strain gauge, the difference in the two locations is neglected, and the strain gauge is glued on the center of the specimen for all tests.

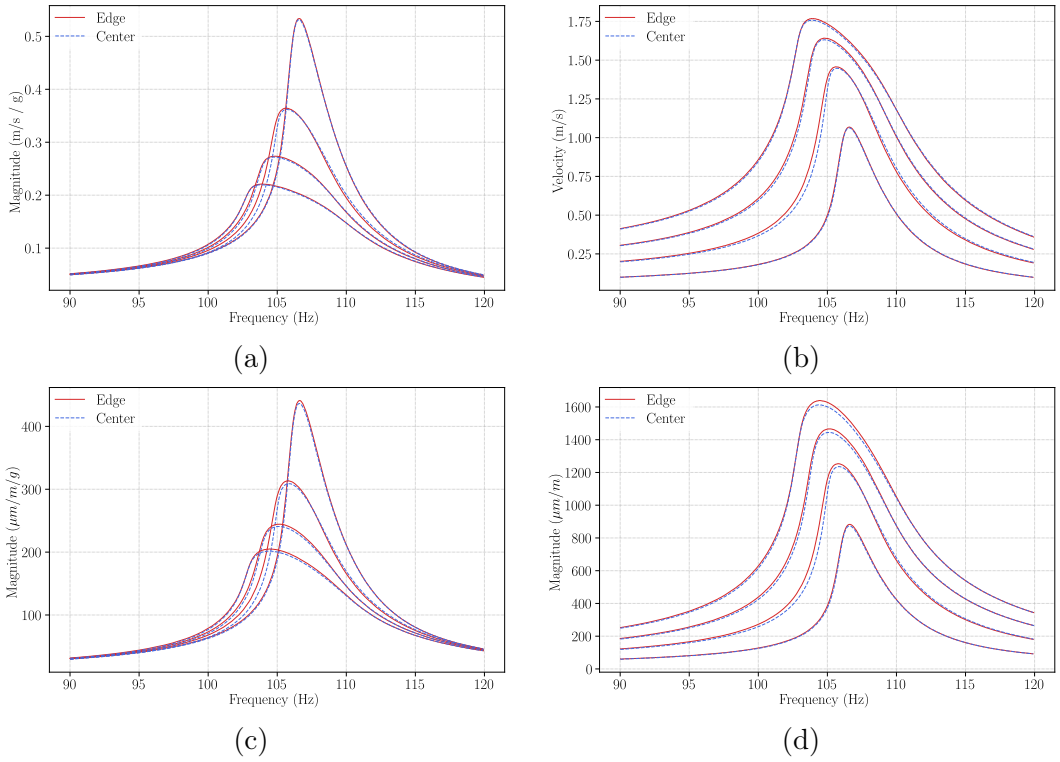

Figure A.11: Comparison between the response in the specimen center and on edge obtained by experimental tests

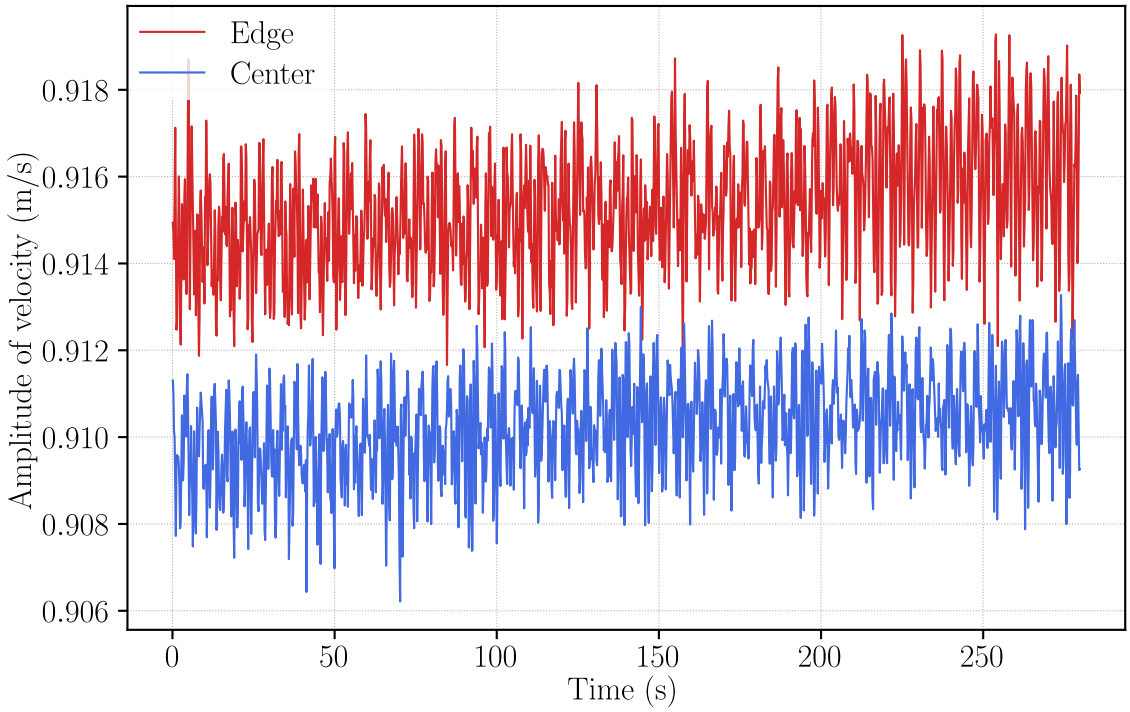

Figure A.12: Velocity response in specimen center and on the edge of the notch

Appendix B
Staircase test data

The detailed data for the specimens in the staircase tests are listed in this section. The specimen names are listed in Tab. B.1.

Table B.1: Effect of dimensions on the resonant frequency

Specimen Id	Thickness (mm)	Length (mm)	Resonant frequency (Hz)
S1	1	100	105
S2L	2	170	107

Table B.2: The specimen, test data and test results from staircase test of specimen S1

Order i	Mass (g)	Strain $(\mu m/m)$	fr^0 (Hz)	Number of cycles $(N, \times 10^5)$ $\%RFC = 1$	$\%RFC = 2$	$\%RFC = 3$	$\%RFC = 4$	$\%RFC = 5$	Result (-)	End of the test $N_{end}(\times 10^5)$	$(\%RFC)$	Number of cracks
1	14.205	1400	102.17	1.97237	-	-	-	-	survival	10.28857	1.89	0
2	13.881	1420	98.26	8.20944	9.19791	9.47587	9.72233	9.97197	failure	10.06509	5.45	1
3	13.702	1400	98.1	-	-	-	-	-	survival	10.53344	0.75	0
4	14.314	1420	102.1	8.79832	9.1802	9.2561	9.29178	9.31036	failure	9.33044	7.66	1
5	14.168	1400	102.11	5.48675	6.14195	6.44087	6.56366	6.62072	failure	6.65164	6.31	2
6	14.145	1380	101.6	-	-	-	-	-	survival	10.30475	0.71	0
7	14.249	1400	102.73	4.79549	-	-	-	-	survival	10.37413	1.22	0
8	14.302	1420	103.43	8.4914	9.09986	9.24076	9.29729	9.32899	failure	9.33455	5.11	1
9	14.09	1400	101.6	0.76433	8.18097	8.68838	8.8883	9.01526	failure	9.06706	5.67	1
10	14.159	1380	101.49	-	-	-	-	-	survival	10.30352	0.6	0
11	13.794	1400	98.32	0.76498	5.07992	7.28616	7.7355	8.00344	failure	8.08092	5.53	2
12	14.063	1380	100.67	-	-	-	-	-	survival	10.20939	0.74	0
13	14.017	1400	99.81	-	-	-	-	-	survival	10.11093	0.83	0
14	14.245	1420	103.28	-	-	-	-	-	survival	10.48336	0.69	0
15	13.928	1440	100.4	0.6515	8.7489	9.69959	9.85773	9.92852	failure	9.98189	6.22	1
16	14.007	1420	101.08	0.19976	7.52629	10.03543	10.80065	11.43074	survival	11.97107	6.63	1
17	14.178	1440	103.36	1.99812	-	-	-	-	survival	10.93874	1.85	0
18	14.128	1460	100.8	5.43833	6.63317	6.84794	7.03775	7.22655	failure	7.47347	6.96	2
19	13.964	1440	103.4	-	-	-	-	-	survival	10.47881	0.8	0
20	14.118	1460	107.04	8.98097	9.70777	-	-	-	failure	9.81153	2.31	1
21	14.177	1440	108.58	7.09969	7.59003	7.74663	7.81466	-	failure	7.84461	4.77	1
22	14.164	1420	108.2	-	-	-	-	-	survival	13.10515	0.43	0
23	14.244	1440	102.96	-	-	-	-	-	survival	11.05515	0.77	0
24	14.27	1460	103.22	7.8618	8.8133	8.9406	8.997	9.0268	failure	9.0287	5.04	1
25	14.259	1440	102.78	5.87758	8.02554	8.34724	8.47644	8.55054	failure	8.61823	5.91	2
26	14.095	1420	100.04	10.06361	-	-	-	-	survival	10.74634	1.63	1
27	13.785	1440	96.58	5.52431	6.44052	6.68414	6.82917	6.9205	failure	6.96115	5.52	1
28	14.091	1420	100.23	5.62697	6.47246	6.60866	6.65233	6.66924	failure	6.6711	5.07	1
29	14.193	1400	102.04	7.13997	7.80374	7.93271	7.98152	8.00566	failure	8.02767	6.22	1
30	14.15	1380	101.98	-	-	-	-	-	survival	10.78397	0.64	0
31	14.136	1400	101.88	-	-	-	-	-	survival	12.76079	0.79	0
32	14.161	1420	102.44	8.72761	9.56921	9.71201	9.76854	9.8021	failure	9.81873	5.71	1

Table B.3: The specimen, test data and test results from staircase test of specimen S2L

Order i	Mass (g)	Strain $(\mu m/m)$	fr^0 (Hz)	Number of cycles $(N, \times 10^5)$ $\%RFC = 1$	$\%RFC = 2$	$\%RFC = 3$	$\%RFC = 4$	$\%RFC = 5$	Result (-)	End of the test $N_{end}(\times 10^5)$	$(\%RFC)$	Number of cracks
1	38.067	1360	107.61	2.59149	3.05248	3.25288	3.38698	3.49539	failure	4.37208	25.53	2
2	37.805	1340	110.15	-	-	-	-	-	survival	10.61576	0.43	0
3	37.656	1360	108.84	5.62984	6.60216	7.05941	7.31311	7.45365	failure	7.62853	7.83	2
4	37.751	1340	107.97	5.08999	5.46754	5.56714	5.60505	5.6238	failure	5.63124	5.62	2
5	37.867	1320	107.54	6.82224	7.28689	7.38994	7.43902	7.46891	failure	7.53573	12.51	2
6	37.714	1300	107.17	5.80151	6.24755	6.34543	6.38341	6.40032	failure	6.42928	13.04	2
7	37.578	1280	107.77	8.71045	9.47744	9.72219	9.82436	9.88239	failure	9.98879	8.15	2
8	38.07	1260	107.69	-	-	-	-	-	survival	11.06315	0.17	0
9	38.116	1280	108.74	9.38336	10.23871	10.66693	10.93543	11.16559	failure	11.39506	6.11	2
10	37.859	1260	107.61	11.47208	-	-	-	-	survival	11.57174	1.06	0
11	38.102	1280	107.8	9.77233	10.53176	10.83959	11.00421	11.09597	survival	11.11085	5.2	1
12	37.918	1300	108.2	-	-	-	-	-	survival	11.03161	0.31	0
13	37.995	1320	107.44	7.84875	8.55759	8.8187	8.95638	9.04595	failure	9.15265	6.74	2
14	37.989	1300	108.42	-	-	-	-	-	survival	11.17851	0.32	0
15	38.09	1320	108.27	8.2753	8.76854	8.9657	9.06988	9.13924	failure	9.40762	26.53	2
16	37.653	1300	108.1	-	-	-	-	-	survival	10.86193	0.4	0
17	37.902	1320	107.99	-	-	-	-	-	survival	11.34238	0.33	0
18	37.878	1340	108.12	7.96203	8.53394	8.69124	8.75389	8.78207	failure	8.80064	6.18	2
19	37.585	1320	106.96	-	-	-	-	-	survival	11.50584	0.98	0
20	37.875	1340	106.98	-	-	-	-	-	survival	10.90555	0.37	0
21	37.768	1360	108.16	8.67703	9.23933	9.50596	9.68059	9.80646	failure	10.26943	17.56	2
22	38.13	1340	108.28	7.34234	8.30292	8.78681	9.08711	9.27518	failure	9.60025	9.37	2
23	37.885	1320	108.64	11.32435	-	-	-	-	survival	11.34391	1.01	1
24	38.079	1340	107.71	5.26093	5.8365	6.02567	6.11642	6.17067	failure	6.28712	10.39	2
25	37.892	1320	107.37	7.15804	7.5988	7.77782	7.88147	7.94862	failure	8.0986	20.42	2
26	37.749	1300	107.12	8.06828	8.70401	8.87666	8.93171	8.95613	failure	9.00014	9.22	2
27	38.126	1280	108.94	9.53908	-	-	-	-	survival	10.66517	2	1
28	38.135	1300	107.93	8.55177	9.21526	9.49407	9.69678	9.85838	failure	10.07815	6.72	2
29	37.965	1280	108.02	10.89935	-	-	-	-	survival	11.33999	1.29	1
30	38.054	1300	107.36	8.04917	8.36178	8.4944	8.55526	8.59102	failure	8.64434	9.18	2
31	38.057	1280	110.14	-	-	-	-	-	survival	11.86388	0.34	0
32	38.105	1300	108.59	10.38954	10.96651	11.16309	11.28775	11.36626	survival	11.45953	9.71	2
33	37.945	1320	107.35	6.59587	7.18665	7.40947	7.54701	7.64956	failure	7.67363	5.26	2
34	38.063	1300	108.29	-	-	-	-	-	survival	12.063	0.36	0
35	38.074	1320	107.8	11.53829	-	-	-	-	survival	11.61006	1.07	1
36	38.094	1340	108.52	-	-	-	-	-	survival	11.57281	0.96	0

Appendix C
Comparison study using the Dixon-Mood method

C.1. Dixon-Mood method

The Dixon-Mood (DM) method was proposed by Dixon and Mood [27] in 1948, which provides approximate formulas of maximum likelihood estimation to calculate the mean and standard deviation of the fatigue limit. This method is a development and simplification from Maximun Likelihood Estimation (MLE) and the parameter distribution is assumed to be a normal distribution. Though there are many post-processing methods that have been studied in recent years, DM is still classic and the most widely used method for staircase data.

In DM method, the less frequency event (survival or failure) is used to calculate the following quantity. The load levels S_a are discrete by step size d and ordinally numbered by j, where $j = 0$ for the lowest load level $S_{a,0}$. Denoting by $n_{c,j}$ the number of the fewer frequency events (survival or failure) at the load level j, two auxiliary values A and B can be calculated by Eq. C.1:

$$\begin{aligned} A &= \sum_{j=0}^{j_{max}} j \times n_{c,j} \\ B &= \sum_{j=0}^{j_{max}} j^2 \times n_{c,j} \\ n_c &= \sum_{j=0}^{j_{max}} n_{c,j} \end{aligned} \tag{C.1}$$

The auxiliary values were used to estimate the mean m_{DM} by Eq. C.2 and the standard deviation s_{DM} by Eq. C.3. The minus sign given in Eq. C.2 is used if the failed specimens are evaluated and otherwise, the plus sign is used.

$$m_{DM} = S_{a,0} + d\left(\frac{A}{n_c} \pm \frac{1}{2}\right) \tag{C.2}$$

$$\begin{aligned} s_{DM} &= 1.62 \times d\left(\frac{Bn_c - A^2}{n_c^2} + 0.029\right) \quad \text{if} \quad \frac{Bn_c - A^2}{n_c^2} \geqslant 0.3 \\ s_{DM} &= 0.53 \times d \qquad\qquad\qquad\qquad\quad \text{if} \quad \frac{Bn_c - A^2}{n_c^2} < 0.3 \end{aligned} \tag{C.3}$$

In which the subscript "DM" represents the Dixon-Mood method. The DM equations for the staircase method are also recommended by ISO 12107[35].

C.2. Standard deviation correction for DM method

The small sample in the staircase test means that a lot of samples are needed under high confidence and high probability, but it is actually impossible to do so much. There is a drawback to the staircase test. The staircase method test is unbiased for the mean value estimation, and the standard deviation estimation is inherently low [118, 36]. One reason is that the staircase method focuses on the majority of the data points near the mean, it is more difficult to get an accurate measure of dispersion

Randall D. Pollak [38, 98] gave detailed research discussing standard deviation estimation and presented a bootstrap correction method.

The deviation bias is a function of both step size(d) and sample size(n) in staircase testing [38]. The staircase method cannot eliminate or avoid this problem, but it can minimize the error of the standard deviation estimation value in terms of optimizing the experimental design [42], improving the data processing [39] and creating correct coefficient.

It can only minimize the error of the variance estimation value in terms of optimizing the experimental design, improving the data processing, and modifying the coefficients. Brownlee [125] corrected the estimation of the mean to improve the situation that the first few trials all have the same outcome, and conclude that over 200 trials would be required to estimate standard deviation within 20% with the confidence of 95%.

Some researchers put forward the corrections for DM method for better estimation of standard deviation.

Svensson-Lorén Correction (SL)

In Svensson's simulation works [20], a linear correction factor was proposed to improve maximum likelihood evaluation procedures.

$$s_{SL} = s_{DM}\frac{n}{n-3} \tag{C.4}$$

A similar equation but with a different constant parameter was also introduced in [42] research.

$$s_{SL} = s_{DM}\frac{n}{n-3.5} \tag{C.5}$$

where s_{SV} represents the Svensson-Lorén corrected standard deviation estimate, and n is the total number of specimens. The equation can improve the low bias of the estimated standard deviation. However, it only considers the sample size and only increases the standard deviation estimated from DM method.

Pollak's Correction (PO)

Based on the Svensson-Lorén equation, Pollak [38] conducted lots of simulation works and proposed a non-linear form including step size.

$$s_{PO} = As_{DM}(\frac{n}{n-3})(1.2\frac{s_{DM}}{d})^b \tag{C.6}$$

Where, the parameters A and b are constant dependent on the number of specimens (as shown in Tab. C.1).

Table C.1: Constants used in standard deviation correction (Eq. C.6)

Number of specimens (n)	A	b
8	1.30	1.72
10	1.08	1.10
12	1.04	0.78
15	0.97	0.55
20	1.00	0.45
30	1.00	0.22
50	1.00	0.15

PO standard deviation shows a more robust than Svensson-Lorén correction in different step size. But the effectiveness of this correction is not good enough, for staircase tests with step size too large or too low may have errors magnified.

Braam-Zwaag Correction (BZ)

Braam and Zwaag [104] proposed a correction equation that accounts for both the sample size as well as the step size to address this standard deviation bias.

$$s_{BZ} = s_{DM} + d \times (\frac{s_{DM}}{n} - 0.95) \times exp(-\frac{n}{4.93\frac{s_{DM}}{n} + 24.48}) \tag{C.7}$$

C.3. Comparison results and discussions

Let's give two figures about median estimation with respect to the number of specimens and step size.

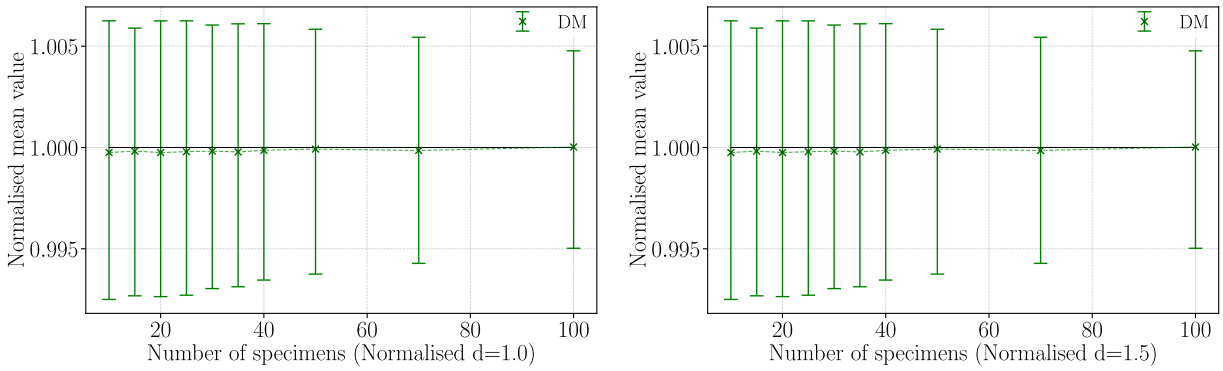

(a) (b)

Figure C.1: Distributions of the median from DM - Number of specimens

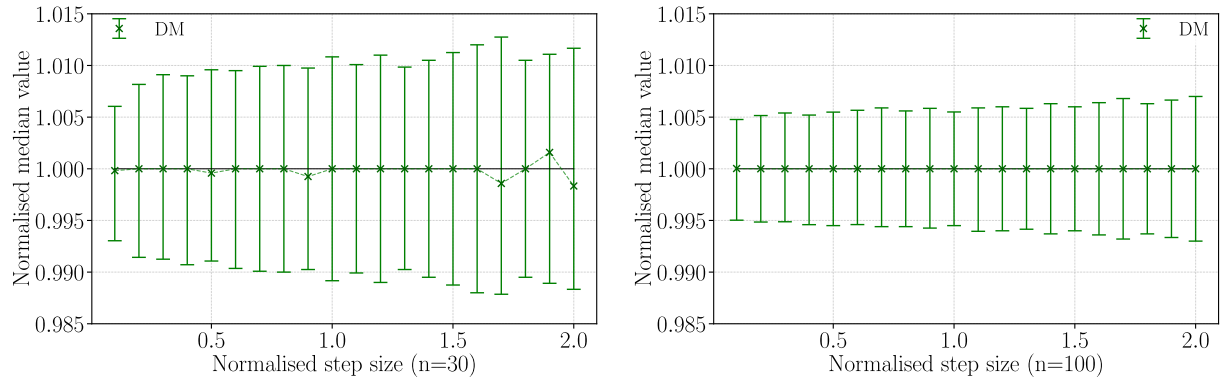

(a) (b)

Figure C.2: Distributions of the median from DM - Normalised step size

From the above figures, the median value from DM method always approaches the true value and is almost independent of the number of specimens and the step size. Next, we will focus on the standard deviation estimation and its corrections (Fig. C.3 and Fig. C.4).

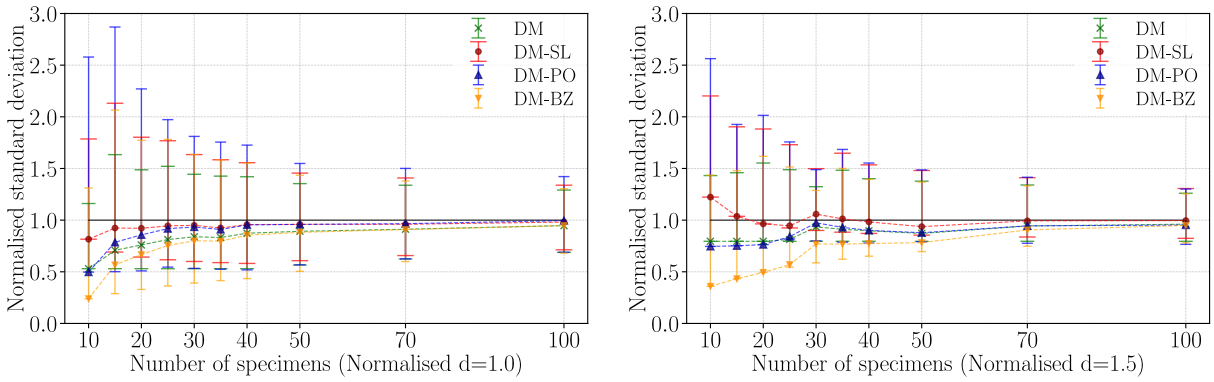

(a) (b)

Figure C.3: Distributions of standard deviation from DM (corrections) - Number of specimens

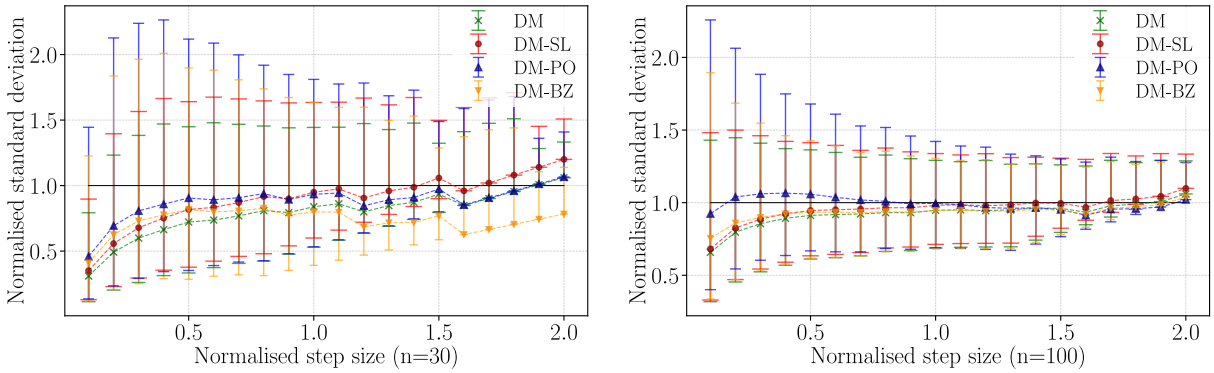

(a) (b)

Figure C.4: Distributions of standard deviation from DM (corrections) - Normalised step size

By comparing the Fig. C.3 and Fig. C.4, some conclusions can been drawn:

1) The uncertainty of mean and standard deviation will decrease with the increase in the number of samples;
2) the estimation of standard deviation is highly affected by the step size.
3) All methods including DM and DM with bootstrap give almost the same and accurate estimation for the mean.
4) From Fig. C.4, the SL correction indeed improves original DM especially for $N = 30$.
5) PO correction include the parameter n and d, so it provides the estimations closer to real value. However, it leads to large diversity and is not easy to use due to the un-constant parameters.
6) From Fig. C.3, and Fig. C.4(a), The BZ correction appears not to better results[38], it is not considered for following comparative study.

Comparatively, DM with Svensson-Lorén(SL) Correction gives the best results.

C.4. Conclusions

It can draw the same conclusions from the figures. For both SL and PO corrections, the results with bootstrap enlarge the bias. if we only focus on SL corrections, the figures also give the same conclusion. Though bootstrap reduced the estimation scatter, it increased the bias and computational cost.

The SL correction improved the standard deviation estimation by a simple equation. Comparatively speaking, DM with Svensson-Lorén(SL) Correction gives the best estimation for standard deviation.

Appendix D
Comparison study with Maximum Likelihood Estimation

D.1. MLE method

The Maximun Likelihood Estimation (MLE) method is the most common technique to analyse the staircase data[39, 56] and general fatigue test data. The purpose is to use the known sample results to infer the most likely (maximum probability) parameter values that lead to such results. The MLE can be used to staircase data with variable step size and any kind of distribution. It is able to derive the estimated distribution parameters, however, the MLE needs a prior assumed distribution.

MLE method

The goal of the MLE is to combine the observations of each specimen in order to estimate the initial distribution. A likelihood function is created to evaluate the parameters of this distribution. In the general case with a dataset containing n samples, the likelihood function L is defined as:

$$\mathrm{L} = \prod_{i=1}^{n} f(S_{a,i}) \tag{D.1}$$

where the f is the PDF of assumed distribution, which is the function of the distribution parameters, such as shape, loc, scale and so on. $S_{a,i}$ is the load amplitude of the specimen i. The evaluation of the distribution parameters is performed by maximizing function L.

MLE with censored data

Considering the data set $\mathbf{X}$=$\{ x_0, ..., x_j, ..., x_n\}$ resulting in the staircase approach, x_j being a state of survival or failure experienced by a specimen (without censor). When the fatigue strengths $S_{a,j}$ of the n specimens are known, For the staircase data, the specimen with failure and with survival gives different information of fatigue limit: the fatigue limit is lower than the applied stress (left censored) in case of failure and the fatigue limit is higher than the applied stress (right censored) in case of survival

(run-out).

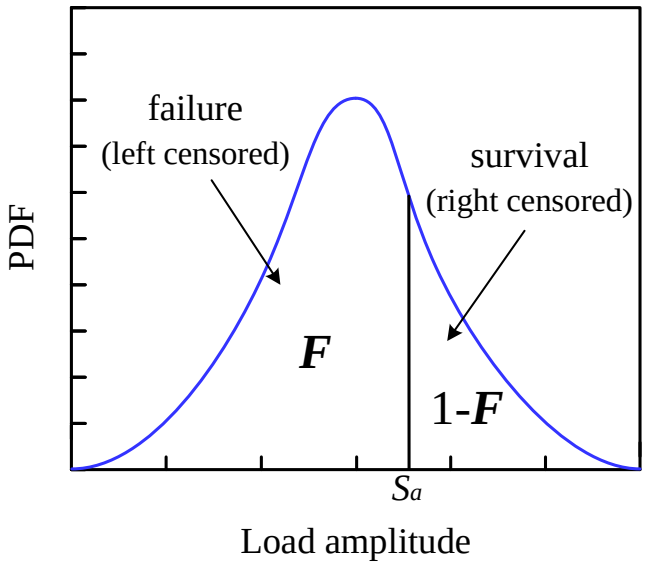

Figure D.1: Left and right censored data distribution and likelihood

As shown in Fig. D.1, if the specimen failed at the load level S_a, the information we derive from the test is that $S_f < S_a$. It corresponds to left censoring and the observed probability is then described using the CDF as Eq. D.2:

$$P(x \leqslant S_a) = F(S_a) \tag{D.2}$$

While it can be known that survival can occur as a result of the load level is less than the corresponding fatigue limit, that is $S_{fl} > S_a$. The right censoring can be expressed as Eq. D.3:

$$P(x \geqslant S_a) = 1 - F(S_a) \tag{D.3}$$

where F is the CDF of the distribution. The maximum likelihood function L is expressed as Eq. D.4

$$\mathrm{L} = \prod_{i=1}^{n} F^{n_{f,i}} (1 - F)^{n_{s,i}} \tag{D.4}$$

The maximization of L results in the estimation of the distribution parameters. The logarithm of the minimized equation is strongly recommended in order to reduce some numerical computational problems. The new function to optimize minimum is:

$$\ln\mathrm{L} = -\sum_{i=1}^{n} [n_{f,i} \ln F + n_{s,i} \ln(1 - F)] \tag{D.5}$$

where 'ln' holds for natural logarithm in this study. The gradient descent methods, such as Newton method, are frequently used to find the extreme value. This study used Broyden–Fletcher–Goldfarb–Shanno (BFGS) algorithm to find the optimum global resolution of the likelihood function. For the staircase data, it should be noted that the MLE with censoring is only suitable for load levels greater or equal to 4 ($j \geqslant 4$).

An example is given as: a staircase including 30 specimens with initial distribution $N\,(400, 10)$. The estimated results of classical MLE and MLE with censoring are listed in Fig. D.2.

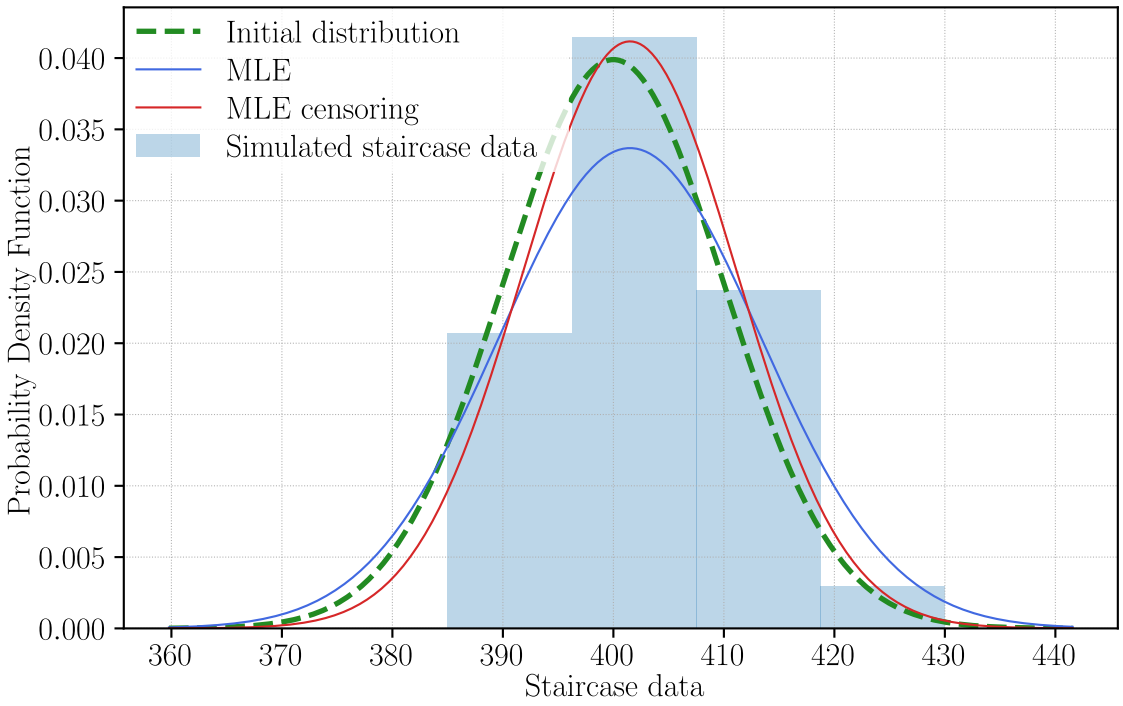

Figure D.2: Comparison of estimated PDF from MLE and MLE with censored data

The optimization of the likelihood function is shown in Fig. D.3. It can be seen that the BFGS algorithm finds the minimum value of the likelihood function and obtain better results in this case.

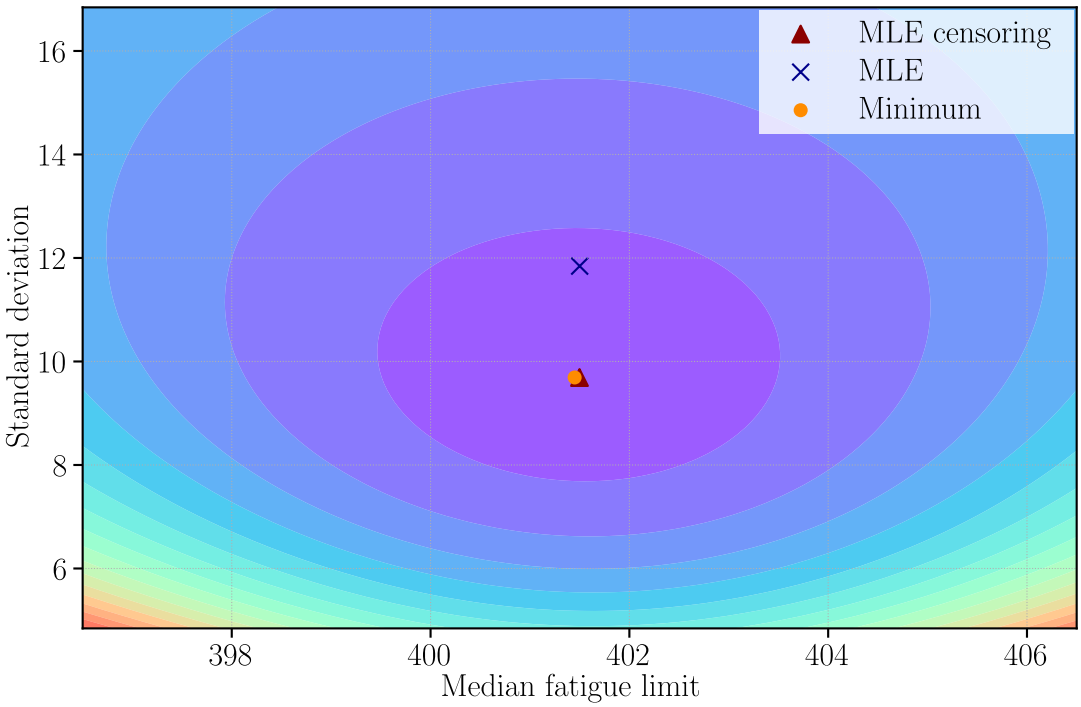

Figure D.3: An example of likelihood function optimization

Corrections to MLE

Müller[40] has concluded that the MLE has a better estimation quality, and he also gave a coefficient(Eq. D.6) to correct logarithmic standard deviation.

$$s_{MUL} = \frac{n-1}{n-6.5} \times s_{MLE} \tag{D.6}$$

This correction is only for logarithmic standard deviation, so it is not considered in this study.

D.2. Comparison results and discussions

Using the simulation described in Section 4.3.1, the median and standard deviation estimation is compared in this section. Firstly, the simulation based on Normal distribution, Lognormal and Weibull distribution will be discussed later. Fig. D.4 and Fig. D.4 show the median estimation with respect to the number of specimens and step size.

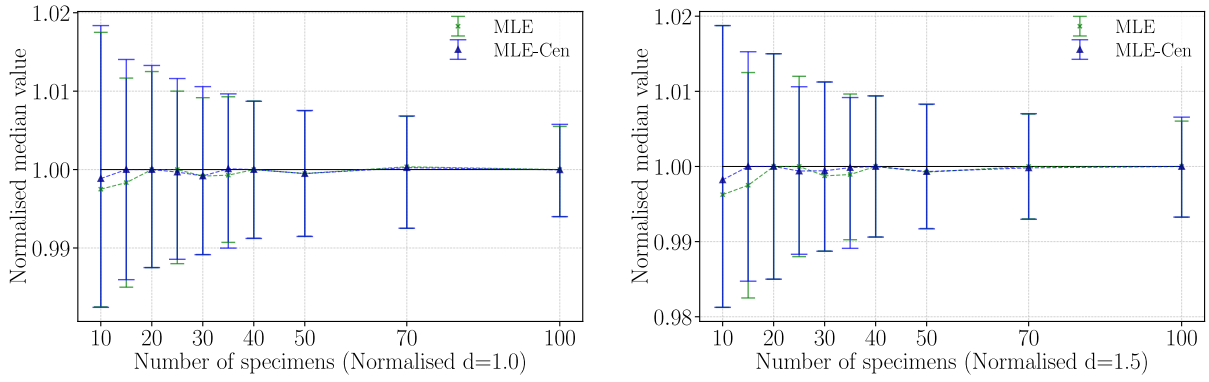

(a) (b)

Figure D.4: Distributions of median from MLE (Normal) - Number of specimens

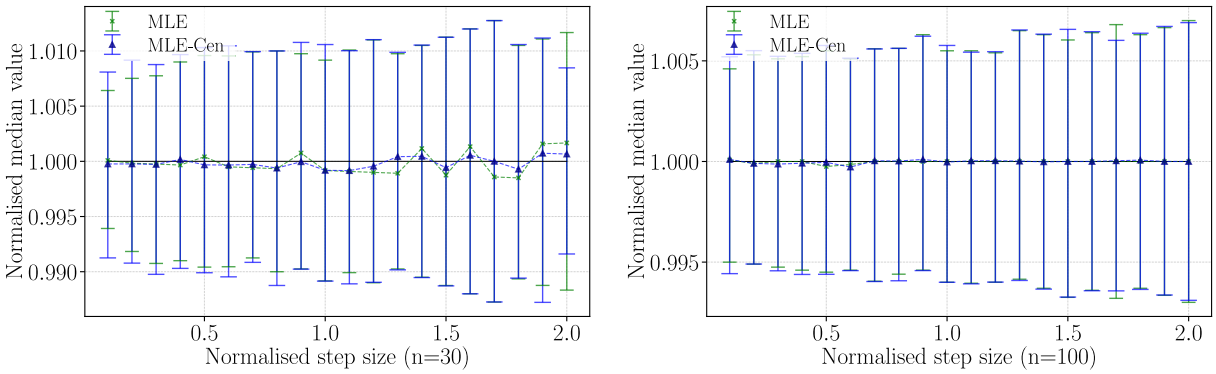

(a) (b)

Figure D.5: Distributions of median from MLE (Normal)- Normalised step size

The median value from MLE method always approach to the true value and almost independent to the number of specimens and the step size. Next, we will focus on the standard deviation estimation and its corrections.

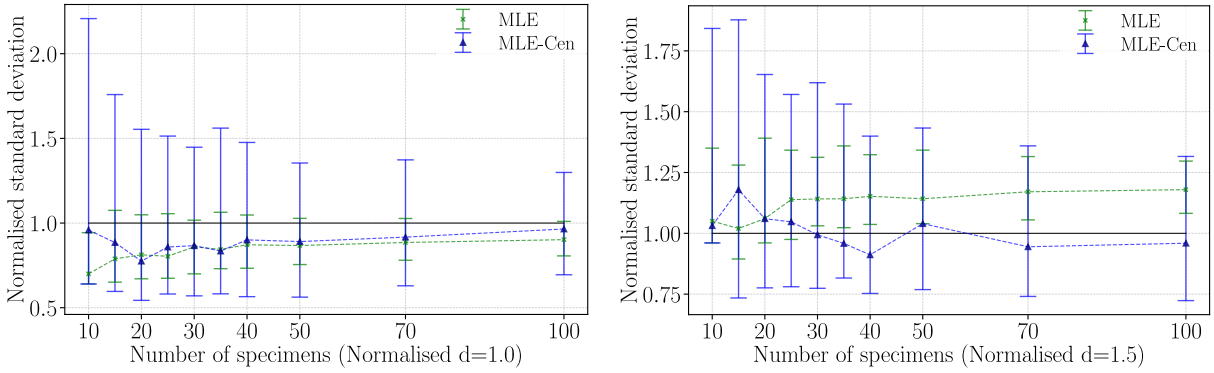

(a) (b)

Figure D.6: Distributions of standard deviation from MLE (Normal) - Number of specimens

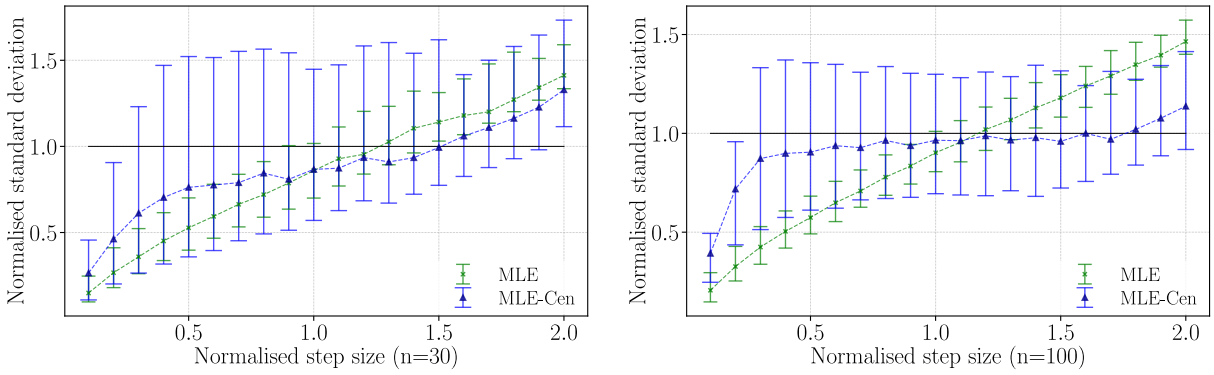

(a) (b)

Figure D.7: Distributions of standard deviation from MLE (Normal) - Normalised step size

From the results of Normal distribution, some conclusions can been drawn:

1) The uncertainty of median and standard deviation will decrease with the increase of number of samples;
2) Both classical MLE and the censoring MLE give perfect estimation to median value. and it is independent to the number of samples and step size.
3) For the classical MLE method, the estimation of standard deviation is highly affected by step size.
4) From Fig. D.7, the censored MLE underestimated standard deviation, but not much.

Next, the estimation based on Lognormal distribution and Weibull distribution are also compared and the results about standard deviation are shown following.

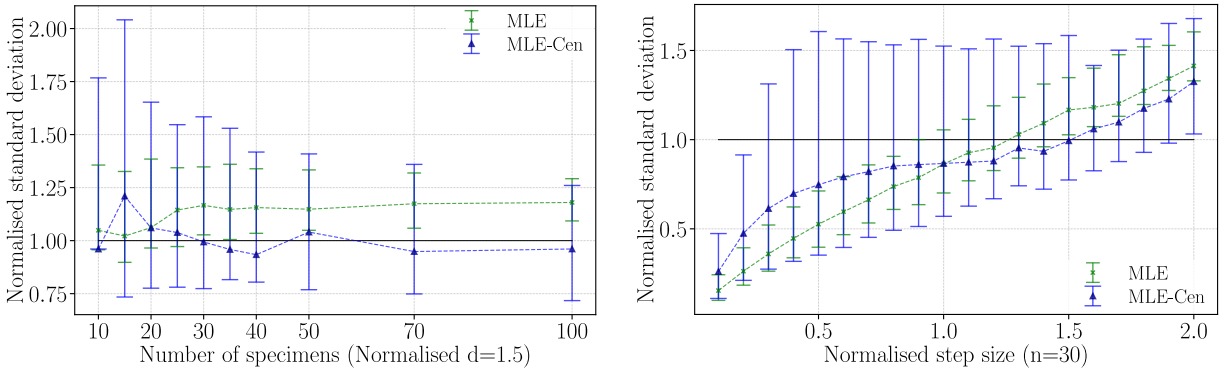

(a) (b)

Figure D.8: Distributions of standard deviation from MLE (Lognarmal)

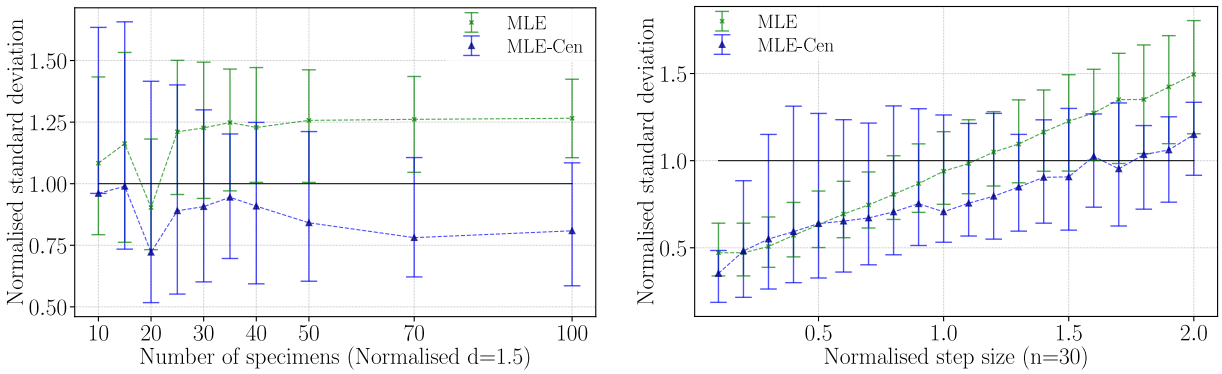

(a) (b)

Figure D.9: Distributions of standard deviation from MLE (Weibull)

Some conclusions can been drawn:

1) There are almost same conclusions for Lognormal distribution and Normal distribution.
2) From Fig. D.9(a), there are a weird peak when $n = 30$. This may caused by Monte-Carlo simulation.
3) From Fig. D.9(b), the MLE with censoring has a poor performance when normalized step size close to 1. However, it is better than classical MLE when normalized step size in range of [1.5-2.0].

D.3. Conclusion

There is no doubt that the MLE with censoring data leads to a better results than classical MLE. Though the correction is not perfect in all case, but it is suitable for most estimation problems.

Appendix E
Distributions: Normal, Lognormal and Weibull

Note that the Normal, Lognormal and Weibull distribution are implied in several studies on staircase test, and represent non-skewed, negative skewed and positive skewed distributions respectively. Hence, this section describes the definition and properties of three distributions. Based on Scipy [112] statistics package (scipy.stats), the formulas are uniformly expressed with location, scale and shape parameters.

For each distribution, the definition of Probability Density Function (PDF) and Cumulative Density Function (CDF) are given. Then we introduce the statistical properties and transformation of distribution parameters and population parameters. Lastly, an example of the distribution with desired mean 400 and desired standard deviation 10 are created. Total 100000 data are sampled from the distribution. And we can obtain the mean, standard deviation and median of sampled data (population), which are consistent with desired mean and desired standard deviation.

In the following formulas:

$f(x)$	: probability density function (PDF)
$F(x)$	: cumulative density function (CDF)
x	: random variates (> 0)
α	: location parameter (> 0)
β	: scale parameter (> 0)
γ	: shape parameter (> 0)
Φ	: CDF of the standard Normal distribution
μ_X	: mean of population
s_X	: standard deviation of population
m_X	: median of population

E.1. Normal distribution

The PDF and CDF of Normal distribution is given such as:

$$\begin{aligned} f(x) &= \frac{1}{\beta\sqrt{2\pi}} \exp\left[-\frac{1}{2}\left(\frac{x-\alpha}{\beta}\right)^2\right] \\ F(x) &= \Phi\left(\frac{x-\alpha}{\beta}\right) \end{aligned} \tag{E.1}$$

where α, β are location (mean) and scale (standard deviation) parameters respectively.

The statistical parameters of Normal distribution can be obtained:

$$\begin{aligned} \mu_X &= m_X = \alpha \\ s_X &= \beta \end{aligned} \tag{E.2}$$

The distribution with desired mean 400 and desired standard deviation 10 are created, and 100000 data are sampled from the distribution. a sample is illustrated in Fig. E.1.

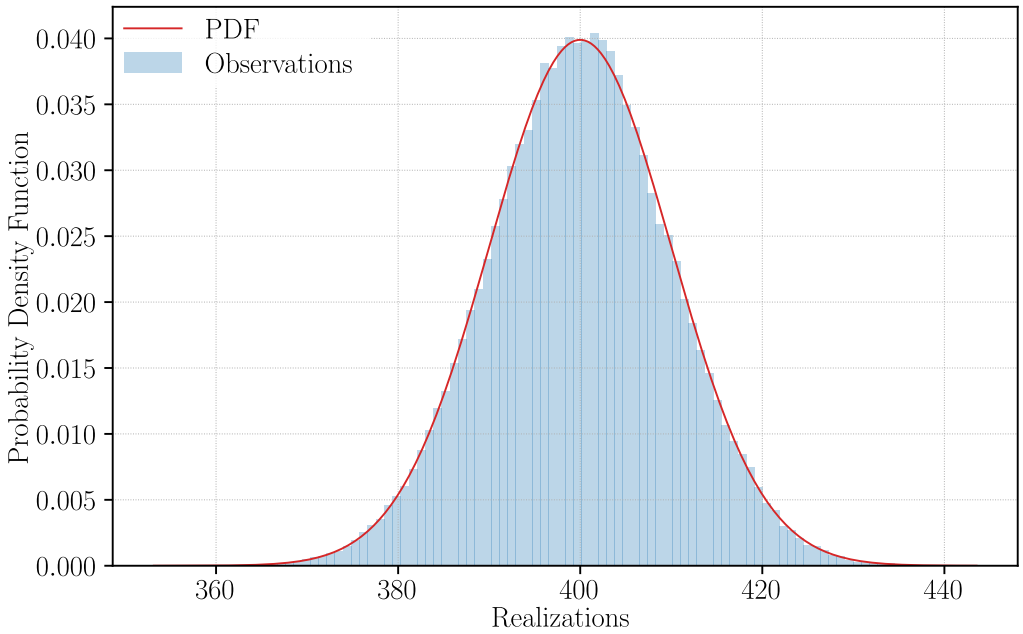

Figure E.1: Normal distribution test

For the observed data, $\mu_X = m_X = 399.9790$ and $s_X = 10.0019$.

E.2. Lognormal distribution

The failure rate curves of Lognormal distribution regularly increase with the fatigue cycling with inherently positively skewed PDF.

The PDF and CDF of Lognormal distribution are given as ref:

$$\begin{aligned} f(x) &= \frac{1}{x\lambda\sqrt{2\pi}} \exp\left(-\frac{\left[\ln\left(\frac{x}{\beta}\right)\right]^2}{2\lambda^2}\right) \\ F(x) &= \Phi\left(\frac{\ln(x)}{\lambda}\right) \end{aligned} \tag{E.3}$$

where λ is the shape parameter (and is the standard deviation s of the Lognormal distribution), β is the scale parameter (and is also the median of the population).

If we want to create a Lognormal distribution from desired population with mean μ_X and s_X:

$$\begin{aligned} \mu &= \ln\left(\frac{\mu_X^2}{\sqrt{\mu_X^2 + s_X^2}}\right) \\ s &= \sqrt{\ln\left(\frac{s_X^2}{\mu_X^2}\right)} \\ \lambda &= s \\ \beta &= \exp(\mu) \quad (= m_X) \end{aligned} \tag{E.4}$$

The statistical parameters of Lognormal distribution can be obtained:

$$\begin{aligned} \mu_X &= \exp\left(\mu + \frac{s^2}{2}\right) \\ s_X &= \sqrt{[\exp(s^2) - 1] \times \mu_X^2} \\ m_X &= \exp(\mu) \end{aligned} \tag{E.5}$$

As shown in Fig. E.2, The Lognormal distribution with desired mean 400 and desired standard deviation 10 are created with 100000 data.

For the observed data, $\mu_X = 400.0116$ and $s_X = 10.0249$, $m_X = 399.9219$.

E.3. Weibull distribution

The PDF and CDF of two-parameter Weibull distribution is given as:

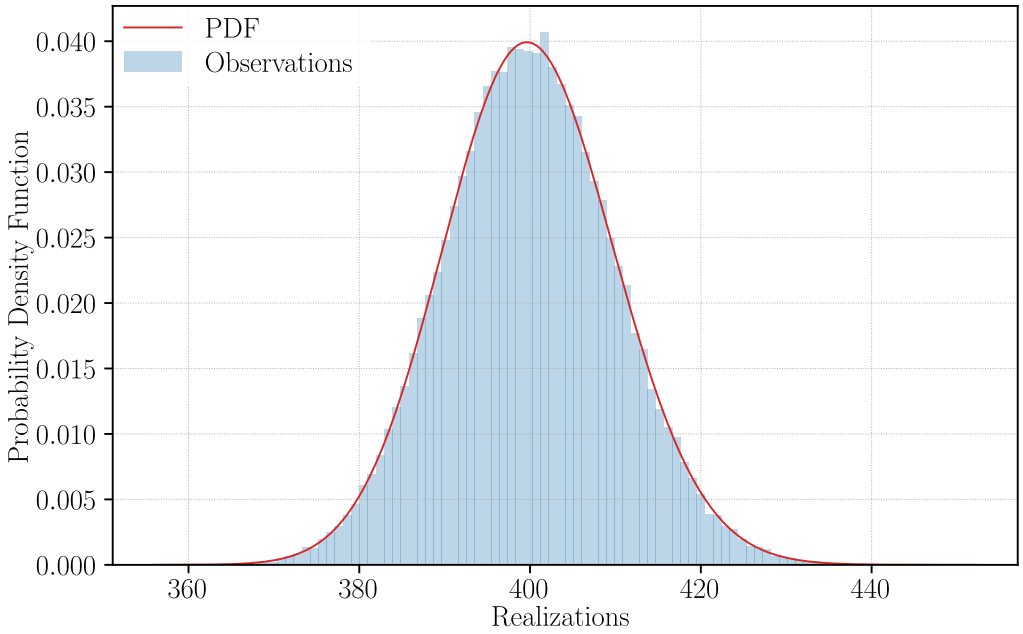

Figure E.2: Lognormal distribution test

$$
\begin{aligned}
f(x) &= \frac{\gamma}{\beta}\left(\frac{x}{\beta}\right)^{\gamma-1}\exp\left[-\left(\frac{x}{\beta}\right)^{\lambda}\right] \\
F(x) &= 1-\exp\left[-\left(\frac{x}{\beta}\right)^{\lambda}\right]
\end{aligned}
\tag{E.6}
$$

The statistical parameters of Weibull distribution can be obtained:

$$
\begin{aligned}
\mu_X &= \beta\Gamma(1+\frac{1}{\lambda}) \\
s_X &= \beta\sqrt{\Gamma(1+\frac{2}{\lambda})-[\Gamma(1+\frac{1}{\lambda})]^2} \\
m_X &= \beta(\ln 2)^{\frac{1}{\lambda}}
\end{aligned}
\tag{E.7}
$$

The shape and scale parameters of the Weibull distribution can be calculated using desired population with mean μ_X and s_X:

$$
\begin{aligned}
\lambda &: \frac{s_X^2}{\mu_X^2}-\frac{\Gamma(1+\frac{2}{\lambda})}{(\Gamma(1+\frac{1}{\lambda}))^2}+1=0 \\
\beta &= \mu_X\Gamma(1+\frac{1}{\lambda})
\end{aligned}
\tag{E.8}
$$

In the fatigue analysis, the shape parameter (λ) of a Weibull distribution should be greater than 1 in order to have the meaning of failure rate curve increases with the fatigue cycling. Generally, for $\lambda < 2.6$ the Weibull PDF is positively skewed (has a right tail), for $2.6 < \lambda < 3.7$ its coefficient of skewness approaches zero (no tail).

Consequently, it may approximate the normal pdf, and for $\lambda > 3.7$ it is negatively skewed (left tail).

As shown in Fig. E.2, The Weibull distribution with desired mean 400 and desired standard deviation 10 are created with 100000 data.

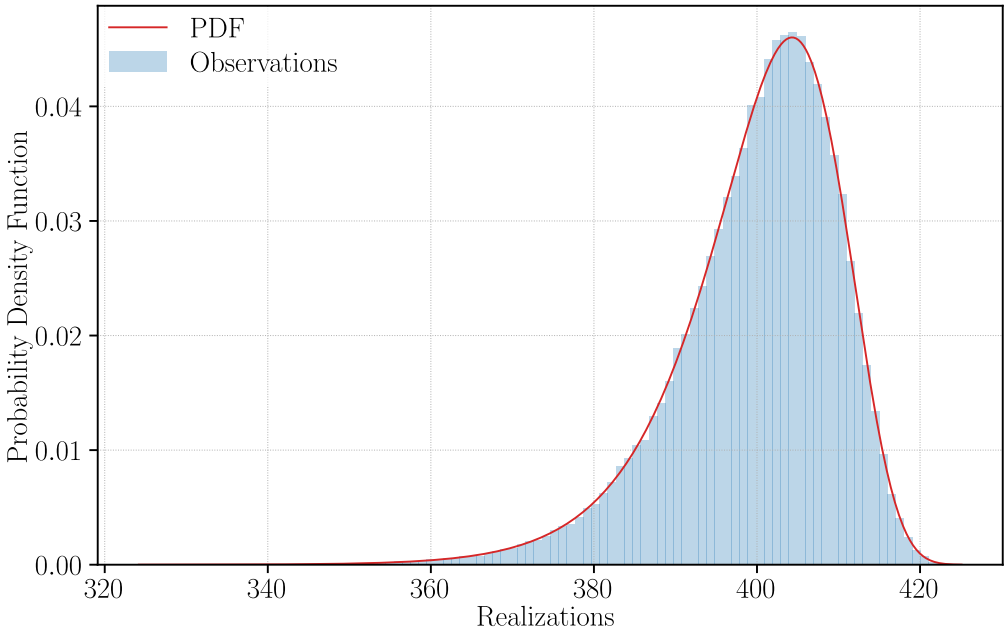

Figure E.3: Weibull distribution test

For the observed data, $\mu_X = 399.9766$ and $s_X = 10.0523$, $m_X = 401.5406$.

ÉVALUATION PROBABILISTE DES LIMITES DE FATIGUE ET AMÉLIORATION PAR DES ESSAIS EXPÉRIMENTAUX ET NUMÉRIQUES

Lujie Shi

Laboratoire de Mécanique de Normandie
INSA Rouen Normandie, France

Annexe F
Résumé en français

F.1. Introduction générale

Presque tous les équipements mécaniques sont soumis à des vibrations. Les charges vibratoires transférées aux structures réduisent la durée de vie et entraînent des fissures dues à la fatigue. Par conséquent, l'exigence d'une distribution probabiliste de la fatigue est critique en ce qui concerne la sécurité des structure. Comme la limite de fatigue indique l'amplitude de charge endurable sous un nombre de cycles suffisamment élevé, l'obtention de la limite de fatigue d'un matériau est cruciale pour la conception de la fatigue structurelle. Cependant, la machine expérimentale, le protocole d'essai et la méthode statistique posent certains problèmes.

La limite de fatigue est un paramètre important qui reflète la performance des matériaux en matière de fatigue. L'évaluation de la limite de fatigue dans la conception technique est encore fortement basée sur le test expérimental, en particulier la méthode de l'escalier. Cependant, l'essai conventionnel présente des limites intrinsèques concernant la dérivation des données et son influence sur la caractérisation de la fatigue. Pour surmonter ces limites dans l'évaluation de la limite de fatigue, les solutions appropriées pourraient résider dans la machine de test, le post-traitement des données et la stratégie d'essai. Les objectifs sont de réaliser l'essai de fatigue sur agitateur électro-dynamique et de réduire l'erreur d'estimation de la limite de fatigue dans l'évaluation des données et le protocole d'essai.

Cette thèse développe des expériences et des statistiques basées sur la méthode de l'escalier pour l'évaluation de la distribution des limites de fatigue. Elle détaille le processus de conception comprenant le but du développement de contrôle de la déformation pour les tests de fatigue, l'évaluation de l'incertitude, une méthode statistique initiale pour le post-traitement et l'optimisation de la conception du protocole de test en utilisant l'algorithme de Bayes.

Les principaux axes de recherche de ce document sont organisés comme suit :

Chapter F.2 : court revue de la limite de fatigue et de la méthode de l'escalier démontrant le but du développement de la méthode d'essai expérimentale de contrôle de la déformation, de la technique d'évaluation des données avec cor-

rection de l'écart type et de la conception du protocole d'essai basée sur le théorème de Bayes.

Chapter F.3 : description d'une méthode d'essai expérimentale de contrôle des vibrations basée sur la déformation réalisée sous agitateur électro-dynamique. Ce chapitre détaille une procédure d'essai en escalier avec un banc de flexion vibratoire et la sélection des paramètres. Les résultats des essais avec cette méthode offrent un ensemble de données pour la quantification des incertitudes et l'étude statistique.

Chapter F.4 : présentation du Bootstrap utilisé pour caractériser la moyenne et l'écart type de la distribution de la limite de fatigue à partir des données issues de la méthode des escaliers, ainsi que l'incertitude associée à cette méthode d'essai. Les résultats comparent la distribution de la limite de fatigue du DC01.

Chapter F.5 : traitement statistique des données d'essais de fatigue sur éprouvettes. Une nouvelle méthode d'évaluation basée sur l'estimation de la densité du noyau est proposée pour estimer la limite de fatigue à partir des essais en escalier. Une étude basée sur la simulation est réalisée en utilisant plusieurs distributions de probabilité avec différents coefficients de variation.

Chapter F.6 : proposition d'un processus de conception de test avec le théorème bayésien en ce qui concerne à la fois la considération scientifique et l'exigence d'ingénierie.

Cette thèse se conclut avec des perspectives de travail (Chapter F.7).

F.2. Chapitre 1 : Vue d'ensemble de la limite de fatigue

Lors de la sélection d'un matériau pour la conception, il est crucial de connaître les conditions de fonctionnement auxquelles il sera soumis. Dans des conditions de chargement cyclique, la distribution statistique de la limite de fatigue est généralement requise pour délimiter la plage de fonctionnement en cas de fatigue à un nombre de cycle élevé. La limite de fatigue est un niveau de contrainte en dessous duquel la rupture par fatigue ne se produira pas même sous un nombre suffisamment élevé de cycles de charge appliqués à la structure.

Depuis longtemps, la limite de fatigue est considérée comme une propriété essentielle du matériau. C'est une constante matérielle utilisée pour évaluer la valeur d'un matériau et un paramètre nécessaire à la conception de structures résistantes à la fatigue. Dans la conception mécanique d'un matériau, il est important de comprendre

non seulement la limite de fatigue moyenne, mais aussi la variance de cette résistance et la probabilité de rupture pour une certaine amplitude de contrainte spécifique.

En ingénierie, la courbe S-N et la limite de fatigue sont souvent utilisées pour évaluer la performance des matériaux et des structures en termes de fatigue. Les spécimens sont testés à différents niveaux de contrainte et le nombre de cycles correspondant (durée de vie en fatigue) est mesuré. Les résultats expérimentaux sont habituellement présentés sous la forme d'un diagramme $logS - logN$ (voir Fig. F.1).

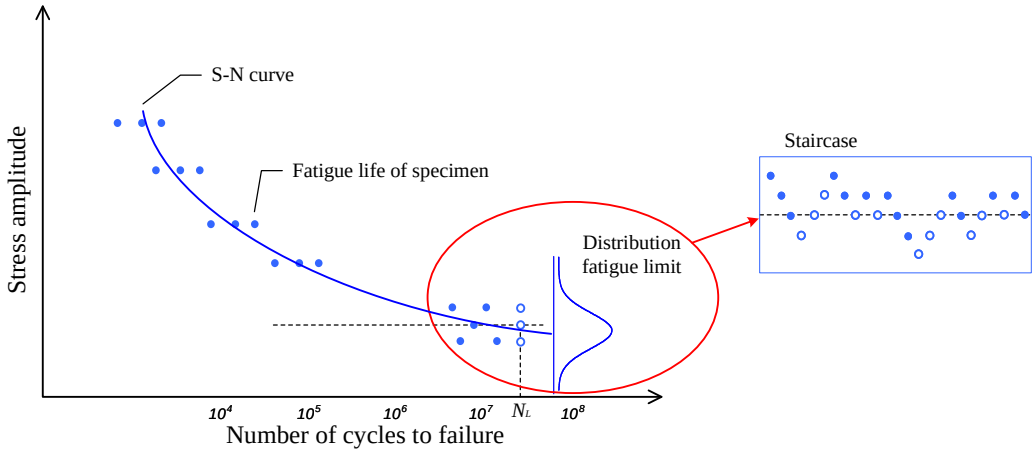

FIGURE F.1 : Courbe S-N et test de l'escalier

Comme le montre la Fig. F.1, il est normal que la limite de fatigue soit déduite de la courbe S-N. Cette dernière peut obtenir une valeurde limite de fatigue mais ne peut pas fournir une distribution statistique. En considérant la limite de fatigue comme une valeur aléatoire, la méthode de l'escalier [27] est beaucoup plus adaptée à la précision de l'estimation de la limite de fatigue.

Dixon et Mood [27] ont proposé une méthode classique de test de sensibilité en 1948 : méthode de l'escalier. Elle est largement utilisée dans les secteurs de la machinerie, de la médecine, de la pyrotechnie, etc. Avec cette méthode, les essais de fatigue sont effectués séquentiellement sur des spécimens soumis à un cycle de contrainte d'amplitude constante jusqu'à un nombre prédéterminé de cycles N_L. La première éprouvette est testée à une amplitude de charge initiale choisie arbitrairement. En supposant que l'éprouvette "survive" (runout) jusqu'à N_L cycles, l'amplitude de charge appliquée à l'éprouvette suivante est augmentée d'un pas d. Inversement, si l'éprouvette est marquée comme "défaillante", alors l'amplitude de la charge appliquée à l'éprouvette suivante sera diminuée d'un pas d. La taille du pas est généralement constante pendant toute la durée de l'expérience. Cette procédure est répétée en séquence. Les niveaux de charge étant augmentés et diminués par paliers jusqu'à ce que le nombre de spécimens soit atteint. Par conséquent, l'approche de l'escalier fournit une estimation raisonnable de la limite de fatigue médiane, car environ la moitié des spécimens

échouent et les autres non[37].

En résumé, la méthode d'essai en escalier a été largement utilisée pour évaluer la distribution des limites de fatigue. Elle présente deux caractéristiques remarquables : tout d'abord, de par sa nature, cette méthode tend à concentrer les données près de la moyenne. Ensuite, elle permet une simplicité relative de l'analyse statistique des données obtenues. Cependant, cette méthode présente également trois défauts : premièrement, le test n'a pas de caractéristique d'optimisation mathématique. De plus la précision de l'estimation avec la même taille d'échantillon doit être encore augmentée ou bien la taille de l'échantillon doit être réduite pour la même précision d'estimation. Deuxièmement, la taille du pas de contrainte doit être estimée avant le test. Si la taille de pas est trop grande, la probabilité de générer des données invalides augmente, ce qui accroît l'incertitude de l'essai. Troisièmement, l'estimation de l'écart-type est systématiquement moins précise et inférieure à la valeur réelle. Par conséquent, cette étude a réalisé l'essai de fatigue expérimental par la méthode de l'escalier mais a également amélioré cette méthode en termes de post-traitement et de stratégie d'essai.

F.3. Chapitre 2 : Contrôle expérimental des vibrations basé sur la déformation

Cette étude est une combinaison d'essais expérimentaux de fatigue à amplitude constante avec la technique de contrôle des déformations et la méthode de l'escalier pour évaluer la limite de fatigue dans le domaine des déformations. Le contrôle des déformations permet de réaliser des essais de fatigue en régime permanent jusqu'à la rupture grâce à une jauge de déformation collée au centre de la section réduite de l'éprouvette. Une procédure d'essai en escalier avec un banc de flexion vibrant, comprenant la sélection des paramètres, est détaillée dans ce travail. L'analyse des résultats est basée sur l'estimation de la densité du noyau. Elle est utilisée pour accéder à la limite de fatigue sur une distribution non paramétrique. Des échantillons d'acier à faible teneur en carbone avec une zone de fatigue ont été sélectionnés pour évaluer les caractéristiques statistiques de la limite de fatigue. Les résultats mettent en évidence l'efficacité de la méthode de l'escalier combinée à celle des déformations contrôlées pour atteindre la limite de fatigue.

Dans cette étude, l'agitateur électro-dynamique, refroidi par l'air, est relié à l'éprouvette par une table vibrante. Les expériences sont réalisées sur des éprouvettes en acier

à faible teneur en carbone soumises à une excitation cyclique sinusoïdale en déformation par flexion.

L'essai de fatigue avec contrôle de déformation est mis en œuvre avec la technique SRTD [77]. Les conditions de résonance sont maintenus automatiquement tout au long de l'essai même si un changement se produit (fissure, par exemple). Il y a deux caractéristiques dans le SRTD avec contrôle de la déformation. Tout d'abord, il s'agit de contrôler l'amplitude de la déformation pour maintenir une valeur constante. L'agitateur ajuste l'accélération de base pour atteindre le niveau de déformation nécessaire à l'essai de fatigue. Ensuite, le SRTD maintient la différence de phase entre les signaux d'excitation et de réponse à 90 degrés, ce qui garantit que la fréquence d'excitation et la fréquence de résonance de l'échantillon restent les mêmes, car une réduction de la fréquence de résonance est observée lorsqu'une fissure se produit. En général, l'amplitude de déformation forme une boucle fermée dans l'essai SRTD, ce qui garantit une amplitude de déformation constante et le maintien à la fréquence de résonance. Ainsi, le contrôle de la déformation a une réponse très stable dans l'essai SRTD.

Dans l'expérience, le contrôle de la déformation dans le vibrateur pour l'essai de fatigue est validé par la méthode de l'escalier. Le diagramme en escalier de l'essai en escalier est présenté dans la Fig. F.2.

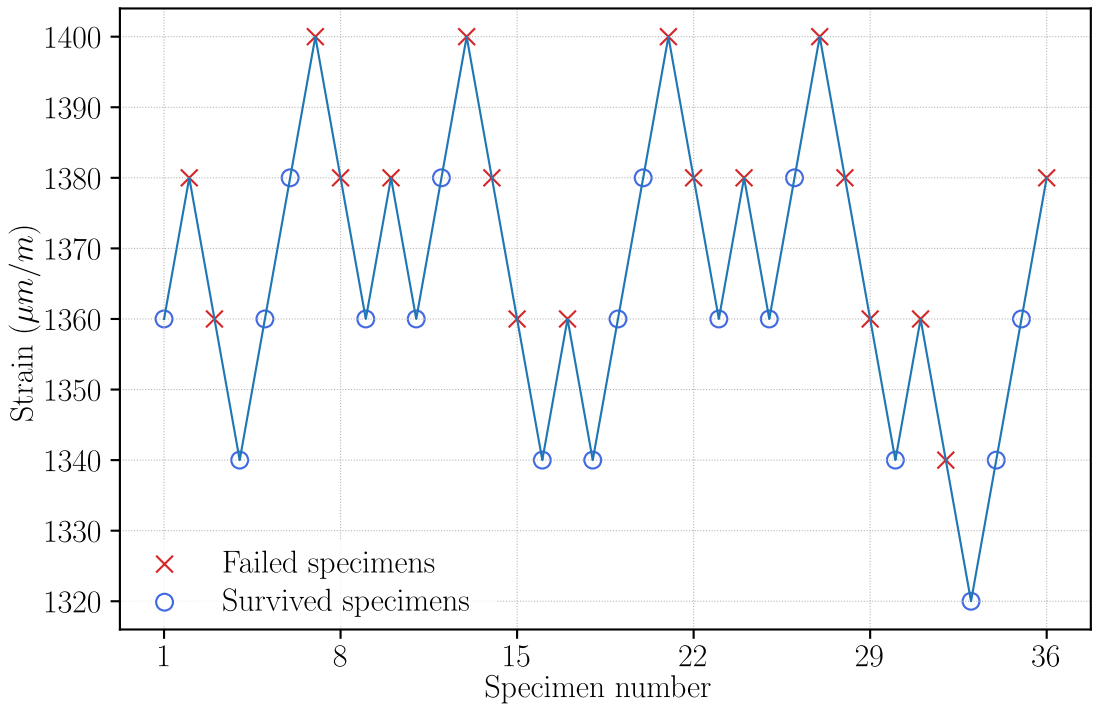

FIGURE F.2 : Diagramme up–and–down pour les échantillons d'acier DC01

Pour conclure, les résultats montrent les niveaux de déformation à la valeur pré-

définie et maintenue constante pendant l'essai, indépendamment de la variation de la fréquence. Ces données démontrent la fiabilité du contrôle de la déformation lors d'un essai de fatigue par vibration sur l'agitateur électro-dynamique.

F.4. Chapitre 3 : Évaluation de l'incertitude par les méthodes de rééchantillonnage

Le post-traitement donne une estimation précise de la distribution de la limite de fatigue. Cependant, on peut se demander quels seront les résultats si l'essai en escalier est effectué plus d'une fois sur le même système d'essai.

Le Bootstrap est une méthode non paramétrique qui repose sur le rééchantillonnage des échantillons observés. Le point clé du bootstrap est l'échantillonnage non ordonné avec remplacement. Combinée à la méthode de l'escalier, une procédure bootstrap est proposée comme l'Algorithm F.1 :

Tout d'abord, une analyse de sensibilité est effectuée pour simuler la variation du facteur d'incertitude en fonction du nombre de spécimens dans un seul échantillonnage et des périodes d'échantillonnage. Ensuite, un total de 100 bootstrap avec 100 échantillons dans chaque échantillonnage est effectué. Nous avons constaté que l'incertitude pour l'estimation de l'écart-type est très élevée, bien plus élevée que l'estimation de la moyenne.

Pour valider la technique de contrôle de la déformation et l'essai en escalier par des méthodes statistiques, trois types de spécimens avec des dimensions différentes ont été utilisés. Sur la base des différents résultats expérimentaux obtenus, le bootstrap est utilisé pour analyser la relation entre les résultats et les causes de leur dispersion. Plusieurs facteurs principaux, notamment la fréquence de résonance et l'épaisseur, sont impliqués dans la dispersion des résultats des tests de fatigue. Ils sont discutés à la fin.

Algorithm F.1: Bootstrap

L'ensemble de données en escalier qui comprend n simples est représenté par $X = [x_1, x_2, ..., x_n]$, et la taille de l'étape est d
Définir N comme le nombre d'échantillons dans un seul échantillonnage et M comme les durées d'échantillonnage
Déterminer tous les niveaux de déformation (ou de contrainte) $L = [l_1, l_2, ...l]$
Diviser X en différentes parties selon les différents niveaux de déformation (ou de contrainte) l, soit $X^l = [x_1^l, x_2^l, ..., x^l]$, c'est-à-dire $X^1 \cup X^2 \cup ...X^l = X$
Pré-requis : Sélectionner aléatoirement un niveau de souche d'essai l
Obtenir toutes les données de test du niveau de souche l
foreach *i in M* **do**
    Réinitialiser l'ensemble de données en escalier $X = [x_1, x_2, ..., x_n]$
    foreach *j in N* **do**
        Echantillonner une donnée x à partir de X^l de façon aléatoire
        if *l'échantillon x est défaillant* **then**
            $l = l - d$ // l'échantillon suivant est sélectionné parmi les spécimens du niveau inférieur
        else
            $l = l + d$ // l'échantillon suivant est sélectionné parmi les spécimens du niveau supérieur
        end if
        Obtenir tous les points de test dans le nouveau niveau X^l
    end foreach
    Obtenir les résultats de l'échantillonnage : $\widetilde{X} = [x_1, x_2, ..., x_N]$
    Estimer la distribution de la limite de fatigue par la même méthode de post-traitement
end foreach
Obtenir tous les résultats de l'échantillonnage : $[\widetilde{X}_1, \widetilde{X}_2, ..., \widetilde{X}_M]$ et les facteurs d'incertitude correspondants

F.5. Chapitre 4 : Méthode d'évaluation non paramétrique dans un test d'escalier pour la limite de fatigue

Les travaux précédents ont fourni des résultats d'essais expérimentaux en escalier. Ainsi, une méthode de post-traitement est nécessaire pour obtenir la distribution de la limite de fatigue.

Une nouvelle méthode d'évaluation basée sur l'estimation de la densité du noyau (KDE) est proposée pour estimer la distribution de la limite de fatigue à partir d'essais en escalier sans connaissance préalable. Le PDF de tous les échantillons est ensuite estimé par la somme de ces densités du noyau. Sur la base de données expérimentales,

l'estimation du KDE avec la règle de Scott et la largeur de bande améliorée conduit à un PDF estimé lisse. Puisque la correction linéaire élargit l'incertitude de l'estimation [38], le développement d'une approche non linéaire pour réduire le biais de l'écart type est nécessaire.

L'estimation proposée de la limite de fatigue basée sur le KDE avec correction du biais est exprimée par pseudo-code dans l'Algorithm F.2.

Algorithm F.2: Méthode non paramétrique d'estimation de la limite de fatigue

Data: L'ensemble de données sur les escaliers : $\mathbf{X} = \{x_1, x_2, ..., x_n\}$, la taille de l'escalier : d

1 Calcul de la largeur de bande h par la règle de Scott;

2 (m, s) de KDE avec une largeur de bande h ;

3 Correction de s ;

Result: La médiane estimée m et l'écart type estimé s de la distribution de la limite de fatigue

Une simulation numérique modélisant l'essai en escalier est réalisée avec différentes distributions et coefficients de variation. La valeur médiane (m) et l'écart-type (s) sont utilisés dans ce travail pour décrire la distribution des limites de fatigue. Il apparaît que la méthode KDE a un résultat estimé conforme à la méthode MLE. La médiane et l'écart-type des estimations de KDE et MLE convergent les uns vers les autres. En comparant les distributions estimées par KDE, MLE et DM, les principaux résultats peuvent être tirés :

(1) : MLE distingue les spécimens en fonction du résultat de l'échec ou de la survie, tandis que KDE ne requière pas cette information

(2) KDE a un résultat estimé selon la méthode MLE. La médiane et l'écart-type des estimations de KDE et MLE convergent les uns vers les autres

(3) DM donne un plus grand écart-type de la limite de fatigue. Alors qu'après la correction de l'écart-type dans la méthode KDE, la valeur prédite devient beaucoup plus petite

Pöur conclure, la méthode KDE proposée réduit considérablement le biais de l'écart-type de la limite de fatigue à partir d'essais sur petits échantillons. De plus, les performances de cette méthode sont insensibles aux paramètres d'essai de la méthode de l'escalier.

F.6. Chapitre 5 : Plan d'expérience optimal en escalier par échantillonnage bayésien à entropie maximale

Pour remédier aux défauts intrinsèques de la méthode d'essai conventionnelle en escalier, ce chapitre propose une méthode d'essai optimisée, basée sur les Echantillonages Bayésiens à Entropie Maximale (BMES) et les Echantillonages Latins Hypercubes (LHS) pour déterminer la distribution de la limite de fatigue de la structure. Cette méthode combine les informations préalables avec les informations de l'échantillon pour obtenir la probabilité postérieure. La distribution de la limite de fatigue est estimée sur la base de la probabilité postérieure, ce qui réduit l'erreur d'analyse statistique causée par les caractéristiques du petit échantillon de l'essai de limite de fatigue.

Pour le premier spécimen, la priorité initiale est créée à partir de la priorité nulle comme détaillé dans Section 5.2.3. Les contraintes possibles proviennent de la plage de la médiane de distribution des limites de fatigue dans le paramètre d'entrée. La fonction d'utilité, décrite dans Section 5.3.2, est utilisée pour rechercher la contrainte de charge. Après l'essai, l'amplitude de la contrainte et le résultat de l'essai (survie ou échec) sont obtenus, et la postérieure est mise à jour sur la base de ce résultat d'essai. Cette dernière devient l'antérieur pour le spécimen suivant.

Cette procédure est répétée pour les autres échantillons avec BMES jusqu'à ce que la postérieure ait une convergence. Cela signifie qu'une seule distribution peut être estimée à partir de la postérieure. À partir de cette étape, le LHS est appliqué pour déterminer la contrainte de charge et mettre à jour la postérieure. Ensuite, les LHS et BMES sont utilisés alternativement pour déterminer la contrainte de charge. La postérieure est mise à jour après chaque test, quel que soit le LHS ou le BMES. Enfin, la valeur postérieure $P(\boldsymbol{\theta}|\boldsymbol{x}_{1:n})$ est obtenue après un total de n spécimens.

La postérieure finale, $P(\boldsymbol{\theta}|\boldsymbol{x}_{1:n})$, présente la probabilité des observations compte tenu des paramètres possibles du modèle. L'estimation des paramètres du modèle est obtenue en recherchant le maximum dans la postérieure après le dernier spécimen. Le protocole optimal de l'escalier est donné dans l' Algorithm F.3.

Par rapport à la méthode de l'escalier classique, les avantages de la méthode Bayes-LHS peuvent être énumérés comme suit :

(1) Cette méthode évite l'utilisation d'une contrainte de départ devinée et d'une taille de pas fixe. Elle sélectionne artificiellement la gamme des paramètres possibles du modèle avant le test bayésien en escalier.

Algorithm F.3: Framework of Bayes-LHS staircase protocol

Data: Distribution ; plages de la médiane et de l'écart-type ;
Générer le paramètre de modèle $\boldsymbol{\theta}$. Initialisation de l'antériorité $P(\boldsymbol{\theta})$; **if** $P(\boldsymbol{\theta}|\boldsymbol{x}_{1:i})$ *convergence* **then**
  Déterminer l'amplitude de la contrainte de charge par BMES
else
  Déterminer l'amplitude de la contrainte de charge par LHS et BMES alternativement
end if
Tester l'éprouvette
Calculer la postérieure $P(\boldsymbol{\theta}|\boldsymbol{x}_{1:n})$ et l'entropie de Shannon après chaque test
Postérieure finale
Result: La médiane estimée m et l'écart type estimé s de la distribution de la limite de fatigue

(2) L'utilisation d'informations antérieures pendant le test permet une convergence plus rapide [116], ce qui signifie moins de spécimens pour atteindre les mêmes résultats.
(3) Très peu d'informations sont nécessaires sur le jeu d'échantillons avant le test.
(4) Il n'est pas nécessaire d'utiliser une méthode de post-traitement. Le paramètre du modèle de distribution est obtenu directement à partir du modèle postérieur.

En outre, par rapport à la méthode bayésienne en escalier, la méthode Bayes-LHS optimisée fournit un protocole de calcul plus rapide tout en conservant l'exactitude et la précision.

F.7. Chapitre 6 : Conclusion et perspectives

Le présent travail décrit le sujet de l'évaluation des limites de fatigue. La thèse couvre des aspects allant des expériences de fatigue mécanique aux méthodes statistiques. Ce dernier chapitre résume ce que nous avons appris des travaux précédents et indique les directions les plus prometteuses pour les recherches futures.

Selon la revue de la littérature, l'évaluation de la limite de fatigue est un problème pratique difficile car l'éprouvette est exposée à des conditions de vibration, ce qui est crucial pour une conception structurelle fiable. Pour parvenir à une distribution de probabilité de la limite de fatigue, les principaux défis proviennent de la méthode d'essai expérimentale et d'une technique d'évaluation avancée des données d'essai.

L'évaluation de la limite de fatigue commence par l'essai expérimental. Un banc de

vibration est une solution raisonnable pour réduire la durée de l'essai de fatigue. En revanche, l'essai de limite de fatigue exige que l'éprouvette soit soumise à une amplitude de contrainte constante pendant un certain nombre de cycles. Une technique de contrôle de la déformation appliquée à un electro-dynamic shaker est proposée pour réaliser un essai à amplitude de déformation constante. L'efficacité de l'approche proposée a été démontrée par des essais de flexion de plaques d'acier DC01 à leur première fréquence de résonance. Le contrôle de la déformation à la résonance (amplification du signal) et l'excitation à relativement haute fréquence permettent de réduire le temps d'essai pour atteindre un grand nombre de cycles. Cette approche est donc efficace pour tester la méthode de l'escalier. Le seuil de fatigue et la dispersion de l'acier DC01 sont estimés par les résultats de l'escalier. Les résultats montrent une bonne répétabilité avec la méthode de l'escalier.

La méthode statistique offre des approches permettant de fournir les distributions des limites de fatigue pour chaque essai en escalier. La question clé est : quels sont les résultats d'une nouvelle exécution de l'essai de l'escalier ? Une analyse d'incertitude est effectuée pour évaluer les distributions des limites de fatigue d'un matériau obtenues à partir de l'essai en escalier. Pour cela, nous avons appliqué la méthode de rééchantillonnage, leave-one-out et bootstrap sur les données de l'escalier afin de déduire la dispersion de la moyenne et l'écart type de la distribution. Les résultats de cette étude ont mis en évidence la forte incertitude inhérente à l'estimation de l'écart-type. Les résultats du rééchantillonnage bootstrap montrent que l'écart-type de la limite de fatigue présente une grande dispersion, ce qui permet de conclure qu'il faut être prudent pour utiliser les résultats des escaliers dans la conception de la fatigue.

Pour réduire cette incertitude, nous proposons d'utiliser l'estimation de la densité du noyau (KDE) dans cette étude en raison de son caractère non paramétrique et de son indépendance par rapport au modèle de distribution. Pour la comparer à d'autres méthodes basées sur des hypothèses, la KDE est testée sur différentes distributions afin de valider son efficacité. La dépendance de l'hyperparamètre KDE est également étudiée et optimisée pour améliorer ses performances dans l'évaluation de la limite de fatigue. De plus, comme la méthode de l'escalier nécessite de définir une taille de pas initiale, un facteur corrigé non linéaire est formulé pour réduire son influence dans l'estimation de l'écart-type. L'approche numérique utilise la simulation de Monte-Carlo et permet d'examiner l'effet du nombre de spécimens et de la taille du pas. La performance de l'estimation est évaluée sur la moyenne et l'écart-type de la limite de fatigue impliquant différentes distributions et coefficients de variation.

Dans le but de résoudre la limitation de la taille des marches dans la méthode de l'escalier, un protocole d'escalier Bayes-LHS est présenté pour supprimer la taille des marches dans l'escalier conventionnel. La théorie bayésienne des essais de fatigue et des Bayesian Maximum Entropy Sampling (BMES) est détaillée, puis le protocole d'es-

calier bayésien est fourni avec un exemple. Cette étude appelée méthode Bayes-LHS enrichit l'approche Bayes avec les Latin Hypercube Sampling (LHS). Cette proposition est décrite pour la procédure en escalier. Les résultats sont suffisamment optimistes pour considérer que le protocole Bayes-LHS pourrait remplacer la méthode classique de l'escalier pour l'estimation des limites de fatigue.

Bibliography

[1] William F. Hosford. *Mechanical Behavior of Materials*. Cambridge University Press, 2005.

[2] Lujie Shi et al. « Approach and Application of Semi-Blind Source Separation for Aero-Engine Vibration Signals Using ICA-R ». In: *Journal of Physics: Conference Series* 1215.1 (May 2019), p. 012030.

[3] Air Accident Investigation Bureau of Singapore. *Airbus A330-343, registration B-HLM engine fire event*. Tech. rep. Singapore: Ministry of Transport, 2014.

[4] Yong Liu et al. « Fatigue limit prediction of notched plates using the zero-point effective notch stress method ». en. In: *International Journal of Fatigue* 151 (Oct. 2021), p. 106392.

[5] Uwe Zerbst, Mauro Madia, and Michael Vormwald. « Applying fracture mechanics to fatigue strength determination – Some basic considerations ». en. In: *International Journal of Fatigue* 126 (Sept. 2019), pp. 188–201.

[6] Matteo Luca Facchinetti. « Fatigue tests for automotive design: optimization of the test protocol and improvement of the fatigue strength parameters estimation ». en. In: *Procedia Engineering* 133 (2015), pp. 21–30.

[7] Cyprian T. Lachowicz and Robert Owsiński. « Comparative Analysis of Fatigue Energy Characteristics of S355J2 Steel Subjected to Multi-Axis Loads ». en. In: *Materials* 13.11 (May 2020), p. 2470.

[8] I. M. W. Ekaputra et al. « Fatigue Strength Analysis of S34MnV Steel by Accelerated Staircase Test ». en. In: *Open Engineering* 10.1 (May 2020), pp. 394–400.

[9] Jifa Mei et al. « The fatigue limit prediction of notched components – A critical review and modified stress gradient based approach ». en. In: *International Journal of Fatigue* 135 (June 2020), p. 105531.

[10] Yukitaka Murakami et al. « Essential structure of S-N curve: Prediction of fatigue life and fatigue limit of defective materials and nature of scatter ». en. In: *International Journal of Fatigue* 146 (May 2021), p. 106138.

[11] A. Fernández-Canteli et al. « Considerations about the existence or non-existence of the fatigue limit: implications on practical design ». en. In: *International Journal of Fracture* 223.1-2 (May 2020), pp. 189–196.

[12] Jaap Schijve. « Fatigue of structures and materials in the 20th century and the state of the art ». en. In: *International Journal of Fatigue* 25.8 (Aug. 2003), pp. 679–702.

[13] Luca Susmel. « Fundamentals of fatigue assessment ». en. In: *Multiaxial Notch Fatigue*. 2009, pp. 33–97.

[14] Yves Nadot. « Fatigue from Defect: Influence of Size, Type, Position, Morphology and Loading ». en. In: *International Journal of Fatigue* 154 (Jan. 2022), p. 106531.

[15] Masahiro Endo and Takashi Matsuo. « A practical method for fatigue limit prediction in ductile cast irons ». en. In: *Fatigue & Fracture of Engineering Materials & Structures* 42.9 (Sept. 2019), pp. 2106–2119.

[16] Howard E. Boyer. *Atlas of Fatigue Curves*. Materials Park, Ohio: ASM lnternatlonal, 1986.

[17] J. Schijve. « Fatigue predictions and scatter ». en. In: *Fatigue & Fracture of Engineering Materials and Structures* 17.4 (Apr. 1994), pp. 381–396.

[18] Ying Min Low. « A variance reduction technique for long-term fatigue analysis of offshore structures using Monte Carlo simulation ». en. In: *Engineering Structures* 128 (Dec. 2016), pp. 283–295.

[19] Francis G Pascual and William Q Meeker. « Estimating Fatigue Curves with the Random Fatigue-Limit Model ». en. In: (1999), p. 34.

[20] Thomas Svensson. « Random Features of the Fatigue Limit ». en. In: *extrems* (1999), p. 12.

[21] Claudio Baptista, Antonio Reis, and Alain Nussbaumer. « Probabilistic S-N curves for constant and variable amplitude ». en. In: *International Journal of Fatigue* 101 (Aug. 2017), pp. 312–327.

[22] S. Lambert, E. Pagnacco, and L. Khalij. « A probabilistic model for the fatigue reliability of structures under random loadings with phase shift effects ». en. In: *International Journal of Fatigue* 32.2 (Feb. 2010), pp. 463–474.

[23] S Lin. « Evaluation of the staircase and the accelerated test methods for fatigue limit distributions ». en. In: *International Journal of Fatigue* 23.1 (Jan. 2001), pp. 75–83.

[24] Y. X. Zhao and Y. Zhang. « Improved measurement on probabilistic fatigue limits/strengths by test data from staircase test method ». en. In: *International Journal of Fatigue* 94 (Jan. 2017), pp. 58–80.

[25] A. Cetin, G. Härkegård, and A. Naess. « The fatigue limit: An analytical solution to a Monte Carlo problem ». en. In: *International Journal of Fatigue* 55 (Oct. 2013), pp. 194–201.

[26] Jing Li et al. « Evaluation of the Methods for Estimating the Fully Reversed Unnotched Fatigue Limits of Steels ». en. In: *Advances in Materials Science and Engineering* 2019 (July 2019), pp. 1–11.

[27] W. J. Dixon and A. M. Mood. « A method for obtaining and analyzing sensitivity data ». In: *Journal of the American Statistical Assiciation* 43.241 (1948), pp. 109–126.

[28] T. Nicholas. « Step loading for very high cycle fatigue: STEP LOADING FOR HCF ». en. In: *Fatigue & Fracture of Engineering Materials & Structures* 25.8-9 (Sept. 2002), pp. 861–869.

[29] Adam Lipski. « Determination of Fatigue Limit by Locati Methodusing S-N Curve Determined by Means of Thermographic Method ». en. In: *Solid State Phenomena* 223 (Nov. 2014), pp. 362–373.

[30] A.P Boresi and T.J. Dolan. *An appraisal of the prot method of fatgiue testing Part I.* Tech. rep. AD0001785. Denfense Technical Information Center, 1953.

[31] Masatoshi Kuroda et al. « Historical Review on Origin and Application to Metal Fatigue of Probit and Staircase Methods and Their Future Prospects ». en. In: *Journal of the Society of Materials Science,* 70.3 (2021), pp. 221–228.

[32] Mauro Ricotta et al. « Comparison of Experimental Thermal Methods for the Fatigue Limit Evaluation of a Stainless Steel ». en. In: *Metals* 9.6 (June 2019), p. 677.

[33] W. A. Hijab. « A Statistical Appraisal of the Prot Method for Determination of Fatigue Endurance Limit ». In: *Journal of Applied Mechanics* 24.2 (1956), pp. 214–218.

[34] O.H. Basquin. « The exponential law of endurance tests ». In: *American Society for Testing and Materials Proceedings* 10 (1910), pp. 625–630.

[35] BS ISO 12107. *Metallic materials- Fatigue testing - Statistical planning and analysis of data.* en. 2003.

[36] MIL-STD-331D. *Fuzes, ignition safety devices and other related components, environmental and performance tests for.* en. 2017.

[37] W. J. Dixon. « Staircase bioassay the up-and-down method ». In: *Technical Session: Toxicokinetic Models For Extrapolation From Animal To Human* 15.1 (1991), pp. 47–50.

[38] R. Pollak, A. Palazotto, and T. Nicholas. « A simulation-based investigation of the staircase method for fatigue strength testing ». en. In: *Mechanics of Materials* 38.12 (Dec. 2006), pp. 1170–1181.

[39] V. Roué et al. « Simulation-based investigation of the reuse of unbroken specimens in a staircase procedure: Accuracy of the determination of fatigue properties ». en. In: *International Journal of Fatigue* 131 (Feb. 2020), p. 105288.

[40] Christian Müller et al. « Accuracy of fatigue limits estimated by the staircase method using different evaluation techniques ». en. In: *International Journal of Fatigue* 100 (July 2017), pp. 296–307.

[41] B. R. Rabb. « Staircase testing – confidence and reliability ». In: *Transactions on Engineering Sciences* 40 (2003), pp. 447–464.

[42] Kim R.W. Wallin. « Statistical uncertainty in the fatigue threshold staircase test method ». en. In: *International Journal of Fatigue* 33.3 (Mar. 2011), pp. 354–362.

[43] Isamu Yoshimoto. « Fatigue test by staircase method with small samples ». In: *Bulletin of JSME* 5.18 (1962), pp. 211–221.

[44] Daniel Grove and Felician Campean. « A comparison of two methods of analysing staircase fatigue test data ». en. In: *Quality and Reliability Engineering International* 24.4 (June 2008), pp. 485–497.

[45] Salim Çalişkan and Riza Gürbüz. « Determining the endurance limit of AISI 4340 steels in terms of different statistical approaches ». en. In: *Frattura ed Integrità Strutturale* 15.58 (Sept. 2021), pp. 344–364.

[46] Przemysław Strzelecki and Janusz Sempruch. « Experimental method for plotting S-N curve with a small number of specimens ». en. In: *Polish Maritime Research* 23.4 (Dec. 2016), pp. 129–137.

[47] Y Zhao and B Yang. « Probabilistic measurements of the fatigue limit data from a small sampling up-and-down test method ». en. In: *International Journal of Fatigue* 30.12 (Dec. 2008), pp. 2094–2103.

[48] Andressa Borin Venturini et al. « Step-stress vs. staircase fatigue tests to evaluate the effect of intaglio adjustment on the fatigue behavior of simplified lithium disilicate glass-ceramic restorations ». en. In: *Journal of the Mechanical Behavior of Biomedical Materials* 113 (Jan. 2021), p. 104091.

[49] Mohammad Jamalkhani Khameneh and Mohammad Azadi. « Reliability prediction, scatter-band analysis and fatigue limit assessment of high-cycle fatigue properties in EN-GJS700-2 ductile cast iron ». en. In: *MATEC Web of Conferences* 165 (2018). Ed. by G. Hénaff, p. 10012.

[50] Theodore Nicholas. *High cycle fatigue: a mechanics of materials perspective*. en. OCLC: ocm69733162. Oxford: Elsevier, 2006.

[51] R Morrissey and T Nicholas. « Staircase testing of a titanium alloy in the gigacycle regime ». en. In: *International Journal of Fatigue* 28.11 (Nov. 2006), pp. 1577–1582.

[52] Carlos C Engler-Pinto Jr et al. « Statistical approaches applied to very high cycles fatigue ». en. In: *Fourth International Conference on Very High Cycle Fatigue*. 2007, p. 9.

[53] Nabil Swadi. « Estimation of fatigue properities of 35NCDV12 alloy steel under chromium coating using the staircase method ». In: *The Iraqi Journal For Mechanical And Material Engineering* 12.1 (2012).

[54] Braitner Lobato Silva, Jorge Luiz Almeida Ferreira, and J. A. Araújo. « Use of the parallel-projected and staircase method to predict fatigue strength of ASTM A743 CA6NM alloy steel ». In: 2009.

[55] Hongqian Xue et al. « Fatigue life assessment of a high strength steel 300 M in the gigacycle regime ». en. In: *Theoretical and Applied Mechanics Letters* 2.3 (2012), p. 031006.

[56] Xin Bai et al. « Measurement and estimation of probabilistic fatigue limits using Monte-Carlo simulations ». en. In: *International Journal of Fatigue* 95 (Feb. 2017), pp. 229–235.

[57] Brecht Van Hooreweder et al. « Fatigue strength analysis of notched aluminium specimens using the highly stressed volume method ». en. In: *Fatigue & Fracture of Engineering Materials & Structures* 35.2 (2011), pp. 154–159.

[58] Lujie Shi, Leila Khalij, and Christophe Gautrelet. « Experimental strain-based vibration control to obtain the fatigue strain limit by the staircase method ». en. In: *Strain* 58.2 (Apr. 2022), e12408.

[59] Galal S A Shawki. « A Review of Fatigue Testing Machines ». en. In: *Engineering Journal of Qatar University* 3 (1990), pp. 55–69.

[60] Wenjie Peng et al. « A Brief Review of the Application and Problems in Ultrasonic Fatigue Testing ». en. In: *AASRI Procedia* 2 (2012), pp. 127–133.

[61] Leila Khalij, Christophe Gautrelet, and Alain Guillet. « Fatigue curves of a low carbon steel obtained from vibration experiments with an electrodynamic shaker ». en. In: *Materials & Design* 86 (Dec. 2015), pp. 640–648.

[62] M. R. Machado, A. Appert, and L. Khalij. « Spectral formulated modelling of an electrodynamic shaker ». en. In: *Mechanics Research Communications* 97 (Apr. 2019), pp. 70–78.

[63] Julian M. E. Marques et al. « An Overview of Fatigue Testing Systems for Metals under Uniaxial and Multiaxial Random Loadings ». en. In: *Metals* 11.3 (Mar. 2021), p. 447.

[64] Christophe Gautrelet et al. « Linearity investigation from a vibratory fatigue bench ». en. In: *Mechanics & Industry* 20.1 (2019), p. 101.

[65] Chan-Jung Kim. « Experimental spectral damage prediction of a linear elastic system using acceleration response ». en. In: *Mechanical Systems and Signal Processing* (2011), p. 11.

[66] Tommy J. George et al. « Development of a novel vibration-based fatigue testing methodology ». en. In: *International Journal of Fatigue* 26.5 (May 2004), pp. 477–486.

[67] Benjamin Ellyson et al. « Characterization of bending vibration fatigue of WBD fabricated Ti-6Al-4V ». en. In: *International Journal of Fatigue* 101 (Aug. 2017), pp. 36–44.

[68] Benjamin Ellyson, Mathieu Brochu, and Myriam Brochu. « Characterization of bending vibration fatigue of SLM fabricated Ti-6Al-4V ». en. In: *International Journal of Fatigue* 99 (June 2017), pp. 25–34.

[69] Martin Česnik, Janko Slavič, and Miha Boltežar. « Uninterrupted and accelerated vibrational fatigue testing with simultaneous monitoring of the natural frequency and damping ». en. In: *Journal of Sound and Vibration* 331.24 (Nov. 2012), pp. 5370–5382.

[70] Alexandre Presas et al. « Fatigue life estimation of Francis turbines based on experimental strain measurements: Review of the actual data and future trends ». en. In: *Renewable and Sustainable Energy Reviews* 102 (Mar. 2019), pp. 96–110.

[71] R Procházka and J Džugan. « Strain controlled cyclic tests on miniaturized specimens ». en. In: *IOP Conference Series: Materials Science and Engineering* 179 (Feb. 2017), p. 012060.

[72] C Williams. « A practical method for statistical analysis of strain–life fatigue data ». en. In: *International Journal of Fatigue* 25.5 (May 2003), pp. 427–436.

[73] Patricio E. Carrion and Nima Shamsaei. « Strain-based fatigue data for Ti–6Al–4V ELI under fully-reversed and mean strain loads ». en. In: *Data in Brief* 7 (June 2016), pp. 12–15.

[74] BS-EN-10130-2006. *Cold rolled low carbon steel flat products for cold forming -Technical delivery conditions*. 2006.

[75] ISO 5344:2004. *Electrodynamic vibration generating systems — Performance characteristics*. en. 2004.

[76] Aymeric Appert et al. « Development of a test bench for vibratory fatigue experiments of a cantilever beam with an electrodynamic shaker ». en. In: *MATEC Web of Conferences* 165 (2018). Ed. by G. Hénaff, p. 10007.

[77] Mohamad Ahmadi Tafti. « Experimental high cycle fatigue testing and shape optimization of turbine blades ». en. PhD thesis. University of Toronto: University of Toronto, 2013.

[78] ANSYS. *Ansys GRANTA EduPack software*.

[79] J I Huertas et al. « Resonant fatigue test bench for shaft testing ». en. In: *Fatigue & Fracture of Engineering Materials & Structures* 40.3 (Mar. 2017), pp. 364–374.

[80] Matjaž Mršnik, Janko Slavič, and Miha Boltežar. « Frequency-domain methods for a vibration-fatigue-life estimation – Application to real data ». en. In: *International Journal of Fatigue* 47 (Feb. 2013), pp. 8–17.

[81] Primož Ogrinec et al. « Vibration fatigue at half-sine impulse excitation in the time and frequency domains ». en. In: *International Journal of Fatigue* 123 (June 2019), pp. 308–317.

[82] Gautrelet Christophe, Khalij Leila, and Machado Marcela Rodrigues. « Resonance track-and-dwell testing for crack length measurement on 304L stainless steel ». en. In: *Mechanics & Industry* 21.6 (2020), pp. 1–8.

[83] M. Liakat and M.M. Khonsari. « On the anelasticity and fatigue fracture entropy in high-cycle metal fatigue ». en. In: *Materials & Design* 82 (Oct. 2015), pp. 18–27.

[84] Martin Česnik et al. « Frequency-based structural modification for the case of base excitation ». en. In: *Journal of Sound and Vibration* 332.20 (Sept. 2013), pp. 5029–5039.

[85] ASTM E739-10. *Practice for Statistical Analysis of Linear or Linearized Stress-Life and Strain-Life Fatigue Data*. en. 2015.

[86] Yung-Li Lee and Jwo Pan, eds. *Fatigue testing and analysis: theory and practice*. en. OCLC: ocm56338563. Amsterdam ; Boston: Elsevier Butterworth-Heinemann, 2005.

[87] C. L. Shen, P. H. Wirsching, and G. T. Cashman. « Design Curve to Characterize Fatigue Strength ». en. In: *Journal of Engineering Materials and Technology* 118.4 (Oct. 1996), pp. 535–541.

[88] P Lorenzino and A. Navarro. « The variation of resonance frequency in fatigue tests as a tool for in-situ identification of crack initiation and propagation, and for the determination of cracked areas ». en. In: *International Journal of Fatigue* 70 (2015), pp. 374–382.

[89] Jan Papuga. *FatLim - Database of Fatigue Limits (http://www.pragtic.com/vmat.php)*.

[90] T Delahay and T Palinluc. « Estimation of the fatigue strength distribution in high-cycle multiaxial fatigue taking into account the stress–strain gradient effect ». en. In: *International Journal of Fatigue* 28.5-6 (May 2006), pp. 474–484.

[91] Chiara Colombo et al. « Rapid estimation of fatigue limit for C45 steel by thermography and digital image correlation ». en. In: *The Journal of Strain Analysis for Engineering Design* (Dec. 2020), p. 030932472097528.

[92] Zhenjie Teng et al. « A unified fatigue life calculation based on intrinsic thermal dissipation and microplasticity evolution ». en. In: *International Journal of Fatigue* 131 (2020), p. 8.

[93] Lujie Shi, Hao Bai, and Leila Khalij. « Uncertainty evaluation by the bootstrap for the staircase fatigue limit test data ». en. In: 2021, pp. 446–447.

[94] Alexander Klawonn and Tilmann Beck. « Efficient staircase testing of probabilistic Haigh diagrams ». en. In: *International Journal of Fatigue* 137 (Aug. 2020), p. 105627.

[95] Aleksander Karolczuk and Marta Kurek. « Fatigue life uncertainty prediction using the Monte Carlo and Latin hypercube sampling techniques under uniaxial and multiaxial cyclic loading ». en. In: *International Journal of Fatigue* 160 (July 2022), p. 106867.

[96] B Efron. « Bootstrap Methods: Another Look at the Jackknife ». In: *The Annals of Statistics* 7.1 (1979), pp. 1–26.

[97] Davide Leonetti, Johan Maljaars, and H.H. (Bert) Snijder. « Uncertainty analysis of constant amplitude fatigue test data employing the six parameters random fatigue limit model ». en. In: *MATEC Web of Conferences* 165 (2018). Ed. by G. Hénaff, p. 10016.

[98] Randall D Pollak. « Analysis of Methods for Determining High Cycle Fatigue Strength of a Material With Investigation of Ti-6Al-4V Gigacycle Fatigue Behavior ». en. PhD thesis. AIR FORCE INSTITUTE OF TECHNOLOGY, 2005.

[99] N. Tsutsumi, Y. Murakami, and V. Doquet. « Effect of test frequency on fatigue strength of low carbon steel ». en. In: *Fatigue & Fracture of Engineering Materials & Structures* 32.6 (2009), pp. 473–483.

[100] Manel Dallali et al. « Effect of geometric size deviation induced by machining on the vibration fatigue behavior of Ti-6Al-4V ». en. In: *Fatigue & Fracture of Engineering Materials & Structures* (Apr. 2022), ffe.13699.

[101] A. Narumoto, S. Matsumoto, and Y. Kawai. « Effect of Plate Thickness on the Fatigue Strength of Cruciform Welded Joints ». In: 1987.

[102] G Bhuyan and O Vosikovsky. « Effect of thickness on fatigue behaviour of notched plates ». en. In: *International Journal of Fatigue* 11.4 (July 1989), pp. 261–267.

[103] Lujie Shi et al. « A non-parametric evaluation method in staircase test for improving fatigue limit assessment ». en. In: *Probabilistic Engineering Mechanics* 70 (Oct. 2022), p. 103373.

[104] JJ Braam and S. van der Zwaag. « A Statistical Evaluation of the Staircase and the ArcSinP Methods for Determining the Fatigue Limit ». In: *Journal of Testing and Evaluation* 26.2 (1998), pp. 125–131.

[105] J Zhang and DB Kececioglu. « New approaches to determine the endurance strength distribution ». In: Washington, 1998, pp. 297–301.

[106] Hao Bai. « Machine learning assisted probabilistic prediction of long-term fatigue damage and vibration reduction of wind turbine tower using active damping system ». en. PhD thesis. Normandie Université, 2021.

[107] Ekaterina Plesovskaya and Sergey Ivanov. « An empirical analysis of KDE-based generative models on small datasets ». en. In: *Procedia Computer Science* 193 (2021), pp. 442–452.

[108] Murray Rosenblatt. « Remarks on Some Nonparametric Estimates of a Density Function ». In: *The Annals of Mathematical Statistics* 27.3 (1956), pp. 832–837.

[109] Nils-Bastian Heidenreich, Anja Schindler, and Stefan Sperlich. « Bandwidth selection for kernel density estimation: a review of fully automatic selectors ». en. In: *AStA Advances in Statistical Analysis* 97.4 (Oct. 2013), pp. 403–433.

[110] F. Pedregosa, G. Varoquaux, and A. Gramfort. « Scikit-learn: Machine Learning in Python ». In: *Journal of Machine Learning Research* 12 (2011), pp. 2825–2830.

[111] Simon J Sheather and M.Chris Jones. « A Reliable Data-Based Bandwidth Selection Method for Kernel Density Estimation ». In: *Journal of the Royal Statistical Society. Series B: Methodological* 53 (1991), pp. 683–690.

[112] Pauli Virtanen et al. « SciPy 1.0: fundamental algorithms for scientific computing in Python ». en. In: *Nature Methods* 17.3 (Mar. 2020), pp. 261–272.

[113] Y. Zhao, Q. Gao, and J. Wang. « An approach for determining an appropriate assumed distribution of fatigue life under limited data ». en. In: *Reliability Engineering & System Safety* 67.1 (Jan. 2000), pp. 1–7.

[114] Przemysław Strzelecki and Tomasz Tomaszewski. « Application of Weibull distribution to describe S-N curve with using small number specimens ». In: *AIP Conference Proceedings*. Fojutowo, Poland, 2016, p. 020007.

[115] Frank Nielsen. « On the Jensen–Shannon Symmetrization of Distances Relying on Abstract Means ». en. In: *Entropy* 21.5 (May 2019), p. 485.

[116] CM Magazzeni et al. « Bayesian Optimised Collection Strategies for Fatigue Testing – Constant Life Testing ». en. In: (2021), p. 32.

[117] Christopher Massimo Magazzeni et al. « Bayesian optimized collection strategies for fatigue strength testing ». en. In: *Fatigue & Fracture of Engineering Materials & Structures* (Oct. 2022), ffe.13859.

[118] Carlos C. Engler-Pinto et al. « Statistical Approaches Applied to Fatigue Test Data Analysis ». en. In: Apr. 2005, pp. 2005–01–0802.

[119] Rocío Alcalá-Quintana and Miguel García-Pérez. « A comparison of fixed-step-size and Bayesian staircases for sensory threshold estimation ». en. In: *Spatial Vision* 20.3 (2007), pp. 197–218.

[120] Xiaoyang Li et al. « A Bayesian Optimal Design for Sequential Accelerated Degradation Testing ». en. In: *Entropy* 19.7 (July 2017), p. 325.

[121] Ivo Babuska et al. « Bayesian inference and model comparison for metallic fatigue data ». en. In: *Computer Methods in Applied Mechanics and Engineering* 304 (June 2016). arXiv: 1512.01779, pp. 171–196.

[122] P. Sebastiani and H. P. Wynn. « Maximum entropy sampling and optimal Bayesian experimental design ». en. In: *Journal of the Royal Statistical Society: Series B (Statistical Methodology)* 62.1 (Feb. 2000), pp. 145–157.

[123] Michael D. Shields and Jiaxin Zhang. « The generalization of Latin hypercube sampling ». en. In: *Reliability Engineering & System Safety* 148 (Apr. 2016), pp. 96–108.

[124] Grégory Barbier. « Fatigue biaxiale à grand nombre de cycles: étude expérimentale et modèle d'endommagement à deux échelles probabiliste ». en. PhD thesis. École normale supérieure Paris-Saclay, 2019.

[125] K. Brownlee, J. Hodges, and M Rosenblatt. « The up-and-down method with small samples ». In: *Journal of the American Statistical Association* 48.262 (1953), pp. 262–277.